Advancing Energy Transition: Statistical Approaches to Pan-European Feed-in Data Sets, Enhanced Data Quality and Improved Forecasting

Zur Erlangung des akademischen Grades eines
Doktors der Ingenieurwissenschaften

(Dr.-Ing.)

von der KIT-Fakultät für Wirtschaftswissenschaften
des Karlsruher Instituts für Technologie (KIT)

genehmigte

Dissertation

von

M.Sc. Mira Watermeyer

Tag der mündlichen Prüfung: 15.06.2023

Referent: Prof. Dr. Oliver Grothe
Korreferent: Prof. Dr. Hans Manner

Karlsruhe 2023

Danksagung

Während meines Studiums weckte sich bei mir die Begeisterung für mathematische Modelle ebenso wie für die Energiewirtschaft. Durch meine Promotion erhielt ich von Herrn Professor Dr. Oliver Grothe die Möglichkeit, diese Interessen miteinander zu verbinden sowie mein Fachwissen auszubauen und zu vertiefen. Daher gebührt mein besonderer Dank meinem Doktorvater Herrn Professor Dr. Oliver Grothe für diese Chance, die umfassende Betreuung und das entgegengebrachte Vertrauen. Durch die sehr gute Zusammenarbeit, seine Hilfsbereitschaft, anregende Diskussionen und neue Denkanstöße konnte ich viel lernen und mich sowohl fachlich als auch persönlich weiterentwickeln.

Ebenso bedanken möchte ich mich bei meinem Korreferenten Herrn Professor Dr. Hans Manner, meinem Prüfer Herrn Professor Dr. Fabian Krüger und dem Vorsitzenden der Prüfungskommission, Herrn Professor Dr. Clemens Puppe für die Zeit und das Interesse, sich mit meiner Arbeit auseinanderzusetzen und diese zu bewerten.

Ich danke außerdem meinen Koautoren Herrn Professor Dr. Felix Müsgens und Thomas Möbius für die gute Zusammenarbeit. Gemeinsam erhielten wir die Gelegenheit, am Forschungsprojekt "ProKoMo" des Bundesministeriums für Wirtschaft und Klima mitzuwirken. Der dadurch entstandene fachliche und persönliche Austausch hat meine Promotionszeit bereichert. Mein Dank gilt ebenso dem BMWK für diese Möglichkeit.

Zudem möchte ich mich bei meinem Koautoren und Kollegen Fabian Kächele sowie meiner Koautorin und wissenschaftlichen Hilfskraft Franziska Scheller bedanken. Die gemeinsame Forschung und der Gedankenaustausch haben mir sehr viel Freude bereitet.

Diese Arbeit entstand während meiner Zeit als wissenschaftliche Mitarbeiterin am Lehrstuhl Analytics and Statistics des Instituts für Operations Research am Karlsruher Institut für Technologie. Ich danke Anika Kaplan, Fabian Kächele, Jonas Rieger und Parzival Borlinghaus für diese Zeit. Durch ihre Unterstützung, die tolle Zusammenarbeit und das persönliche Verhältnis, Kaffee, Grillabend und Squash-Spiel inklusive, habe ich mich sehr wohl gefühlt. Mein Dank gilt auch Marion Rihm, die mir so oft weitergeholfen hat und als gute Seele immer da war. Darüber hinaus möchte ich mich bei unseren wissenschaftlichen Hilfskräften Huidi, Tim, Tim und Franziska bedanken.
Ebenso bedanke ich mich bei Fenja Scheu für die Motivation und die vielen Gespräche während meiner Promotionszeit.

Abschließend möchte ich mich von Herzen bei meiner Familie und meinen Freunden bedanken, die stets an mich glaubten. Insbesondere danke ich meinen Eltern Petra und Dr. Heinrich Jürgen Watermeyer, die mir diesen Lebensweg ermöglicht, immer an mich geglaubt und mich immer bedingungslos unterstützt haben. Nicht zuletzt gilt mein großer Dank Tobias Wälde. Seine Motivation, Rücksicht und Geduld sowie seine grenzenlose Unterstützung und sein Verständnis waren unverzichtbar für das Gelingen meiner Dissertation. Durch ihn habe ich die Kraft und den Mut gefunden, diese Herausforderung zu meistern.

Abstract

The energy transition is increasing the share of renewable energy sources in electricity generation and thus the complexity and uncertainty in the electricity market. Comprehensive and large-scale data sets as well as accurate forecasts are crucial for political, financial and operational decision-making. Past and current research in this area focusses on improving data quality and data forecasting. In particular, probabilistic forecasts have gained raising interest in recent years due to increased market uncertainty. This thesis presents contributions which address these challenges by using statistical methods and models. The work thus contributes to improving the data basis, data quality and forecast accuracy of various variables such as load, prices or renewable energy generation, and provides methods to quantify the increased uncertainty.

Specifically, this work develops a comprehensive, high-resolution data set for the European mainland, which includes hourly electricity generation from renewable energy sources and realistic layouts. The layouts reflect the allocation of installed wind and solar energy capacities. For the calculation of the data set, physical and statistical methods are combined. By providing the source code, the layouts and time series can be individually adjusted, updated, and used for accurate, geographically high-resolution forecasts and nowcasts.

Furthermore, the day-ahead load forecast published by the transmission system operators of the European electricity grid for their respective market areas is improved using a time series model. This model maps the forecast error solely to past values of the load forecast, the realised load, and the observed load forecast error itself. The model and source code are freely available, so that the increased forecast accuracy through this method provides added value to the variety of models that use this load forecasts as an input variable.

In addition, this work presents a method for forecasting prediction errors that combines various statistical modelling approaches to create both classical point forecasts and modern density forecasts. The multidimensional forecast error model increases the reliability of existing forecasts and supplements them with probability statements. The model is developed as a ready-to-use application with available source code. The effectiveness of the method is demonstrated using three real data applications.

Finally, the presented methods are used to develop a novel open-source hybrid model that combines fundamental and statistical methods. The statistical models provide a crucial added value; they improve a techno-economic electricity market model. In doing so, the resulting and presented multi-step hybrid model generates accurate point and probabilistic forecasts for day-ahead electricity market prices.

Contents

List of Figures **vii**

List of Tables **xi**

List of Abbreviations **xiii**

1 Introduction **1**

2 High-Resolution Working Layouts and Time Series for Renewable Energy Generation in Europe **5**
2.1 Introduction 5
2.2 Data 8
2.3 Methodology 11
2.3.1 Calculation of Renewable Power Generation 11
2.3.2 Weather Cell Combination 19
2.3.3 Layout Estimation 21
2.4 Results 26
2.5 Summary and Concluding Remarks 41

3 Enhancing Energy System Models Using Better Load Forecasts **43**
3.1 Introduction 43
3.2 Literature 45
3.3 Data 48
3.3.1 TSO-based Load Forecast Data 48
3.3.2 Input Data for the Energy System Model 51
3.4 Methodology 54
3.4.1 Model for Load Forecast Error 55
3.4.2 Energy System Model 58
3.5 Results 65
3.5.1 Improved Load Data and Achieved Error Reduction 66
3.5.2 Impact of Improved Load Data on an Energy System Model 68
3.6 Concluding Remarks 72

4 Forecast the Forecast Error 75
4.1 Introduction . . . 75
4.2 Data . . . 79
4.3 Methodology . . . 80
4.3.1 Point Forecast . . . 81
4.3.2 Probabilistic Forecast . . . 85
4.4 Evaluation Methods . . . 86
4.4.1 Point Forecast Evaluation . . . 86
4.4.2 Probabilistic Forecast Evaluation . . . 88
4.5 Real Data Examples and Validation . . . 89
4.5.1 Point Forecasts . . . 90
4.5.2 Probabilistic Forecasts . . . 98
4.6 Example use Cases for Probabilistic Forecasting . . . 104
4.7 Concluding Remarks . . . 107

5 A Hybrid Model for Day-Ahead Electricity Price Forecasting 109
5.1 Introduction . . . 109
5.2 Literature . . . 112
5.3 Data . . . 120
5.4 Methodology . . . 125
5.4.1 Stochastic Data Pre-Processing Step . . . 125
5.4.2 Parameter Density Forecast Step . . . 128
5.4.3 Energy System Optimisation Step . . . 129
5.4.4 Stochastic Data Post-Processing Step . . . 136
5.5 Hybrid Model Results . . . 140
5.6 Analysis of Individual Model Steps . . . 150
5.6.1 Load Forecasts . . . 150
5.6.2 Price Estimators After the Energy System Optimisation Step . . . 150
5.6.3 Improvement of Price Estimators . . . 152
5.7 Concluding Remarks . . . 159

6 Conclusion 161

Appendices 163

A Data, Code and Sources Availability 164

B Nomenclature for the Techno-Economic Energy System Model 166

C Supplementary Material for the Load Forecast 168

D Heat Maps of the Univariate DM Tests 170

Own Publications **177**

Bibliography **178**

List of Figures

2.1 Nodes of the European transmission network. 10
2.2 Power of LongiSolar LR4-72HBD solar panel depending on radiation and cell temperature. 16
2.3 Power curves Siemens SWT 107 and MHI Vestas V164 with corresponding parameters of the fitted polynomials and change-point. 19
2.4 Nodes of the European transmission network and assigned weather cells of the ERA5 data set. 20
2.5 Pearson correlation of power signals of 2019 from neighbouring transmission nodes for k-nearest neighbours and given distance per renewable generator type. 22
2.6 Actual and estimated PV generation for Germany and Denmark in July 2022. 26
2.7 Actual and estimated onshore wind generation for Germany and Denmark in July 2022. 27
2.8 Actual and estimated offshore wind generation for Germany and Denmark in July 2022. 27
2.9 Predicted onshore wind generation for Germany and Denmark in July 2022. 29
2.10 Predicted PV generation for Germany and Denmark in July 2022. 29
2.11 Estimated PV capacity layout for Germany and Denmark in 2022. 31
2.12 Estimated onshore wind capacity layout for Germany and Denmark in 2022. 32
2.13 Estimated offshore wind capacity layout for Germany and Denmark in 2022. 33
2.14 Estimated node capacity for offshore wind for Germany and Denmark per year. 34
2.15 Estimated node capacity for onshore wind for Germany and Denmark per year. 35
2.16 Estimated node capacity for solar for Germany and Denmark per year. . 35
2.17 Actual, estimated and predicted PV generation for Germany and Denmark in July 2022 for the OLS regression. 36
2.18 Actual, estimated and predicted onshore wind generation for Germany and Denmark in July 2022 for the OLS regression. 37

2.19 Actual, estimated and predicted offshore wind generation for Germany and Denmark in July 2022 for the OLS regression. 37
2.20 With an OLS regression estimated onshore wind capacity layout for Germany for 2019 and 2022. 38

3.1 Actual load and TSOs' day-ahead load forecast and error of TSOs' day-ahead load forecast in 2017. 49
3.2 Average weekly pattern of TSOs' day-ahead load forecast errors from 2016 to 2019. 51
3.3 Scatter plot of TSOs' day-ahead load forecast error and TSOs' day-ahead load forecast error one hour before. 52
3.4 Illustration of the energy system model's rolling window. 60
3.5 Average percentage MSE improvement for the day-ahead load forecast for each hour of a day and for each weekday. 68
3.6 Average percentage MSE improvement of day-ahead load prediction and day-ahead price estimators for each hour of a day. 70
3.7 Percentage error reduction of the price estimator and the load in different time periods. 71
3.8 Relative error reduction of the price estimator in different price segments of the respective year from 2017 to 2019. 72

4.1 Average forecast error of the day-ahead load forecast $\hat{Y}$ for the hours of the day. 91
4.2 Coefficients estimated by linear regression for the day-ahead load, wind generation and price forecast error forecast for an exemplary time period. 93
4.3 Multivariate DM test for the day-ahead load, wind generation and price forecast. 96
4.4 RMSE of the sub-models' forecasts of the forecast error for the hours of the day for load, wind generation and price. 97
4.5 Univariate DM test for the day-ahead wind generation forecast for hours 4 and 15 of the day. 98
4.6 Discrete PIT for the QRA-based probabilistic day-ahead load, wind generation and price forecast error forecast. 103
4.7 Discrete PIT for the distribution-based probabilistic day-ahead load, price and wind generation forecast error forecast. 103
4.8 Probability for the overestimation of the load for each hour of the week. 105
4.9 Probability for the overestimation of the day-ahead wind generation and day-ahead price for each hour of the week. 106
4.10 Box plot of the 90 % prediction interval's width of the day-ahead load, wind generation and price forecast error for each hour of the day. 106

5.1 Schematically illustration of the hybrid model. 111
5.2 Geographical scope of the energy system model. 120
5.3 Illustration of the rolling window for the energy system optimisation step. 131
5.4 RMSE for base, peak and off-peak hours. 143
5.5 RMSE for hours at different day-ahead price quantiles. 144
5.6 RMSE of the LEAR model's day-ahead price forecast for base, peak and off-peak hours and for hours at different day-ahead price quantiles. . . . 145
5.7 Number of actual prices included in the quantiles estimated in the forecast period from 2017 to 2020. 146
5.8 Number of actual prices included in the quantiles estimated in the 2017 to 2020 forecast period, separated for peak (left) and off-peak (right) hours. 147
5.9 Box plot of the 90 % prediction interval for each hour of the day. 148
5.10 Average spread between the predicted 5 % and 95 % quantiles for the hours of the week. 148
5.11 Day-ahead price forecast, lower-bound forecast and upper-bound forecast. 149
5.12 Probability of negative day-ahead prices. 150
5.13 Mean price estimator errors for the hours of the week after the energy system optimisation step. 153
5.14 Mean price estimator errors for the hours of the day in each year after the energy system optimisation step. 153
5.15 Correlation of possible exogenous variables and the price estimation error. 154
5.16 RMSE for univariate and multivariate post-processing sub-models for each hour of the day. 156
5.17 Mean price forecast errors of the individual sub-models and the combined sub-models for the hours of the day in each year. 157
5.18 Mean price forecast errors of the individual sub-models and the combined sub-models for the hours of the week. 157
5.19 P-value of Diebold-Mariano test for all parts of the stochastic post-processing step. 158
5.20 Average RMSE improvement in day-ahead price forecasts for each hour of the day and each day of the week. 159

D.1 Univariate DM tests for the day-ahead electricity load forecast for hours 0 to 11 of the day. 171
D.2 Univariate DM tests for the day-ahead electricity load forecast for hours 12 to 23 of the day. 172
D.3 Univariate DM tests for the day-ahead wind generation forecast for hours 0 to 11 of the day. 173
D.4 Univariate DM tests for the day-ahead wind generation forecast for hours 12 to 23 of the day. 174

D.5 Univariate DM tests for the day-ahead electricity price forecast for hours 0 to 11 of the day. 175
D.6 Univariate DM tests for the day-ahead electricity price forecast for hours 12 to 23 of the day. 176

List of Tables

2.1 Countries in the European transmission network used in this study. 9
2.2 Variables of the ERA5 data set used in this study. 11
2.3 RMSE of the elastic-net year- and country-wise estimation and prediction for PV, onshore wind and offshore wind generation relative to the respective hourly generation average. 28
2.4 Actual installed onshore wind, offshore wind and PV capacity and estimated onshore wind, offshore wind and PV capacity of Denmark and Germany for each year. 30
2.5 RMSE of the OLS regression year- and country-wise estimation and prediction for PV, onshore wind and offshore wind generation relative to the respective hourly generation average. 36
2.6 With an OLS regression estimated onshore wind, offshore wind and PV capacity of Denmark and Germany for each year. 36
2.7 Actual installed onshore wind capacity and estimated onshore wind capacity of all countries for each year. 39
2.8 Actual installed offshore wind capacity and estimated offshore wind capacity of all countries for each year. 40
2.9 Actual installed PV capacity and estimated PV capacity of all countries for each year. 40

3.1 Descriptive statistics of TSOs' load forecast errors for the years 2016 to 2019. 50
3.2 Means, standard deviations and error measures for the original TSOs' day-ahead load forecast and the improved day-ahead load forecast. . . . 66
3.3 Error measures for the price estimators of the *em.power dispatch* model comparing the improved load forecasts by original load forecasts. 69

4.1 RMSE for the weighted and non-weighted final forecasts of the day-ahead load, wind generation and price forecast error. 92
4.2 Error measurements RMSE and MAE of the day-ahead load forecast error time series. 94

4.3 Error measurements RMSE and MAE of the day-ahead wind generation forecast error time series. 94
4.4 Error measurements RMSE and MAE of the day-ahead electricity price forecast error time series. 95
4.5 CRPS for the probabilistic forecast of the day-ahead wind generation forecast error. 100
4.6 CRPS for the probabilistic forecast of the day-ahead load forecast error. 101
4.7 CRPS for the probabilistic forecast of the day-ahead price forecast error. 102

5.1 Overview of required data. 121
5.2 RMSE and MAE of day-ahead electricity price forecast through the presented hybrid model, the agent-based model and the LEAR model. . . . 142
5.3 RMSE and MAE for the TSOs' day-ahead load forecast and the improved day-ahead load forecast. 151
5.4 Descriptive statistics of the errors of the price estimators after the energy system optimisation step. 152
5.5 Descriptive statistics of the day-ahead price forecast error of the hybrid model. 154
5.6 Error measurements RMSE and MAE of the sub-models' error time series. 155

C.1 Weekday wise averaged descriptive statistics of TSOs' load forecast errors for the years 2016 to 2019. 168
C.2 Hourly averaged descriptive statistics of TSOs' load forecast errors for the years 2016 to 2019. 169
C.3 Error measures for the the improved day ahead load forecast with a rolling window length of three and six month. 169

List of Abbreviations

AE	Absolute error
ANFIS	Adaptive neuro-fuzzy inference system
ANN	Artificial neural network
APARCH	Autoregressive conditional heteroscedastic
API	Application programming interface
BNetzA	Bundesnetzagentur
CDS	Climate Data Store
CHP	Combined heat and power
CNN	Convolutional neural network
CO_2	Carbon dioxide
CRPS	Continuously ranked probability score
DM	Diebold Mariano
DNN	Deep neuronal network
ECMWF	European Centre for Medium-Range Weather Forecasts
EEX	European Energy Exchange
ENTSO-E	European Network of Transmission System Operators for Electricity
EPEX	European Power Exchange
ERA5	ECMWF Reanalysis v5
ETS	Exponential smoothing
EU	European Union
GAMS	General Algebraic Modeling Language
GARCH	Generalised autoregressive conditional heteroscedastic
GEBCO	The General Bathymetric Chart of the Oceans
GEFCom	Global Energy Forecasting Competition
GLM	Generalised linear model
JAO	Joint Allocation Office
LB	Ljung-Box
LEAR	Lasso estimated autoregressive
LSTM	Long short-term memory
MAE	Mean absolute error
MAPE	Mean absolute percentage error
MS	Markov regime-switching
MSE	Mean squared error

MWh	Megawatt-hour
NTC	Net transfer capacity
OLS	Ordinary least squares
PIT	Probability integral transform
PL	Pinball loss
PSP	Pumped storage plants
PV	Photovoltaic
QRA	Quantile regression averaging
RES	Renewable energy sources
RMSE	Root mean squared error
RNN	Recurrent neural network
(S)AR(I)MA(X)	(Seasonal) Autoregressive (Integrated) Moving Average (with exogenous factors)
SE	Squared error
SVM	Support vector machine
TSO	Transmission system operator
TVP	Time-varying parameter
UBA	Umweltbundesamt
VAR	Vector autoregressive
Wh	Watt-hour
Ws	Watt-second

1. Introduction

The energy market is a complex and interdependent system. Due to the need to reduce net greenhouse gas emissions and the energy transition, the entire energy system is changing. The shift towards renewable energy sources, which are weather-dependent and fluctuating, is transforming the electricity system into a decentralised network. This leads to new challenges for politics and especially for companies in energy markets, which are already facing strong competition due to liberalisation. With this growing complexity, competition and uncertainty, comprehensive and large-scale data sets as well as accurate forecasts for and within the energy landscape are crucial for financial and operational decisions and regulatory interventions in the energy sector. The growth of renewable energy sources and fluctuating commodity prices has further increased uncertainty, making it essential to record and quantify this uncertainty. Concluding, data sets, accurate forecasts and the quantification of uncertainty are more critical than ever in the energy sector and essential for the growth and success of the energy market and the energy transition.

The thesis tackles the complex challenges facing the energy sector by presenting four approaches that leverage statistical methods and models. In the first approach, we present a comprehensive data set with a high spatial resolution containing layouts with estimates of installed wind and solar capacities as well as wind and solar power generation time series for the whole of mainland Europe. It is calculated by using physical and statistical methods. Since the provided synthetic data set with its open source code is the first one with such a high spatial resolution and for such a large area, it expands the renewable energy database. For other variables, e.g., load, there already exist data sets. In the second contribution of this thesis, we apply statistical methods to this data and thus, significantly improve the day-ahead load forecast of the transmission system operators (TSOs) with a time series model. Following the idea of enhancing forecasts, the third

contribution provides a general and ready-to-use approach to improve day-ahead forecasts. Therefore, forecast errors are predicted both precisely and probabilistically, so that the increased uncertainty in energy markets can be quantified. In the fourth contribution, we combine previous approaches to improve a techno-economic energy system model with statistical methods and thus generate accurate day-ahead price forecasts while keeping interpretability. Therefore, different statistical approaches complement the energy system model, melting together to one united hybrid model type.

In the following, the structure and contributions of the thesis are outlined. In Chapter 2, we provide the mentioned data-driven layouts representing installed wind and photovoltaic capacity for about 1,500 nodes in continental Europe. We convert high-resolution numerical weather data into synthetic generation data using physical models of wind turbine power curves and solar module efficiency curves to describe the potential wind and solar power generation at each node. These synthetic and upscaled data are regressed on actual feed-in data at country-specific resolution for each hour based on elastic-net approaches, with the estimated coefficients describing the installed capacity at each node. Regularisations applied via the elastic-net allow for realistic estimates of the allocation of installed capacity, enabling the layouts to be used for accurate forecasts and nowcasts. The inclusion of onshore wind, offshore wind, and PV in the analysis provides generator type-specific, detailed information. The large-scale time series data, which include daily updates of energy feed-ins and information on the allocation of wind and PV capacities, present a comprehensive data set. We offer the necessary source code to generate, modify and customise the layouts and time series to meet the requirements of specific applications. This chapter is based on: O. Grothe, F. Kächele, and M. Watermeyer (2023), High-Resolution Working Layouts and Time Series for Renewable Energy Generation in Europe: A Data-Driven Approach for Accurate Fore- and Nowcasting, *Paper submitted to Renewable Energy* (Grothe et al., 2023b).

To improve existing load data, we present a statistical model to reduce the forecast errors of the TSOs' hourly day-ahead load forecasts in Chapter 3. Using only the publicly available TSO-based load forecasts in a common time series model, we avoid the need for additional data and provide an accurately improved day-ahead load forecast. Since the source code is openly available, we make the approach accessible to all users

and researchers. We demonstrate the value of improving in real-time the quality of load forecasting as an input variable in techno-economic energy system models through an empirical study. By showing that techno-economic energy system models perform significantly better compared to the TSO data with the improved load data, we provide valuable insights for many stakeholders in the power sector, especially energy system model developers who want to improve the validity of their models. This chapter is based on: T. Möbius, M. Watermeyer, O. Grothe and F. Müsgens (2023), Enhancing energy system models using better load forecasts, *Energy Systems*, 1868–3975 (Möbius et al., 2023).

In Chapter 4, we use and develop statistical models to generally improve forecast models and data. The chapter presents a flexible approach to calculate point and probabilistic forecasts of the error in short-term forecasts of various target variables. We interpret the forecast errors as an hourly high-frequency time series and split it into 24 daily time series, capturing intraday dependencies and structures as well as specific characteristics of each hour of the day. We use univariate and multivariate seasonal time series models across different calibration windows to predict the forecast error time series. The forecasts of the individual models are combined into expected values, e.g., the point forecasts, and hourly probabilistic forecasts via Quantile Regression Averaging for the hourly prediction errors. Thus, we link point and probabilistic forecasts, increase the accuracy of existing forecasts and additionally quantify uncertainties due to forecast inaccuracies. Market participants can incorporate them into risk assessments, trading strategies and power plant dispatch planning. By publicly releasing the source code, we provide a ready-to-use application, empowering others to forecast the prediction errors of their own forecasts and customise the model to suit their requirements. Overall, our approach represents a significant step forward in improving the accuracy of day-ahead forecasting in the energy sector. This chapter is based on: M. Watermeyer and F. Scheller (2023), Forecast the forecast error: Improving point forecasts and generating density forecasts in energy markets, *Working paper* (Watermeyer and Scheller, 2023).

Continuing, in Chapter 5, we build upon the ideas presented in previous chapters by using statistical methods to improve a techno-economic market model. This results in what we call a hybrid model, enriching the literature on hybrid models. Given that the

model's complete source code is accessible online, researchers are able to implement our methodology and adapt it to suit different electricity markets. Our approach generates highly accurate day-ahead price forecasts that are comparable to benchmarks in the literature. To enhance the energy system model, we adopt the general idea of improving the day-ahead load forecast and develop a new, simple approach for two-day-ahead load forecasts. We also create prediction intervals for selected input parameters of the energy system model, enabling us to account for uncertainty in the operational decisions of market participants in the model. After calculating the optimisation of the energy system model, we use a multidimensional model that incorporates both univariate and multivariate approaches to map the errors resulted from the day-ahead price estimators. This approach enables us to capture seasonal effects and complex price structures. By modelling and improving the error of the price estimators, we generate more accurate day-ahead price forecasts. In addition, we calculate prediction intervals and probability densities for day-ahead prices using Quantile Regression Averaging, which allows us to quantify uncertainty. This approach has practical applications, such as enabling power plant operators to assess the probability of negative prices occurring during a given hour. Altogether, through the statistical methods, our approach marks a significant advance in improving the usefulness of power system models for short-term price forecasting. This chapter is based on: M. Watermeyer, T. Möbius, O. Grothe and F. Müsgens (2023), A hybrid model for day ahead electricity price forecasting: Combining fundamental and stochastic modelling, *Paper submitted to Energy Economics* (Watermeyer et al., 2023).

Chapter 6 concludes this thesis. The appendix contains some additional topics belonging to the individual chapters.

2. High-Resolution Working Layouts and Time Series for Renewable Energy Generation in Europe: A Data-Driven Approach for Accurate Fore- and Nowcasting

This chapter is based on Grothe et al. (2023b)[1].

2.1. Introduction

To reduce net greenhouse gas emissions, the EU, like most countries worldwide, is expanding renewable energy generation capacities (European Commission, 2019; European Commission et al., 2021). The energy system, which has so far been based on conventional and centralised electricity generation, transforms into a decentralised system dependent on generators with high weather-conditional variability (Morales et al., 2014; Gil et al., 2012; Antweiler and Müsgens, 2021; Beran et al., 2019; Pape et al., 2016). Because of this, the integration of renewable energy sources poses challenges for the electricity market, including the need for detailed information and accurate forecasts of feed-in from individual generators as well as on different aggregation levels. The interconnection of the European power grids and the impact of weather on renewable energy output also

[1]The work was partly supported by the German Federal Ministry of Economic Affairs and Climate Action through the research project "ProKoMo - Better price forecasts in the energy sector by combining fundamental and stochastic models" within the Systems Analysis Research Network of the 6th energy research program. Further, we thank Yanting Liu and Rafael Weinert for coding assistance.

calls for merged data sets of installed capacities and feed-in on a large-scale, i.e., covering the entire continent (González-Aparicio et al., 2017). However, actual feed-in data sets are often not publicly available, and even the sole information on the spatial allocation of installed renewable generation capacity is only available with a time lag, if at all. We, therefore, derive high spatial resolution hourly wind and solar feed-in time series calculated from weather data for mainland Europe. We also provide working layouts with an estimated, realistic allocation of installed wind and solar capacities across the continent. The data set has been generated with great methodical care. Users may update it at any time using our code with the flexibility to limit their analysis to the regions or aggregation levels that interest them.

Calculating feed-in of renewable energy sources is not new to the existing literature. For example, researchers use statistical methods and calculate or predict the feed-in by time series models and deep learning (see, e.g., Wang et al., 2019; Li et al., 2020; Shahid et al., 2020; Maciejowska et al., 2021; Ali et al., 2021). A comprehensive overview of very short-term forecasting wind and solar generation is provided by Tawn and Browell (2022), whereas Rajagukguk et al. (2020) focus on deep-learning methods for short-term forecasting solar irradiance and PV power of single solar panels. Detailed reviews concerning solar generation forecasting are given by Ahmed et al. (2020), and wind generation forecasting by Wang et al. (2011). Other works directly use weather data for weather-to-energy conversion techniques trained on historical data. Thus, instead of time series approaches, they develop physical models like we do, at least partly in this chapter. A short overview of the calculation of feed-in data from weather data is provided by Koivisto et al. (2020) (see also the references therein). Studies using weather-to-energy conversions to calculate the generation of renewable energy sources can be found, for example, in Staffell and Pfenninger (2016); Staffell and Green (2014); Kubik et al. (2013); Barthelmie et al. (2010); Baker et al. (1990); Rose and Apt (2015); Hughes (2012); Sunderland et al. (2016) for wind and in Kenny and Fiedler (2022); Frank et al. (2021); Huld et al. (2011); Huld and Amillo (2015); Pfenninger and Staffell (2016); Piasecki et al. (2019) for solar.

Approaches that rely on weather-to-energy conversion require detailed data on the locations and specifics of the installed turbines and solar panels, which are often not

publicly available for macro-scale regions due to economic interests and high administrative burdens, as stated above. Researchers have therefore tried to circumvent this lack of data by using layouts only for specific regions or countries, such as Germany or Denmark, where information is publicly available (see, e.g., Engelhorn and Müsgens (2018); Olauson and Bergkvist (2015); Grothe et al. (2022)). Additionally, Andresen et al. (2014) used layouts based on site attractiveness and policy targets to calculate possible trajectories of wind and solar power generation depending on the future share of renewables in electricity generation and other supply and demand factors, and Andresen et al. (2015) generated forecasts based on the government's expansion plans and targets. Another option is chosen by Jensen and Pinson (2017), who assumed wind and solar generators to be uniformly distributed over mainland Europe for a first layout and proportionally distributed to the population for a second layout. By doing so, they come up with a comprehensive data set for a European electricity system. However, due to their strong assumptions on the spatial distribution of generators, Jensen and Pinson (2017) did not intend the estimated hourly feed-in of these layouts to actually conform to the observed feed-in.

In contrast, we develop synthetic yet realistic capacity layouts for renewable energy generation plants. The provided layouts are learned from observed data, have a high spatial resolution, and result in a comprehensive and precise data set for the feed-in of renewable energy sources. We focus on wind and photovoltaic (PV) energy, as these have the largest share of renewable generation capacity and exhibit a high degree of weather dependency. We provide information on potential installed wind, onshore and offshore, and PV capacities as well as on the feed-in generated with these capacities, scaled to the network nodes of the main continental European transmission network. The estimated layouts are derived as follows. We convert high-resolution numerical weather data into energy signals using physical models from the power curves of wind turbines and solar modules. Hereby, we carefully consider parameters like the wind conditions at hub height, the sun's incidence angle on the solar panels as well as the weather-dependent proportions of direct and diffuse irradiation. Resulting energy signals are then mapped to 1,494 main nodes of the European transmission network to form synthetic power outputs. We next use the synthetic outputs to explain actual measured wind and solar feed-in with an

elastic-net regression approach and come up with an estimate of installed wind and solar capacities at each node, which builds our *working layout* for renewable energy sources in mainland Europe. We show that using our working layouts in weather-to-energy conversion approaches leads to precise estimates of the actual electricity feed-in. Further, the working layouts inherit most of the characteristics of the true layouts for places where the true layout is known. Thus, the layouts can be used to map and forecast the generated feed-in in the European transmission network. Finally, we use our layouts to create a comprehensive data set for mainland Europe, including the hourly resolution wind, onshore and offshore, and PV power generation from 2019 to 2022 and high-resolution layouts of installed wind and PV capacities. By making the code publicly available, we enable others to generate results for a specific time horizon and tailor them to their needs. Additionally, we provide a detailed methodology for converting weather data to wind and especially to solar generation, filling a gap in previous research by providing a comprehensive understanding of this conversion process and the required variables.

The remainder of the chapter is structured as follows. First, the data used in our approach are presented in Section 2.2. In Section 2.3, we explain the layout generation step-by-step, including a detailed description of the weather-to-energy conversion, the cell-to-node allocation and the layout estimation. Section 2.4 presents the results and evaluations of the layout and the feed-in data sets. We conclude in Section 2.5.

2.2. Data

Our analysis is based on high-resolution historical weather data and the main continental European transmission network nodes. The nodes belong to a network model which comprises 1,494 buses, shown in Figure 2.1. It is based on the European Network of Transmission System Operators for Electricity (ENTSO-E) grid map and was first developed by Hutcheon and Bialek (2013). We use the geographical locations of this network, which are transformed by Jensen and Pinson (2017) and are available at Jensen et al. (2017). The network captures countries of mainland Europe, listed in Table 2.1.

For the weather data, we use high-resolution historical weather data, i.e., data which is often provided from reanalysis data, where weather measurements, models and numerical

Table 2.1.: Countries in the European transmission network used in this study.

Country	Abbreviation
Albania	ALB
Austria	AUT
Belgium	BEL
Bulgaria	BGR
Bosnia Herzegovina	BIH
Switzerland	CHE
Czechia	CZE
Germany	DEU
Denmark	DNK
Spain	ESP
France	FRA
Greece	GRC
Croatia	HRV
Hungary	HUN
Italy	ITA
Luxembourg	LUX
North Macedonia	MKD
Montenegro	MNE
Netherlands	NLD
Poland	POL
Portugal	POR
Romania	ROU
Serbia	SRB
Slovakia	SVK
Slovenia	SVN

model predictions are combined into one large comprehensive data set. More specifically, our analysis uses the *ERA5 hourly data on single levels from 1959 to present* reanalysis data set (Hersbach et al., 2018) for the years 2019 to 2022. Since the data set includes more than 250 variables, we only use an excerpt with the variables given in Table 2.2 for each location.

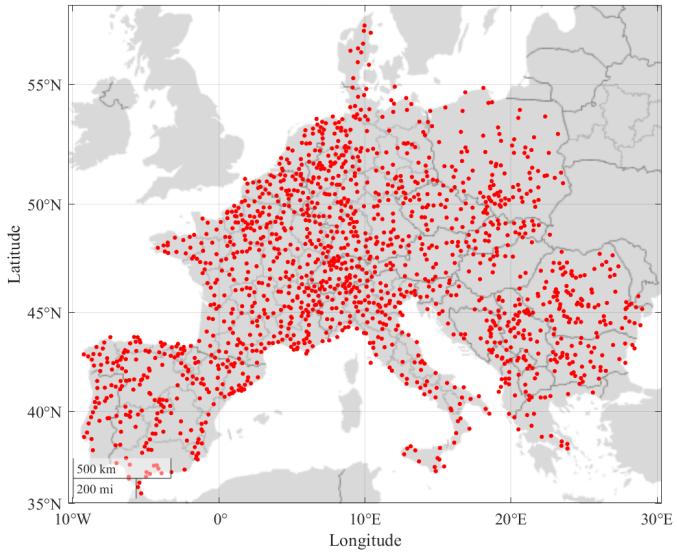

Figure 2.1.: Nodes of the European transmission network, marked in red.

The data is accessed via the *Python™ CDS Toolbox API*[2]. We also use sea depth data extracted from the GEBCO data[3] and match it to the coordinates of the ERA5 data to exclude locations where offshore wind farms are technically not possible or not profitable yet.

Hourly actual feed-in data for every country is provided by the ENTSO-E transparency platform (ENTSO-E Transparency Platform, 2023a). Note this important point: Since the feed-in and weather data have different accumulation schemes, with the weather data containing accumulated data for the hour ending at the timestamp, and the feed-in data accumulating over the hour following the timestamp, it is necessary to align the two data sets with each other. To clarify, the 10 a.m. timestamp, for example, refers to 10 a.m. to 11 a.m. in the feed-in data and to 9 a.m. to 10 a.m. in the weather data; thus, we reduce the timestamps in the feed-in data by one hour.

[2]The documentation of the toolbox is available under *https://cds.climate.copernicus.eu/toolbox/doc/api.html*, accessed on 17-01-2023

[3]The data is available under *https://download.gebco.net/*, accessed on 15-12-2022

Table 2.2.: Variables of the ERA5 data set used in this study.

Variable	Naming ERA5	Description
u	100m u-component of wind	Eastward component of the 100 m wind
v	100m v-component of wind	Northward component of the 100 m wind
z_0	Forecast surface roughness	Aerodynamic roughness of surface
t_a	2m temperature	Temperature of air at 2m above the surface
ρ	Forecast albedo	Reflectivity of the earth's surface
I_{bn}	Total sky direct solar radiation at surface	Amount of direct solar radiation
I_s	Surface solar radiation downwards	Amount of solar radiation that reaches a horizontal plane at the surface of the earth

2.3. Methodology

Our approach is based on comparing synthetic energy signals with the actual feed-in of renewable energy sources. From a high level, we first calculate the nominal power from solar and wind power generators in each weather cell of the ERA5 data set for each hour. Then, each weather cell is assigned to a transmission node within the European electricity grid structure, where we aggregate the information from multiple weather cells. Third, we facilitate an elastic-net regression approach to estimate the number of renewable generators at each transmission node. The installed capacities are then given by the estimated number of renewable generators multiplied by the rated power of the exemplary used generators. The resulting layout information can be used to improve forecasts, enhance grid stability or define expansion goals for renewable energies. In the following, we first discuss the calculation of nominal power for each weather cell and then introduce the weather cell combination and the estimation approach. The entire code of our methodology is provided in a repository on GitHub (*https://github.com/MWaterm/High-Resolution-Working-Layouts-and-Time-Series-for-Renewable-Energy-Generation-in-Europe*).

2.3.1. Calculation of Renewable Power Generation

We calculate the generated power based on historical weather data and the technical specifications of the used renewable generators. More precisely, we transform the measured

solar radiation and wind speeds to nominal power outputs for each weather cell. The transformation is done using the technical specifications of state-of-the-art solar panels and wind turbines. We first consider the calculation of solar power generation followed by wind power generation, onshore and offshore.

Solar

To calculate the nominal power generated by solar panels, it is important to consider both solar radiation and temperature. Solar radiation consists of direct, diffuse, and ground-reflected components, all of which must be taken into account. In the ERA5 data set, the variable *Surface solar radiation downwards* (denoted as I_s) represents the total amount of solar radiation that a pyranometer would measure, including both direct and diffuse radiation. To separate these components, we subtract the direct radiation component given in the variable *Total sky direct solar radiation at surface* (denoted as I_{bn}). We then calculate the ground-reflected component using the *Forecast albedo* variable (denoted as ρ), which measures the Earth's surface reflectivity. Since radiation is measured in Joule per square meter [$\mathrm{J/m^2}$], we convert it to Watt-hours [Wh] by dividing by 3,600. This is because one Joule equals one Watt-second ($1\,\mathrm{J} = 1\,\mathrm{Ws}$), which is approximately $0.00027777\,\mathrm{W/m^2}$ over the course of one hour.

We now give a compact presentation of the important aspects and formulas for solar conversion. In a nutshell, we first determine the angle of the sun for the given location, time, and date. Then, the actual radiation on the tilted surface of the solar panel is calculated. Third, we use the radiation, ambient temperature, and specifications of the solar panel to determine the cell temperature and, finally, the resulting efficiency. Last, this value is multiplied by the corresponding radiation and discounted for further losses. For more details on the following calculations and formulas, we recommend the excellent books by Kalogirou (2014) and Duffie and Beckmann (2006).

First, the sun's radiation angle is needed, which depends on the date, time, and geographical location. Since the earth's axis of rotation is inclined at an angle of 23.45° from the ecliptic axis of the earth's rotation around the sun, the polar axis is moving with respect to the sun. Thus, we calculate the angle δ, called *declination*, between the normal of the earth's axis of rotation and the sun's rays for each day first. The declination in

radians can be computed by the formula given by Spencer (1971):

$$\begin{aligned}\delta = 0.006918 &- 0.399912 \cdot \cos(\Gamma) + 0.070257 \cdot \sin(\Gamma) \\ &- 0.006758 \cdot \cos(2\Gamma) + 0.000907 \cdot \sin(2\Gamma) \\ &- 0.002697 \cdot \cos(3\Gamma) + 0.00148 \cdot \sin(3\Gamma),\end{aligned} \tag{2.1}$$

where the *day angle* Γ in radians is given by

$$\Gamma = \frac{2\pi \cdot (N-1)}{365} \tag{2.2}$$

and N is the day of the year. Further, we consider the change of declination during the day as constant (see, e.g., Duffie and Beckmann, 2006; Kreith and Kreider, 1978) and adjust it with the *hour angle* h. Since the earth does a full rotation (i.e., 360°) within 24 hours of the day, each hour accounts for a change of ±15° from the solar noon (positive numbers for afternoon hours). The apparent solar time AST, needed for computations, is given by

$$AST = LST + ET \pm 4 \cdot (SLon - LLon),$$

with $SLon$ and $LLon$ being the standard and local longitude to correct for the sun's traverse within a timezone (about 1° in 4 minutes). There, $SLon$ is a selected meridian near the centre of a timezone. The sign is positive (+) if the location is west of Greenwich and negative (–) otherwise. ET is the *equation of time* accounting for different lengths of the day within the year calculated by

$$ET = 9.87 \cdot \sin(2B) - 7.53 \cdot \cos(B) - \sin(B),$$

where $B = (N - 81) \cdot 360/364$. For the hour angle h in degrees follows

$$h = (AST - 12) \cdot 15. \tag{2.3}$$

After the adjustments for a date, time and location, we calculate the angle of radiation on a tilted solar panel, the *incidence angle* θ. We denote the *tilt angle* of the panel by

β and the *surface azimuth angle*, i.e., the orientation of the panel (westward orientated panel positive), by Z_S. The incidence angle θ in radians is now calculated by

$$\begin{aligned}\cos(\theta) =& \sin(L)\cdot\sin(\delta)\cdot\cos(\beta) \;-\; \cos(L)\cdot\sin(\delta)\cdot\sin(\beta)\cdot\cos(Z_s)\\ &+\cos(L)\cdot\cos(\delta)\cdot\cos(h)\cdot\cos(\beta)\\ &+\sin(L)\cdot\cos(\delta)\cdot\cos(h)\cdot\sin(\beta)\cdot\cos(Z_S)\\ &+\cos(\delta)\cdot\sin(h)\cdot\sin(\beta)\cdot\sin(Z_s),\end{aligned} \tag{2.4}$$

where δ again is the declination of the sun during the day, L the local latitude and h the hour angle, all converted to radians before plugged into the above equation (Duffie and Beckmann, 2006; Kreith and Kreider, 1978)[4].

With the radiation angles at hand, we next determine the actual radiation at our solar panel. Therefore, we use the model proposed by Reindl et al. (1990a,b) and adjust the given direct normal radiation I_{bn} (*Total sky direct solar radiation at surface*) such that it is assumed to be perpendicular to the earth's surface by $I_b = I_{bn}\cdot\cos(\phi)$, with ϕ being the *solar zenith angle* in radians calculated using Formula (2.4) for a tilt angle of $\beta = 0$ and a surface azimuth angle $Z_S = 0$.

The radiation on a tilted surface (i.e., the solar panel) I_t with tilt angle β converted to radians is then calculated by

$$\begin{aligned}I_t = &\underbrace{\big(I_b + I_d A\big)R_B}_{\text{Direct radiation contribution}} + \underbrace{I_d\big(1-A\big)\left(\frac{1-\cos(\beta)}{2}\right)\cdot\left(1+\sqrt{\frac{I_b}{I_b+I_d}}\sin(\beta/2)^3\right)}_{\text{Diffuse radiation contribution}}\\ &+\underbrace{\big(I_b+I_d\big)\rho\left(\frac{1-\cos(\beta)}{2}\right)}_{\text{Reflected radiation contribution}},\end{aligned} \tag{2.5}$$

where I_b is the direct radiation, I_d the diffuse radiation, and the last term reflects the ground reflected radiation with ρ being the forecast albedo, i.e., the reflectivity of the Earth's surface. Further, R_B is the *bean radiation tilt factor*, which includes the earlier calculated incidence angle θ and is calculated by $R_B = cos(\theta)/cos(\phi)$, both in radians. Next,

[4]Degrees can be converted to radians by multiplying with π and dividing by 180.

A is the anisotropy index defined as $A = I_{bn}/I_{ex}$ where I_{ex} is the extraterrestrial radiation depending on the day of the year N, i.e., $I_{ex} = 1366.1\,\mathrm{W/m^2} \cdot [1 + 0.033 \cdot \cos\big(360N/365\big)]$ (see Kalogirou, 2014, Section 2).

Last, the calculated radiation I_t and the ambient temperature t_a serve as input for the conversion to a power signal. Here we use the *LongiSolar LR4-72HBD* as a benchmark solar cell and leverage its technical characteristics to calculate the corresponding nominal power. It is a rather modern solar cell used in several European solar power plants. The efficiency of the solar panel generally depends on its temperature t_c and the radiation I. To account for both, we start with the efficiency given in the data sheet of the solar panel, the reference efficiency η_r, for testing conditions and correct it iteratively with the estimated cell temperature t_c similar to other authors (cf., Kalogirou 2014, Section 9.5; Durisch et al. 2000 or Beyer et al. 2004). The cell temperature t_c is estimated based on radiation I_t, the temperature of the ambient air t_a, and the temperature-related efficiency of the solar panel $\eta_{t_c}(I)$, which we set to the reference efficiency for the first approximation. For the calculation follows

$$t_c(I_t, t_a) = (t_c^{NOCT} - t_a^{NOCT}) \cdot \frac{I_t}{I^{NOCT}} \cdot \left(1 - \frac{\eta_{t_c}}{\xi}\right) + t_a, \tag{2.6}$$

where super-script $NOCT$ denotes the *Nominal Operating Cell Temperature* and radiation at nominal operating cell temperature given in the data sheet and the transmittance–absorptance product ξ is set to 0.9 to account for reflected energy at the panel (Duffie and Beckmann, 2006, Section 23).

Afterwards, the temperature-related efficiency η_{t_c} is updated via

$$\eta_{t_c} = \eta_r + \mu_\eta\big(t_c - t^{NOCT}\big), \tag{2.7}$$

with the temperature coefficient of maximum power efficiency μ_η calculated by $\mu_\eta = \eta_r \cdot \mu_V/V_{mp}$. There, η_r again denotes the reference efficiency, μ_V the temperature coefficient of open-circuit voltage, and V_{mp} the voltage at maximum power all given in the data sheet of the solar panel (Duffie and Beckmann, 2006, Section 23.2). Formulas (2.6) and (2.7) demonstrate the high interdependence between the cell temperature and the actual efficiency of the solar cell. Since the first estimate of the cell temperature

is calculated based on the reference efficiency η_r, the estimates of both variables are updated. Therefore, we use the same formulas but now based on the first estimates of both variables to approximate the true values of t_c and η_{t_c}. Thus, the cell temperature t_c is updated with the first estimate of the efficiency η_{t_c} by Formula (2.6). Afterwards, η_{t_c} is updated a second time using the new value of t_c. This two-step update has shown to be sufficiently precise in simulations and further updates do only account for marginal improvements in precision. We display the resulting power of the solar cell, depending on radiation and cell temperature, in Figure 2.2.

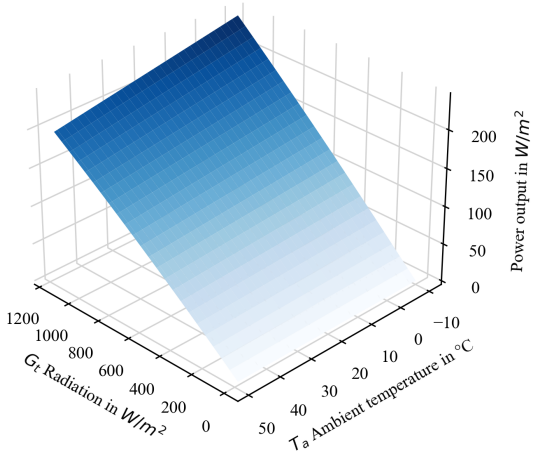

Figure 2.2.: Power of LongiSolar LR4-72HBD solar panel depending on radiation and cell temperature.

In the last step, the calculated efficiency η_{t_c} (Formula (2.7)) is multiplied by the actual radiation per square meter on the tilted surface I_t, the area of the solar panel S and a discount value of 95 % to account for further losses, e.g., the efficiency of the inverter. Converted from the measured unit Watt [W] in Megawatt [MW], the resulting power p_s emerges to

$$p_s = \big(\eta_e \cdot I_t \cdot S\big)/1000 \cdot 95\,\%. \tag{2.8}$$

We use hourly data and assume constant power generation within one hour, so the actual power and the produced energy within the hour measured in [MWh] have the

same absolute value. For all calculations, we set the tilt angle $\beta = 45°$ and assumed that 50 % of solar panels are installed facing south while 25 % are facing westwards and eastwards, respectively. These values have shown to be optimal settings for estimating the data set created in this work for mainland Europe in previous intensive analyses and reflect the non-optimal conditions in reality.

Remark 2.3.1. *Specific radiation may vary widely within a single grid box/weather cell, depending on clouds or other local characteristics. However, since our goal is to estimate the renewable layout on a regional basis, i.e., on grid nodes, the resolution provided in the ERA5 data (average over each model grid box) is sufficient for our usage.*

Wind

Next, we calculate the electricity resulting from wind power generation. To do so, we leverage the wind speeds given in the ERA5 data set (Hersbach et al., 2018). For each weather-cell location, we extract the lateral wind speed components u and v in [m/s] at 100 m above ground and compute the absolute wind speed v_{100} from these two orthogonal components by

$$v_{100} = \sqrt{u^2 + v^2}. \tag{2.9}$$

In the subsequent step, these wind speeds in a height of 100 m have to be transformed to the hub height of the used benchmark wind turbine. For the adaption of wind speed to the hub height, we follow Grothe and Müsgens (2013), Katzenstein et al. (2010) and Seinfeld and Pandis (2016), and assume a logarithmic velocity profile:

$$v_{hub} = v_{100} \cdot \left(\frac{log(h_{hub}) - log(z_0)}{log(100) - log(z_0)} \right). \tag{2.10}$$

Here, z_0 corresponds to the surface roughness depending on the typical landscape, atmospheric conditions or state of the ocean in the weather cell and is provided in the ERA5 data set (Hersbach et al., 2018).

The calculated wind speeds are now transformed to nominal power outputs using the turbine's power curves, i.e., a function that maps the wind speed in [m/s] to power in

[MW]. Again, feeding in for an hour with that power leads to produced energy measured in [MWh] of the same absolute value.

We consider two different turbines for onshore and offshore installation. For the onshore component, we use the *Siemens SWT 107* wind turbine with a nominal power of 3.6 MW and a hub height of 90 m. For the offshore component, we use the *MHI Vestas V164* wind turbine with a nominal power of 9.5 MW and a hub height of 105 m. We resort to these two frequently used types as reference turbines for all weather cells, which form a cross-section of older and newer turbines with their hub height and nominal power. To obtain a functional relationship at each wind speed, we fit a combination of third-order polynomials to the point-wise given nominal power of both turbines (Archer and Jacobson, 2007). A piece-wise definition of the function resulting in the actual power output p_w is given by

$$p_W(v_h) = \begin{cases} 0, & \text{if } v_{hub} < v_{min} \\ \alpha_1 v_{hub}^3 + \beta_1 v_{hub}^2 + \gamma_1 v_{hub} + \delta_1, & \text{if } v_{min} < v_{hub} < v_{split} \\ \alpha_2 v_{hub}^3 + \beta_2 v_{hub}^2 + \gamma_2 v_{hub} + \delta_2, & \text{if } v_{split} < v_{hub} < v_{rated} \\ p_{rated}, & \text{if } v_{rated} < v_{hub} < v_{max} \\ 0, & \text{if } v_{max} < v_{hub}, \end{cases}$$

where v_{hub} is the wind speed at hub height. Further, v_{min} is defined as cut-in speed, i.e., the minimum wind speed required for electricity production, and v_{rated} is the minimum wind speed for the rated power (related to this, p_{rated} is the rated power of the wind turbine). At the top end, v_{max} determines the cut-out speed, i.e., the maximum wind speed where the turbine is operated and is set to $v_{max} = 25\,\text{m/s}$ for all turbines. Further, we define v_{split} as the turning point within our functional representation, where we change to the second polynomial. This point is located where the concavity of a fitted third-order polynomial on the power curve changes sign (see Archer and Jacobson (2007) for details). The resulting power curves are depicted in Figure 2.3. In the following, we denote the actual power of onshore turbines as p_{wl} and offshore generation as p_{wo}.

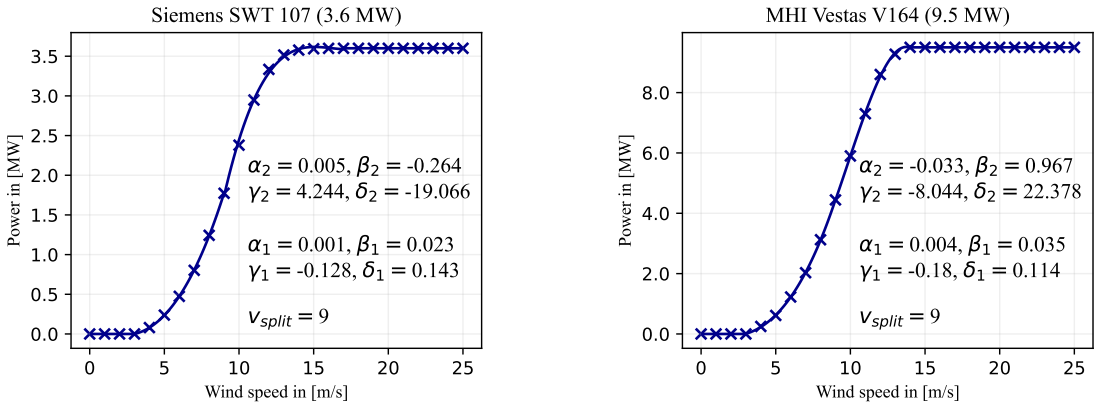

Figure 2.3.: Power curves Siemens SWT 107 (left) and MHI Vestas V164 (right) with corresponding parameters of the fitted polynomials and change-point v_{split}.

2.3.2. Weather Cell Combination

In the previous section, we calculated the nominal power of solar panels and wind turbines in each of the 15,292 weather cells in the ERA5 data set. We now aim to assign each weather cell to one grid node to aggregate the generated power of multiple weather cells to one transmission node. The aggregated power is later used for the estimation of the renewable energy layout by an elastic-net.

Therefore, we first map each weather cell c (thus its renewable generators) to its closest transmission node $n_i,\ i \in \{1, \dots, N\}$, of all N transmission nodes since this connection is the cheapest and most efficient. Further, we filter the resulting allocation and only keep a mapping of a weather cell c to its transmission node n_i if the corresponding distance $d(c, n_i)$ is smaller than the maximal distance between any two adjacent transmission nodes, i.e.,

$$d(c, n_i) \overset{!}{<} d(n_k, n_\ell) \text{ for all } k, \ell = 1, \dots, N.$$

This condition ensures that we only take weather cells with a reasonable distance to the power grid into account, e.g., cells covering the coastal area (used for offshore wind constructions) but not the complete ocean. For the special case where no weather cell is assigned to a transmission node, we assign the closest weather cell to this node as well. Note that this is only the case for 25 nodes in total, thus leading to 25 weather cells

which are assigned to two nodes: the node closest to the weather cell and the node for which the weather cell is the closest. Figure 2.4 visualises the resulting assignment of all used weather cells (small dots) to the network nodes (fat dots). Weather cells that are assigned to a node are coloured correspondingly. The double-assigned weather cells are colour-coded to their nearest node.

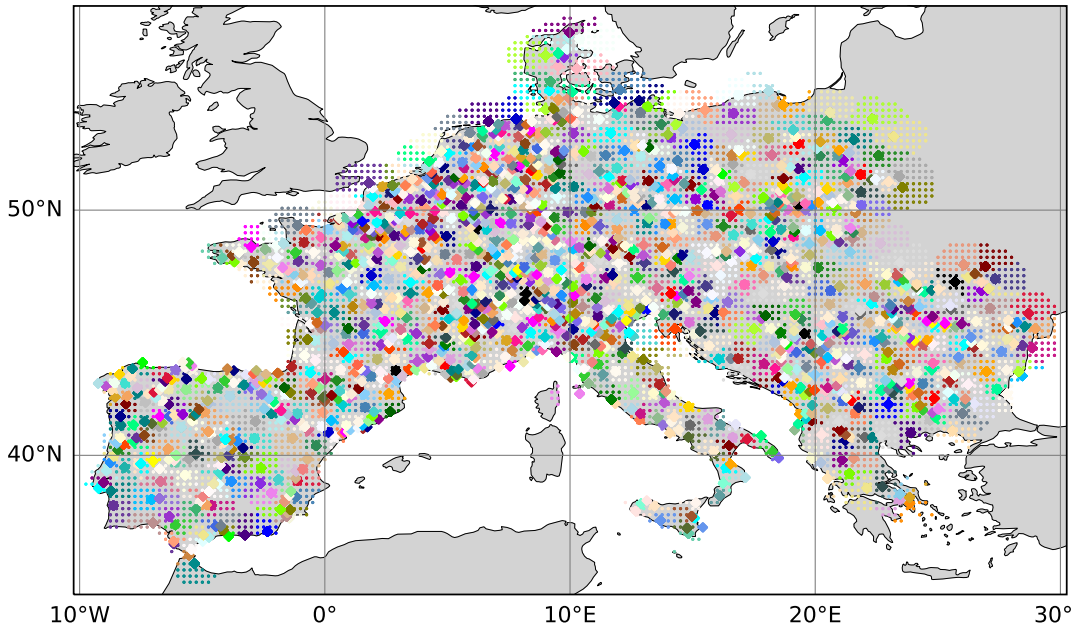

Figure 2.4.: Nodes of the European transmission network (fat) and assigned weather cells (small) of the ERA5 data set.

In the last step, the nominal power signals of all weather cells associated with a transmission node are averaged by generator type. To do so, we classify each weather cell depending if it is mainly covering ocean or land. The ocean weather cells are not considered for averaging solar signals, while the land cells are ignored for calculating the average offshore wind power signals. We distinguish onshore and offshore wind power signals in the same manner and further exclude offshore weather cells with a sea depth $\geq 70\,\mathrm{m}$ due to technical and construction restrictions of offshore wind turbines.

The result is a power signal for each transmission node, scaled to the nominal power of one representative renewable generator by type.

2.3.3. Layout Estimation

Now, the allocation and, thus, the working layouts of renewable energy generators across Europe are estimated from derived power signals per transmission node and actual feed-in data of solar and wind power. The actual generation data for onshore wind power in_{wl}, offshore wind power in_{wo}, and solar in_s are openly available on a country level at the ENTSO-E transparency platform for the years 2019 to 2022 (ENTSO-E Transparency Platform, 2023a). For the estimation, we facilitate the condition that the total feed-in of wind and solar power has to be the sum of the produced power at all transmission nodes, i.e., the power signal of a single solar cell or wind turbine multiplied by the number of installed generators, at country-based resolution for each hour. Thus, the feed-in in_s, in_{wl} and in_{wo} for each country at any time-step $t = 1, \ldots, T$ is given by

$$in_s = \sum_{n=1}^{N} w_s^{(n)} \cdot p_s^{(n)} \qquad \text{Solar Feed-in,} \tag{2.11}$$

$$in_{wl} = \sum_{n=1}^{N} w_{wl}^{(n)} \cdot p_{wl}^{(n)} \qquad \text{Onshore Feed-in,} \tag{2.12}$$

$$in_{wo} = \sum_{n=1}^{N} w_{wo}^{(n)} \cdot p_{wo}^{(n)} \qquad \text{Offshore Feed-in,} \tag{2.13}$$

where $w_s^{(n)}$, $w_{wl}^{(n)}$ and $w_{wo}^{(n)}$ denote the unknown weights (i.e., number of generators) of solar, onshore and offshore wind power generators at each transmission node $n = 1, \ldots N$. Hence, the layout estimation aims to estimate the values of $w_s^{(n)}$,$w_{wl}^{(n)}$, and $w_{wo}^{(n)}$ such that the Mean Squared Error (MSE) is minimised for each generator type separately. From a technical perspective, this requires solving the popular *least squares* problem and corresponds to a linear regression setup. Such a setup is known to be unstable for highly correlated regressors, which leads to poorly determined estimated coefficients with high variance (cf., Hastie et al., 2001, Section 3.4). Since we expect weather data of neighbouring cells to be highly correlated, we also expect the given aggregated power

signals $p_{(\cdot)}$ of each transmission node to be highly correlated with its neighbouring signals. Figure 2.5 analyses the correlation of energy signals from neighbouring transmission nodes with respect to distance. The left plot visualises the mean correlation of every transmission node with its k-nearest-neighbours, while the right plot shows the mean correlation of all transmission nodes and all of their neighbours within the given distance in [km]. As expected, we observe strongly correlated signals, with the correlations slightly decreasing in growing distances. Thus, the problem at hand shows high collinearities in the data and an alternative to using a simple linear regression is called for.

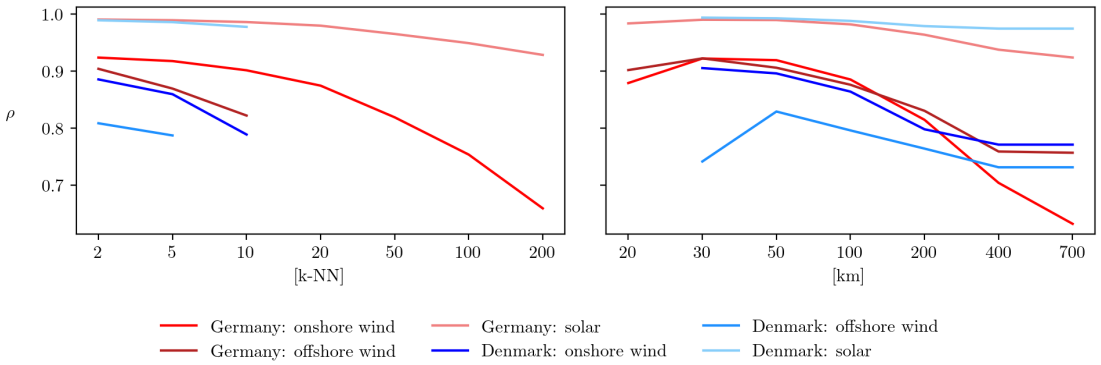

Figure 2.5.: Pearson correlation of power signals of 2019 from neighbouring transmission nodes for k-nearest neighbours (left) and given distance (right) per renewable generator type.

Therefore, the final estimation is done by using a regularised linear regression model for each generation type and country, i.e., an *elastic-net* with a L_1 and a L_2 regularisation term (see Zou and Hastie, 2005). Within this framework, we optimise the strength of the regularisation via 10-fold cross-validation. Further, a non-negativity restriction for the coefficients is introduced to avoid unrealistic solutions, i.e., physically impossible solutions like a negative number of generators. The resulting optimisation problem is solved for each country and each year. Since the shrinkage of the estimated parameters is directly related to the variance of the features, i.e., the input signals, we standardise

the features before optimising the parameters by

$$\tilde{p}_{s,t}^{(n)} = \frac{p_{s,t}^{(n)} - \overline{p}_{s}^{(n)}}{\sigma_{s}^{(n)}} \qquad \text{Solar,} \tag{2.14}$$

$$\tilde{p}_{wl,t}^{(n)} = \frac{p_{wl,t}^{(n)} - \overline{p}_{wl}^{(n)}}{\sigma_{wl}^{(n)}} \qquad \text{Onshore,} \tag{2.15}$$

$$\tilde{p}_{wo,t}^{(n)} = \frac{p_{wo,t}^{(n)} - \overline{p}_{wo}^{(n)}}{\sigma_{wo}^{(n)}} \qquad \text{Offshore,} \tag{2.16}$$

where $\tilde{p}_{\cdot,t}^{(n)}$ is the standardised power signal per generator type at time t and node n, $\overline{p}_{\cdot}^{(n)}$ the mean of all power signals at node n and $\sigma_{\cdot}^{(n)}$ the standard deviation of the power signals at node n. Note that doing so requires an intercept ($w_{\cdot}$) during estimation, which will result in nearly zero after reversing the standardisation. With this, the optimisation problem for the case of solar is given by

$$\arg\min_{w_s} \left(in_s - \tilde{w}_s - \sum_{n=1}^{N} \tilde{w}_s^{(n)} \cdot \tilde{p}_s^{(n)} \right)^2 \tag{2.17}$$

$$+ \lambda \cdot \alpha \sum_{n=0}^{N} |\tilde{w}_s^{(n)}| + 0.5 \cdot \lambda \cdot (1-\alpha) \sum_{n=0}^{N} (\tilde{w}_s^{(n)})^2. \tag{2.18}$$

There, (2.17) minimises the difference between the true feed-in and our models' prediction, and (2.18) includes the regularisation terms[5]. The parameters $\tilde{w}_s^{(n)}$ denote the estimated weights in the standardised setup. The standardisation is reversed after the optimisation to result in the installed capacities, i.e., by multiplying the calculated parameter values with the standard deviation of the corresponding original input data:

$$w_s^{(n)} = \tilde{w}_s^{(n)} \cdot \sigma_s^{(n)}. \tag{2.19}$$

The same optimisation is done for every year, both wind power generation types and each country separately.

[5] The hyperparameter α compromises between the L_1 and a L_2 regularisation term and is set to 0.7, as it has shown to be the best choice in our studies. The parameter λ is the cross-validated strength of regularisation.

Using an elastic-net regularisation is useful for two reasons. First, as we have seen in Figure 2.5, aggregated power signals of the transmission nodes are highly correlated. We tackle this problem by using the L_2 regularisation term, which causes the regressors to act more like an orthogonal system, hence resulting in more stable estimations and a lower MSE (Hoerl and Kennard, 2000). Further, the L_2 penalty causes the resulting loss function to be strongly convex and avoids grouping effects of correlated variables (Zou and Hastie, 2005). The grouping effect means that within a heavily correlated group of regressors, it can be difficult to estimate the effects of each variable on the dependent variable accurately since another variable might partially or fully capture the effects of one variable. In our case, that would result in an estimation where all the weight is randomly assigned to a few transmission nodes. Besides the purely mathematical motivation of an easier and better estimation, the L_2 regularisation penalises very high negative and positive coefficients and thus avoids technically impossible solutions. Additionally, regularisation reduces the number of estimated weights to stabilise the estimation with limited data and results in a more realistic, compact model. A compact model improves the overall interpretability of results and reduces the noise in the estimated coefficients. Since the discussed L_2 penalty can not set coefficients to zero, the L_1 regularisation here comes into play. It forces some of the estimated weights to zero, reducing the overall complexity. In summary, we use the L_2 ridge-like regularisation to shrink the coefficients of correlated predictors towards each other and the L_1 lasso-like regularisation to select variables, e.g., important generator locations, in the elastic-net approach.

The estimated weights represent the total installed generation units at the considered locations. By multiplying these with the nominal power of the used example generators, i.e., the nominal power of both wind turbines and the solar panel, we obtain the estimated capacities at each node. Altogether, the elastic-net results in completely data-driven layouts of renewable energy sources for each European country.

Remark 2.3.2. *The estimation of installed capacities can also be done using standardised relative power signals. Relative power signals are derived by dividing the actual power signal of onshore, offshore and solar ($p_{wl}^{(n)}$, $p_{wo}^{(n)}$ and $p_s^{(n)}$) by the nominal power of the used power generator. These (standardised) relative power signals can now be used to replace the (standardised) actual power signals in the optimisation problem of the elastic-net*

(Formulas (2.17)-(2.18)). Thus, the estimated and rescaled weights from the elastic-net directly correspond to the estimated installed capacity at each transmission node. Note that using relative or actual power signals results in the same estimated layout.

Estimated on such spatially and temporally high resolution, the working layouts mimic the wind, onshore and offshore, and solar power generation and realistically reflect the allocation of installed capacities over the landscape. However, *working layout* means here that the installed plants belonging to the estimated capacities are optimally utilised and *working*. They are always online and on the grid and are only limited by the level of wind and solar irradiation. Due to the objective of a purely data-driven approach, we do not make any assumptions about possible deviations of the potentially and optimally generated amount, e.g., due to self-consumption or storage in individual household batteries or the curtailment of PV and wind power plants, which is done to ensure grid stability. For example, in Germany, PV power plants with a nominal power of up to 25 kW were only allowed to feed in a maximum of 70 % of their nominal power until the beginning of 2023 due to concerns about grid congestion (Federal Office of Justice and Federal Ministry of Justice, 2021, §9(2)), and onshore wind energy is the most de-regulated energy source, followed by offshore wind energy (Bundesnetzagentur für Elektrizität, Gas, Telekommunikation, Post und Eisenbahnen and Bundeskartellamt, 2022). Due to the optimal utilisation of wind turbines and solar modules, we further do not consider wake effects of wind turbines standing next to each other in wind farms (e.g., Barthelmie et al., 2010) and other possible reasons for losses, e.g., the age of the turbines and modules (Staffell and Green, 2014). We, therefore, expect that the actual installed capacity is higher than technically necessary and that the estimated working layouts represent a lower bound compared to the actual total installed capacity.

Note that ignoring the high collinearity in our data and estimating the capacities by an ordinary least squares (OLS) regression also delivers suitable results, but only with respect to the production data. The layouts are able to mimic the actual power generation similarly well, but constitute highly unrealistic spatial allocations of the installed capacities. For example, onshore wind power generation in Germany is only allocated over 55 of 227 transmission nodes in 2022 (see Section 2.4 for more details).

2.4. Results

In this section, we exemplary report the results for Germany and Denmark in detail. We analyse the ability of the estimated working layouts to mimic the actual feed-in of electricity per generator class (onshore wind, offshore wind, PV) and depict these layouts for solar and wind power generators across the countries for 2019 to 2022. We further demonstrate that the estimated layouts have been rather stable over the years and match the true installed capacities' allocation. In this context, we also present the results of the estimation with a non-regulated regression approach for comparison. Finally, we give a brief overview of the estimates for all countries of mainland Europe. The entire data set can be downloaded through the following link: *https://doi.org/10.6084/m9.figshare.22439254.v3*.

Turning to the exemplary analysis, we first assess the ability of the estimated layouts to mimic the actual feed-in per generator type (onshore/offshore wind, PV). Figure 2.6 depicts the actual and estimated PV generation for Germany (left) and Denmark (right) in July 2022. Besides minor deviations in the peak of each day, the estimation fits the actual generation and the changes between low- and high-generation days are captured very well.

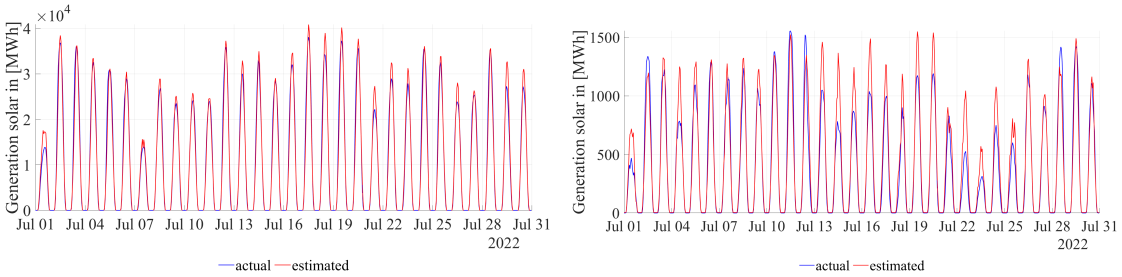

Figure 2.6.: Actual and estimated PV generation for Germany (left) and Denmark (right) in July 2022.

Similar observations can be made when considering the onshore wind generation in Figure 2.7 and offshore wind generation in Figure 2.8. Both types of wind generation are characterised by higher volatility, but the estimation generally fits the feed-in very well. Looking at the offshore wind feed-in in Denmark in detail, we notice a drop in wind generation on July 17th, 2022, which is not reflected in the estimate. This drop may be

due to the curtailment of wind turbines and, thus, the limitation of wind energy. Since the approach presented here is based on converting weather data to feed-in data, it is not able to consider such curtailments.

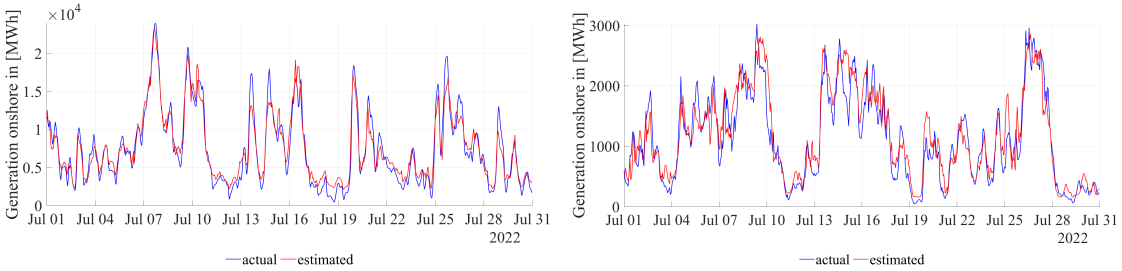

Figure 2.7.: Actual and estimated onshore wind generation for Germany (left) and Denmark (right) in July 2022.

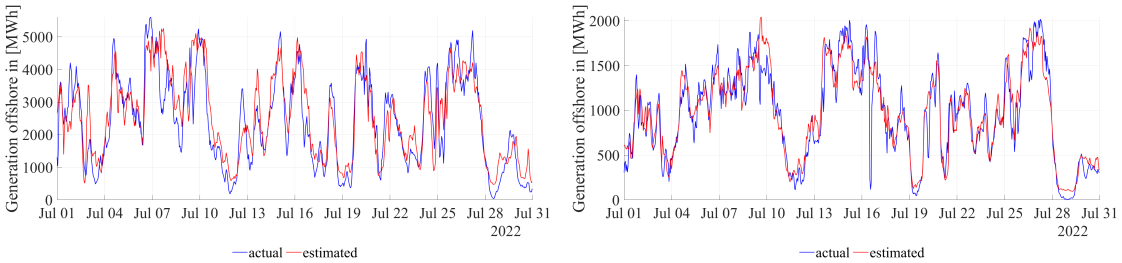

Figure 2.8.: Actual and estimated offshore wind generation for Germany (left) and Denmark (right) in July 2022.

Overall, the estimated capacity layouts seem to mimic the actual feed-in of renewable energy sources very well, only using a weather-to-energy-conversion scheme based on the physical characteristics of the benchmark generators. With these estimated capacity layouts, forecasts can be made in a consecutive step. To prove the concept, we use the layouts estimated for one year to calculate the feed-ins in the following year, which we call predictions in the following. Table 2.3 reports the *Root Mean Squared Error* (RMSE) for the estimations (est.) and the predictions (pred.) relative to the respective realised hourly generation average. For the RMSE in the case of solar, we only consider values of hours with an actual solar feed-in bigger than zero, thus excluding nighttime hours. We observe that the absolute RMSE increases with the amount of onshore or offshore

wind and solar generation and their installed capacity, but the relative RMSE does not. This means that the accuracy of the estimates and predictions does not decrease with higher installed capacity and generation from a relative point of view. We further see that the RMSE of the estimates and predictions for the German layouts are higher than for the Danish layouts because installed capacity and generation quantity are higher. Still, the relative RMSE is lower for all generation types in Germany. We conclude that the estimates and predictions for Germany are more accurate. Further, in both countries, the estimations' RMSE is lower than the RMSE of the predictions (relative and absolute). The latter could be improved by, e.g., not using the layout based on 2019 for the whole prediction of 2020 but scaling it with information on expansions of onshore, offshore and solar power plants or calculating layouts on a rolling basis. Besides the slightly higher RMSE, the layouts allow a good approximation of the feed-ins in the context of a prediction, as illustrated exemplary in Figure 2.9 for the actual, estimated and predicted onshore wind power generation and in Figure 2.10 for solar generation for Germany (left) and Denmark (right) in July 2022.

Table 2.3.: RMSE of the elastic-net year- and country-wise estimation and prediction for PV, onshore wind and offshore wind generation relative to the respective hourly generation average.

			2019	2020	2021	2022
PV	DEU	est.	0.2176	0.2028	0.2477	0.2040
		pred.		0.2354	0.2530	0.2999
	DNK	est.	0.2901	0.2631	0.3850	0.3597
		pred.		0.5089	0.3993	0.6162
Onshore	DEU	est.	0.1358	0.1412	0.1462	0.1577
		pred.		0.1545	0.2242	0.2121
	DNK	est.	0.2966	0.3115	0.2997	0.2853
		pred.		0.3151	0.3673	0.3572
Offshore	DEU	est.	0.2648	0.2653	0.3189	0.2861
		pred.		0.2964	0.3418	0.2886
	DNK	est.	0.3027	0.2505	0.2846	0.1986
		pred.		0.2823	0.3489	0.2706

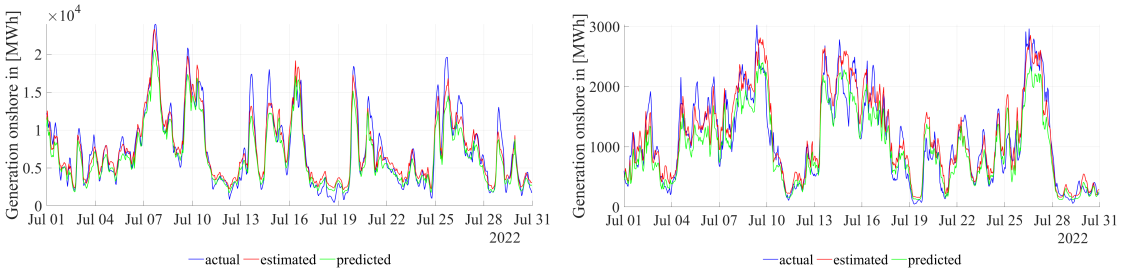

Figure 2.9.: Predicted onshore wind generation for Germany (left) and Denmark (right) in July 2022.

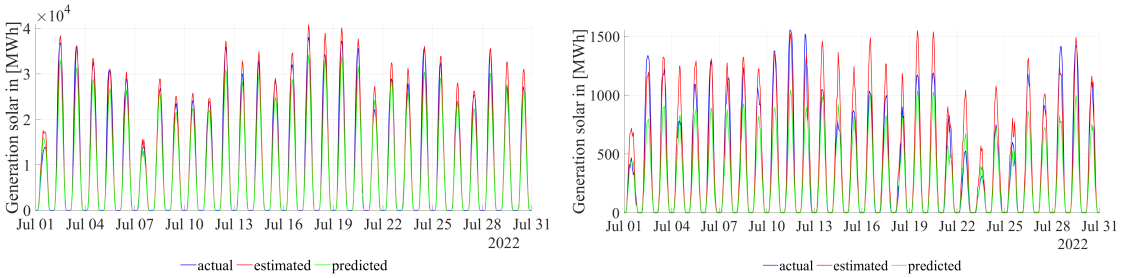

Figure 2.10.: Predicted PV generation for Germany (left) and Denmark (right) in July 2022.

In the following, we directly analyse the estimated layouts and, thus, the estimated capacities. Table 2.4 compares the current total installed capacity of Denmark and Germany with the estimated total installed capacity for each year from 2019 to 2022. Thereby, the estimated total installed capacity is the sum of the estimated installed node capacities. The estimated total capacity of wind, onshore and offshore, and solar energy for Denmark and Germany deviates from the actual one in all years. As expected, due to various factors limiting the measured feed-in, less capacity is required overall than is actually installed. We see that our approach requires about 44 % less installed capacity for Germany and 13 % less for Denmark to generate the given amount of feed-in. For wind, onshore and offshore, the deviation is smaller. In general, the deviation shows the high potential of renewable energy sources. Even without further expansion, optimal and unrestricted use of the installed plants would lead to increased power production from renewable energies.

Table 2.4.: Actual installed onshore wind, offshore wind and PV capacity (ENTSO-E Transparency Platform, 2023d; International Renewable Energy Agency, 2023) and estimated onshore wind, offshore wind and PV capacity of Denmark and Germany for each year in [MW].

		PV		Onshore		Offshore	
		DNK	DEU	DNK	DEU	DNK	DEU
Actual installed	2019	1,014	45,299	4,426	52,792	1,700	6,393
	2020	1,013	48,206	4,402	53,184	1,700	7,504
	2021	1,300	53,302	4,481	54,499	1,700	7,774
	2022	1,536	57,744	4,644	55,289	2,305	7,787
Estimated installed	2019	641	24,842	3,327	47,064	1,316	5,084
	2020	804	27,248	3,069	48,530	1,400	5,567
	2021	930	28,622	2,802	51,010	1,804	5,672
	2022	1,341	32,285	3,218	51,354	2,042	5,232
Perc. deviation	2019	37%	45%	25%	11%	23%	20%
	2020	21%	43%	30%	9%	18%	26%
	2021	28%	46%	37%	6%	-6%	27%
	2022	13%	44%	31%	7%	11%	33%

Looking at the estimated working layouts, which are presented in Figure 2.11, more closely, we see that solar is mostly evenly distributed across Denmark. This aligns with our expectations since professional solar parks are emerging in every region, and PV panels are becoming more popular even for private households and investors. In Germany, we can also observe PV capacity distributed all over the land, but with a higher concentration in the south, especially in Bavaria. This reflects that Bavaria is the federal state with the most installed greenfield and rooftop PV capacity (50Hertz Transmission GmbH et al., 2023).

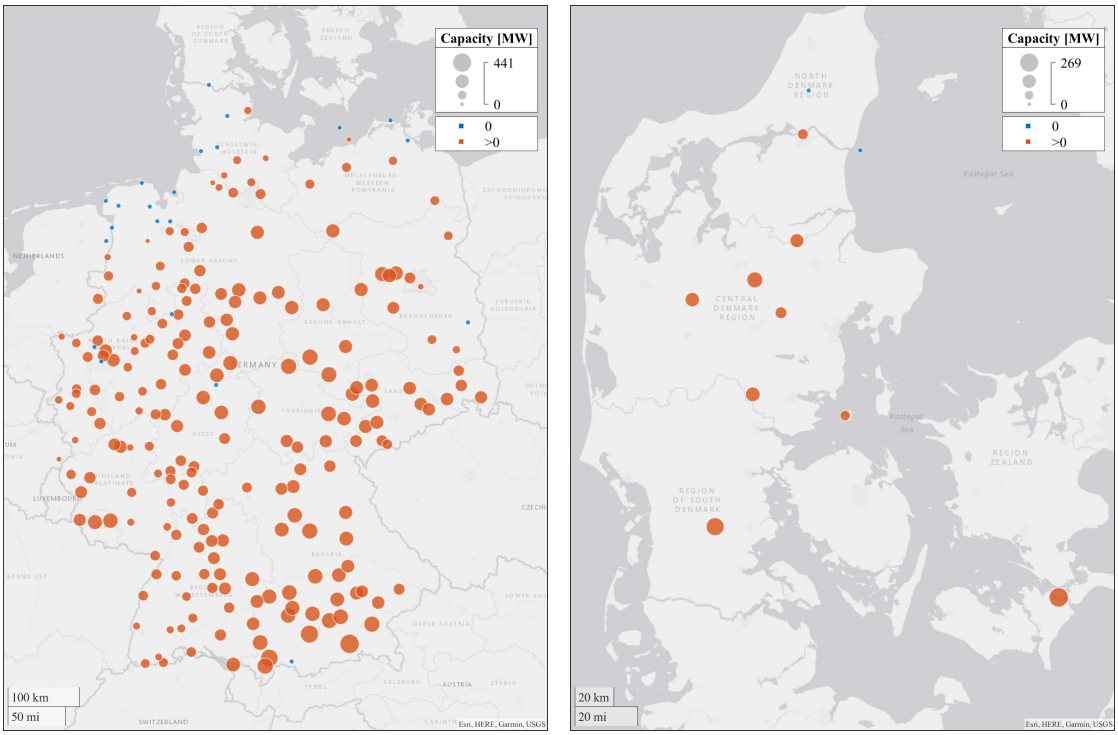

Figure 2.11.: Estimated PV capacity layout for Germany (left) and Denmark (right) in 2022.

For the estimated German onshore wind capacities in Figure 2.12, we observe more estimated capacities in the north than in the south of Germany. Interestingly, this reflects the allocation of wind turbines in Germany, where high wind-powered electricity generation in the north is often a problem for the nationwide grid infrastructure (TenneT TSO GmbH, 2023; TransnetBW GmbH, 2023; Federal Office of Justice and Federal Ministry of Justice, 2022a; 50Hertz Transmission GmbH et al., 2023; Bundesnetzagentur für Elektrizität, Gas, Telekommunikation, Post und Eisenbahnen and Bundeskartellamt, 2022). In Denmark, onshore wind capacity is not as evenly distributed as solar, with the highest installed capacity in the transmission node characterising the area of South Denmark (see Figure 2.12). Compared to the other Danish transmission nodes, it captures the widest area and, thus, has a high potential for onshore wind power plants, represented by the layout's estimation. However, as with solar energy, Denmark's estimated onshore

wind capacities are distributed throughout the country. This also corresponds to the allocation of installed wind turbines in Denmark (see Andresen et al., 2015).

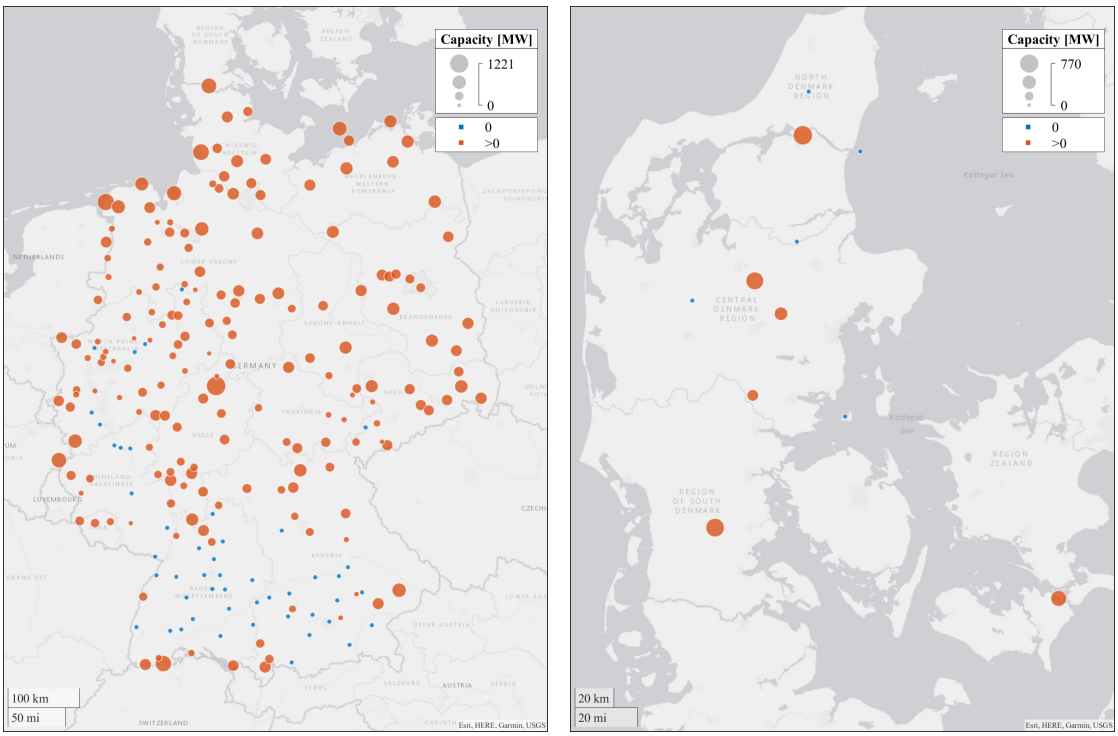

Figure 2.12.: Estimated onshore wind capacity layout for Germany (left) and Denmark (right) in 2022.

Turning to Figure 2.13, we see the estimated offshore wind capacity layout for Germany and Denmark. In Germany, most estimated high-capacity nodes are nearest nodes to the biggest offshore wind farms *GodeWind, Borkum Riffgrund* and *Hohe See* in the North Sea and *Baltic Eagle* in the Baltic Sea, as analysed in Grothe et al. (2022). For Denmark, the transmission nodes have a larger catchment area than in Germany and, therefore, capture the installed capacity over a larger area, representing it on landscape nodes. This means that individual wind farms cannot be fully identified. Still, the two big wind farms *Horns Rev* in the North Sea and *Kriegers Flak* in the Baltic Sea as well as the haven *Esbjerg*, the central point for offshore wind energy in Denmark's North Sea, are

represented in their corresponding nearest nodes with a high estimated installed capacity. Thus, we can conclude the layout identifies and maps big wind farms.

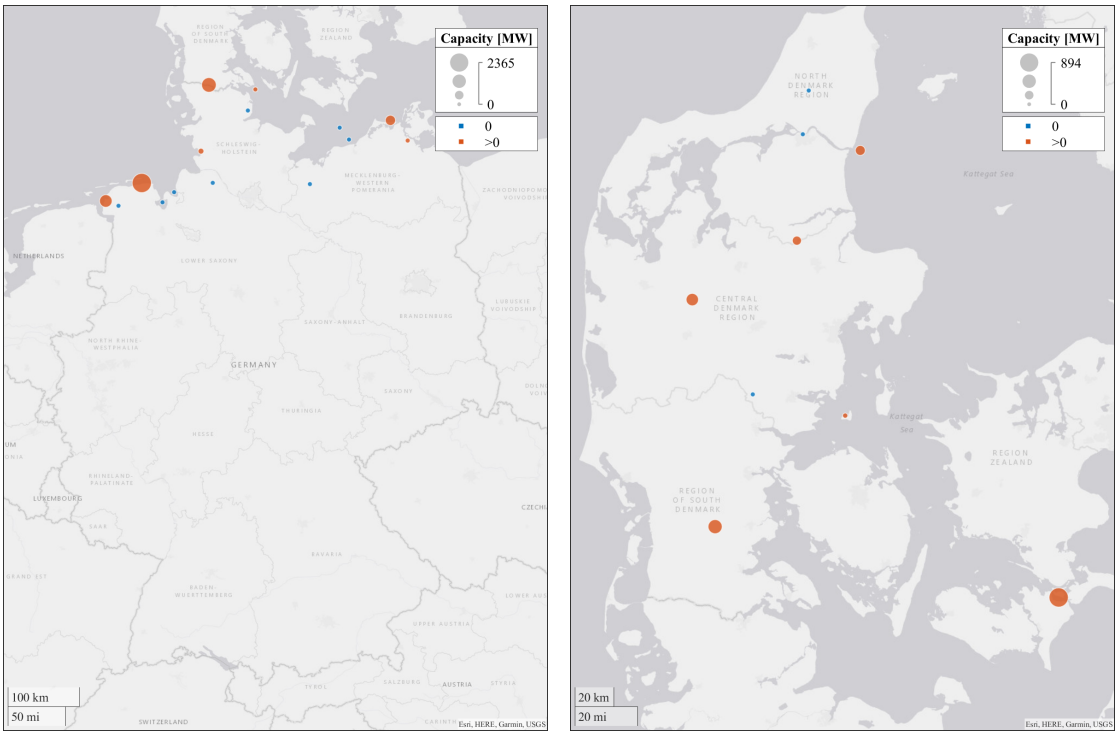

Figure 2.13.: Estimated offshore wind capacity layout for Germany (left) and Denmark (right) in 2022.

Next, we investigate how stable the estimated capacity layouts are across the different years. We define stable estimates as those where capacities are allocated to the same transmission nodes each year. So a transmission node does not have any estimated capacity in one year, high estimated capacity the next year and none estimated capacity in the third year again. Therefore, we compare the estimated capacity per transmission node from 2019 to 2022 and analyse the development of offshore wind capacity exemplary. Due to the small number of nodes in Germany (15 nodes) and Denmark (nine nodes), the results for this generation type can be presented clearly. For onshore wind and solar,

the capacity developments at the individual nodes are more difficult to determine due to the high number of 227 transmission nodes for Germany.

Figure 2.14 plots the estimated capacity in [MW] per transmission node for offshore wind power generators for Germany and Denmark from 2019 to 2022. We can observe peaks to occur usually at the same transmission node. The estimated capacities do not fluctuate strongly over the years in both Germany and Denmark. In particular, no strong jumps from minimum to maximum values and back are observed. The almost constancy of the node capacities indicates a rather stable estimation over the years.

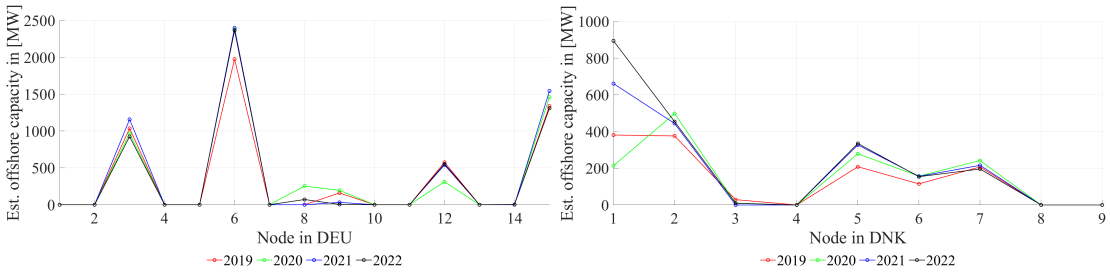

Figure 2.14.: Estimated node capacity for offshore wind for Germany (left) and Denmark (right) per year.

Figures 2.15 and 2.16 show the estimated installed capacity per transmission node for onshore wind and solar power generators from 2019 to 2022. As with offshore wind capacities, a stable level can be observed for onshore wind and solar capacities at the individual transmission nodes in Denmark. Here, the peaks usually occur at the same transmission nodes every year, too. We cannot observe details for the case of solar and onshore wind in Germany; however, the general level seems stable for most transmission nodes over the years.

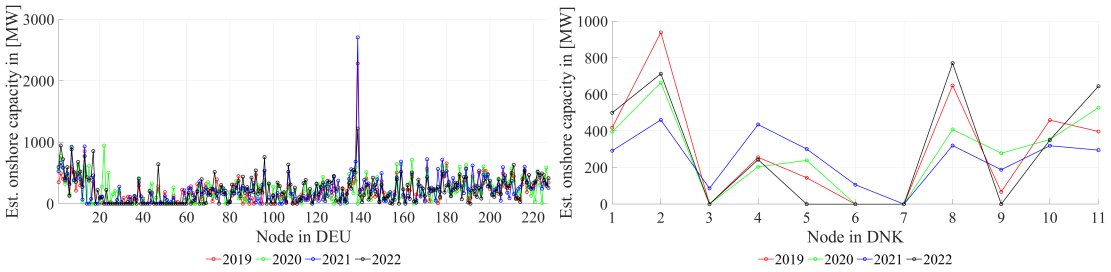

Figure 2.15.: Estimated node capacity for onshore wind for Germany (left) and Denmark (right) per year.

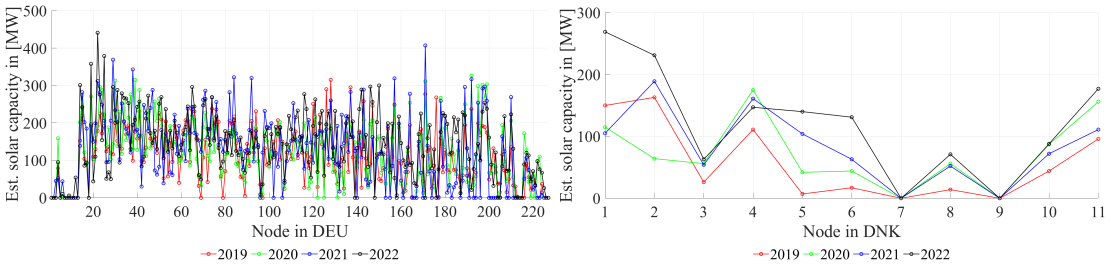

Figure 2.16.: Estimated node capacity for solar for Germany (left) and Denmark (right) per year.

The contrary can be observed for results estimated by a non-regularised regression model. In the following, we provide a short overview of the results using a standard, non-regularised regression model for capacity estimation. We observe that the total estimated installed capacity is comparable to the elastic-net estimation, but more nodes are set to an installed capacity of zero. Corresponding relative RMSE values, the total installed capacity per production type and the estimated generation for July 2022 for Germany and Denmark are shown in Table 2.5 (RMSE), Table 2.6 (total installed capacities) and Figures 2.17 (PV generation), 2.18 (onshore wind generation), 2.19 (offshore wind generation).

Table 2.5.: RMSE of the OLS regression year- and country-wise estimation and prediction for PV, onshore wind and offshore wind generation relative to the respective hourly generation average.

			2019	2020	2021	2022
PV	DEU	est.	0.2146	0.1995	0.2437	0.1994
		pred.		0.2337	0.2526	0.2994
	DNK	est.	0.2897	0.2618	0.3834	0.3586
		pred.		0.5085	0.3994	0.6140
Onshore	DEU	est.	0.1329	0.1377	0.1430	0.1533
		pred.		0.1531	0.2255	0.2106
	DNK	est.	0.2959	0.3104	0.2986	0.2849
		pred.		0.3159	0.3708	0.3514
Offshore	DEU	est.	0.2638	0.2614	0.3168	0.2832
		pred.		0.2909	0.3386	0.2879
	DNK	est.	0.3026	0.2504	0.2845	0.1982
		pred.		0.2817	0.3485	0.2690

Table 2.6.: With an OLS regression estimated onshore wind, offshore wind and PV capacity of Denmark and Germany for each year in [MW].

	PV		Onshore		Offshore	
	DEU	DNK	DEU	DNK	DEU	DNK
2019	24,591	631	48,115	3,358	5,144	1,325
2020	26,988	800	48,742	3,113	5,634	1,407
2021	28,166	921	52,136	2,862	5,741	1,819
2022	31,987	1,326	51,094	3,255	5,294	2,058

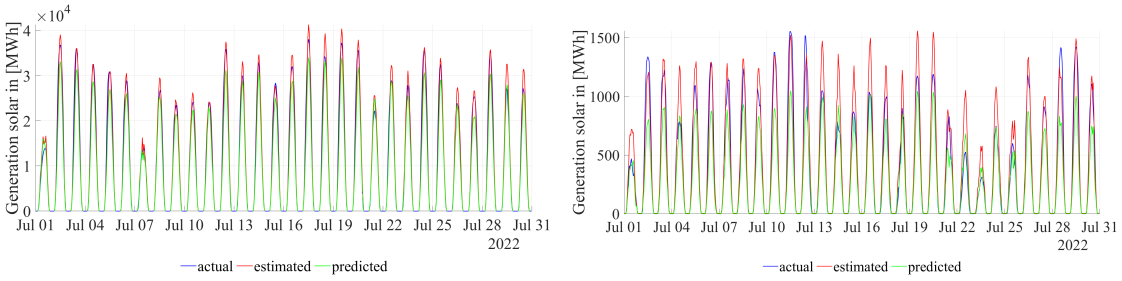

Figure 2.17.: Actual, estimated and predicted PV generation for Germany (left) and Denmark (right) in July 2022 for the OLS regression.

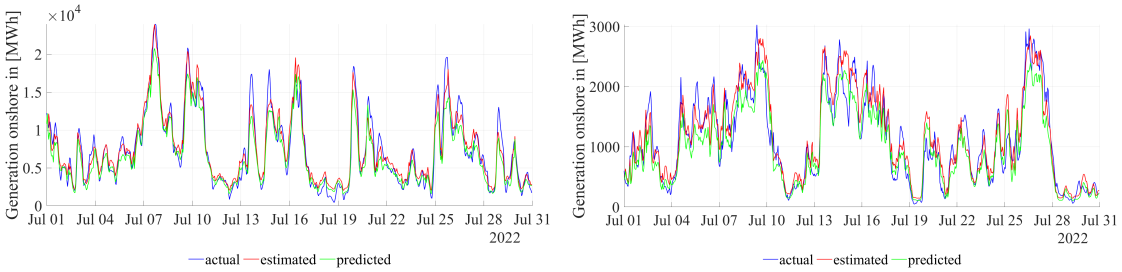

Figure 2.18.: Actual, estimated and predicted onshore wind generation for Germany (left) and Denmark (right) in July 2022 for the OLS regression.

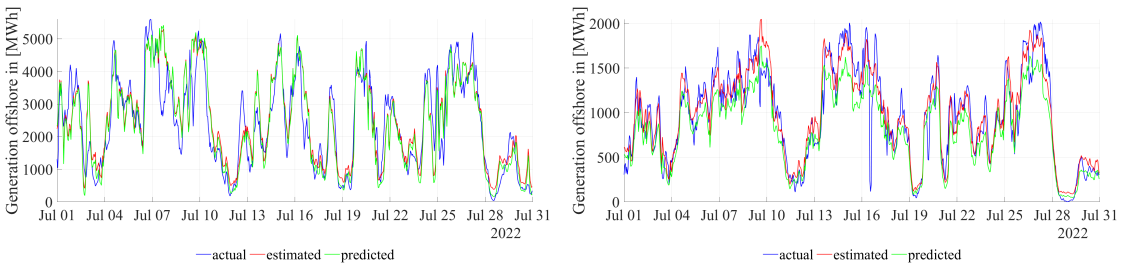

Figure 2.19.: Actual, estimated and predicted offshore wind generation for Germany (left) and Denmark (right) in July 2022 for the OLS regression.

Exemplary, Figure 2.20 shows the installed capacity for each German transmission node in 2019 and in 2022 estimated by the non-regularised linear regression. We observe that, especially in the south, a large proportion of the nodes are assumed to have zero installed capacity, which does not correspond to a realistic capacity allocation. For example, wind turbines are actually installed in the Swabian Alb, located roughly in the middle-east of the federal state Baden-Wuerttemberg (see, e.g., Bundesnetzagentur, 2019).

Consequently, the example of the onshore wind capacity allocation for Germany shows that the generated feed-in quantity relates to the installed capacity at a few grid nodes, which varies over the years. Due to a large number of transmission nodes and their highly correlated nature, capacities can not be estimated in a stable manner and a realistic allocation. Thus, the estimated layouts can be used for feed-in forecasts of individual countries but do not provide any information on the allocation of installed capacities

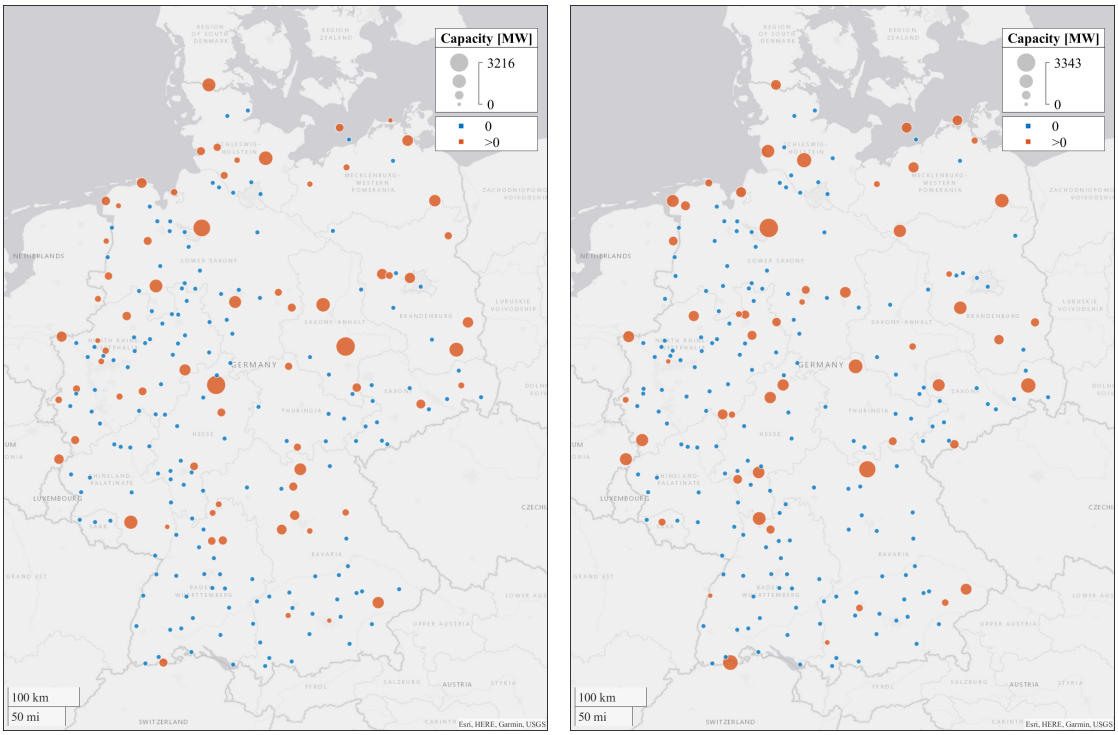

Figure 2.20.: With an OLS regression estimated onshore wind capacity layout for Germany for 2019 (left) and 2022 (right).

and generation. We prevent such behaviour using the proposed elastic-net regression, resulting in stable results for Denmark and Germany.

Last, we report the estimated total installed capacity for each country of mainland Europe, compared with the current total installed capacity in Tables 2.7 (onshore wind), 2.8 (offshore wind) and 2.9 (PV). Therefore, we first use data from the ENTSO-E transparency platform (ENTSO-E Transparency Platform, 2023a). We fill in missing values with data provided by the online data query tool IRENASTAT (International Renewable Energy Agency, 2023), where the value of a year reflects the actual installed capacity at the end of the previous year. Values that have been supplemented accordingly are marked with a star (*) in the tables. Due to missing feed-in data provided by the ENTSO-E transparency platform (ENTSO-E Transparency Platform, 2023a), not all

countries can be fully estimated. Note that for the Netherlands, solar generation data provided by ENTSO-E Transparency Platform (2023a) is incomplete for all years and, thus, the estimated capacities are far too low.

Table 2.7.: Actual installed onshore wind capacity (ENTSO-E Transparency Platform, 2023d; International Renewable Energy Agency, 2023) and estimated onshore wind capacity of all countries for each year in [MW].

	actual				estimated			
	2019	2020	2021	2022	2019	2020	2021	2022
Austria	3,035	3,133	3,198	3,500	3,406	4,093	4,570	4,160
Belgium	2,248	2,416	2,629	2,787	1,375	1,556	1,922	
Bulgaria	700	700	705	705	751	822	723	667
Bosnia Herzgovina	87	87	145	135	105	78	161	367
Switzerland	75*	75*	87*	87*	2,705	1,876	2,350	
Czechia	316	339	339	339	303	316	333	310
Germany	52,792	53,184	54,499	55,289	47,064	48,530	51,010	51,354
Denmark	4,426	4,402	4,481	4,644	3,327	3,069	2,802	3,218
Spain	22,961	24,447	26,664	27,735	22,961	24,332	31,046	
France	13,610	16,578	17,217	19,516	15,134	16,848		18,191
Greece	2,355	3,153	3,755	4,150	3,131	3,092	4,803	4,908
Croatia	616	739	796	925	668	859	1,021	1,304
Hungary	327	323	323	323		351	377	378
Italy	9,617	10,224	10,302	10,658	21,354	19,702	24,668	
Luxembourg	154	154	167	167	105	111	133	135
North Macedonia	35	37*	35	37		32	54	59
Montenegro	118	118	118	118	209	117	312	382
Netherlands	3,436	3,527	4,188	5,310	1,182	1,661	1,769	1,939
Poland	5,808	5,953	6,570	7,950	5,779	6,149	6,935	7,887
Portugal	5,127	5,181	5,183	5,328	6,138	6,425	6,539	6,900
Romania	2,968	2,972	2,957	2,957		3,774		
Serbia	398	397	429	533				664
Slovakia	3	3	3	4*			2	2
Slovenia	3	3	3	2		1	2	2

In line with previous findings for Germany and Denmark, our analysis reveals that estimated total capacity of wind, onshore and offshore, and solar differs from current capacity in all years. This discrepancy can be attributed to various factors, such as limitations in measured feed-in, which results in less capacity being required overall than what is actually installed.

As a result, accurate estimation of total capacity and generation can be challenging, but the approach presented here provides valuable information on the allocation of installed renewable energy capacity and generation.

Table 2.8.: Actual installed offshore wind capacity (ENTSO-E Transparency Platform, 2023d; International Renewable Energy Agency, 2023) and estimated offshore wind capacity of all countries for each year in [MW].

	actual				estimated			
	2019	2020	2021	2022	2019	2020	2021	2022
Belgium	1,548	2,254	2,254	2,254				
Germany	6,393	7,504	7,774	7,787	5,084	5,567	5,672	5,232
Denmark	1,700	1,700	1,700	2,305	1,316	1,400	1,804	2,042
France	2*	14	10	20				
Netherlands	957	957	2,460	2,460	833	1,243	2,214	2,165
Portugal	0	8*	25	25	0	13	14	29

Table 2.9.: Actual installed PV capacity (ENTSO-E Transparency Platform, 2023d; International Renewable Energy Agency, 2023) and estimated PV capacity of all countries for each year in [MW].

	actual				estimated			
	2019	2020	2021	2022	2019	2020	2021	2022
Austria	1,193	1,333	1,851	2,500	356	440	453	403
Belgium	3,369	3,887	4,788	4,788	2,084	2,541	2,908	
Bulgaria	1,059	1,084	1,246	1,726	637	675	740	856
Switzerland	2,173*	2,498*	2,973*	3,449*		1,084	1,056	
Czechia	2,049	2,061	2,054	2,053		1,298	1,286	1,389
Germany	45,299	48,206	53,302	57,744	24,842	27,248	28,622	32,285
Denmark	1,014	1,013	1,300	1,536	641	804	930	1,341
Spain	6,751	8,466	11,390	14,640	4,617	6,439	8,761	
France	8,188	9,438	10,213	13,154	6,264	6,673	7,470	8,347
Greece	2,441	2,606	3,055	3,820	1,756	1,946	2,147	2,598
Croatia	53	53	85	96	35	38	42	47
Hungary	936	1,407	1,829	2,524	766	856	1,254	1,567
Italy	4,717	4,874	4,979	5,137	8,767	9,143	9,177	
Luxembourg	136	170	236	258	73	87	115	146
North Macedonia	21*	26*	94*	94*				
Netherlands	4,608	7,226	11,108	14,911	39	129	201	219
Poland	430	1,310	3,473	6,664		979	2,770	5,402
Portugal	324	413	569	1,032	397	480	650	970
Romania	1,150	1,163	1,145	1,160	616	693	696	845
Serbia	21*	23*	31*	52*				
Slovakia	531	531	532	536*	278	318	283	295
Slovenia	275	278	289	286	130	129	141	141

2.5. Summary and Concluding Remarks

In this chapter, we described a comprehensive methodology for developing synthetic, data-driven, and large-scale capacity layouts for onshore wind, offshore wind and solar power plants. The approach combines high-resolution numerical weather data with physical models of the power curves of wind turbines and solar modules to estimate potential installed wind and solar capacities at each network node of the main continental European transmission network. The methodology includes a country-specific regularised regression approach, combining synthetic outputs with actual measured wind and solar feed-in data to estimate the installed capacity at each node. The estimated layouts mimic the actual generated power by renewable generators very closely and thus are feasible as working layouts for further analysis.

We provide these realistic high-resolution layouts of installed onshore and offshore wind capacities as well as PV capacities in a comprehensive data set for mainland Europe, including generation data from 2019 to 2022 in an hourly resolution of all three types. By making the source code publicly available, we enable others to generate results for a specific time horizon or location and tailor them to their needs. This chapter provided a detailed understanding of the conversion process and the required variables to convert weather data to solar energy information.

Overall, the presented methodology and provided data set offer valuable insights for policymakers and energy companies in designing and implementing renewable energy projects. The approach could be used to make forecasts in the resolution of single grid nodes with a given layout or to study the necessary or recommendable expansion of renewable generation capacities, also taking into account dark windless and sunny strong wind days to increase the share of renewable energies in the electricity mix. Additionally, through the data-driven calculation of layouts and feed-ins via weather-to-energy conversions, the effects of weather phenomena, e.g., storms or heat phases, on power generation from renewable energy sources can be analysed. In future research, the conversion process could be adapted and expanded. For instance, factors such as turbine wake effects, the unavailability of turbines and solar modules, and the efficiency degradation due to the ageing of turbines and modules could be considered. While this may not result in more accurate synthetic energy feed-ins compared to the working

layouts presented here, it would generate layouts aimed at meeting the total actual installed capacity and not only to be proportional to. Finally, the impact of adjusting solar feed-in data to account for stored solar energy and self-consumption can also be explored, considering the likely numerous regional and local differences, which would make this a highly complex and time-consuming undertaking.

In the next chapter, we turn towards broadly provided data sets and improve the transmission system operators' (TSOs) day-ahead load forecast. This is done with a time series model to capture autoregressive dependencies in the forecast.

3. Enhancing Energy System Models Using Better Load Forecasts

This chapter is based on Möbius et al. (2023)[1].

3.1. Introduction

Energy markets are complex and exhibit non-trivial interdependencies, so decisions from policy and industry stakeholders rely on theoretical models and other methodological support. Techno-economic energy system models are widely used in academia, policy-making and industry. Typically, they determine market equilibria, minimising production costs or maximising social welfare. A market's supply and demand sides are equally essential to derive equilibria. Various models have been developed using time series of load data as an essential input on the demand side. On the supply side, models focus on power plants (electricity system models) or gas production (gas systems). Transmission and distribution infrastructure, i.e., connecting supply and demand, can also be included and analysed with energy system models. A strength of these models is that they can provide valuable insights into both causes and effects of current and planned developments, as well as into "what-if" types of analyses. They are capable of reflecting structural breaks better than most other model types. Thus, energy system models are among the essential methodologies for a successful energy transition.

However, they rely on the quality of input data to provide accurate results. Preparing and collecting data for energy system models is a challenge, and tremendous efforts have

[1]The work was supported by the German Federal Ministry of Economic Affairs and Climate Action through the research project "ProKoMo - Better price forecasts in the energy sector by combining fundamental and stochastic models" within the Systems Analysis Research Network of the 6th energy research program.

been done to generate techno-economic data (see, e.g., Schröder et al., 2013; Kunz et al., 2017b) or forecast data (see, e.g., Li et al., 2023), among others. Moreover, literature has shown that widely used input data sets for energy system models, in particular load data and wind or solar forecasts from official sources, often have significant systematic errors (Maciejowska et al., 2021; Hirth et al., 2018). We refer to these results and elaborate on how these errors can be reduced by real-time time series filters. Considering the errors as an econometric time series, serial structures in these errors can be used to predict future errors, which significantly reduces the errors themselves. We then analyse whether using these improved input data in an energy system model will improve model quality.

The contribution of this chapter is threefold. First, we develop and provide a simple time series model reducing forecast errors of hourly day-ahead load predictions of transmission system operators (TSOs) in real-time. We focus on load forecasts because they are the most correlated with the prices of the day-ahead electricity market and have the most potential for improvement compared with wind and photovoltaic (PV) generation forecasts (see, e.g., Maciejowska et al., 2021). One advantage of our approach is that we take publicly available TSO-based load forecasts as given. Thus, in modelling their prediction error directly as a predictable subject, we do not need to develop a complex load forecast model. On a country level, load forecasts are often used to represent the demand on the day-ahead market clearing[2]. Thus, load forecasts are central variables for determining equilibria of demand and supply in energy system models.

Second, we present a fundamental energy system dispatch model called the *em.power dispatch* model, which is developed and calibrated precisely for short-term use in the day-ahead market. A primary objective of this model is to predict wholesale electricity prices. Using a rolling window, it consecutively determines the optimal power plant operation for three consecutive days. Moreover, the model considers hourly net transfer capacities to limit electricity transmission across countries and a formulation for medium- and long-term energy storage.

Third, we demonstrate the value of sequentially and continuously improving the quality of input variables in fundamental energy system models in the empirical part of the chapter. We consider TSOs' day-ahead load forecasts provided by one of the most used

[2]In all main European markets, wholesale electricity prices are determined in the day-ahead market clearing one day before the actual delivery.

data sources (ENTSO-E Transparency Platform, 2021k) and day-ahead prices forecasted with the energy system model for Germany, one of the largest and most liquid electricity markets in the world. By capturing and reflecting systematic biases and autoregressive structures, we reduce the mean squared error (MSE) by 26 % compared to the TSO-based load forecast. Therefore, market participants' expectations of the day-ahead market clearing can be better reflected. As a result, the MSE of the *em.power dispatch* model's price forecast is reduced by nearly 15 % in hours with high prices using the improved load forecast compared to using the TSOs' load forecast. By demonstrating that energy system models with the improved load data perform significantly better compared to the TSO data, we provide valuable insights for many stakeholders in the power sector, particularly energy system model developers seeking to improve the validity of their models. Based on these results, we encourage energy system modellers and all users of fundamental input data to be aware of the predictable structure of their errors. In particular, stochastic modelling of the errors significantly reduces the forecast error of input data. It thus improves the quality of input data as part of sequential data pre-processing in real-time and offers the possibility to enhance the output of fundamental energy system models.

The remainder of the chapter is organised as follows. First, we examine the literature on energy systems modelling, data quality and time series modelling in Section 3.2. Section 3.3 presents the data used in this application. In Section 3.4, we provide and explain the methodology for the model improving the load forecasts and the energy system model used to evaluate the impact of the improved load data. The results are presented in Section 3.5. Finally, a conclusion is drawn in Section 3.6.

3.2. Literature

This chapter addresses energy system modellers who model energy systems with a high degree of detail and therefore require large and as accurate as possible data sets. Out of a wide range of modelling applications, examples include the determination and assessment of long-term investment decisions for generation and storage capacities (e.g., Nahmmacher et al., 2016; Schill and Zerrahn, 2018), implications on short-term operational decisions (e.g., Schill et al., 2017), transmission expansion planning (e.g., Egerer et al., 2021; Sauma

et al., 2006) as well as the evaluation of carbon reduction paths (e.g., Vaillancourt et al., 2017), of support schemes for a renewable energy system (e.g., Kitzing et al., 2017) and of interdependencies between energy sectors (e.g., Lienert and Lochner (2012) for electricity and gas markets, Heinisch et al. (2021) for transport, electricity and district heating, Koirala et al. (2021) for electricity, hydrogen and methane). Moreover, scholars develop stochastic models to assess the impact of uncertainty on a power system (Riepin et al., 2021), for example, to quantify the expected costs of ignoring uncertainty of critical parameters in the electricity and gas sector. Möst and Keles (2010) provide an overview and classification of stochastic models dealing with uncertainty in the power sector. With regard to uncertainty, scholars analyse the effect of risk preferences (e.g., Möbius et al., 2021; Ambrosius et al., 2022).

In particular, this chapter analyses the impact of better load forecasts on the day-ahead forecast of wholesale electricity prices using a fundamental energy system model. Estimating wholesale electricity prices is essential for making optimal economic decisions (e.g., investment and dispatch of various technologies) and policy decisions (e.g., calculating the implications of a coal phase-out). Wholesale electricity prices can be forecasted with multiple methodologies, all with their unique advantages and disadvantages. Energy system models perform exceptionally well at structural breaks, are based on a broad economic theoretical foundation explaining causality, and provide additional information beyond the forecast. Consequently, much attention has been paid in the literature to simulate or predict electricity prices with energy system models. Hirth (2013) simulates electricity prices to quantify the drop in the market value of variable renewables. Additionally, Eising et al. (2020) quantify market values for renewables generating electricity prices in a future power system with the help of an energy system model. Engelhorn and Möbius (2022) derive market prices assuming different weather years and quantify weather-specific market values for a comprehensive database of onshore wind capacities in Germany. Qussous et al. (2022) use an agent-based model with rule-based bidding strategies to reproduce spot prices for the German bidding zone.

Market power and strategic behaviour are other applications of wholesale price forecasts with energy system models. When modelling competitive market prices and comparing them with actual prices, they were able to point to serious problems (e.g., Müsgens

(2006a) and Weigt and von Hirschhausen (2008) for Germany, Borenstein et al. (2002) for the United States).

These and many other model applications have a dedicated empirical focus. Thus, the high quality of input data is vital. For the European electricity sector, data is conveniently gathered and made publicly available by transmission system operators (TSOs) via the transparency platform of the European Network of Transmission System Operators for Electricity (ENTSO-E) (ENTSO-E Transparency Platform, 2023b). The platform is a very ambitious and unique project to provide an extensive data set for electricity markets and is thus both well-known and widely used. Nevertheless, the data presented on the platform is not without its shortcomings regarding completeness and quality (see Hirth et al., 2018). Furthermore, Maciejowska et al. (2021) analyse the quality of load data for the Germany-Luxembourg bidding zone. They detect a bias in TSO load forecasts and develop an alternative load prediction model that incorporates information from these forecasts to remove the bias and thus achieve an enhanced load prediction. Cancelo et al. (2008) analyse the forecast errors of the Spanish day-ahead TSO load forecasts in detail for serial structures and influences of special days such as Christmas holidays or New Year's Eve. Hence, researchers using such empirical data should raise awareness and be targeted at improving data quality.

We aim to provide energy system modellers with a methodology to enhance the quality of their results by improving the input data. Concerning load data, a comprehensive literature review of various methods and models for energy demand forecasting is given by Suganthi and Samuel (2012) and Singh et al. (2012). Among others, approaches for stand-alone load forecasting models are presented by Weron and Misiorek (2005); Weron (2006); Naz et al. (2019); Lin et al. (2018); Rodrigues and Trindade (2018); Wu et al. (2019); Tan et al. (2010); Chen et al. (1995); Al-Hamadi and Soliman (2004); Wang et al. (2023) and Yang et al. (2013).

Load forecasts are publicly available. However, they can be improved with a simple and straightforward approach. Given a series of load forecasts with forecasting errors that still show a predictable structure, the method proposed in this chapter offers a possibility to enhance existing forecasts. We improve the forecasts by modelling and removing predictable parts of the errors needing no other information than the forecast

error itself. Implicitly, Yang et al. (2013) use a similar step since they remove a structure from their forecasting model (first stage) in a second stage by a time series approach. However, they rely on neural networks, while we propose a simple time series model.

In energy system modelling, activities to improve input data can be described as data pre-processing or, more precisely, continuous data processing and enhancement with subsequent use. Such continuous data processing is typically not performed for energy system models. We believe this is a methodological gap in the literature and aim to bridge it by providing an approach to sequentially improving input data and sequentially using these continuously improved data sets in an energy system model. We demonstrate the effectiveness in an empirical application, focusing on the effect of better load forecasts for electricity price forecasts derived from energy system models.

3.3. Data

Energy system models require extensive input data to model market equilibria on both the demand and the supply sides. Since this work focuses on a day-ahead time horizon, TSO-based load forecasts published by ENTSO-E may be used as predictors for the demand side. However, as was pointed out in the literature section, the quality of these load forecasts is debated and will be improved in this work. In Section 3.3.1, we first provide a detailed overview of the TSO-based load forecast data and forecast errors. Moving to the supply side of the energy system model, data on techno-economic parameters for conventional generation, renewables, storage and electricity transmission are of the utmost importance and are presented in Section 3.3.2.

3.3.1. TSO-based Load Forecast Data

The load data set we use for our analysis contains hourly day-ahead load forecast data and hourly actual load data from January 1st, 2016, until December 31st, 2019, for Germany and Luxembourg. It was downloaded from the ENTSO-E transparency platform (ENTSO-E Transparency Platform, 2021k) in quarter-hourly resolution, given in [MW], and transformed in hourly resolution in [MWh]. Missing values were replaced by the

average of the value of the previous week and the week after[3]. An illustration of the time series of the actual load, TSOs' load forecast and the resulting error, computed as the difference between actual load and load forecast, is shown in Figure 3.1.

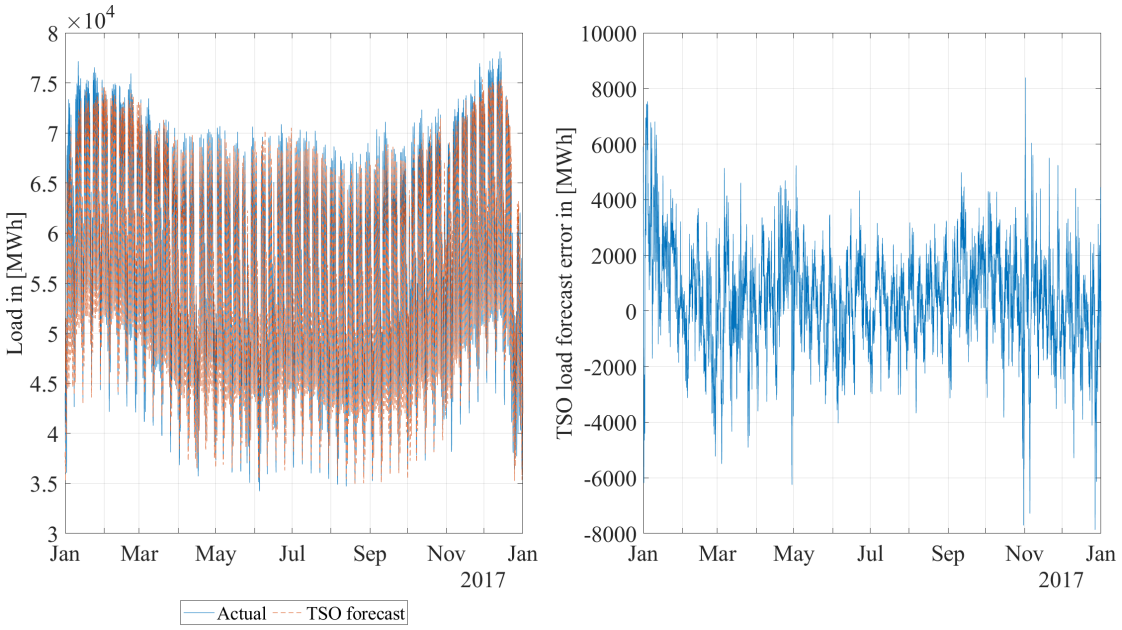

Figure 3.1.: Actual load and TSOs' day-ahead load forecast in 2017 (left) and error of TSOs' day-ahead load forecast in 2017 (right).

For the considered years, Table 3.1 contains descriptive statistics of the TSOs' load forecast errors defined as $\varepsilon_t := L_t - \hat{L}_t$, meaning actual load minus TSOs' load forecast. Thus, a positive error states an underprediction of load.

The TSOs' forecast data is mean-biased, as discussed in Maciejowska et al. (2021). In our analysis, we find systematic underpredictions with a mean error of 881.29 MWh across all years and positive mean errors for every year.

However, the absolute level of the error and whether the TSO under- or overpredicts in its forecasts depend on the day of the week and the hour of the day. Figure 3.2 states the averaged hourly forecast errors in a week. Broadly, we can observe underprediction

[3]There are 1,105 missing values in the hourly TSOs' load forecast and 38 missing values in the hourly actual load data.

Table 3.1.: Descriptive statistics of TSOs' load forecast errors for the years 2016 to 2019; except for LB hypothesis, all variables are given in [MWh].

	total	2016	2017	2018	2019
mean	881.29	1,555.38	446.50	298.60	1,222.84
median	892.75	1,468.00	479.50	395.63	1,195.75
minimum	-20,358.00	-7,752.50	-7,868.50	-20,358.00	-7,415.00
maximum	12,930.75	12,930.75	8,392.50	9,045.25	9,635.25
5%-quantile	-2,477.50	-1,684.03	-2,413.75	-3,180.63	-2,266.13
95%-quantile	4,294.40	4,894.20	3,099.38	3,644.75	4,811.38
std.	2,149.75	2,079.19	1,746.54	2,341.68	2,128.55
LB hypothesis	1.00	1.00	1.00	1.00	1.00

during weekdays and overprediction on the weekends, especially on Saturdays. During the day, in the morning and the evening hours, the error of the TSOs' day-ahead load forecast is generally positive and higher than in the other hours of the day. With an average error of 943.53 MWh at 6 a.m. and 1,180.48 MWh at 7 p.m., the prediction error in these hours is higher by 7 % (34 %) than the mean error of the entire time period considered (compare with Table 3.1). These are the hours when the workday begins or ends and where production ramps up or down. Although the standard deviation of the forecast in these hours is not significantly larger than in the other hours, it appears that the load in these hours is still more challenging to forecast on average than in the other hours of the day (see weekday-wise descriptive measurements in Appendix Table C.2 for more details).

Finally, we perform Ljung-Box (LB) tests to verify the auto-correlation of the TSOs' load prediction errors. The null hypothesis at a 5 % significance level is rejected for all years, which indicates a strong auto-correlation of the errors. Comparing the errors with those one hour before (see Figure 3.3), we can see a highly linear dependence.

In summary, the load data shows high auto-correlated TSOs' forecast errors, which average 1.56 % of the total load's mean. The mean absolute error of the TSOs' load forecast is 1,776 MWh (3.14 % of the total load's mean). The TSOs' forecast errors are biased with some seasonal structures in the bias and are highly auto-correlated. Hence, autoregressive type models could improve the TSOs' load forecast.

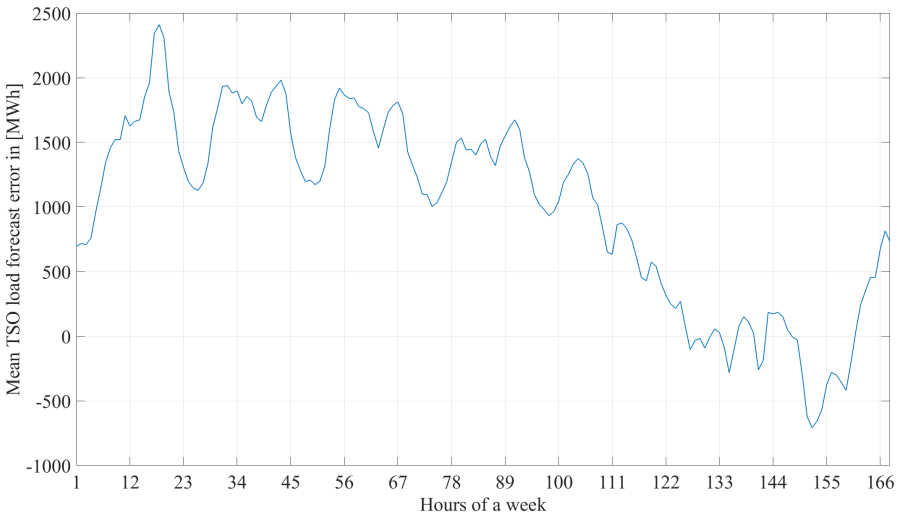

Figure 3.2.: Average weekly pattern of TSOs' day-ahead load forecast errors from 2016 to 2019.

3.3.2. Input Data for the Energy System Model

Aiming to analyse the impact of improved day-ahead load forecasts on the accuracy of electricity price forecasts, which are derived using an electricity system model, we develop and parameterise a European electricity market model with data from January 1st, 2017, until December 31st, 2019. A meaningful empirical parameterisation of such models requires extensive input data derived from various sources. To model the demand side, the load data presented in the previous Section 3.3.1 is essential. Furthermore, there is typically an option to shed load during supply scarcities. In our application, we assume the costs for load shedding to be 3,000 €/MWh.

On the supply side, several technologies are available for electricity generation and storage. Our energy system model distinguishes ten conventional thermal generation technologies, which form 30 capacity clusters according to a power plant's commissioning year. We provide each of the capacity clusters with different efficiencies, minimum outputs and efficiency losses in part-load operations, which are derived from Schröder et al. (2013) and Open Power System Data (2020a). The capacity, fuel type, generation technology and commissioning date are derived from ENTSO-E Transparency Platform (2021i),

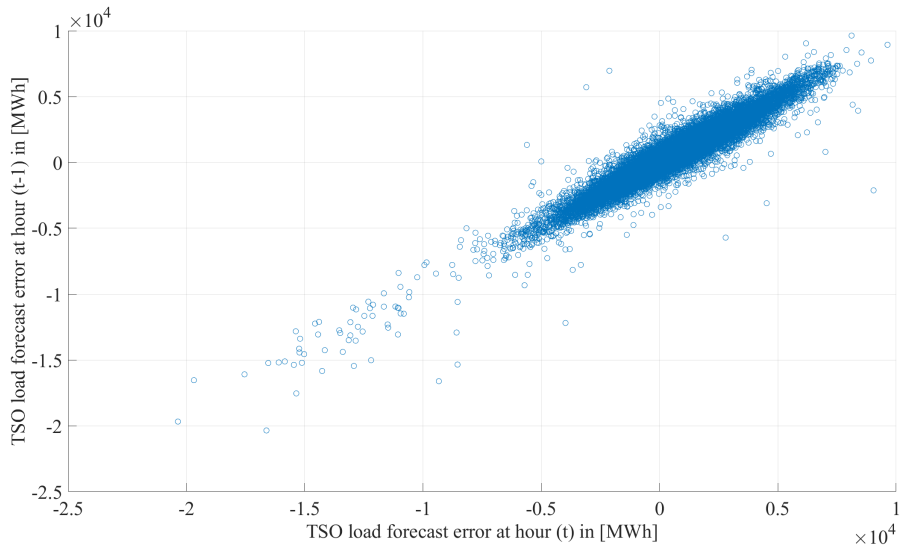

Figure 3.3.: Scatter plot of TSOs' day-ahead load forecast error and TSOs' day-ahead load forecast error one hour before.

Open Power System Data (2020a) and EBC (2021). For power plants on the German market, we additionally use data from BNetzA (2021) and UBA (2020). Fuel costs, costs for CO_2 emissions and the power plant efficiency determine the variable generation costs of conventional thermal technologies. For fuel costs, we use daily gas prices that are provided by EEX (2021), and monthly coal and oil prices from DESTATIS Statistisches Bundesamt (2021). Fuel costs for nuclear, lignite and waste are derived from ENTSO-E (2018). These are assumed to be constant over time. Prices for CO_2 certificates are implemented as weekly values from Sandbag (2020).

The process of starting up power plants requires the use of fuel, emits CO_2 and leads to material wear in the plant. Data for start-up times, secondary fuel usage and depreciation are derived from Schröder et al. (2013).

The ability to generate electricity depends not only on the installed capacity but also on the technical availability of the plants. Therefore, we consider all scheduled and non-scheduled power plant outages known before the day-ahead market's closure. Hourly outages are derived from ENTSO-E Transparency Platform (2021m).

Since combined heat and power (CHP) plants are used in most electricity markets, electricity and heat supplies are linked. To account for this dependency, we provide these units with a must-run condition that ensures their operation at certain minimum output levels. These output levels are derived in two steps. First, we determine an hourly heat-demand factor consisting of a temperature-dependent (spatial heating) and temperature-independent (warm water and process heat) part. The temperature-dependent heat demand is generated with heating degree days using mean temperature data from Open Power System Data (2020b). We derive the temperature-independent heat demand using the hourly and daily consumption patterns from Hellwig (2003). Second, we use the heat-demand factor to allocate annual electricity generation volumes by CHP plants to single hours. The annual technology-specific electricity generation by CHP units is taken from European Commission (2021).

In addition to conventional thermal technologies, we consider renewable energy sources (RES), energy storage, hydro-reservoirs and run-of-river. Intermittent RES such as onshore wind, offshore wind and PV are implemented by hourly availability factors that are derived from feed-in forecasts from ENTSO-E Transparency Platform (2021g). We do not also improve these forecasts by sequentially modelling their forecast errors in order to clearly measure the impact on the quality of the price forecast when we improve the forecast of the variable that not only offers the greatest potential for improvement but is also most strongly correlated with day-ahead electricity spot market prices (e.g., load). Biomass is implemented as base-load as the historic operation is at a constant level (compare ENTSO-E Transparency Platform, 2021a).

We exclusively consider pumped storage plants (PSP) for energy storage that actively charge and discharge. The overall turbine capacity of PSPs is made available by ENTSO-E Transparency Platform (2021i), and the efficiency of a storage cycle is around 75 % (Schröder et al. (2013)). For PSPs, the energy storage capacity and the turbine capacity are linked. Assuming an energy-power factor of nine, the plant can generate electricity at full load for nine hours until the storage is empty.

Long-term PSP, as well as hydro-reservoirs, are assigned a variable generation cost, i.e., the value for water consumption. Using historical electricity prices from ENTSO-E Transparency Platform (2021c) and the observed generation and pumping activities in the

respective hour from ENTSO-E Transparency Platform (2021a), a step-wise merit-order for long-term PSP and hydro-reservoirs is constructed. Run-of-river and mid-term PSP[4] are subject to seasonal variations, which we acknowledge by a monthly availability factor derived from historical generation data from ENTSO-E Transparency Platform (2021a).

The German electricity market is highly integrated into the European system. Total interconnector capacity amounts to 27 GW, which is more than 30 % of the German peak load[5]. Both annual aggregated exports (around 13 % of annual German consumption in 2019) and imports (around 7 % in 2019) are significant. Hence, we parameterise a Pan-European electricity market model which includes the bidding zones of most EU-27 member states[6], Norway, Switzerland and the United Kingdom[7]. Within Germany, day-ahead electricity prices are derived following the principle of a bid-based economic dispatch, neglecting the physical transmission constraints within the market zone. Since the energy system model has its focuses on the analyse of day-ahead prices, we follow this approach and treat all of Germany, plus Luxembourg, as one bidding zone[8]. Thus, in total, we include 23 different markets in the analysis, which will be referred to as "nodes" in the formal model, connected by net transfer capacities (NTCs). We implement hourly day-ahead forecasts for NTCs that are made available by ENTSO-E Transparency Platform (2021e) and JAO Joint Allocation Office (2021).

3.4. Methodology

In the following, we present our two components to analyse the value of improved day-ahead load forecasts for electricity price forecasts derived by an electricity system model: a time series model for the sequential load data pre-processing and improvement in Section

[4]Note that we call it mid-term because we focus on the day-ahead market with an hourly granularity, as opposed to short-term storage with an intra-hourly resolution closer to time of delivery.

[5]Note that the availability of the interconnectors depends on various factors (e.g., congestion within a market zone).

[6]Bulgaria, Cyprus, Greece, Iceland, Ireland, Malta and Romania are not included.

[7]Note that we aggregate the bidding zones of Spain and Portugal to one market, "Iberian peninsula", and the bidding zones of Lithuania, Estonia and Latvia to one market, "Baltic". Also, note that we consider the different bidding zones within countries. However, we aggregate the following zones: in Norway NO1-NO5, in Sweden SE1-SE3, and in Italy all zones except IT-North.

[8]Note that the market area, Germany-Luxembourg-Austria, was split into two market zones (Germany-Luxembourg and Austria) in 2018. Our model accounts for this fact.

3.4.1 and the dispatch market model that is used to generate price estimators in Section 3.4.2. The entire source code of both the time series model and the dispatch market model, the used input data which we could provide public, and the generated results are provided in a repository on GitHub (*https://github.com/ProKoMoProject/Enhancing-Energy-System-Models-Using-Better-Load-Forecasts*). The proposed pre-processing is implemented in MATLAB®[9], and the dispatch model is coded in GAMS[10].

3.4.1. Model for Load Forecast Error

To improve load forecasts, we use a well-known time series approach that achieves a trade-off between performance and complexity. The approach is based on the idea of forecasting the TSOs' load forecast error and using this to enhance the load prediction. Thus, we model the time series of forecast errors. For this reason, and to obtain a low-parameter model, we do not use exogenous variables such as feed-in of renewable energy or weather in our model for forecasting the load forecast error, in contrast to the main load forecasting methods in the literature, which include temperature and weather data in particular, e.g., Cancelo et al. (2008); Al-Hamadi and Soliman (2004); Amjady (2001); Wu et al. (2019) and Li et al. (2021). We propose a purely endogenous time series approach that can be applied using TSOs' load forecast error alone as input data. It is detached from the outgoing model, which, in general, already includes exogenous variables. With forecasting the forecast error, the resulting load prediction $\hat{L_t}^*$ at time t is then given by

$$\hat{L_t}^* = \hat{L}_t + \hat{\varepsilon}_t, \tag{3.1}$$

where $\hat{L}_t$ is the original TSOs' load prediction and $\hat{\varepsilon}_t$ is our forecasted TSOs' load prediction error. Thus, $\hat{L}^*$ is an improved load forecast in which we adjust the original forecast for predictable structure in its error.

For the overall setup, the subindex t will denote consecutive hours. So, $\hat{L}_1$, for instance, is the load forecast for the first hour of the considered time period, and $\hat{L}_{123}$ is the forecast for the hour 123. This fits best into the observation process of the actual load data. For example, in contrast to electricity prices for which we observe a realisation of

[9] Version R2020b
[10] GAMS General Algebraic modelling System Version 41

24 daily hourly prices at the same time, load data can theoretically be observed hour by hour. For day-ahead electricity prices, alternative parameterisations such as modelling every day as a 24-dimensional vector, or using 24 time series each for one hour of the day, would be more appropriate (see, e.g., Ziel and Weron, 2018a).

Furthermore, we decompose the time series into the sum of a seasonal component and a remaining stochastic component. As we do not observe any trend in the forecast error data in Section 3.3.1, we do not use the usual trend component of such decomposition models (see, e.g., Lütkepohl (2005); Hyndman and Athanasopoulos (2021); Box et al. (2015) for comprehensive introductions into time series models). Together, the model is

$$\varepsilon_t = SC_t + RC_t, \tag{3.2}$$

where ε_t is the TSOs' load forecast error, SC_t is a seasonal and RC_t is the remaining component at time t.

The forecast errors' average sizes depend on the specific hour of the week (see Section 3.3.1), so the seasonal component SC_t captures a weekly season, consisting of an average value for each of the 24x7 hours of the week. This means addressing the hour of the day and the day of the week with a total of 168 dummy variables, as given by

$$HoW_t^{h,d} = \begin{cases} 1, & \text{if } t \text{ is the h-th hour of the d-th day of the week,} \\ 0, & \text{otherwise.} \end{cases}$$

Here, $h = 1, ..., 24$ denote the hours of the day and $d = 1$ (Monday), $\ldots$, 7 (Sunday) the days of the week.

The seasonal component SC_t for time t is now defined by Formula (3.3), with (3.4) being the average of TSOs' forecast errors from the hours of the week from the time period used to estimate the model (e.g., the last l_w hours).

$$SC_t = \sum_{h=1}^{24} \sum_{d=1}^{7} HoW_t^{h,d} \cdot HS^{h,d}, \tag{3.3}$$

$$HS^{h,d} := \frac{\sum_{s=t-h-l_w-23}^{t-h-24} \varepsilon_s \cdot HoW_s^{h,d}}{\sum_{s=t-h-l_w-23}^{t-h-24} HoW_s^{h,d}}, \tag{3.4}$$

The rest of the time series $RC_t = \varepsilon_t - SC_t$ is modelled by the econometric SARMA $(1,1)\text{x}(1,1)_{24}$ model given in Formula (3.5), i.e., a (S)easonal (A)uto(R)egressive (M)oving (A)verage model. Here, the value RC_t at hour t depends on its previous value at $t-1$ as well as the previous model error ψ_{t-1}. Additionally, the model contains a 24-hour seasonal part which captures stochastic seasonal behaviour in contrast to the more deterministic seasonal structure filtered by SC_t. Formally, the seasonal part leads to direct effects of all variables lagged by another 24 hours on RC_t, as given by

$$\begin{aligned} RC_t =& \phi_0 + \phi_1 \cdot RC_{t-1} + \phi_{24} \cdot RC_{t-24} - \phi_1\phi_{24} \cdot RC_{t-25} \\ &+ \omega_1 \cdot \psi_{t-1} + \omega_{24} \cdot \psi_{t-24} + \omega_1\omega_{24} \cdot \psi_{t-25} \\ &+ \psi_t, \end{aligned} \tag{3.5}$$

where the innovations are assumed to be homoscedastic and normally distributed, which means $\psi_t \sim N(0, \sigma_\varepsilon^2)$. Assuming a normal distribution for the innovations is a simplification and idealisation.

We calibrate and estimate the model on a rolling window. The window length, denoted by l_w, is an integer multiple of 24 and thus contains full days only. The window is also rolled over full days in each step to further reflect the daily availability of load data and, thus, the error of the TSOs' load forecast. In this work, we decide on one window length l_w to estimate the model. Alternatively, one could average multiple models calibrated on different window lengths, e.g., as proposed in Maciejowska et al. (2021); Ziel and Weron (2018a); Marcjasz et al. (2018). However, in this study, where the simplicity and usability of the model are important considerations, we believe such an increase in complexity would not be justified.

The estimated model is used to recursively (i.e., on an hour-by-hour basis) predict the hours of the next day. Since we rely on an autoregressive time series model, we

need load data from the last hours for prediction, which enter the model as explanatory variables. Although load generation can theoretically be observed hourly, in practice, the load values of the previous hours are available with a time lag, meaning they may not be available as explanatory variables when forecasting the following hours. A solution is to replace unavailable variables with recursively forecasted variables based on the last available observations.

To ensure data availability in the sense of a day-ahead forecast at all times, we only use load observations up to yesterday's last hour for TSO data as inputs if we make predictions today for tomorrow. Today's hours must be replaced by forecasts based on yesterday. More clearly, let $t = 8785$ be the first hour of January 1st, 2017, for simplicity, and let x be the hour of January 1st from which we forecast the next day's hours. In the further course, we assume $x = 12$, so we forecast the next day's hours between 11 a.m. and 12 a.m. today. Depending on availability, actual TSOs' load forecast errors ε_t enter our model or forecasted ones. For hour $t \leq x - 12$, we use the observed errors ε_t and the forecasted ones $\hat{\varepsilon}_t$ for $t > x - 12$. We want to predict the load for the next day's 24 hours, thus, $x + 13$ to $x + 37$. Due to the information delay and ensuring data availability, we do not indicate the actual load of hours $x - 11$ to $x - 1$. We also have no information about the hours x to $x + 12$ lying in the future. For this reason, we first estimate the model based on the last available l_w observations (i.e., of hours $x - 12 - (l_w + 1)$ to $x - 12$). From that, we predict the errors of the TSOs' load forecast of the next 48 hours ($x - 11$ to $x + 37$), i.e., of the hours of January 1st and 2nd, and use the last 24 predicted values, meaning the values at hours $x + 13$ to $x + 37$, for improving the original load forecasts of the following day. Note that by rolling over the estimation window daily, we ensure that the prediction of TSOs' forecast errors for all load periods of one day is based on the same estimated model.

3.4.2. Energy System Model

We develop a new energy system model, the *em.power dispatch* model, to derive wholesale day-ahead electricity price forecasts. The model is formulated as a linear optimisation problem minimising total system costs and includes a detailed representation of central techno-economic aspects of the European electricity sector. In particular, the model

dispatches various generation technologies to satisfy electricity demand. In addition to power plant dispatch in Germany, the model considers international trade between the markets described in Section 3.3.2, electricity production by combined heat and power plants, energy storage and control power provision. To ensure a linear formulation of such a highly complex system, we form capacity clusters, parameterised as described in Section 3.3.2. Within each technology cluster, capacity can be started-up and electricity can be produced in marginal increments (see, e.g., Müsgens, 2006a). The advantage of this approach is twofold. First, computational efforts are reduced. Second, the marginal of the demand restriction is differentiable at each point and can thus be interpreted as a wholesale market price estimator. Additionally, the accuracy of modelling large energy systems, in particular, remains reasonably high (see Müsgens and Neuhoff, 2006).

Considering all economic and technical restrictions, the model solves the cost minimisation problem and determines i) the optimal dispatch decision for all considered infrastructure elements, such as generation technologies, energy storage and cross-border transmission capacities, and ii) the short-run marginal system cost that determines the price estimators for the day-ahead market in hourly resolution.

Furthermore, as our research analyses the impacts on day-ahead price forecasts, we set up the model to reflect the information available to market participants on the day before delivery. Thus, we consider that market participants do not have perfect foresight for the upcoming days. We achieve this with a rolling window model that is repeatedly solved and provides information for 24 day-ahead hours of one "target day" in each model run. To reduce the problem of starting and ending values, in particular for power plant start-ups and pump storage plants, each model run includes three days, as shown in Figure 3.4. In this setting, the 24 hours of the respective target day are represented by the second day of the horizon $(d + 1)$. This is following the EPEX spot market organisation, where 24 hourly day-ahead prices are determined at 12 p.m. on the day before delivery (d). In addition to the target day $(d + 1)$, we also include the day before (d) and the day after $(d + 2)$. Note that we include a water value to increase the accuracy of seasonal hydro-storage modelling.

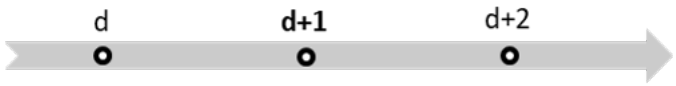

Figure 3.4.: Illustration of the energy system model's rolling window.

As with the improvement of the load forecast, this approach is repeated continuously ("rolling window"), once for each day of the observation period. At each iteration, the input data for $d+1$ and $d+2$ are limited to the values available on day d (i.e., forecasts), so that the incoming day-ahead load forecast is successively improved and processed in our approach. Correctly parameterised, our model uses the same data as market participants (e.g., energy suppliers, direct marketers, investment banks) when forecasting the day-ahead prices to optimise their portfolio. Given this day-ahead focus of our analysis, installed and available capacities are exogenous. The model endogenously optimises power plant dispatch only.

Our rolling window approach to forecasting hourly prices implies that we forecast three years with 365 daily model runs each year. As each model run comprises 72 hourly dispatch decisions with numerous variables in 23 model regions, the total number of variables is 340 million. In the following, we present the mathematical formulation of our model. A nomenclature containing all indices, parameters and variables of the energy system model formulation is provided in Appendix B[11].

The objective function in Formula (3.6) minimises total system costs and accounts for all costs that generation units face in the short-term. We include costs at full load operation ($vc^{FL}_{i,n,t}$), additional costs for units that operate at partial load ($vc^{ML}_{i,n,t} - vc^{FL}_{i,n,t}$), and start-up costs ($sc_{i,n,t}$). Note that we apply a linear formulation of the unit commitment, and all units have to produce at least a minimum output level. Additionally, we account for load shedding costs ($voll$) and penalty payments for curtailing renewables ($curtc$).

Since we apply our model with a rolling window, we consider three days in each model run. Modelling an additional day before and after the target day seems appropriate for storages with large energy-to-power ratios, which are essentially operated on a daily

[11] In the nomenclature, subindices d, h have to be pooled to the subindex t used in this chapter.

cycle (e.g., the largest German pump storage facility, *Goldisthal*, can store enough energy for nine hours of full load operation). However, other storages (both PSP and seasonal storages without pumps) have a storage cycle longer than three days. Therefore, we model PSP in two types: as mid-term storage that operates a storage cycle within a three-day horizon, and as long-term storage that operates a storage cycle longer than three days. The dispatch of mid-term storage is determined endogenously, with the exogenous restriction that they both start and end the cycle with reservoir levels at 30 %. The approach is different for long-term PSPs, which are assigned a water value ($wv_{stl,n,t}$) that is implemented as a variable cost factor for electricity generation ($G_{stl,n,t}$) and consumption ($CL_{stl,n,t}$). We assume that 70 % of the pump storage capacity is optimised in the medium-term. The remaining 30 % are long-term PSPs.

Compared to pumped storage plants, hydro-reservoirs have a natural water feed-in and do not perform a pumping process. However, the water budget for electricity generation is limited according to seasonal inflow volumes. Therefore, we also apply a water value for electricity generation by hydro-reservoirs.

$$\begin{aligned}\min TC = &\sum_{i,n,t} G_{i,n,t} \cdot vc^{FL}_{i,n,t} + \sum_{i,n,t} SU_{i,n,t} \cdot sc_{i,n,t} \\ &+ \sum_{i,n,t} (P^{on}_{i,n,t} - G_{i,n,t}) \cdot (vc^{ML}_{i,n,t} - vc^{FL}_{i,n,t}) \cdot g^{min}_i / (1 - g^{min}_i) \\ &- \sum_{stl,n,t} CL_{i,n,t} \cdot wv_{stl,n,t} + \sum_{n,t} SHED_{n,t} \cdot voll \\ &+ \sum_{n,t} CURT_{res,n,t} \cdot curtc\end{aligned} \tag{3.6}$$

Market clearing is ensured by Formula (3.7). For all T hours of the given rolling window, demand ($d_{n,t}$) must equal the sum of generation ($G_{i,n,t}$), load shedding ($SHED_{n,t}$) and electricity imports ($FLOW_{nn,n,t}$), reduced by electricity consumption of mid-term energy storage ($CM_{stm,n,t}$), long-term energy storage ($CL_{stl,n,t}$) and electricity exports

$(FLOW_{n,nn,t})$.

$$\begin{aligned} d_{n,t} = & \sum_{i} G_{i,n,t} - \sum_{stm \subset I} CM_{stm,n,t} - \sum_{stl \subset I} CL_{stl,n,t} + SHED_{n,t} \\ & + \sum_{nn} (FLOW_{nn,n,t} - FLOW_{n,nn,t}) \\ & \forall n, nn \in N, t \in T \end{aligned} \tag{3.7}$$

The dual variable of the demand constraint Formula (3.7) is used as an hourly day-ahead wholesale electricity price estimator. As we want to analyse how well these price estimators based on different demand forecasts fit real-world day-ahead prices, we compare them and compute error measures.

Electricity generation by capacity cluster is limited by an upper and a lower bound. The upper bound is formalised in Formula (3.8) and ensures that electricity generation does not exceed the running capacity ($P^{on}_{i,n,t}$) in the cluster. The possible electricity generation by running capacity is further limited by the reserve for positive control power provision ($PCR_{i,n,bp}, SCR^{pos}_{i,n,bs}$). The lower bound is presented in Formula (3.9) and states that running capacities must operate at least at a minimum power level, including the capacity reserved for negative control power provision ($PCR_{i,n,bp}, SCR^{neg}_{i,n,bs}$). Note that primary control power ($PCR_{i,n,bp}$) in Germany is provided synchronously, i.e., a unit has to provide both positive and negative primary control power. Different products for positive and negative control power were introduced for secondary control power. Since fast-reacting units (e.g., hydro- and open-cycle gas turbines) can be started-up to provide a positive-minute reserve, the effect on the running capacities is neglected. In addition, we assume that a negative-minute reserve is provided by multiple market players, not necessarily by power plants. The hours that belong to bidding blocks are mapped for primary control power by *bp* and secondary control power by *bs*.

$$\begin{aligned} G_{i,n,t} \leq & P^{on}_{i,n,t} - PCR_{i,n,bp|t \in bp} - SCR^{pos}_{i,n,bs|t \in bs} \\ & \forall bp \in BP, bs \in BS, i \in I, n \in N, t \in T \end{aligned} \tag{3.8}$$

$$G_{i,n,t} \geq P^{on}_{i,n,t} \cdot g^{min}_{i} + PCR_{i,n,bp|t\in bp} + SCR^{neg}_{i,n,bs|t\in bs} \quad \forall bp \in BP, bs \in BS, i \in I, n \in N, t \in T \tag{3.9}$$

The running capacity of a power system is limited by the installed capacity ($cap_{i,n,t}$) in combination with either the availability factor ($af_{i,n,t}$) or power plant outages ($out_{i,n,t}$), as shown in Formula (3.10). For thermal generation capacities, we use hourly power plant outages. Renewables are provided with an hourly availability factor and hydroelectric units with a monthly availability factor.

$$P^{on}_{i,n,t} \leq cap_{i,n,t} \cdot af_{i,n,t} - out_{i,n,t} \qquad \forall i \in I, n \in N, t \in T \tag{3.10}$$

Formula (3.11) tracks start-up activities ($SU_{i,n,t}$) that increase the running capacity from one hour to another. Due to the non-negativity condition, start-ups are either positive or zero.

$$P^{on}_{i,n,t} - P^{on}_{i,n,t-1} \leq SU_{i,n,t} \qquad \forall i \in I, n \in N, t \in T \tag{3.11}$$

The delta between available feed-in from intermittent renewables and their actual generation defines the curtailment of renewables ($CURT_{res,n,t}$), given by

$$cap_{res,n,t} \cdot af_{res,n,t} = G_{res,n,t} + CURT_{res,n,t} \qquad \forall res \in I, n \in N, t \in T. \tag{3.12}$$

Some power plants are active in the heat market in addition to the electricity market. The model thus implements a must-run condition for such units on the electricity market, which varies over time (e.g., higher in the winter season due to space heating). Depending on hourly heat demand, Formula (3.13) states that the output of a combined heat and power unit is at least equal to the electricity generation linked to the heat production ($chp_{i,n,t}$):

$$chp_{i,n,t} \leq G_{i,n,t} \qquad \forall i \in I, n \in N, t \in T. \tag{3.13}$$

The cross-border electricity transfer ($FLOW_{n,nn,t}$) is constrained by the net transfer capacity ($ntc_{n,nn,t}$):

$$FLOW_{n,nn,t} \leq ntc_{n,nn,t} \qquad \forall n, nn \in N, t \in T. \tag{3.14}$$

Formula (3.15) describes the state of the storage level of a mid-term storage. It is increased by the generation ($G_{stm,n,t}$) and decreased by the consumption while charging ($ST^{in}_{stm,n,t}$). The efficiency of an entire storage cycle (η_{stm}) is assigned to the charging process.

$$\begin{aligned} &SL_{stm,n,t} = SL_{stm,n,t-1} - G_{stm,n,t} + CM_{stm,n,t} \cdot \eta_{stm} \\ &\forall stm \in I, n \in N, t \in T \end{aligned} \tag{3.15}$$

The maximum energy storage capacity ($SL_{stm,n,t}$) of a mid-term storage is defined by the maximum installed turbine capacity times an energy-power factor (epf), given by

$$SL_{stm,n,t} \leq cap_{stm,n,t} \cdot epf \qquad \forall stm \in I, n \in N, t \in T. \tag{3.16}$$

Restricting the turbine and pumping capacity, the pumping capacity is assumed to be lower than the turbine capacity:

$$G_{stm,n,t} + 1.1 \cdot CM_{stm,n,t} \leq cap_{stm,n,t} \qquad \forall stm \in I, n \in N, t \in T. \tag{3.17}$$

At the beginning and end of each model run, all mid-term storages must be filled with 30 % of their energy level:

$$SL_{stm,n,tfirst} = 0.3 \cdot cap_{stm,n,t} \qquad \forall stm \in I, n \in N, tfirst \in T, \tag{3.18}$$

$$SL_{stm,n,tlast} = 0.3 \cdot cap_{stm,n,t} \qquad \forall stm \in I, n \in N, tlast \in T. \tag{3.19}$$

Long-term storage is not subject to a storage mechanism. However, the electricity generation and consumption of long-term storage units are also restricted by the installed capacity of long-term storage, given by

$$G_{stl,n,t} + CL_{stl,n,t} \leq cap_{stl,n,t} \qquad \forall stl \in I, n \in N, t \in T. \tag{3.20}$$

Formulas (3.21), (3.22) and (3.23) ensure the control power provision for primary, positive secondary and negative secondary control power:

$$\sum_i PCR_{i,n,bp} = pr_n \qquad \forall bp \in BP, n \in N, \tag{3.21}$$

$$\sum_i SCR^{pos}_{i,n,bs} = sr^{pos}_n \qquad \forall bs \in BS, n \in N, \tag{3.22}$$

$$\sum_i SCR^{neg}_{i,n,bs} = sr^{neg}_n \qquad \forall bs \in BS, n \in N. \tag{3.23}$$

The non-negativity constraint is presented in Formula (3.24).

$$\begin{aligned} 0 \leq & CL_{stl,n,t}, CM_{stm,n,t}, CURT_{res,n,t}, G_{i,n,t}, FLOW_{n,nn,t}, P^{on}_{i,n,t}, \\ & PCR_{i,n,bp}, SCR^{neg}_{i,n,bs}, SCR^{pos}_{i,n,bs}, SHED_{n,t}, SL_{stm,n,t}, SU_{i,n,t} \\ & \forall bp \in BS, bs \in BS, i \in I, n \in N, t \in T \end{aligned} \tag{3.24}$$

We use both models presented alternately. To predict the next day, we first forecast the load forecast error with the load forecast improvement model and thus enhance the day-ahead load forecast. As one input data, it enters the power system model, which estimates the next day's prices using the presented approach. This sequence is repeated continuously day by day over the rolling window for all points in time in our observation period.

3.5. Results

This work explores two different methodologies that are combined. It presents a forecast error improvement model for load forecasts based on data from ENTSO-E, and develops the energy system model *em.power dispatch* which is built for day-ahead wholesale price forecasts. We present the results accordingly. First, we show the performance our approach to model the load forecast error. Therefore, we use statistical data and different error measures for various time periods of the enhanced load forecast. With our approach we are able to reduce the RMSE of load forecast error by 22.5 %. Second, we analyse the impact of the improved forecast on the resulting price estimates of the *em.power dispatch*

model. Therefore, we compare the resulting price estimators generated with the original TSOs' load forecast $\hat{L}$ and the enhanced load forecast $\hat{L}^*$ with the actual price observed at the day-ahead market using several error measures: MSE, root mean squared error (RMSE), and mean average error (MAE). We find that during hours with relatively high prices, the usage of improved load forecasts leads to a reduction of prices' forecast mean squared error by nearly 15 %.

3.5.1. Improved Load Data and Achieved Error Reduction

In the following, we quantify the forecast error improvement model described in Section 3.4.1. Therefore, we compare the improved load forecast $\hat{L}^*$ and the TSOs' load forecast $\hat{L}$ with actual load data L. For the error improvement model, we use a rolling window width of one year (i.e., $l_w = 8760$), which yields the lowest (out of sample) error measures compared with a width of three months and six months (see Appendix Table C.3). For this reason, the prediction of the forecast error, and thus the out-of-sample period, begins on January 1st, 2017. Table 3.2 shows the mean and standard deviation as well as the error measures MSE, RMSE and MAE of the TSOs' load forecast and of the enhanced load forecast, and its percentage improvement.

Table 3.2.: Means, standard deviations and error measures (MSE, RMSE, MAE) for the original TSOs' day-ahead load forecast (TSO) and the improved day-ahead load forecast (Impr.). MSE is given in [(MWh)^2], and all other variables in [MWh].

	year	total	2017	2018	2019
mean	TSO	655.98	446.50	298.60	1,222.84
	Impr.	-98.89	-229.06	-36.32	-31.29
std.	TSO	2,125.72	1,746.54	2,341.68	2,128.55
	Impr.	1,743.89	1,465.74	2,043.67	1,665.56
MSE	TSO	4,948,990.80	3,249,416.14	5,572,010.71	6,025,545.56
	Impr.	3,050,928.19	2,200,617.23	4,177,415.90	2,774,751.43
	% Improvement	38.35	32.28	25.03	53.95
RMSE	TSO	2,224.63	1,802.61	2,360.51	2,454.70
	Impr.	1,746.69	1,483.45	2,043.87	1,665.76
	% Improvement	21.48	17.71	13.41	32.14
MAE	TSO	1,691.37	1,396.45	1,726.67	1,951.00
	Impr.	1,253.95	1,106.12	1,372.55	1,283.17
	% Improvement	25.86	20.79	20.51	34.23

While the load was severely underestimated in the TSOs' forecast with a mean of 656.0 MWh, it is slightly overestimated in the improved model with -98.9 MWh. Looking at the individual annual mean values, the high negative value in 2017 is particularly striking. The reason for this is the very strong underestimation of the TSOs' load forecast in 2016, with an average deviation of 1555.4 MWh (see Section 3.3.1). The influence of errors from the year 2016 has a large impact due to the rolling window period of 365 days, especially on the model estimates of the first days and months of 2017. A shorter window period of three months sinks the annual mean value of 2017 but has a minor improvement in error measures (see Appendix Table C.3). The standard deviation of the improved load forecast is lower than the standard deviation of the TSOs' load forecast across all years.

The error measures MSE and MAE given in Table 3.2 show a significant improvement of the load forecast. With a RMSE of 2,224.63 MWh, we achieve a 21.48 % improvement over the TSOs' load forecast for the period from January 1st, 2017, to December 31st, 2019. The most considerable improvement can be observed in 2019 with 32.14 %. A breakdown of the improvement among the components (seasonal and remaining) of the model shows that both the seasonal and remaining component account for a large share of the improvement, and neither component dominates.

Maciejowska et al. (2021) also improve the TSOs' load forecast. From October 1st, 2016, to September 30th, 2019, they achieve an enhancement in RMSE over 365 days from a minimum of 23.71 % to a maximum of 34.38 %. Comparing both, achieving a slightly higher improvement also means using a multivariate modelling framework with six different rolling window widths, and consequently six model estimates and six point forecasts for each hour of the forecast period. Our approach is intended to allow a user with less modelling expertise and computational capacity to enhance the commonly used TSOs' forecast of load. With a less complex, univariate model, we still achieve substantial improvement and thus error measurements that are comparable with error measurements in the literature (e.g., in Do et al., 2016; Ziel, 2018; Li et al., 2021).

To better attribute and understand the effect of load improvement on price, we also determine the percentage improvement in MSE for the hours of the day, and the days of the week, as shown in Figure 3.5. The observed daytime and weekday structures in the

TSOs' load forecast error are also evident in the improvement. During the day, hours two to five and 16 to 20 achieve the most considerable percentage improvement. Weekdays can be improved more than weekends; Tuesdays and Wednesdays show an especially strong improvement. In the TSOs' load forecast, these are the hours and days that have the largest mean error. Therefore, hours and days that have a sizeable mean error are the ones that have the most potential for improvement. Enhancing the load forecast by reducing this error is the primary goal of modelling and predicting the error of the TSOs' load forecast.

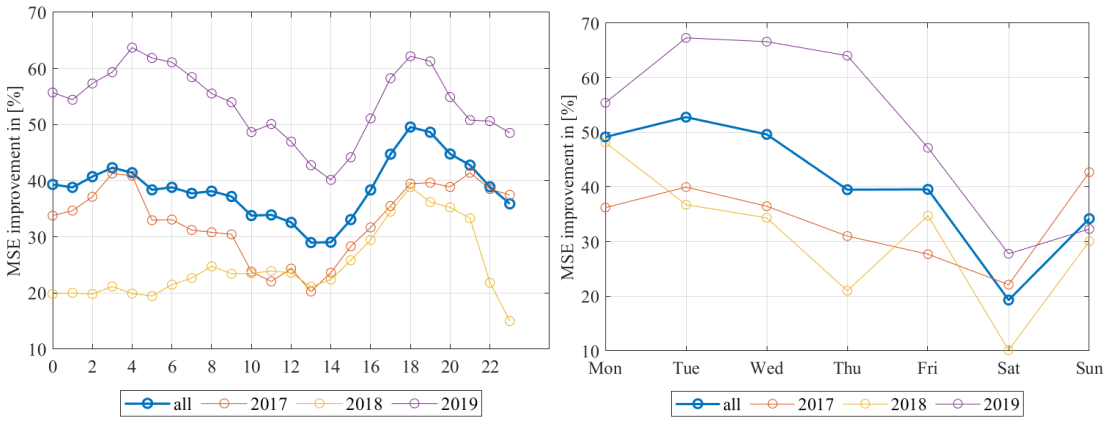

Figure 3.5.: Average percentage MSE improvement for the day-ahead load forecast for each hour of a day (left) and for each weekday (right).

3.5.2. Impact of Improved Load Data on an Energy System Model

In the previous Section 3.5.1, we proved that, with a relatively straightforward approach, the TSOs' load data can be significantly improved. Thus, this approach is particularly suitable for energy system modellers to enhance critical input data. In the following, we quantify the impact of the improved load forecast on day-ahead wholesale price forecasts based on the *em.power dispatch* model. To do this, we run the model twice, first using the original TSO-based load forecasts $\hat{L}$ and second, using the improved load forecasts $\hat{L}^*$ presented in Section 3.5.1. For both cases, we derive estimates of the day-ahead wholesale

electricity prices and calculate error measures comparing the results to actual observed prices.

Using the improved load data set, we see an overall reduction in the error of the price estimators. For the entire time horizon, Table 3.3 states a reduction of the MSE by 1.75 %, the RMSE by 0.88 % and the MAE by 0.42 %.

Comparing our results with those of other models in the same modelling class, we find that our model generates very good price estimates. Qussous et al. (2022), for example, report an MAE of 9.44 €/MWh for 2017, 8.88 €/MWh for 2018 and 6.69 €/MWh for 2019.

Table 3.3.: Error measures for the price estimators of the *em.power dispatch* model comparing the improved load forecasts (Impr.) by original load forecasts (Orig.), given in [$(\text{MWh})^2$] for MSE, in [MWh] for RMSE and MAE.

	total		2017		2018		2019	
	Impr.	Orig.	Impr.	Orig.	Impr.	Orig.	Impr.	Orig.
[1] MSE	89.15	90.73	133.13	135.29	72.47	73.22	61.84	63.70
[2] RMSE	9.44	9.53	11.54	11.63	8.51	8.56	7.86	7.98
[3] MAE	5.94	5.96	6.75	6.80	5.98	6.04	5.09	5.28
Reduction [1]	1.75%		1.62%		1.04%		3.01%	
Reduction [2]	0.88%		0.81%		0.52%		1.49%	
Reduction [3]	0.42%		0.85%		1.02%		3.65%	

Table 3.3 further shows disaggregated error measures by year. It can be seen that an improvement in the error measure is achieved in all three years. However, the magnitude of this improvement varies; the relative error reduction is largest in 2019 and smallest in 2018. This observation correlates with the magnitude of the annual improvement in the load forecast, shown in Figure 3.5.

Furthermore, we analysed whether the improvement of the load estimator and the price estimator correlate with the hour of the day. Figure 3.6 shows the average percentage improvement of the MSE of the day-ahead load prediction per hour of the day (left) and of the day-ahead price estimators (right). It can be seen that an hour's load and hour's price improvement do not correlate. Depending on the respective hour of the day, improvement of load prediction seems to have a different impact on the resulting price estimator.

The reason for this discrepancy is twofold: i) the model is more sensitive in one hour than in another hour, depending on the respective position in the merit order, and ii) an improvement in the load forecast in one hour may affect another hour due to temporal interdependencies such as storage operation and unit commitment decisions.

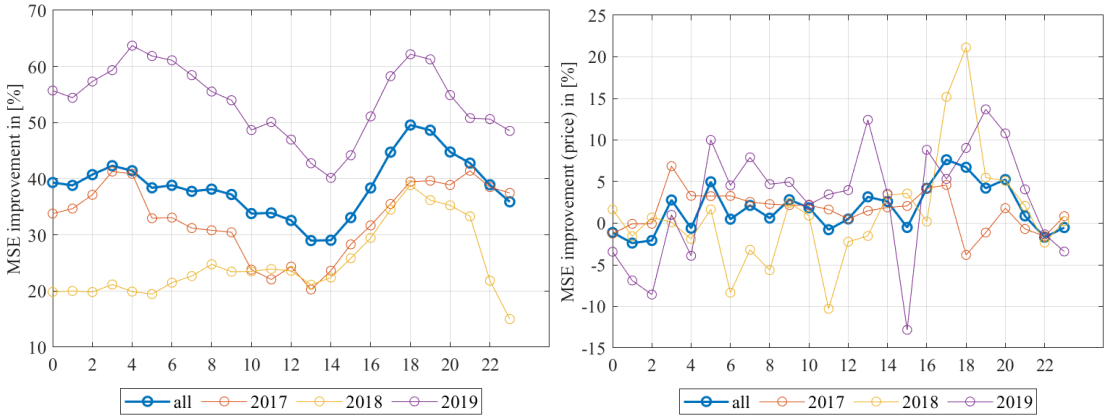

Figure 3.6.: Average percentage MSE improvement of day-ahead load prediction (left) and day-ahead price estimators (right) for each hour of a day.

Having shown that the impact of better load forecasts on price forecasts derived in an energy system model is positive on average but varies between hours, we now examine the extent of error reduction at different points in time, starting with differentiation between high (peak) and low demand (off-peak) periods. Figure 3.7 states the error reduction of the price estimator and of the load forecast for the entire time period and the time categories peak, off-peak, weekdays and weekend days. Peak hours are defined as those between 8 a.m. and 8 p.m. from Monday to Friday, while off-peak hours are all remaining hours. The most considerable error reduction of the price estimators is observed in peak hours and on weekdays in general. In off-peak hours, the effect on the price estimators is relatively low. On weekends, this observation correlates with the improvement of the load data, both of which are at their minimum. However, in off-peak hours, the impact on the price estimator is negligible, despite the great improvement in the load forecast.

As such, the model benefits significantly from improved load input data during peak hours and in total on weekdays, where demand and price levels are generally higher than off-peak hours and especially on weekends.

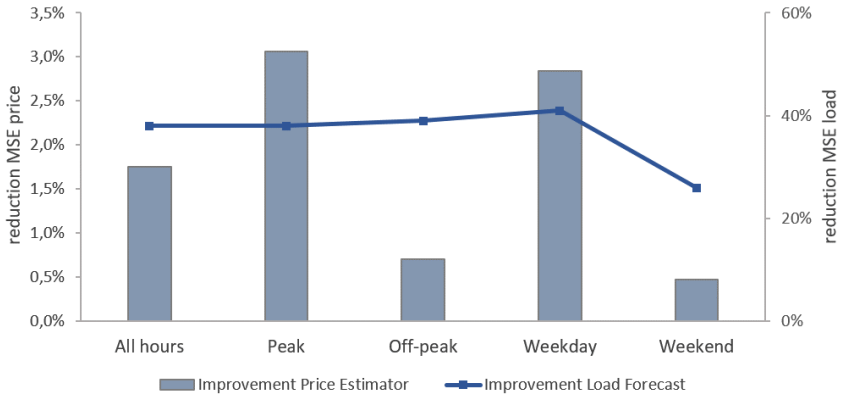

Figure 3.7.: Percentage error reduction of the price estimator and the load in different time periods.

Based on the observation that price forecasts improve more during peak periods than in off-peak periods, we analyse the relation between wholesale price and forecast improvement. Figure 3.8 shows the improvement of the price estimators for five different price segments where electricity prices are equally separated in 20 % quantiles based on their level. The first quantile (q1) represents the lowest 20 % quantile and the last quantile (q5) the highest 20 % quantile of electricity prices of the respective year between 2017 and 2019.

It can be seen that the error reduction of the price estimators is most relevant in hours with high and medium prices. Overall, the largest improvement can be observed in 2018 and 2019 with an MSE reduction of nearly 15 %, here at times with the 60-80 % highest prices. In contrast, the improved load forecast data does not lead to a better price estimator in low-price periods. In all years, we even observe an increasing error in these price ranges. In summary, the improved load forecast is most beneficial for the model in the hours when the market equilibrium is found on the right side in the merit order, i.e., where changes or errors in the demand have the highest price impact.

Figure 3.8.: Relative error reduction of the price estimator in different price segments of the respective year from 2017 to 2019, starting with the lowest 20 % quantile of electricity prices (q1) to the highest 20 % quantile (q5).

Hence, our analysis shows that the price forecasts are generally better when either demand is high or prices are high. As traded volumes (in monetary terms) are the product of prices and volumes, it is interesting to note that price forecast improvement is highest when it matters the most.

3.6. Concluding Remarks

We confirmed the results from previous studies that input data for energy system models, especially day-ahead load forecast data, are biased and inaccurate. Nevertheless, many modellers use them unfiltered. Therefore, we showed to what extent load forecasts can be improved and how improved input data affect the quality of energy system models' results. Thus, this chapter aims at energy system modellers who want to provide empirically meaningful results and therefore need large and accurate data sets.

We presented a simple time series model to improve the TSO-based load forecast data provided by ENTSO-E. The model captures and removes systematic biases and autoregressive structures present in the load forecast errors. Answering the research question, we found that it can be straightforward to improve input data. Using the

example of German day-ahead load forecasts, we were able to reduce the RMSE of the errors by 22.5 %. Since the model is applied to observed forecast errors rather than to the load data itself and does not include load-specific external variables, it can be easily transferred to pre-processing other quantities of interest.

To analyse the effect of enhanced load forecasts on electricity system models, we fed the improved load forecast data into the *em.power dispatch* model. The model is used to generate price estimates for the German day-ahead electricity market, and we presented the structure, assumptions, and optimisation equations of the model in detail. Concerning the effect of sequentially pre-processed inputs, we found that the benefits of sequentially improved load forecasts strongly depend on the respective price level, with more extensive benefits for higher price levels. This is a universal result in line with fundamental theory since the impact of load changes on price changes increases with the overall level in merit order markets. The work showed that in phases of relatively high prices, as in 2018 and 2019, the continuous and sequential, i.e., day-by-day, load data pre-processing led to an average reduction of *em.power dispatch*'s prices forecast MSE by nearly 15 %. Hence, our analysis demonstrated that forecasts tend to be more accurate with stochastic data pre-processing when the demand and prices are high. As the value of traded energy is the product of prices and volumes, the accuracy of forecasts is enhanced most when it matters the most. With this analysis, we proved that the quality of the model results benefits from better data input.

Based on these findings, we recommend energy system modellers to carefully analyse not only the structure and equations of their models but also the quality of input data. We demonstrated in the empirical setting of the German wholesale electricity market that input data can be improved significantly and that these improvements can be achieved with straightforward time series models. Furthermore, we showed that the results of the energy system model benefited from the improved input data.

Although our results are generalised, further research should extend our analysis by evaluating the impact of better load forecasting using different energy system models and models that focus on markets other than Germany. Furthermore, scholars may investigate the quality of other input parameters, such as wind and PV generation forecasts. Modellers focusing on, for example, CO_2 emissions or the use of power plants

and energy storage can also use our approach and analyse how the quality of their results can be improved.

In the next chapter, we extend the idea of improving a forecast by forecasting the forecast error within an approach to calculate point and probabilistic forecasts of the error of short-term forecasts of various target variables.

4. Forecast the Forecast Error: Improving Point Forecasts and Generating Density Forecasts in Energy Markets

This chapter is based on Watermeyer and Scheller (2023)[1].

4.1. Introduction

Forecasting plays a crucial role in the energy sector, enabling financial and operational decisions and regulatory interventions. Day-ahead forecasts are particularly critical for developing supply strategies and production plans that maximise a company's margins and ensure reliable grid operations. Forecast errors in the short-term electricity market can have significant financial and operational impacts on all market participants.

However, with the advent of smart grids, the growth and integration of renewable energy sources, and fluctuating commodity prices that increase uncertainty in future supply, demand and prices, forecasting is becoming increasingly complex. It is crucial to quantify the uncertainty caused by forecast errors and to take this into account when making decisions. Doing so not only minimises the risk of losses and wrong decisions but also provides a significant competitive advantage for companies in power system planning and operations (Nowotarski and Weron, 2018; Hong et al., 2016, 2020), leading to better

[1]The work was supported by the German Federal Ministry of Economic Affairs and Climate Action through the research project "ProKoMo - Better price forecasts in the energy sector by combining fundamental and stochastic models" within the Systems Analysis Research Network of the 6th energy research program.

market positions and increasing profits for companies. Therefore, accurately forecasting and quantifying uncertainty is more important than ever in the energy sector.

In many cases, the time series of forecast errors, i.e., the difference between the actual and the forecasted value, exhibit predictable structures like seasonality and autocorrelation (Weron and Ziel, 2019). To optimise the prediction model, it is essential to analyse the prediction errors. For example, Maciejowska et al. (2021) develop enhanced day-ahead load and wind generation forecasts including day-ahead load and wind generation forecasts which are made available by the transmission system operators (TSOs). Schön et al. (2019) present a model for the prediction of thunderstorms by using the prediction error of a first prediction model as a feature for a second, different prediction model, and Yang et al. (2013) develop a two-stage approach for day-ahead load forecasts, removing structures in the forecast error of their first stage Seasonal Autoregressive Integrated Moving Average (SARIMAX) model in modelling the forecast error with a neuronal network in a second stage. Forecasting day-ahead electricity prices, Kontogiannis et al. (2022) develop a deep neuronal network (DNN) with an additional autoregressive module to compensate for errors by forecasting them and thus improving the forecast of the DNN. Angamuthu Chinnathambi et al. (2019) analogous develop a two-stage approach for hourly electricity spot price forecasts, predicting first the prices with an ARIMA model and second the residuals of this forecast with a Generalised Linear Model (GLM), alternatively with a Support Vector Machine (SVM) to enhance forecast accuracy.

Although improving point forecasts can help reduce losses and erroneous decisions, e.g., in hedging a portfolio based on wrong expectations, forecast errors remain an inherent risk and mean uncertainty for market participants. Effective risk management strategies such as diversification and hedging mitigate the impact of forecast errors. In addition, understanding the limitations and uncertainties of forecasts can help market participants to make more informed decisions and to avoid over-reliance on imperfect predictions.

To address this issue, approaches in various fields have been developed to model the uncertainty of forecast errors with probabilistic forecasts, e.g., by Krüger and Nolte (2016) and Clark et al. (2020). In general, probabilistic forecasting is quite young for predicting energy market variables. The Global Energy Forecasting Competition (GEFCom2014) served as a catalyst for the growing interest in recent years (see Hong et al., 2016,

2020). Gneiting and Katzfuss (2014) provide a review of the method of probabilistic forecasting, and Nowotarski and Weron (2018) overview the different applications of historical simulation, distribution-based prediction intervals and Quantile Regression Averaging (QRA) approaches to generate probabilistic wind generation, load and price forecasts. QRA was first used by Nowotarski and Weron (2015) to predict different quantiles of the response variable by combining predictions from multiple quantile regression models. Since QRA estimates the predictive distribution in a data-driven way and takes point predictions into account, it is not only based on historical data. Thus, the approach becomes less sensitive to structural changes in the data than other methods, e.g., historical simulation (Nowotarski and Weron, 2015). Manner et al. (2019) propose another approach for quantile forecasting in developing a dynamic vine copula approach to predict the joint distribution of the day-ahead prices of interdependent electricity markets. To improve energy forecasts with prediction intervals, Kaack et al. (2017) compare the forecast performance of different empirical density forecasting methods. While Muniain and Ziel (2020) and Phipps et al. (2022) estimate uncertainties of wind generation forecasts and Ludwig et al. (2022) of load and wind generation forecasts, Grothe et al. (2023a) propose a method for generating multivariate probabilistic forecasts by modelling cross-hour dependencies. Their approach is applied to existing point forecasts. Also, Janke and Steinke (2020) generate probabilistic forecasts in a post-processing step. A hybrid model combining point and probabilistic forecasting in four steps is developed by Maciejowska and Nowotarski (2016) and by Watermeyer et al. (2023). The latter quickly applies the idea presented here in developing a hybrid model for day-ahead price forecasts.

In this chapter, we propose a novel approach to improve the accuracy of day-ahead electricity market quantity forecasts by forecasting prediction errors. Our methodology is grounded in fundamental principles and based on deep and comprehensive analyses, making it robust and generally applicable. Through the detailed analyses of forecast errors resulting from model imperfections, we identify patterns and quantify the uncertainty of forecasts. By incorporating this information into the underlying quantity forecasts, our methodology leads to more accurate and reliable day-ahead forecasts, making it a valuable tool for power system planning and operations. It enables companies to make accurate

financial and operational decisions and regulatory interventions, ensuring reliable grid operations and maximising their margins.

Our approach uses univariate and multivariate seasonal time series models and combinations of these to predict the time series of forecast errors $\varepsilon_{d,h},\ h = 1, ..., 24,\ d = 1, ..., D$. We interpret the forecast errors as an hourly, high-frequency time series and as 24 daily time series, referring each to one hour of the day. Models for both approaches are based on ARMA models, where past values explain future values. By averaging over arbitrary hyperparameters, such as rolling window sizes, the framework becomes robust to random missteps by potential users.

Training a model to explain and forecast prediction error patterns can be beneficial in terms of forecast accuracy. An improved day-ahead point forecast $\widehat{Y}_{d,h}$ at hour h and day d can be obtained by adding the day-ahead forecast of the prediction error $\hat{\varepsilon}_{d,h}$ to the initial point prediction (see Brockwell and Davis, 2016):

$$\widehat{Y}_{d,h} = \hat{Y}_{d,h} + \hat{\varepsilon}_{d,h},\ h = 1, ..., 24, d = 1, ..., D. \tag{4.1}$$

Additionally, through forecasting prediction errors, we can generate probabilistic forecasts. Therefore, we combine individual point forecasts of the forecast error using QRA and, on their basis, forecast the quantiles $q, q \in (0, 1)$ of the forecast error individually for each hour. Forecasting these quantiles corresponds to the estimation of the discrete predictive cumulative distribution function of the prediction error $\varepsilon_{d,h}$, which is directly connected with the predictive cumulative distribution function of the quantity $Y_{d,h}$ at time (d, h):

$$\hat{F}^{-1}_{Y_{d,h}}(q) = \hat{Y}_{d,h} + \hat{F}^{-1}_{\varepsilon_{d,h}}(q)\ with\ h = 1, ..., 24, d = 1, ..., D. \tag{4.2}$$

By estimating probabilistic forecasts and prediction intervals, our approach allows market participants to account for the risk of forecast inaccuracy.

The presented approach can be adapted to various applications in the energy sector. We demonstrate our approach for three real data examples using a day-ahead electricity price forecast, a day-ahead load forecast, and a day-ahead wind generation forecast. We analyse the results in detail and illustrate the value of the additional information

the generated point and density forecasts added. By making the source code publicly available, we enable others to forecast prediction errors of their forecasts and tailor the model to their needs.

The remainder of the chapter is structured as follows. Section 4.2 describes which data are suitable for using our presented approach. It also contains all the data details of the three exemplary model applications. In Section 4.3, we first explain the methodology of improving hourly short-term predictions in forecasting the forecast error and then of generating probabilistic forecasts for the forecast error. Afterwards, we present methodologies for evaluating point and density forecasts in detail in Section 4.4. A proof of concept is given in Section 4.5 analysing and describing the results of our approach implemented for the TSOs' day-ahead load forecast error, the TSOs' wind generation forecast error and the error of a day-ahead electricity price forecast which is generated with the LEAR benchmark model introduced by Lago et al. (2021). In Section 4.6, we provide exemplary use cases for probabilistic forecasts. We conclude this chapter in Section 4.7.

4.2. Data

In this section, we define the generally necessary input data to apply the presented methodology for the point and probabilistic forecast of prediction errors. Furthermore, we describe the data used for the model validation.

We validate our approach and demonstrate its versatility by providing three real data examples of its application. These examples present how our approach can be used to improve point forecasts and generate density forecasts for a wide range of target variables. Suppose that a quantity $Y_{d,h},\ h = 1, ..., 24, d = 1, ..., D$ is observed hourly over days D and aimed to be predicted in a day-ahead setting. For that purpose, initial point forecasts $\hat{Y}_{d,h},\ h = 1, ..., 24, d = 1, ..., D$ for the target variable, calculated with some model, are already given. The forecast's accuracy is assessed by comparing the forecasts with their corresponding observations as soon as the latter is available. For a forecasting model with an additive prediction error, subtracting the forecast from the observation for each

point in time yields the prediction error time series:

$$\varepsilon_{d,h} = Y_{d,h} - \hat{Y}_{d,h}, \;\; h = 1, ..., 24, d = 1, ..., D. \tag{4.3}$$

We first produce forecasts of the German TSOs' day-ahead wind generation forecast error using data from 2019 to 2022. The transparency platform of the European Network of Transmission System Operators for Electricity (ENTSO-E) provides the forecast and actual wind generation data (ENTSO-E Transparency Platform, 2023a,c).

Second, we use the German TSOs' hourly day-ahead electricity load forecast and load observations from 2019 to 2022. Again, the data are provided by the ENTSO-E transparency platform (ENTSO-E Transparency Platform, 2023e).

Third, we apply our approach to the errors of a price forecast for the German day-ahead electricity spot market[2] generated with a LEAR model. The model's day-ahead price forecast developed by Lago et al. (2021) is one of the most accurate in current research, especially for statistical time series modelling. Since its source code is freely available via the Python™ package *epftoolbox*, we fit the model with the same data sources used by Lago et al. (2021), extended for years 2016 up to 2020. The actual day-ahead electricity prices for this period and bidding zone are available on the transparency platform (ENTSO-E Transparency Platform, 2022).

4.3. Methodology

This section presents the components of the forecast error model, starting with the methodology for point forecasting the forecast error and improving the quantity's point prediction in Section 4.3.1. Afterwards, we introduce the approach for probabilistic forecasting the forecast error in Section 4.3.2. On a GitHub repository (*https://github.com/MWaterm/Forecast-the-forecast-error*), we provide the entire source code of the presented model, implemented as a ready-to-use application.

[2]The German electricity spot market is understood as the joint bigging zone of Germany and Luxembourg since October 1st, 2018, and of Germany, Luxembourg and Austria before.

4.3.1. Point Forecast

The day-ahead prediction error model estimates the time series $\varepsilon_{d,h},\ h = 1, ..., 24$ and $d = 1, ..., D$. Please note that in the following, if $h - 1$ is equal or smaller than zero, we have to shift one day backwards, and if $h + 1$ is bigger than 24, we have to shift one day ahead. The error prediction model aims to capture structures not explained by the given day-ahead forecast model. Therefore, we combine several successful approaches in day-ahead energy forecasting, focusing on seasonality and dependency modelling by combining uni- and multivariate models as well as multiple training data lengths.

Seasonally recurring patterns are often observed in energy and forecast error time series. Hence, we decompose the forecast error time series $\varepsilon_{d,h}$ into a seasonal component $\varsigma_{d,h}$, which is characterised by a recurring behaviour after a known period δ, measured in days, and a remaining noise component $\nu_{d,h}$ (among others, see, e.g., Brockwell and Davis, 2016; Lütkepohl, 2005; Hyndman and Athanasopoulos, 2021; Box et al., 2015):

$$\varepsilon_{d,h} = \varsigma_{d,h} + \nu_{d,h}. \tag{4.4}$$

To deseasonalise the forecast error time series, we consider weekly recurring patterns and holiday effects by applying the classical decomposition algorithm. Here, the seasonal component $\varsigma_{d,h}$ is determined by

$$\varsigma_{d,h} = \sum_{wd=1}^{7} \sum_{\tilde{h}=1}^{24} HoW_{d,h}^{\tilde{h},wd} \cdot HS^{\tilde{h},wd}, \tag{4.5}$$

where $HS^{\tilde{h},wd}$ is the average of the forecast errors for the hour $h = 1, ..., 24$ and weekday $wd = 1$ (Monday), ..., 7 (Sunday), and $HoW_{d,h}^{\tilde{h},wd}$ describes dummy variables to address the hour of the day and the day of the week. If the prediction error time series is already deseasonalised and thus, does not contain seasonal patterns, the seasonal component $\varsigma_{d,h}$ is set to zero. Otherwise, we assume $\varsigma_{d,h} \neq 0$ and calculate the seasonal component by Formula (4.5). According to Formula (4.4), the estimates of the seasonal component are subtracted from the corresponding prediction errors, and the component $\nu_{d,h}$ remains.

For this remaining noise component, we combine a univariate model, which describes the forecasting error time series as a whole, and a multivariate model where every hour

of the day is modelled separately, motivated by an extensive study of Ziel and Weron (2018b). They provide evidence that there is no out-performance of one model type compared to the other across different data sets, seasons of the year and hours of the day. For the univariate case we choose an ARMAX(p, q) model introduced by Box and Jenkins (1970), with $p \in \{1, 2, 24, 168\}$, $q = 1$, given by

$$\begin{aligned}
\nu_{d,h} =& \phi_0 + \phi_1 \nu_{d,h-1} + \phi_2 \nu_{d,h-2} + \phi_3 \nu_{d-1,h} + \phi_4 \nu_{d-7,h} + \omega_1 \xi_{d,h-1} && (4.6)\\
&+ \omega_1 \cdot \nu_{min,d-1} + \omega_2 \cdot \nu_{max,d-1} + \omega_3 \cdot M_{h,d} && (4.7)\\
&+ \sum_{m=0}^{k} \omega_{m+3} X_{m,d,h} && (4.8)\\
&+ \xi_{d,h}, && (4.9)
\end{aligned}$$

where $\{\xi_{d,h},\ h = 1, ..., 24, d = 1, ..., D\} \sim WN(0, \sigma^2)$. The AR and MA terms are represented in (4.6). Thereby, the autoregressive order $p \in \{1, 2\}$ aims to capture the information contained in the forecasting errors of the two previous hours, $p = 24$ captures daily and $p = 168$ weekly recurring patterns. In (4.7), the first three exogenous variables describe the prior day's minimum and maximum forecast error value ($\nu_{d-1,min}, \nu_{d-1,max}$) and a dummy variable $M_{d,h}$ indicating public holidays. Depending on the forecast error, in (4.8), further exogenous variables $X_{m,d,h}$ with $m = 0, ..., k$, $k \in \mathbb{N}_0$, which increase the forecast error's forecast performance, can be included, e.g., a day-ahead load forecast for modelling the price forecast error.

For the multivariate model approach, we split the data into 24 forecasting error time series, each representing one hour of the day. Each of them is modelled with a separate ARX(p) model, $p \in \{1, 2, 7\}$:

$$\begin{aligned}
\nu_{d,h} =& \phi_0 + \phi_1 \cdot \nu_{d-1,h} + \phi_2 \cdot \nu_{d-2,h} + \phi_3 \cdot \nu_{d-7,h} && (4.10)\\
&+ \omega_1 \cdot \nu_{d,h-1} + \omega_2 \cdot \nu_{d-1,min} + \omega_3 \cdot \nu_{d-1,max} + \omega_4 \cdot M_{d,h} && (4.11)\\
&+ \sum_{m=0}^{k} \omega_{m+4} X_{m,d,h} && (4.12)\\
&+ \xi_{d,h}. && (4.13)
\end{aligned}$$

Here, (4.10) represents the AR terms, where $p \in \{1, 2\}$ aims to capture the information contained in the forecasting errors one day and two days before the current point in time and $p = 7$ models weekly recurring patterns. The exogenous variables in (4.11) are similar to the ones incorporated in the multivariate model. In addition, they contain the prediction errors of the hour before the modelled one, $\nu_{d,h-1}$. Thereby, the otherwise independent 24 models for each hour are interconnected. For the additional exogenous variables $X_{m,d,h}$ with $m = 0, ..., k$ in (4.12), we assume $k \in \mathbb{N}_0$, so other variables that influence the level of the prediction error can be included.

The sub-models are estimated on a rolling window approach to calculate individual forecasts, where the window length l is set to an integer multiple of 24 to contain full days only. The window is rolled over by full days in each step to ensure that the prediction of forecast errors for all periods of one day is based on the same estimated model parameters, with l training observations used to estimate the model's parameters. Recursive predictions are made for the next day's periods, and unavailable values are replaced with recursively forecasted values.

To ensure data availability for day-ahead forecasts, the model uses observations up to yesterday's last hour as inputs when predicting tomorrow's values. Values of today's hours ($l+1$ to $l+24$) are replaced by forecasts based on yesterday's values. The day-ahead forecast of the forecast error is covered in the forecast values $l + 25$ to $l + 48$. Forecasting day-ahead electricity price prediction errors draws an exception because today's electricity prices are already known due to the bidding system of the spot markets. Therefore, values of the next day's 24 hours can be predicted directly. Our model takes this into account, and the forecast values for hours $l + 1$ to $l + 24$ describe the forecast for the next day.

We vary the training data length by performing parameter estimations and calculating forecasts for n different window lengths, as shown to be effective in the literature (see Marcjasz et al., 2018). Note that the rolling window lengths can be specified individually for flexibility. In doing so, for each hour, we get $2n$ individual forecasts of the forecast error, which are derived from the n univariate and the n multivariate model estimations. Since the combination of individual forecasts leads to more accurate point forecasts, we average the $2n$ individual forecasts for the final point forecasts of the prediction errors. We use a

non-weighted average approach as well as optimal weights $\hat{w}_h^{(i)}, h = 1, ..., 24, i \in (1, ...2n)$ calculated by a non-negative least-squares regression approach. Due to the use of different model frameworks, the informative value of the individual sub-models with regard to the forecast error can vary depending on the hour of the day. For this reason, the regression approach relates the individual point forecasts of an hour of the day and the actual observations of the forecast error of an hour of the day, given for $h = 1, ..., 24$ by

$$\begin{aligned} &\varepsilon_{d,h} = w_h \cdot Z_{(d,h)}, \\ &w_h^i \geq 0 \quad \forall i \in (1, ...2n), \end{aligned} \tag{4.14}$$

where $Z_{(d,h)} = [\hat{\varepsilon}_{d,h}^{(1)}, \hat{\varepsilon}_{d,h}^{(2)}, ..., \hat{\varepsilon}_{d,h}^{(2n)}]$ contains the $2n$ individual point predictions from the uni- and multivariate models for time (d, h), and w_h is the vector of weights of the individual sub-models. For one forecast day, we thus set up 24 regression approaches and calculate 24 different sub-model weights. The coefficients $w_h^{(i)}$ of all 24 regressions are estimated by a historical data window rolled over full days. The window length is set to the maximum of the window lengths which are used to estimate the individual sub-models.

For each individual target variable, the final point prediction is determined by the averaging method that triggers the more accurate prediction relative to the root mean squared error (RMSE). The more volatile the optimal weighting of the individual error point predictions, the more likely it is that the unweighted approach will provide the best solution. Estimating optimal weights with a regression approach introduces additional noise, which increases inaccuracy, especially for volatile weights, and can lead to inefficiencies (see, e.g., DeMiguel et al., 2009). In this case, we follow the more robust method of non-weighted averaging the $2n$ individual forecasts. In the other one, we use the approach of optimal weight calculation. Concluding, accurate point forecasts of the prediction error can significantly improve the initial day-ahead forecast of the target variable, as shown in Formula (4.1).

4.3.2. Probabilistic Forecast

Next, the $2n$ individual point forecasts are combined to derive valuable probabilistic forecasts that capture the uncertainty associated with the forecast error. A detailed description of the methodology is given in this subsection.

The predictive cumulative distribution function $\hat{F}_{\varepsilon_{d,h}}$ of the prediction error $\varepsilon_{d,h}$ describes the estimation of the true cumulative distribution function. By applying quantile regression to the pool of point forecasts $\hat{\varepsilon}_{d,h}$ of the prediction error $\varepsilon_{d,h}$ at time (d,h), we discretely estimate the predictive distribution at multiple quantile levels q, $q \in (0,1)$. The conditional q-th quantile is modelled by

$$Q_{\varepsilon_{d,h}}(q|X_{d,h}) = X_{d,h}\beta_q, \tag{4.15}$$

with $Q_{\varepsilon_{d,h}}(q|\cdot)$ being the prediction error at the q-th quantile, conditional on additional information, and $X_{d,h}$ the vector of regressors. Here, $X_{d,h} = [1, \hat{\varepsilon}^{(1)}_{d,h}, \hat{\varepsilon}^{(2)}_{d,h}, ..., \hat{\varepsilon}^{(2n)}_{d,h}]$ contains the value one for the intercept and the $2n$ point forecasts for the prediction error from the uni- and multivariate models for time (d,h), and $\varepsilon_{d,h}$ is the observed, externally given prediction error at the time (d,h). The variable β_q describes the vector of parameters for the q-th quantile, which is estimated by minimising the pinball loss function of this particular q-th quantile, as shown in Formula (4.16) and done by Nowotarski and Weron (2015):

$$\hat{\beta}_q = \arg\min_{\beta} \Big[\sum_{\{(d,h):\varepsilon_{d,h} \geq X_{d,h}\beta\}} (q - \mathbf{1}_{\varepsilon_{d,h} < X_{d,h}\beta})(\varepsilon_{d,h} - X_{d,h}\beta) \Big], \tag{4.16}$$

where $\mathbf{1}$ is the indicator function.

The coefficients of the regressors are estimated by a calibration window of one year, rolled over by full days to ensure that the day-ahead probabilistic predictions of the forecast error for one day are based on the same estimated vector. Note that we have tested different calibration window lengths for different quantities. While shorter windows resulted in less accurate predictions, longer windows did not increase the accuracy significantly.

4.4. Evaluation Methods

This section describes the methodologies used to evaluate the presented approach. It includes the improvement of the initial day-ahead forecast of the target variable, which is achieved through the forecast error's point forecast with the forecast error model in Section 4.4.1, and the probabilistic predictions of the forecast error in Section 4.4.2.

4.4.1. Point Forecast Evaluation

We introduce performance criteria to evaluate the point forecasts and the improvement of the initial day-ahead forecast. We focus on the mean absolute error (MAE) and the RMSE defined as the square root of the mean squared error (MSE).

The theoretical foundation of these criteria are scoring functions S. They evaluate how accurate the point predictions $\hat{\varepsilon}_{d,h}$, $\hat{Y}_{d,h}$ and $\widehat{Y}_{d,h} = \hat{Y}_{d,h} + \hat{\varepsilon}_{d,h}$ are relative to the realisations $\varepsilon_{d,h}$ and $Y_{d,h}$. Scoring functions depend on the observation and its forecast and are negatively oriented, meaning that a smaller value indicates a more accurate forecast (Gneiting, 2011). The two scoring functions used in this work are the squared error (SE) with $SE(Y_{d,h}, \hat{Y}_{d,h}) = (Y_{d,h} - \hat{Y}_{d,h})^2$ for the RMSE and the absolute error (AE) with $AE(Y_{d,h}, \hat{Y}_{d,h}) = |Y_{d,h} - \hat{Y}_{d,h}|$ for the MAE. Taking the mean over all forecast points T yields the general form of the performance criteria RMSE and MAE that are used for ranking point forecasts from the different models (Gneiting, 2011):

$$\bar{S} = \frac{1}{T} \sum_{\tilde{d}=1}^{T/24} \sum_{h=1}^{24} S(\hat{Y}_{\tilde{d},h}, Y_{\tilde{d},h}). \tag{4.17}$$

Note that mean forecasts, i.e., forecasts where the parameters of the underlying model have been estimated by a least squares approach and thus by minimising the sum of $SE(\cdot)$, should focus on the MSE or RMSE as consistent performance criteria. For median forecasts, i.e., forecasts where the parameters have been estimated by minimising the sum of the absolute deviation $AE(\cdot)$ between estimated and observed values, the MAE is the consistent performance criteria choice (Gneiting, 2011). Although our model produces mean forecasts for the forecast error, the underlying input forecast $\hat{Y}_{d,h}$ for the

quantity $Y_{d,h}$ can be both a mean and a median forecast. For this reason, we report both performance criteria.

In addition, we provide the arithmetic mean over specific forecast points, calculating a yearly, a weekday and an hourly RMSE and MAE to make the performance more transparent across years, days and hours.

We want to emphasise that even though percentage errors like the well-known mean absolute percentage error (MAPE) have the advantage of making it possible to compare errors across different data sets (see, e.g., Petropoulos et al., 2022), they have the drawback of becoming very large when the values of the observations are close to zero, and very small in case of spikes, regardless of the actual absolute errors. For observations that take negative values, the percentage errors can take negative values too and become hard to interpret (Weron and Ziel, 2019). As we aim to stay in a general setting with the option of correcting different day-ahead forecasts for energy variables, we refrain from using percentage errors.

To analyse the statistical significance of the difference in forecast performance between the enhanced point forecast $\widehat{Y}_{d,h}$ and the underlying input forecast $\hat{Y}_{d,h}$, we use a modified Diebold-Mariano (DM) test (Diebold and Mariano, 1995), as recommended by Lago et al. (2021). The test first measures the difference in the accuracy of two models M_1 and M_2 by calculating the difference δ of each model's MSE in Formula (4.18), and then performs two one-sided hypothesis tests to determine whether the difference in the MSE is statistically significant. First, the null hypothesis H_0 is defined by the expected MSE difference $E(MSE_{M_1} - MSE_{M_2})$ being smaller or equal to zero. Second, the alternative hypothesis H_1 is defined by the expected MSE differential being bigger or equal to zero. If the null hypothesis is rejected and the alternative hypothesis is accepted, it suggests that model M_1 is more accurate than the other. To determine which model is more accurate than the other at which significance level, i.e., at which probability of a correct statement, we report the p-values of the hypothesis tests.

$$\begin{aligned} \delta_{d,h} &= (Y_{d,h} - \hat{Y}_{d,h})^2 - (Y_{d,h} - \widehat{Y}_{d,h})^2 \\ &= \varepsilon_{d,h}^2 - \xi_{d,h}^2 \end{aligned} \tag{4.18}$$

We perform the DM test jointly for all hours, calling it multivariate (see, e.g., Ziel and Weron, 2018b; Lago et al., 2021), and independent for every hour of the day (univariate), meaning 24 independent tests (see, e.g., Lago et al., 2021), by using the implemented test algorithm in the *epftoolbox* of Lago et al. (2021). The first version gives us a qualitative, clear comparison of the forecasts over the entire period, while the second version provides detailed information on the individual accuracy per hour.

4.4.2. Probabilistic Forecast Evaluation

Probabilistic forecasting aims to construct predictive distributions that maximise sharpness subject to calibration (Gneiting and Katzfuss, 2014). Calibration refers to the accuracy of a probabilistic forecast regarding the actual occurrence of events relative to the predicted probabilities. A forecast is said to be well calibrated if the predicted probabilities match the observed frequencies and thus, for example, if a $(1-\alpha)$ prediction interval covers indeed $(1-\alpha) \times 100\,\%$ of the observed variable for which the prediction interval is constructed (Gneiting and Katzfuss, 2014; Diebold and Mariano, 2002; Nowotarski and Weron, 2018). Sharpness, however, refers to the degree of concentration and spread of the predicted probabilities. A forecast is said to be sharp if it assigns high probabilities to a small number of possible outcomes and low probabilities to the rest (Gneiting and Katzfuss, 2014; Diebold and Mariano, 2002).

One way to assess calibration and sharpness simultaneously is through scoring rules. Like scoring functions, they are numerical and negatively oriented penalties that aim to be minimised. The most commonly used scoring rule is the continuously ranked probability score (CRPS). It is specified directly in terms of the predictive cumulative distribution function $\hat{F}$ and the observation ε. One can show that the CRPS can be expressed as an integral over linear quantile scores $PL(\cdot)$ at different quantile levels:

$$CRPS(\hat{F}, \varepsilon) = \int_0^1 PL(\hat{q}_{\alpha,\varepsilon}, \varepsilon, \alpha) d\alpha, \tag{4.19}$$

with $\hat{q}_{\alpha,\varepsilon}$ being the quantile function and ε being the observed prediction error (Nowotarski and Weron, 2018). The linear quantile score defined as pinball loss (PL) is given by

$$PL(\hat{q}_{\alpha,\varepsilon}, \varepsilon, \alpha) = \begin{cases} (1-\alpha)(\hat{q}_{\alpha,\varepsilon} - \varepsilon) & \text{for } \varepsilon < \hat{q}_{\alpha,\varepsilon} \\ \alpha(\varepsilon - \hat{q}_{\alpha,\varepsilon}) & \text{for } \varepsilon \geq \hat{q}_{\alpha,\varepsilon} \end{cases} \tag{4.20}$$

(Weron and Ziel, 2019). Thus, the CRPS can be approximated by calculating the average linear quantile scores at several equally spaced levels (Nowotarski and Weron, 2018).

We report the CRPS for the entire forecast period jointly for all hours and individually for each hour. In comparing the 24 probabilistic forecast error forecasts, we provide a deeper analysis of forecast accuracy and the level of uncertainty for the hours of the day.

Additionally, we evaluate the density forecast's calibration in isolation by applying the Probability Integral Transform (PIT) proposed by Dawid (1984). The PIT is the random variable $PIT_{d,h} = \hat{F}_{\varepsilon_{d,h}}(\varepsilon_{d,h})$, where $\hat{F}_{\varepsilon_{d,h}}$ is the fixed, nonrandom predictive cumulative distribution function for an observed forecast error $\varepsilon_{d,h}$. If $\hat{F}_{\varepsilon_{d,h}}$ is continuous and $\varepsilon_{d,h} \sim \hat{F}$, $PIT_{d,h}$ is standard uniform. The other way around, the probabilistic cumulative distribution function $\hat{F}_{\varepsilon_{d,h}}$ is probabilistically calibrated if $PIT_{d,h}$ has a standard uniform distribution. In the case of non-uniformity, U-shaped histograms indicate that the tails of the predictive distribution are not heavy enough, and inverse U-shaped histograms correspond to predictive distributions with too fat tails (see, e.g., Gneiting and Katzfuss, 2014).

4.5. Real Data Examples and Validation

This section provides validation of our forecast error model by three real data examples of load, price and wind generation forecast errors. The results of the three applications of our forecast error model are presented in two parts. In Section 4.5.1, we evaluate the generated point forecasts for the three time series of the prediction errors. We show to what extent the calculated point forecast of the forecast error improves and influences the day-ahead forecast of the target variable. A comprehensive overview of the probabilistic forecasts of the forecast errors for the three examples wind generation, load and price

is provided in Section 4.5.2. We use the scoring functions and scoring rules defined in Section 4.4 to evaluate the point and probabilistic forecasts and illustrate the validation.

4.5.1. Point Forecasts

To forecast the forecast errors for the three real data examples, we choose $n = 3$ different rolling window lengths comprising 44, 48 and 52 weeks of historical data for the model estimations. Thus, we get six individual point forecasts for each hour and each example. Further, the three exemplary variables, wind generation, load and price, require different specifications of the presented model. For the first example, no adjustments are needed. For the second example, we use the additional seasonal component, and for the third, an additional exogenous variable. In the following, we describe the respective model design and the corresponding properties in detail.

In the context of TSOs' day-ahead wind generation forecasting, we use the basic form of the model from Section 4.3.1, with no seasonal component and no additional exogenous variables, leading to $\varsigma_{d,h} = 0$ and $k = 0$.

Concerning the load forecast error example, previous studies, such as Maciejowska et al. (2021) and Möbius et al. (2023), have shown that the errors of TSOs' day-ahead load forecast often exhibit strong seasonalities. For instance, Figure 4.1 indicates that the day-ahead load forecast consistently underestimates the load during certain hours of the day, with the greatest underestimation occurring in the morning (4 a.m. to 8 a.m.) and late afternoon (4 p.m. to 8 p.m.) every day of the week. To address this issue, we deseasonalise the time series of the forecast error by adding a seasonal component $\varsigma_{d,h} \neq 0$ to the model, which is calculated and forecasted using Formula (4.5). Since we do not include additional exogenous variables, $k = 0$ holds.

For the day-ahead price forecast error example, an analysis of the error reveals that some variation can be explained by the TSOs' day-ahead wind generation forecast available on the transparency platform (ENTSO-E Transparency Platform, 2023b). Therefore, we include an additional exogenous variable in the univariate and multivariate model frameworks (Formula (4.8) and (4.12)), setting $k = 1$. Since there is no clear evidence of a deterministic seasonality, we also choose $\varsigma_{d,h} = 0$.

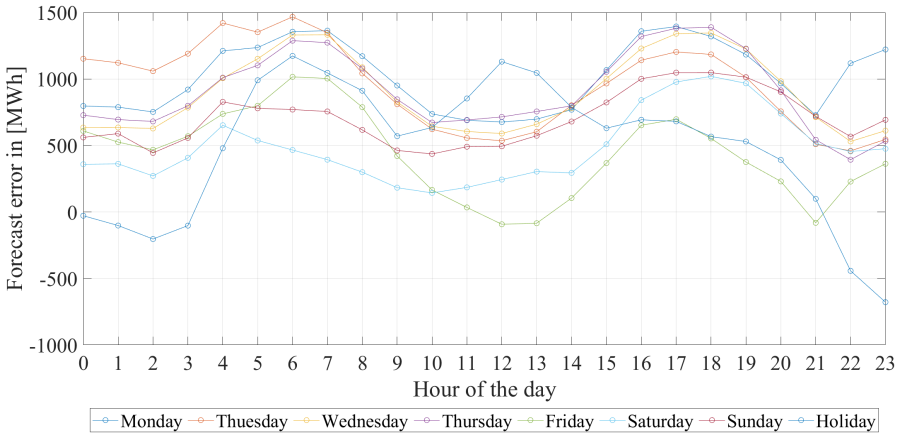

Figure 4.1.: Average forecast error of the day-ahead load forecast $\hat{Y}$ for the hours of the day.

In the following, we present the results of all three data examples together. The error of the error forecasts, by definition, equals the error of the improved point forecasts. Thus, considering and evaluating the error of the error forecast also directly implies the evaluation of the improved point forecasts $\widehat{Y}$ modified via Formula (4.1). By definition, the error of the error forecasts equals the error of the improved point forecasts.

First, we take a look at the calculation of the final point forecast and thus at the methodology for combining the six individual sub-models. For all three data examples, we calculate the final point forecast firstly as an arithmetic mean and secondly via a regression with the least squares approach. To estimate the non-negative coefficients and hence the weights, we use one year of the predicted error forecasts so that we obtain robust estimates. Table 4.1 compares the RMSE of the final forecasts calculated by the weighted combination and by the arithmetic mean of the forecasts of each sub-model. For the load and the wind generation example, the RMSE of the regressed forecast is smaller than the RMSE of the arithmetic forecast. In contrast, the combination approach using the arithmetic mean achieves a more accurate forecast for the price example.

Figure 4.2 shows the daily re-estimated optimal weights of all sub-models and all three real data examples. It supports and justifies the RMSE observations. For load and wind power, the estimated values of the coefficients do not show sharp jumps and

behave stably, so the weights calculated based on history are good estimators for the forecast. For the price example, we find stronger fluctuations in the coefficients. The optimal weights slightly vary from day to day and from hour to hour, so they can only be inadequately approximated from historical data. For this reason, the final forecast resulting from the unweighted average of the individual forecasts is slightly more accurate than the weighted average.

Table 4.1.: RMSE for the weighted and non-weighted final forecasts of the day-ahead load, wind generation and price forecast error in [MWh] and [€/MWh].

	load	wind	price
weighted	1862.38	1526.23	7.21
arithmetic	1879.45	1545.82	7.19

We now take a look at the error measures achieved with the six individual sub-models *UV44w, UV48w, UV52w, MV44w, MV48w* and *MV52w* as well as with the combination of the forecasts $\widehat{Y}$. The RMSE and the MAE are reported in the Tables 4.2 for the load, 4.3 for the wind generation and 4.4 for price example. Turning to the load example (Table 4.2), the prediction of the load forecast error leads to a significant improvement in the day-ahead forecast of the output variable, with a reduction of 33 % in the RMSE and 36 % in the MAE. The improvements are also observable for individual years, e.g., in 2021, the weighted forecast combination achieves the highest improvement amounting 42 % in the RMSE. Thereby, the weighted combination of the individual forecasts reaches the lowest error measures. Just the same, in the wind power example (Table 4.3), combining all individual sub-model forecasts by the weighted regression approach results in the most accurate prediction of the forecast error and the greatest improvement for the initial day-ahead wind power forecast for each considered period. The reduction achieves 7 % in the RMSE and 9 % in the MAE over the entire period. In comparison, in the price example (Table 4.4), we can observe a reduction of the amount of the forecast errors through its prediction with our model which achieves 5 % in the RMSE and 4 % in MAE. Even if the (non-weighted) combined forecast reduces the error measures, it does not always result in the lowest error measures. For example, over the entire period, the lowest RMSE is achieved by the univariate sub-model with a calibration window of 52 weeks

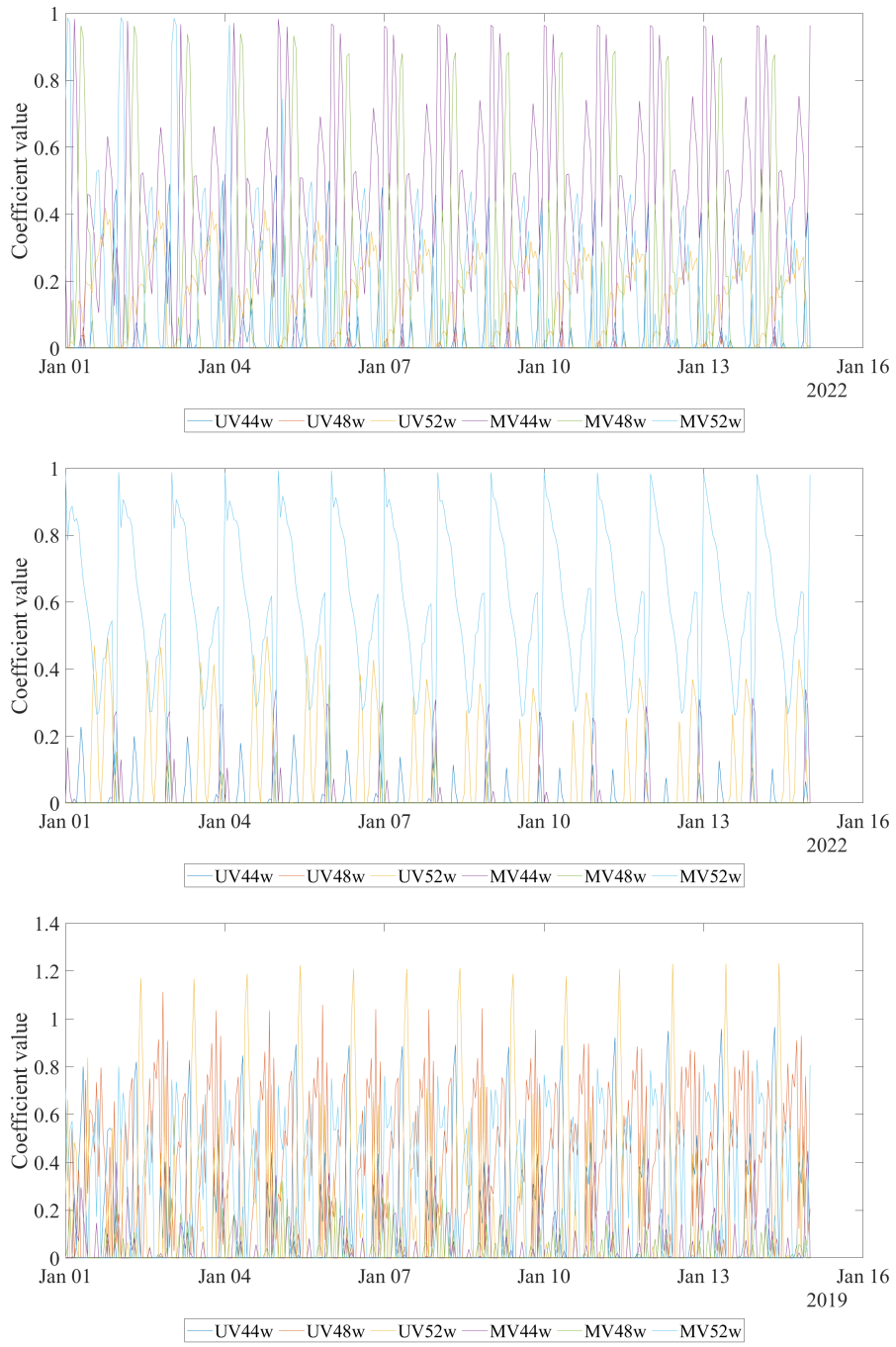

Figure 4.2.: Coefficients estimated by linear regression for the day-ahead load (top), wind generation (middle) and price (bottom) forecast error forecast for an exemplary time period.

(7.23 €/MWh), and for 2019 by the univariate sub-model with a calibration window of 48 weeks.

Table 4.2.: Error measurements RMSE and MAE of the day-ahead load forecast error time series in [MWh].

		$\hat{Y}$	UV44w	UV48w	UV52w	MV44w	MV48w	MV52w	$\widehat{Y}$	
RMSE	total	2,797.83	2,018.21	2,011.80	1,999.52	1,950.34	1,959.67	1,964.84	1,862.38	33 %
	2021	2,888.61	2,015.22	1,991.30	1,977.97	1,676.00	1,671.33	1,670.66	1,667.36	42 %
	2022	2,704.01	2,021.20	2,032.09	2,020.83	2,190.58	2,210.71	2,220.38	2,038.83	25 %
MAE	total	2,186.77	1,537.39	1,538.63	1,534.07	1,457.30	1,462.01	1,466.40	1,391.54	36 %
	2021	2,256.01	1,540.12	1,533.00	1,530.38	1,218.69	1,217.51	1,217.64	1,213.26	46 %
	2022	2,117.53	1,534.65	1,544.27	1,537.75	1,695.91	1,706.51	1,715.15	1,569.83	26 %

Table 4.3.: Error measurements RMSE and MAE of the day-ahead wind generation forecast error time series in [MWh].

		$\hat{Y}$	UV44w	UV48w	UV52w	MV44w	MV48w	MV52w	$\widehat{Y}$	
RMSE	total	1,641.70	1,640.25	1,639.26	1,635.99	1,578.17	1,568.29	1,559.49	1,526.23	7 %
	2021	1,590.34	1,595.04	1,590.21	1,584.31	1,518.31	1,498.28	1,484.09	1,461.76	8 %
	2022	1,691.50	1,684.24	1,686.90	1,686.07	1,635.84	1,635.31	1,631.41	1,588.09	6 %
MAE	total	1,179.11	1,178.04	1,177.13	1,174.07	1,116.33	1,108.15	1,102.70	1,071.08	9 %
	2021	1,153.04	1,156.89	1,153.75	1,148.61	1,067.36	1,052.41	1,043.40	1,022.83	11 %
	2022	1,205.18	1,199.18	1,200.51	1,199.54	1,165.31	1,163.89	1,162.00	1,119.34	7 %

The multivariate DM test, implemented by the *epftoolbox* of Lago et al. (2021), has been used to determine whether one model significantly outperforms another based on the RMSE scoring function. The test results are shown in heat maps in Figure 4.3. The maps illustrate the p-values of the hypothesis that the model's forecast on the y-axis is significantly more accurate than the forecast on the x-axis. A p-value close to zero indicates a significantly higher forecast accuracy of the model on the x-axis than of the model on the y-axis. For all three examples, the test confirms the previous results and shows that combining all individual sub-models significantly improves the forecast model. Analysing the results of the multivariate DM test in more detail, the combined forecast $\widehat{Y}$ is significantly more accurate than the forecasts of the individual sub-models for the load and the wind generation example. In comparison, for the price example, the combined forecast is solely significantly more accurate than the forecasts of the multivariate sub-models. However, this does not mean that the predictions of the univariate models outperform the ones of the combination. The DM test shows that the

Table 4.4.: Error measurements RMSE and MAE of the day-ahead electricity price forecast error time series in [€/MWh].

		$\hat{Y}$	UV44w	UV48w	UV52w	MV44w	MV48w	MV52w	$\widehat{Y}$	
RMSE	total	7.60	7.29	7.24	7.23	7.63	7.40	7.33	7.25	5 %
	2017	7.91	7.56	7.50	7.46	7.76	7.54	7.47	7.42	6 %
	2018	6.96	6.52	6.48	6.50	6.69	6.60	6.59	6.49	7 %
	2019	7.95	7.63	7.55	7.56	8.26	7.78	7.69	7.63	4 %
	2020	7.54	7.40	7.39	7.35	7.73	7.63	7.52	7.39	2 %
MAE	total	4.65	4.52	4.48	4.46	4.73	4.61	4.56	4.48	4 %
	2017	4.55	4.51	4.45	4.40	4.71	4.58	4.49	4.43	3 %
	2018	4.84	4.53	4.50	4.51	4.63	4.59	4.57	4.50	7 %
	2019	4.53	4.49	4.44	4.46	4.78	4.59	4.56	4.47	1 %
	2020	4.65	4.55	4.52	4.50	4.80	4.68	4.61	4.52	3 %

univariate sub-models are not significantly more accurate than the combination for the price example (see Figure 4.3, bottom).

Furthermore, the forecast accuracy and the forecast error prediction have been analysed for each hour of the day. For all three examples, Figure 4.4 shows the forecast error's RMSE scoring function based on the individual hours of the day. Turning to the load example (top in the figure), we indicate the same pattern for every sub-model. The RMSE is lowest for values in the first four morning hours and raises up until 4 p.m., which aligns with the daily cycle of electricity consumption. The figure also indicates that the multivariate model framework forecasts are generally more accurate than the univariate ones, which is confirmed by the multivariate DM test, showing a significantly higher forecast accuracy for the multivariate sub-models compared to the univariate sub-models (see Figure 4.3, top).

Turning to the wind generation example, the dominance of the multivariate sub-models does not hold for values of all hours of the day. While in the first hours of the day, the forecasts of the multivariate sub-models show a very low error, with a clear distance to the error of the univariate sub-models' forecasts, it increases in the course of the morning and is higher than the RMSE of the univariate forecasts from 12 p.m. onward (see Figure 4.4, middle). The univariate DM tests for the 24 hours of the day for the wind power example confirm the significance of this observation. The results for hours four and 15 are shown exemplary in Figure 4.5. The heat maps for the univariate DM test of the other

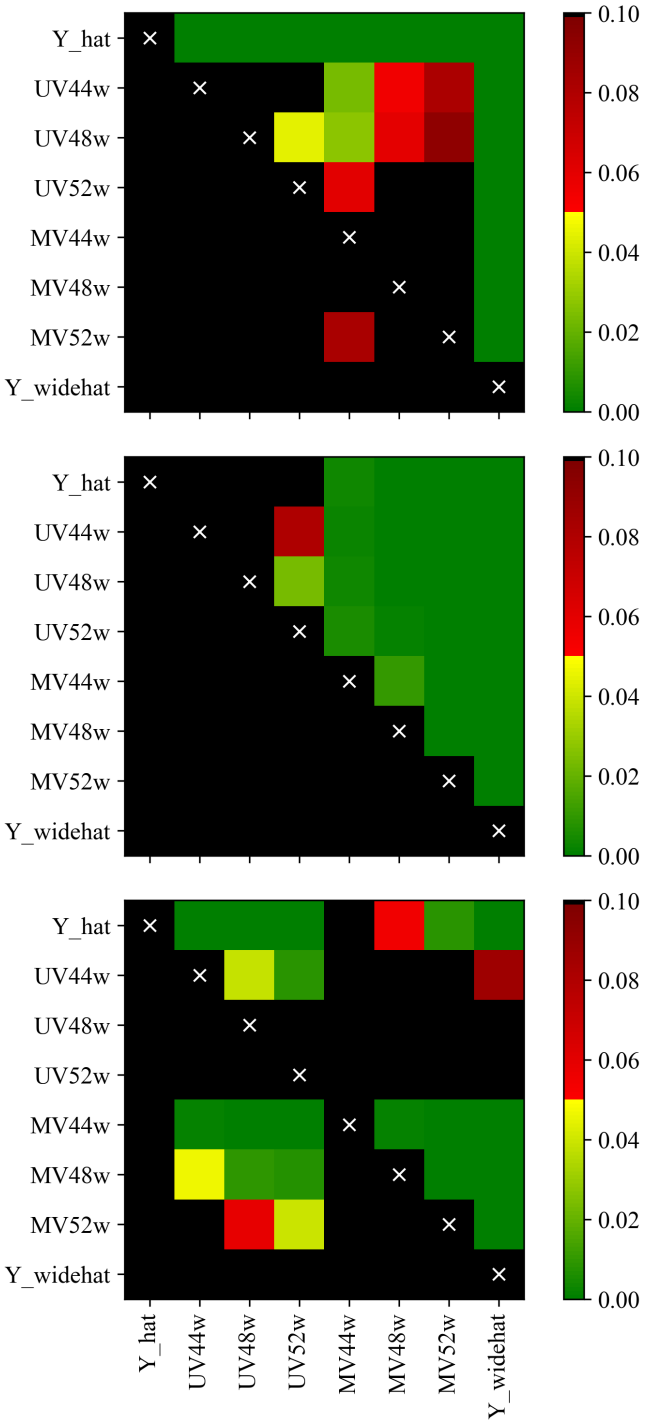

Figure 4.3.: Multivariate DM test for the day-ahead load (top), wind generation (middle) and price (bottom) forecast (output derived with source code from *epftoolbox* by Lago et al. (2021)).

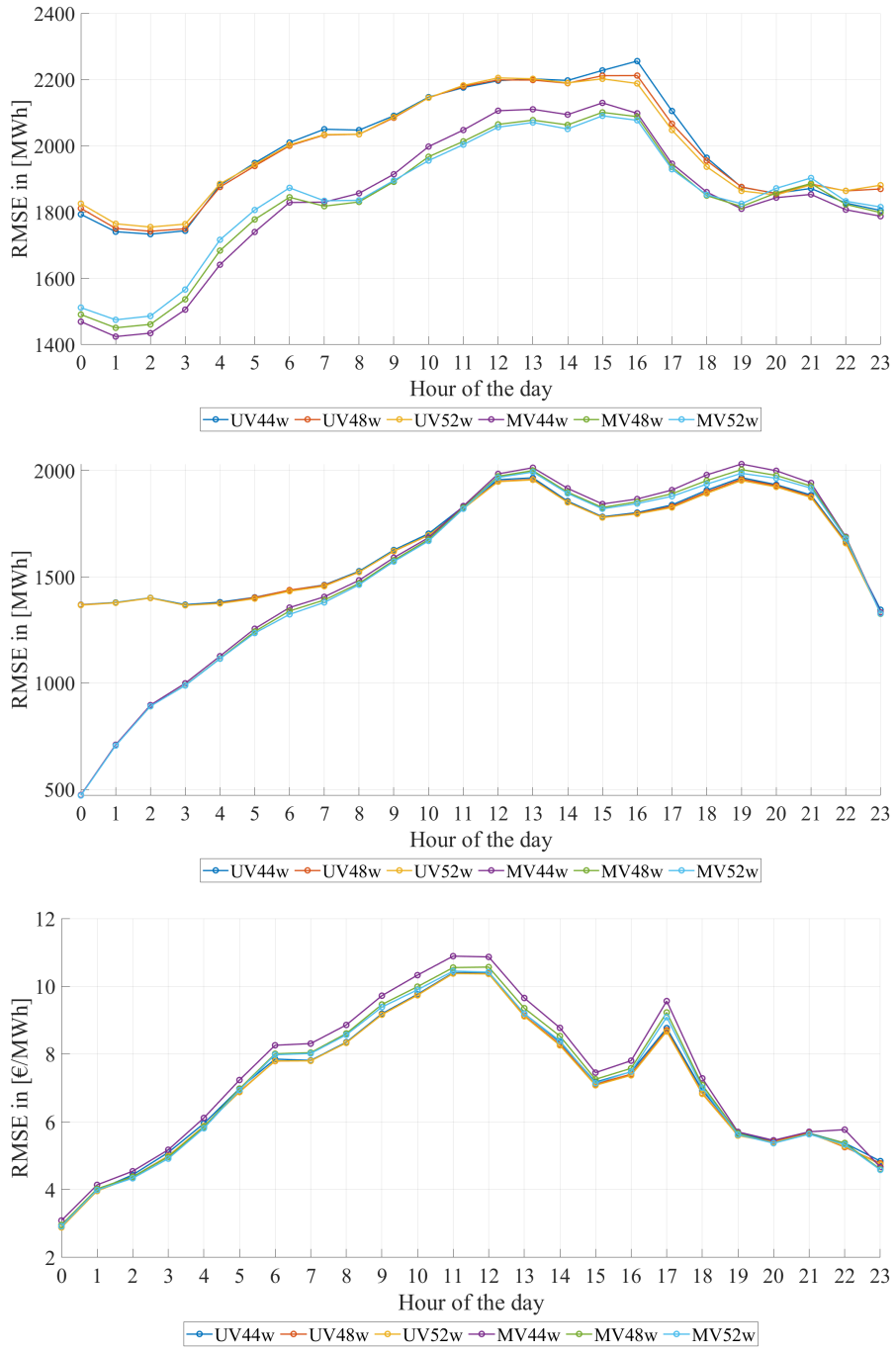

Figure 4.4.: RMSE of the sub-models' forecasts of the forecast error for the hours of the day for load (top), wind generation (middle) and price (bottom).

hours are given in Appendix D. Additionally, we illustrate the results of the univariate DM tests for all hours of the day for the load and for the price example in there.

Turning to the price example, the forecasts of the multivariate sub-models no longer outperform the univariate ones. Figure 4.4 (bottom) illustrates a slightly lower RMSE for forecasts of the univariate sub-models. However, performing the univariate DM tests for all 24 hours of the day shows that this slightly higher accuracy is not significant in most hours.

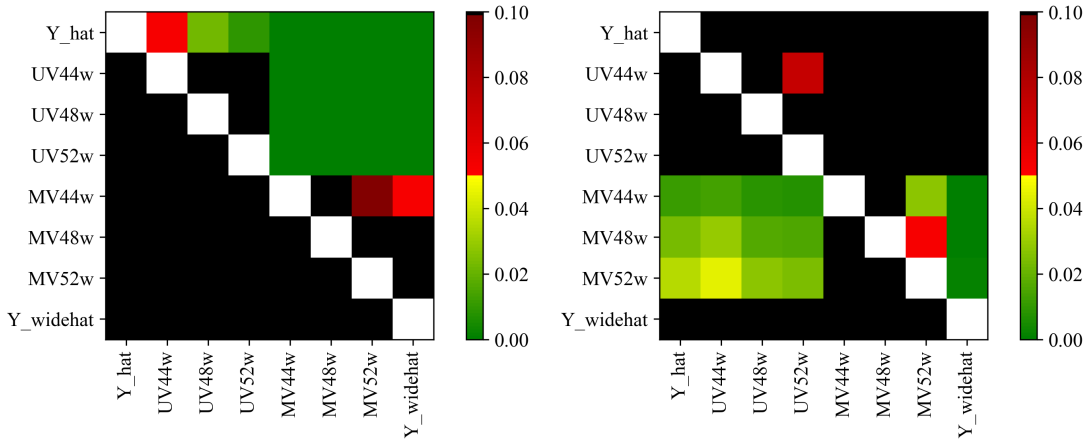

Figure 4.5.: Univariate DM test for the day-ahead wind generation forecast for hours 4 (left) and 15 (right) of the day (output derived with source code from *epftoolbox* by Lago et al. (2021)).

In summary, the examples presented with real data demonstrate that the approach provided here accurately predicts errors in forecasts. Our model's structure and the idea of calculating and combining numerous individual point forecasts for the forecast error allow a wide range of quantities in electricity markets to be used.

4.5.2. Probabilistic Forecasts

We evaluate the accuracy of the probabilistic forecasts using the metrics presented in Section 4.4.2. To rank the results, we compare them with those of four different

distribution-based probabilistic forecasts. For the first one, we continuously estimate the expected value and standard deviation based on the observed errors over the last 312 hours (13 days), such as done by Dudek (2016); Nowotarski and Weron (2018), and use them to forecast hourly values for the quantiles q, $q \in (0, 1)$ of the forecast error assuming normally distributed errors. For the other three distribution-based predictions, we use the information from the estimates of the multivariate framework (see Formula (4.13)). The point forecast of the prediction error describes the expected value of the distribution. The standard deviation is estimated as part of the model estimation so that the normal distribution assumption of the resulting innovations is approximated. We obtain a separate distribution for each hour of the day. Since the sub-model is estimated daily with rolling windows, the expected value and standard deviation are also continuously determined here.

To analyse the overall accuracy of our probabilistic forecasts, we first use the CRPS metric. Tables 4.5, 4.6 and 4.7 summarise the CRPS for the ORA-based (QRA) and distribution-based (d-b) probabilistic forecasts of the day-ahead wind generation, load and price forecast errors, broken down by the hours of the day, to understand the accuracy better. For all three examples, we observe that the quality of the QRA-based probabilistic forecast varies in the hours, with the lowest CRPS for the forecasted values of the first hour of the day. After that, the CRPS rises almost monotonously to its maximal value for load, wind generation and price. However, the hour containing the probabilistic predictions with the highest CRPS is not equal for the three examples. In the wind generation example, the forecasts for the 19th hour reach the maximum CRPS and, thus, less accurate compared to the probabilistic forecasts in the other hours. In the load example, the maximum CRPS occurs in the 15th hour, and in the price example even already in the 11th and 12th hour. We tested to account for this imbalance of CRPS values for the hours of the day. Therefore, we assumed different density functions for every hour of the day and estimated the parameter vector β_q separately based on 24 disjunctive sub-sets, each containing one hour of the day. Doing so resulted in a probabilistic forecast worse than or equal to the univariate QRA approach presented. Further information on our findings can be provided upon request.

Table 4.5.: CRPS for the probabilistic forecast of the day-ahead wind generation forecast error in [MWh].

hour	QRA	d-b (hist.)	d-b (MV44w)	d-b (MV48w)	d-b (MV52w)
0	193.23	368.00	224.74	224.48	224.78
1	225.27	373.70	250.33	250.10	250.33
2	256.17	380.86	278.56	278.23	278.28
3	277.29	377.32	296.13	294.92	294.56
4	297.10	382.53	315.54	313.90	313.29
5	317.88	383.50	341.15	340.11	337.24
6	339.72	386.89	364.81	362.41	357.68
7	354.70	394.97	374.80	372.40	369.02
8	373.13	412.24	392.97	389.79	387.58
9	400.17	439.31	415.45	412.66	410.95
10	421.18	462.92	437.38	434.58	432.40
11	455.60	498.77	480.60	477.04	474.43
12	483.27	525.87	514.34	509.27	506.77
13	483.37	523.71	513.54	508.95	506.55
14	464.25	491.35	483.17	480.28	478.70
15	452.24	473.77	462.29	460.73	459.92
16	467.87	489.68	473.25	472.22	470.63
17	480.10	498.87	488.67	486.77	483.65
18	492.46	505.24	505.94	502.04	498.41
19	499.19	509.03	512.19	508.25	504.72
20	495.22	510.22	504.44	500.49	497.97
21	485.87	503.39	492.85	489.16	487.19
22	411.21	423.75	419.80	418.18	415.85
23	345.52	357.87	346.09	344.83	345.15
total	394.67	444.74	412.04	409.66	407.75

Turning to the distribution-based probabilistic forecasts, it can be seen that the CRPS of these predictions also varies in the hours, taking maxima and minima in other hours in all three examples. In general, comparing probabilistic forecasts calculated by QRA with distribution-based ones, the QRA-based predictions achieve a lower CRPS overall and also in most single hours. Thus, the method of estimating probabilistic forecasts by QRA provides more accurate forecasts than the estimation based on historical distribution parameters.

Reporting the CRPS provides a first overview of the probabilistic forecast's accuracy in terms of sharpness and calibration. To further evaluate the calibration of our probabilistic forecasts for the three real data examples, we use the PIT methodology to plot the histogram of observed forecast errors in the predicted quantiles. Figure 4.6 shows the histograms for the probabilistic forecast of the load, wind generation and price prediction

Table 4.6.: CRPS for the probabilistic forecast of the day-ahead load forecast error in [MWh].

hour	QRA	d-b (hist.)	d-b (MV44w)	d-b (MV48w)	d-b (MV52w)
0	350.59	517.14	498.13	502.11	506.56
1	341.97	500.49	481.66	487.40	492.63
2	347.89	487.72	480.46	486.61	492.51
3	370.72	483.15	491.22	500.27	508.10
4	418.45	492.20	509.62	524.07	535.28
5	445.86	520.53	516.70	530.27	539.73
6	482.63	550.99	537.39	545.62	552.52
7	497.72	557.07	552.29	549.00	550.41
8	510.55	565.86	564.13	556.51	555.25
9	527.90	579.97	577.03	570.26	568.95
10	552.45	600.28	593.52	584.80	579.71
11	565.40	611.96	607.06	597.83	593.13
12	579.50	624.13	613.89	605.05	599.60
13	579.28	625.26	615.34	607.25	602.85
14	578.22	604.89	611.53	602.84	596.74
15	589.40	597.26	622.29	613.33	606.99
16	578.69	580.28	616.55	608.98	600.76
17	532.91	546.90	575.87	570.11	562.80
18	516.22	526.96	555.07	552.16	547.02
19	495.11	518.45	526.02	531.72	530.51
20	503.90	533.41	530.38	539.01	541.23
21	513.60	552.61	531.50	541.92	544.12
22	497.97	530.24	515.80	520.28	520.35
23	503.85	521.47	514.97	517.82	519.30
total	495.03	551.22	551.60	551.88	551.96

errors. A calibrated forecast in a laboratory environment would correspond to a uniform distribution, causing the predicted probabilities to match the observed frequencies of the forecast error over time. While the histograms for load and price show slightly increasing frequencies towards the external quantiles and, thus, a slight U-shape, the histogram for wind power indicates almost identical relative frequencies for all quantiles. In general, all three histograms provide a good approximation of a uniform distribution generated by drawn random numbers. The comparison with the histograms of the distribution-based forecasts demonstrates this calibration since these histograms deviate strongly from a uniform distribution (see Figure 4.7). This confirms that the predicted probabilities reflect the true probabilities of the forecast errors for all three real data examples and validates the effectiveness of our approach across different quantities.

Table 4.7.: CRPS for the probabilistic forecast of the day-ahead price forecast error in [€/MWh].

hour	QRA	d-b (hist.)	d-b (MV44w)	d-b (MV48w)	d-b (MV52w)
0	0.84	1.37	0.93	0.92	0.91
1	1.01	1.47	1.13	1.11	1.11
2	1.09	1.47	1.18	1.15	1.15
3	1.17	1.48	1.27	1.23	1.22
4	1.34	1.57	1.46	1.43	1.42
5	1.62	1.75	1.74	1.70	1.69
6	1.86	1.90	1.93	1.91	1.90
7	1.89	1.91	1.97	1.94	1.92
8	2.02	2.05	2.12	2.09	2.07
9	2.19	2.20	2.33	2.30	2.27
10	2.28	2.27	2.46	2.42	2.39
11	2.43	2.39	2.61	2.55	2.52
12	2.43	2.39	2.66	2.60	2.56
13	2.16	2.13	2.38	2.31	2.28
14	1.96	1.93	2.15	2.09	2.06
15	1.75	1.73	1.87	1.82	1.80
16	1.73	1.68	1.84	1.79	1.77
17	1.96	1.89	2.07	2.01	2.00
18	1.75	1.71	1.80	1.75	1.75
19	1.42	1.46	1.45	1.43	1.43
20	1.34	1.39	1.38	1.37	1.37
21	1.26	1.34	1.33	1.32	1.32
22	1.24	1.36	1.31	1.29	1.29
23	1.17	1.31	1.20	1.18	1.17
total	1.66	1.76	1.77	1.74	1.72

In summary, our evaluation using CRPS and PIT verifies the accuracy and calibration of our probabilistic forecasts for the forecast error of different quantities while also highlighting variations in performance by hour.

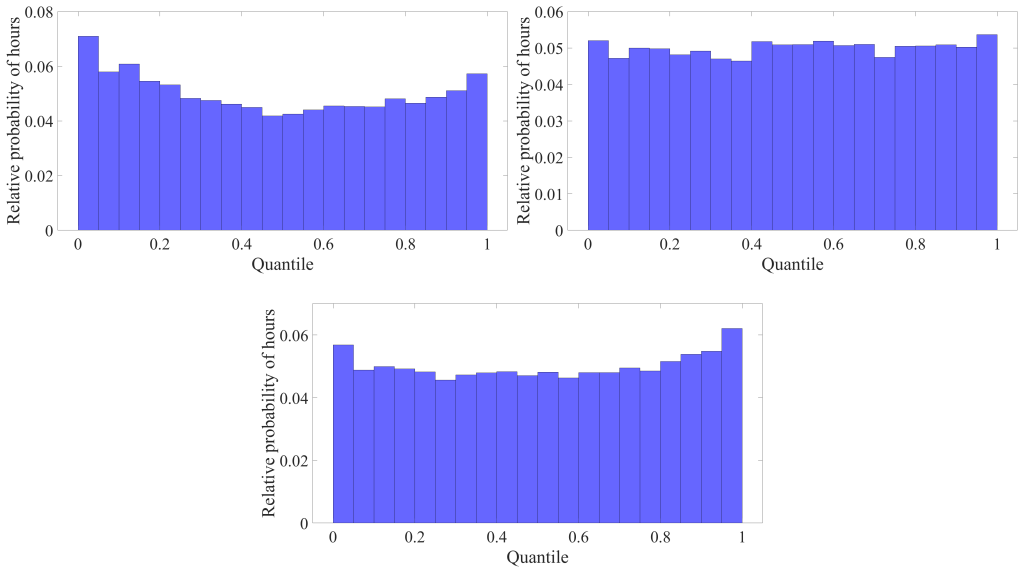

Figure 4.6.: Discrete PIT for the QRA-based probabilistic day-ahead load (top left), wind generation (top right) and price (bottom) forecast error forecast.

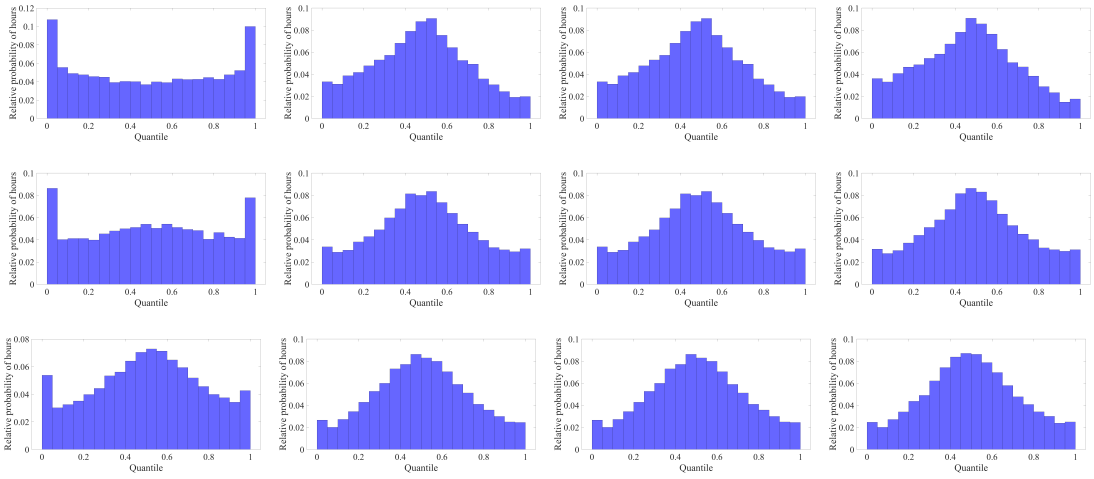

Figure 4.7.: Discrete PIT for the distribution-based probabilistic day-ahead load (top), price (middle) and wind generation (bottom) forecast error forecast. From left to right: estimation of distributional parameters based on historical observations, multivariate sub-model with a window length of 44 weeks, multivariate sub-model with a window length of 48 weeks and multivariate sub-model with a window length of 52 weeks.

4.6. Example use Cases for Probabilistic Forecasting

In this section, we present exemplary statements that can be derived from probabilistic forecasting. The use cases are calculated with the real data examples of day-ahead load, wind generation and price forecast errors. Informed decision-making depends on reliable information, which accurate, calibrated probabilistic forecasts can provide. They can help decision-makers to identify whether a forecast tends to underestimate or overestimate the actual quantity. This information can influence trading strategies, power plant deployment planning, risk calculations, and pricing.

For instance, the probability of negative and positive forecast errors for each hour of the week can indicate the probability of overestimation or underestimation. Figure 4.8 shows the probability of negative day-ahead load forecast errors for each hour of the week and, thus, the probability of load overestimation. The probability of negative load forecast errors is higher in 2022 (over 50 %) than in 2021 (around 20 %), possibly due to a reduction in gas and electricity consumption ordered by politicians to address the energy crisis (Federal Office of Justice and Federal Ministry of Justice, 2022b). The reduction may not be adequately reflected in the load forecasts that include past values, resulting in an increased probability of load overestimation. Irrespective of the year under consideration, the probability of overestimation is higher at the beginning, in the middle and at the end of the day, except for public holidays.

Figure 4.9 shows the probability of overestimation for price and wind generation forecast errors, which have different but identifiable patterns and probabilities. Knowledge of the probability of overestimation can also facilitate market interactions for these variables.

In box plots, Figure 4.10 shows the distribution of the 90 % prediction interval's width for each hour of the day, calculated by the difference between the estimated 95 % quantile and the estimated 5 % quantile. A higher width characterises a broader range of possible values for the forecast error in the occurring hours with the same probability as in lower-width hours. We can observe deviations between the hours of the day for the load and price forecast error, especially in the outliers. A higher width and a higher occurrence of outliers identify hours where, e.g., concerning load forecast errors, trading operations might be necessary and higher cause the expected load is more unsure. Since

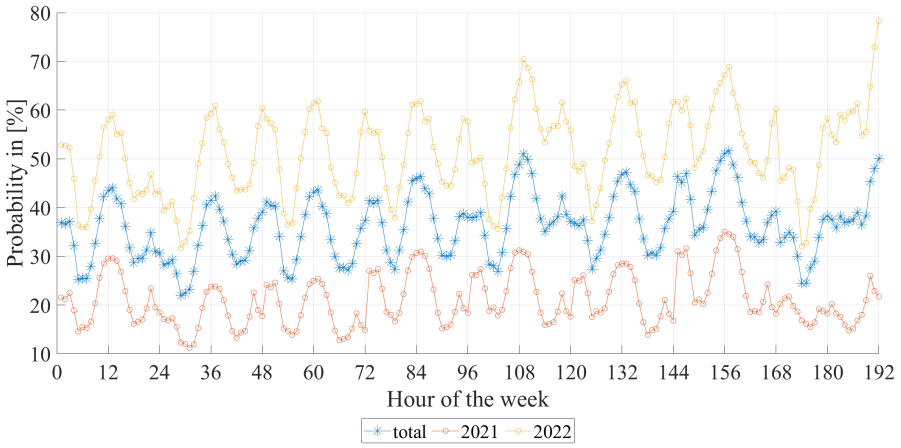

Figure 4.8.: Probability for the overestimation of the load for each hour of the week (including holidays, hours 168 to 192).

we can not observe substantial deviations in the distribution for each wind generation forecast error hour, there is no hour with a more uncertain forecast error.

The calculation of over- and underestimation probabilities by the forecast of the target variable, and the distribution of the width of the prediction interval show two possible applications of probabilistic forecasts. The first one's information can be used to adjust trading strategies and make better decisions regarding resource allocation. For example, suppose the probability of overestimating the load forecast is high. In that case, a trader might want to purchase less electricity on the day-ahead market to avoid paying too much for energy that is not needed. The second one's information can help to quantify uncertainties and provide a measure of risk. For example, suppose the width of the prediction interval is vast. In that case, it may indicate high uncertainty, and traders may want to hedge against potential losses by purchasing options or other financial instruments.

Statements can be made about the forecast itself through the probabilistic predictions of the prediction error by linking the probabilistic prediction error forecasts with the initial forecast of the target variable (see Formula (4.2)). Thus, density forecasts of the target variable become directly possible. These density forecasts can be integrated into procurement strategies, power plant deployment planning, and risk management.

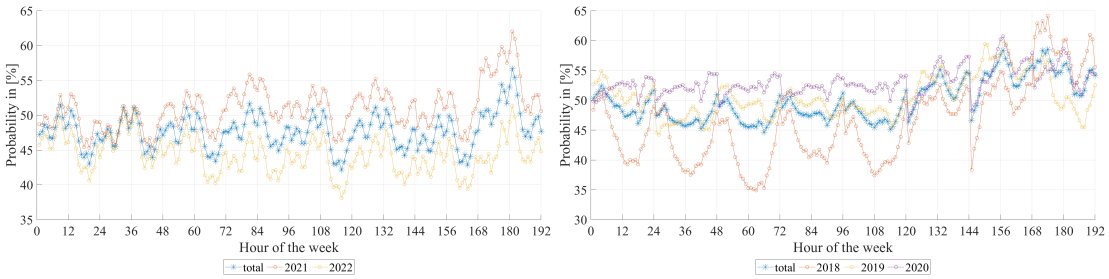

Figure 4.9.: Probability for the overestimation of the day-ahead wind generation (left) and day-ahead price (right) for each hour of the week (including holidays, hours 168 to 192).

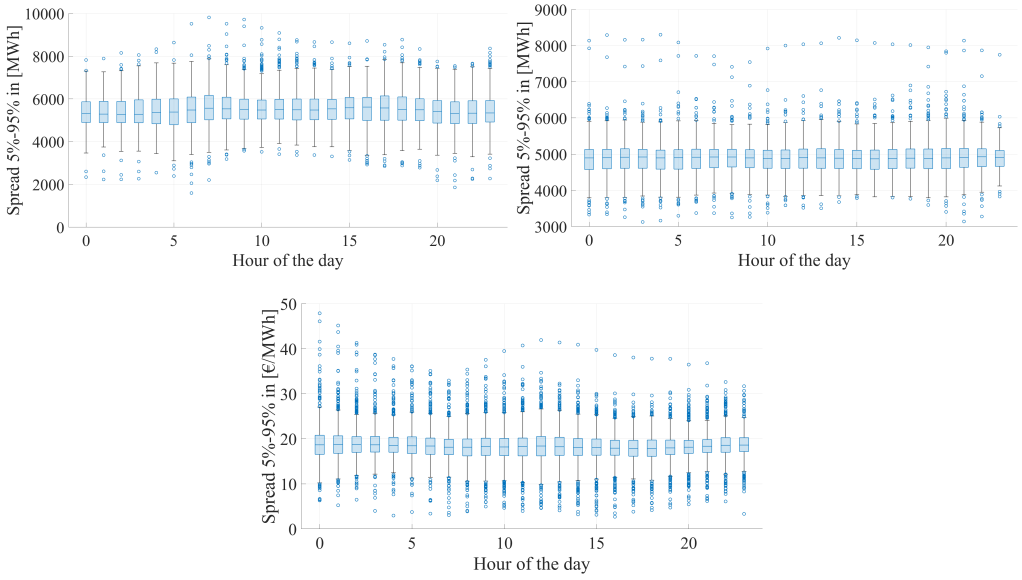

Figure 4.10.: Box plot of the 90 % prediction interval's width of the day-ahead load (top left), wind generation (top right) and price (bottom) forecast error for each hour of the day.

Application examples for probabilistic day-ahead price forecasts are provided by, e.g., Watermeyer et al. (2023). In managing renewable energy sources, probabilistic forecasts can be utilised to optimise energy storage systems and to handle the risks associated with curtailment and imbalance penalties. For example, a power plant operator could use a density forecast to optimise different generation resources, such as wind or solar, based on the expected weather conditions.

4.7. Concluding Remarks

In this chapter, we offered a versatile and adaptable method to predict short-term forecast errors for any target variable and forecast model, along with evaluation techniques. The approach generates point forecasts as well as probabilistic forecasts of the prediction error. For predicting the error, we relied on statistical ARMA models designed in a univariate and a multivariate framework and estimated for several rolling window sizes. This allowed us to average over arbitrary hyperparameters, making the framework robust to random missteps by potential users. We obtained probabilistic forecasts using QRA, applied to a pool of generated point forecasts of the prediction error.

By forecasting the forecast error and generating density forecasts, we improve and extend the initial prediction and address the need for accurate point forecasts as well as for probabilistic forecasts.

We illustrated the validation of our approach by applying our model to three real data examples: electricity load, wind generation and electricity price forecasts. We could significantly improve all three predictions, with price and wind generation point forecasts seeing a reduction of 5 % and 7 % in RMSE and the day-ahead load forecast of 33 %. We analysed the results in detail and showed that, due to the flexible settings of the approach, structures and patterns in the forecast errors can be captured by the model. The probabilistic forecasts are well-calibrated.

Providing density forecasts in addition to point forecasts allows, e.g., to quantify the probability of over- and underestimation of the (point) forecasts and to give information about the uncertainty of the prediction. Since probabilistic forecasts and their practical

application are relatively new in the energy-related literature, we showed the interested reader exemplary use cases for probabilistic forecasts.

Overall, our open-source approach provides a robust and adaptable framework for predicting forecast errors and generating density forecasts, leading to improved accuracy in initial forecasts and valuable insights into the underlying structures of forecast errors.

In the next chapter, we combine the approaches of improving and generating input data in a data pre-processing step as well as forecasting the forecast error in a data post-processing step to enhance a techno-economical market model. In doing so, we provide a hybrid model to generate point and probabilistic day-ahead price forecasts.

5. A Hybrid Model for Day-Ahead Electricity Price Forecasting: Combining Fundamental and Stochastic Modelling

This chapter is based on Watermeyer et al. (2023)[1].

5.1. Introduction

Accurate forecasting in the energy sector is crucial for multiple stakeholders, including industry practitioners, researchers and policymakers. The effectiveness of financial and operational decisions and regulatory interventions depends on accurate predictions of future developments in relevant areas. As a result, the forecasting of electricity prices has become a key area of focus (Weron, 2014). With companies facing increasingly intense competition due to deregulation and liberalisation in the electricity sector, day-ahead price forecasts and insight into the next day's market situation are essential to the development of bidding strategies and production plans that maximise a company's profit margins and ensure a reliable grid operation. Quantifying uncertainty has become increasingly important in recent years due to the growth of renewable energies and the need to integrate them alongside an increase in infrastructural challenges and fluctuating commodity prices, raising uncertainty in the energy market (Nowotarski and Weron,

[1]The work was supported by the German Federal Ministry of Economic Affairs and Climate Action through the research project "ProKoMo - Better price forecasts in the energy sector by combining fundamental and stochastic models" within the Systems Analysis Research Network of the 6th energy research program.

2018; Hong et al., 2016, 2020). Probabilistic forecasts help in the planning and operation of energy systems, allowing for the assessment of uncertainty and the development of future strategies against the background of various probable future events (Amjady and Hemmati, 2006).

We present a novel, open-source hybrid model that forecasts day-ahead electricity prices punctually and probabilistically by combining two main methodological streams: techno-economic energy system modelling and stochastic modelling. Techno-economic models are fundamental energy system models that determine (partial) market equilibria through the bottom-up optimisation of an energy system. They can explain actual developments and reflect structural breaks by identifying techno-economic interdependencies in energy markets. However, when estimating prices in the short term (e.g., day-ahead, intraday), these models exhibit larger and more systematic errors than other model classes. Stochastic models, on the other hand, learn from history and are developed and trained with historical data, enabling them to capture fluctuations and uncertainties in the market, especially in the short term. They offer high flexibility and the ability to specify forecast ranges and distributions. Still, they can only capture structural breaks and changes in external influences ex-post due to their dependence on historical data.

Our proposed hybrid model combines the strengths of techno-economic energy system models and stochastic models to develop a more robust and accurate approach to forecasting electricity prices on the day-ahead market. The model retains the structural statements of techno-economic energy system model and, thus, insights into the driving market mechanisms while incorporating stochastic short-term structures and distribution functions to account for uncertainty. The model uses state-of-the-art methods to generate point and probabilistic price forecasts. These probabilistic price forecasts, with probabilities for each potential price scenario, are increasingly valuable to the industry (e.g., when assessing the probabilities of negative prices or when assessing the overall risk level of the price forecast).

The model is schematically illustrated in Figure 5.1. It employs a rolling-window approach. In each iteration, it forecasts day-ahead prices exclusively through the use of data known prior to the day-ahead market's closure, accurately reflecting the knowledge of stakeholders making decisions in these markets. The model is repeatedly applied each

day (d_n) to generate forecasts for the following 24 hours of the day-ahead market. Each daily forecast includes four steps – stochastic data pre-processing, parameter density forecast, energy system optimisation and stochastic data post-processing – to produce point and probabilistic forecasts.

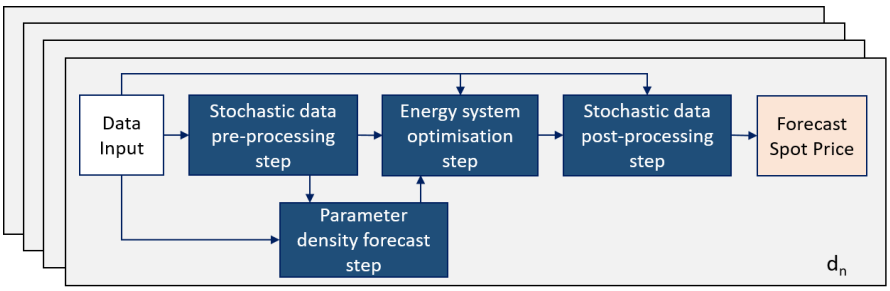

Figure 5.1.: Schematically illustration of the hybrid model.

The first step, stochastic data pre-processing, aims to improve the accuracy of input data in advance of the energy system optimisation step and generates the basis for the parameter density forecast step. In the second step, the parameter density forecast generates prediction intervals for selected input parameters of the third step, energy system optimisation, enabling us to account for uncertainty in the operational decisions of market participants. This third step considers the improved input data from the first and second steps. It forms a stochastic optimisation model that minimises total system costs, identifies the equilibrium between supply and demand and determines the hourly marginal system costs, which can be interpreted as price estimators. These price estimators are the initial values in the fourth and final step, stochastic data post-processing. The errors of the price estimators are mapped by a multidimensional model in which seasonal effects and structures are captured using a combination of univariate and multivariate approaches, resulting in an enhanced price forecast. By modelling and improving the price forecast error, the model calculates forecast intervals and probability densities for the forecast prices, providing a quantification of uncertainty. Finally, our model can combine the strengths of both method classes to achieve excellent state-of-the-art price forecasts, including both point and probabilistic forecasts, to capture the stochastic uncertainty of the market.

This work contributes to the literature in three main ways. First, it presents a novel hybrid model that provides a general framework to combine techno-economic and stochastic energy models. Since the model's source code and algebra are available online, other researchers can apply our methodology and extend it to different time periods and electricity markets around the world. Second, it proves that techno-economic energy system models can contribute to short-term price forecasting, especially when paired with stochastic models for the sake of error improvement. Our hybrid model delivers highly accurate day-ahead price forecasts on top of the insights that techno-economic models provide. We demonstrate its value with an empirical analysis based on European data focusing Germany, the largest European electricity market. Third, our hybrid model provides probabilistic forecasts in addition to point forecasts, enabling power plant operators to, for example, quantify the likelihood of prices becoming negative at any given hour.

The remainder of this chapter is organised as follows. Section 5.2 reviews the existing literature. Afterwards, we provide all of the information necessary to use our model and replicate this study in Section 5.3. Section 5.4 describes our methodology. Following, Section 5.5 presents and evaluates the results of our hybrid model, while Section 5.6 closely analyses individual model steps. Finally, Section 5.7 offers some concluding remarks.

5.2. Literature

Research on electricity prices has garnered the interest of many scholars due to the complexities and extraordinary challenges of achieving high accuracy in forecasting. They have developed and refined numerous methodological approaches to achieve high accuracy and adapt to changes in the electricity market. The number of relevant publications has increased rapidly over the last two decades.

Weron (2014) offers a detailed review of several approaches to forecasting electricity prices, including the following five model classes: multi-agent models, fundamental models, reduced-form models, statistical models, and artificial intelligence models. Previously, Aggarwal et al. (2009) had provided an overview of the methods used in electricity

price forecasting. However, their focus is on stochastic time series, causal and artificial intelligence-based models. Weron and Ziel (2019) and Hong et al. (2020) present a general review of and outlook on energy forecasting. The most recent overview of forecasting theory and practice comes from Petropoulos et al. (2022), who provide an overview of a wide range of theoretical models, methods, principles and approaches to preparing, organising and evaluating forecasts. In addition, they provide several real-world examples of how these theoretical concepts are applied.

Many publications conduct time series analysis based on time series models, which are particularly suitable for short-term electricity price forecasting. Time series models constitute a special subtype of regression model in which target variables y are represented, among other things, by past values of the time series as regressors x. They include autoregressive moving-average (ARMA), generalised autoregressive conditional heteroscedastic (GARCH) and Markov regime-switching (MS) models. Steinert and Ziel (2019), for example, develop an autoregressive model with 24 individual models – one for each hour of the day – that also incorporates electricity futures prices to produce hourly electricity price forecasts. Nowotarski and Weron (2016) refer to the decomposition of values into different components, which is common in time series analysis, and show that the quality of time series models benefits greatly from decomposing a set of electricity prices into a long-term seasonal component and a stochastic component, modelling them independently and combining their forecasts. In an extensive study, Ziel and Weron (2018a) compare two options for the type of time series modelling used with high-frequency data sets. They compare models with univariate model frameworks, where one of these models is constructed for the entire time series, featuring models with multivariate model frameworks, in which each hour of a day is modelled separately and independently. This is initiated by the organisation of electricity markets as day-ahead auctions, as in the U.S. or Europe. Their study shows no clear dominance by one framework, suggesting that the combination of both modelling approaches could improve predictive accuracy.

While Steinert and Ziel (2019), Nowotarski and Weron (2016) and Ziel and Weron (2018a) focus on day-ahead electricity prices in general, Christensen et al. (2012) use a nonlinear variant of the autoregressive conditional risk model to predict price peaks, treating them collectively as a discrete-time point process, Eichler et al. (2014) an

approach based on the autoregressive conditional hazard model, and Manner et al. (2016) the mapping of inter-regional linkages between different electricity markets in a dynamic multivariate binary choice model to predict electricity price spikes. Garcia et al. (2005) develop a GARCH model to predict day-ahead electricity prices, while Hickey et al. (2012) evaluate the accuracy of ARMAX-GARCH models in forecasting short-term prices in the U.S., determining that model choice depends largely on location, horizon and regulation, with asymmetric power autoregressive conditional heteroskedastic (APARCH) models being more appropriate in deregulated markets and GARCH models being better for regulated markets. Bordignon et al. (2013) develop a linear regression model to account for relationships between prices and various price drivers, using a time-varying parameter (TVP) and an MS model to capture peaks and discontinuities. Other examples of applying MS models include Kosater and Mosler (2006) for the German market and Bierbrauer et al. (2004) for the Nordic market. Notably, in a recent paper, Mari and Mari (2022) use deep learning-based regime-switching models to predict electricity prices. Parameter-rich ARX models represent a special type of time series models. The Lasso estimated autoregressive (LEAR) model introduced by Uniejewski et al. (2016) is further developed by Lago et al. (2021).

To provide a set of best practices for evaluating future model developments in electricity price forecasting and comparing state-of-the-art statistical and deep-learning methods, Lago et al. (2021) define a deep neuronal network (DNN) and a LEAR model based on the latest findings. Together with various evaluation metrics, these models are accessible in a Python™ toolbox to evaluate new algorithms. Accordingly, we compare our hybrid model with this statistical LEAR benchmark model.

Deep-learning models (e.g., artificial neural network (ANN), DNN, long short-term memory (LSTM) network, recurrent neural network (RNN), feed-forward neural network) are used in an increasing share of electricity price forecasts. In addition to the cited benchmark model, Panapakidis and Dagoumas (2016), as an example, study ANNs using different inputs and ANN typologies. These authors characterise such models as having comprehensive functionality and a high degree of flexibility. In their analysis of the impact of different markets on one another, Lago et al. (2018) develop a DNN that considers interconnected markets' characteristics to boost forecasting accuracy. Notably, they

show that predicting the price of two markets simultaneously enhances forecast accuracy. Amjady (2006) develops a fuzzy neuronal network that forecasts hourly electricity prices for the Spanish day-ahead market. Notably, the combination of deep learning and time series models can be found in the nonlinear autoregressive neural network of Marcjasz et al. (2019).

To compare time series and neural network models using external regressors, Lehna et al. (2022) use four different forecasting approaches to the German day-ahead electricity market: a seasonal autoregressive integrated moving average (SARIMA) model, an LSTM neural network, a convolutional neural network LSTM (CNN-LSTM) and an extended two-stage multivariate vector autoregressive (VAR) model. While the LSTM model achieves the highest average accuracy, the two-stage VAR model has advantages at shorter prediction horizons. A combination of both methods outperforms each of the individual models in terms of accuracy.

The methods presented so far are fundamentally based on historical day-ahead electricity price time series. Another approach entails using models that simulate the actions of individual market participants (so called agents). Qussous et al. (2022), for example, develop an agent-based model to derive day-ahead prices and simulate the bidding strategies of market participants. To evaluate their model, they reproduce day-ahead electricity prices in the 2016 to 2019 German bidding zone. Compared to other techno-economic approaches to short-term electricity price forecasting, this agent-based model achieves the highest accuracy. Consequently, we compare the hybrid model presented in this work with this model.

Due to their explanatory character in identifying an efficient market outcome and their comprehensive modelling of the entire electricity system, techno-economic energy system models have been employed for the ex-post analysis of electricity prices. Müsgens (2006b) and Borenstein et al. (2002) replicate day-ahead prices to assess the existence of market power in Germany and the U.S., respectively. Keles et al. (2013) investigate on the importance of adequate wind power feed-in time series to obtain better results in electricity price simulation. Hirth (2013) determines the market value of renewables, and Sensfuß et al. (2008) quantify the merit order effect computing day-ahead prices. The merit order effect describes the displacement of fossil fuel generation by renewable energy

sources due to their lower marginal costs and the subsequent decline in total electricity costs. Pape et al. (2016) analyse to what extent day-ahead and intraday electricity prices can be explained and represented by techno-economic energy system models. Notably, however, they show that this method has significant weaknesses in explaining short-term electricity prices compared to other methods.

In contrast to ex-post analyses of electricity prices, which examine actual prices that have already occurred, this article focuses on ex-ante forecasts. Techno-economic energy system models, used for ex-ante prediction, have the key disadvantage they do not use recent historical prices to benchmark their price estimators. As a result, they may struggle to explain random short-term variations compared to econometric models that "learn from the past". However, energy system models possess an advantage in that they are based on established economic theory and replicate the workings of markets. As such, they are able to predict prices independently of past data and are less prone to structural changes in the market and other similar factors. In line with that, we did not find techno-economic energy system model applications to forecasts for ex-ante predictions of short-term electricity prices. However, there are such uses in ex-ante predictions of long-term electricity prices, where random short-term variations are less inherent (see, e.g., Müsgens, 2020; Green and Vasilakos, 2010; Lamont, 2008). In addition, techno-economic energy system models have been employed in bodies of literature that extend beyond price estimates (e.g., to determine the value of demand response (Misconel et al., 2021; Kirchem et al., 2020), to identify an optimal transmission-expansion plan (van der Weijde and Hobbs, 2012), to support decision-making at the municipal level (Scheller and Bruckner, 2019), to analyse the effect of power-to-gas (Lynch et al., 2019), to evaluate policy instruments to reduce CO_2 emissions (Sgarciu et al., 2023)). Additionally, Plaga and Bertsch (2023) thoroughly examines how energy system models can account for climate uncertainty. A comprehensive overview of energy system modelling can be found in Ventosa et al. (2005).

In recent years, hybrid methods have garnered significant attention in electricity price forecasting. Hybrid models are those that combine two or more distinct methods. They aim to use the combined strengths of the employed methods while mitigating their individual weaknesses to achieve better results. Many hybrid methods have been

developed that combine a wide variety of methods. Aggarwal and Tripathi (2017), for example, present a hybrid approach that uses a wavelet transform, a time series time-delay neural network and an error-predicting algorithm to predict day-ahead electricity prices in the ISO New England market. Chang et al. (2019) combine an Adam-optimised LSTM neural network to generate electricity prices with a wavelet transform to decompose an electricity price time series into several series of electricity prices. A combination of an empirical wavelet transform, a support vector regression, a bi-directional LSTM and a Bayesian optimisation is proposed by Cheng et al. (2019). Nazar et al. (2018) apply a three-stage hybrid model to the DK2 area of Nordpool and the Spanish power market. The first stage features a wavelet and Kalman machines to decompose price data into different frequency components. The second stage uses an adaptive neuro-fuzzy inference system (ANFIS) to forecast price frequency components. In the third stage, the output of the second stage is fed into the ANFIS to boost forecasting accuracy. A wavelet transform and an ARMA are paired with a kernel-based extreme learning machine by Yang et al. (2017), and with a radial basis function neural network by Olamaee et al. (2016). Zhang et al. (2020) propose a hybrid model based on variational mode decomposition, self-adaptive particle swarm optimisation, SARIMA and a deep belief network for short-term electricity price forecasting.

Most of the hybrid models mentioned above use statistical and deep learning methods. However, a few applications also combine a techno-economic energy system model with another approach. For example, de Marcos et al. (2019) detail a short-term hybrid electricity price forecasting model for the Iberian market that combines a techno-economic cost-generation optimisation model with an ANN. Gonzalez et al. (2012) propose two hybrid approaches based on a techno-economic electricity market model. Focusing on the day-ahead market in the UK, they combine this model type separately with two other models: a linear autoregressive model with exogenous data on price drivers (ARX model) and a nonlinear logistic regression model with a smooth transition (LSTR model), which is a regime change in times of structural change. Their results support the idea of incorporating fundamental information for better price forecasting. Particularly in highly volatile periods, the nonlinear hybrid model achieves better results. In Möbius et al. (2023), our previous study, we introduced a techno-economic market model tailored

to the day-ahead market and combined it with a stochastic model to enhance day-ahead load forecast accuracy in the estimation of day-ahead electricity prices. We highlighted the positive effects of better load forecasts on the day-ahead price estimators generated with an energy system model. However, this approach merely represents a first step; it does not fully realise the potential of a hybrid model, which seamlessly integrates the strengths of both the techno-economic and the stochastic models.

The literature on electricity price forecasting mostly focuses on developing point forecasting methods for the day-ahead market. However, in recent years, there has been a growing interest in probabilistic forecasting methods (Hong et al., 2020). The Global Energy Forecasting Competition (GEFCom2014) (see Hong et al., 2016) served as a catalyst for this trend, and many studies have been published on this topic in the time since. Nowotarski and Weron (2018) provide a comprehensive overview of the different approaches used in this field. A hybrid model combining point and probabilistic forecasting in four steps was developed by Maciejowska and Nowotarski (2016) for the GEFCom2014.

Common approaches to probabilistic electricity price forecasting include using time series models, such as ARIMA, GARCH and exponential smoothing (ETS) (e.g., Weron and Misiorek, 2008) and using deep learning models. Bootstrapping is widely used in combination with deep learning approaches (e.g., Chen et al., 2012; Wan et al., 2014; Rafiei et al., 2017; Khosravi et al., 2013). On top of deep learning, Zhao et al. (2008) use a support vector machine (SVM) to estimate prediction intervals and density forecasts, and Zhou et al. (2006) use an extended ARIMA model to do the same. An econometric model for probabilistic forecasting is proposed by Panagiotelis and Smith (2008). Manner et al. (2019) use vine-copula models to forecast quantiles for a vector of day-ahead electricity prices from interconnected electricity markets, while Grothe et al. (2023a) propose an approach based on copula techniques that entails generating multivariate probabilistic forecasts by modelling cross-hour dependencies. Considering these dependencies in probabilistic forecasts is uncommon, in contrast to point forecasts. However, including them in the methodology for generating probabilistic price forecasts can enhance forecast accuracy.

Historical simulation and distribution-based prediction intervals are other popular approaches. Historical simulation estimates risks and generates prediction intervals in the simulation of multiple scenarios using historical data; it then uses the results to estimate the probability of different outcomes (e.g., Weron and Misiorek, 2008; Nowotarski and Weron, 2015). Distribution-based prediction intervals are calculated based on the distribution of historical data (e.g., Misiorek et al., 2006; Zhao et al., 2008; Dudek, 2016; Maciejowska et al., 2016; Panagiotelis and Smith, 2008). A theoretical introduction to the generation of prediction intervals based on distribution and historical simulation is provided by Weron (2006).

Quantile regression averaging (QRA) is a method that has risen in prominence recently in probabilistic electricity price forecasting. It combines predictions from multiple quantile regression models, trained to predict a different quantile of the response variable. This method was first formally introduced by Nowotarski and Weron (2015) and has continued to be applied and developed further due to its accuracy (e.g., Maciejowska et al., 2016; Nowotarski and Weron, 2014; Marcjasz et al., 2020; Uniejewski et al., 2019; Uniejewski and Weron, 2021).

Despite the rising prominence of probabilistic forecasts in various models, there is still a general lack of approaches that combine probabilistic forecasting with techno-economic energy system models. We aim to fill this gap in the literature. By adapting and developing an energy system model specifically for the short-term electricity market and combining this model with common stochastic models through multiple steps, we can leverage the strengths of both models and open up the field of short-term electricity price forecasting for energy system models. Having already highlighted the positive effects of combining a stochastic model for better load forecasts with an energy system model for the day-ahead market in Möbius et al. (2023), these building blocks are included in the hybrid model. We demonstrate that a multi-layer hybrid model makes point and probabilistic price forecasting with techno-economic and stochastic models possible.

5.3. Data

In our study, we develop a hybrid model that integrates stochastic modelling approaches and energy system optimisation to forecast wholesale electricity prices. Notably, this energy system optimisation requires multiple inputs. Table 5.1 provides an overview of the necessary input data. In this section, we provide more details on how the data is obtained and applied.

Although our modelling approach can be applied to many markets, our empirical exercise focuses exclusively on the German spot market. However, the high level of integration among European electricity markets and the resulting interdependencies require a comprehensive representation of these markets, particularly during the energy system optimisation step. Figure 5.2 shows the geographical scope of the collected data and the interconnection among European markets. We consider the bidding zones of most of the EU's 27 member states[2] as well as Norway, Switzerland and the United Kingdom[3]. Unless stated otherwise, the collected data is from 2016 to 2020.

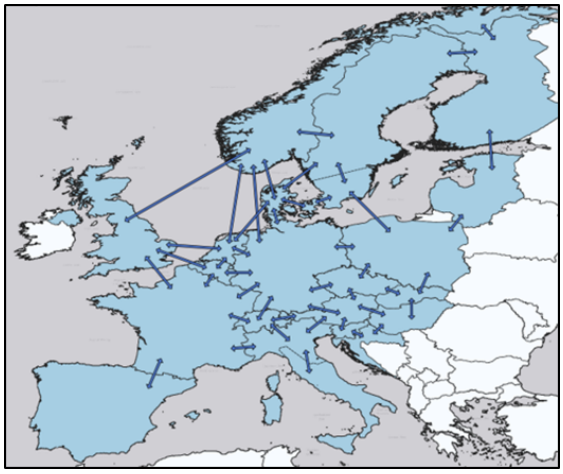

Figure 5.2.: Geographical scope of the energy system model.

[2]Bulgaria, Cyprus, Greece, Iceland, Ireland, Malta and Romania are omitted.

[3]Note that we aggregate the bidding zones of Spain and Portugal to a single "Iberian" market and the bidding zones of Lithuania, Estonia and Latvia to a single "Baltic" market. Additionally, note that we consider the distinct bidding zones within countries. However, we aggregate the following zones: in Norway, zones NO1–NO5; in Sweden, zones SE1–SE3; and in Italy, all zones but IT-North.

Table 5.1.: Overview of required data.

Parameter	Source
CO_2 prices	Sandbag (2020)
Control power procurement	Regelleistung.net (2018)
Efficiency of generation capacities	Schröder et al. (2013), Open Power System Data (2020b)
Efficiency losses at partial load	Schröder et al. (2013)
Electricity demand (load)	ENTSO-E Transparency Platform (2021l)
Energy-power factor (for storages)	own assumption: 9
Fuel prices (Lignite, nuclear, coal, gas, oil)	DESTATIS Statistisches Bundesamt (2021), ENTSO-E (2018), ENTSO-E (2018), EEX (2021)
Generation and storage capacity	BNetzA (2021), UBA (2020), EBC (2021), ENTSO-E Transparency Platform (2021j), Open Power System Data (2020a)
Generation by CHP units	European Commission (2021)
Historic electricity generation	ENTSO-E Transparency Platform (2021b)
Load shedding costs	own assumption: 3,000 €/MWh
Minimum output levels	Schröder et al. (2013)
NTCs	ENTSO-E Transparency Platform (2021f), JAO Joint Allocation Office (2021)
Variable O&M costs	Schröder et al. (2013)
Power plant outages	ENTSO-E Transparency Platform (2021n)
RES feed-in	ENTSO-E Transparency Platform (2021h)
RES curtailment costs	own assumption: 20 €/MWh
Start-up costs	Schröder et al. (2013)
Seasonal availability of hydro power	ENTSO-E Transparency Platform (2021b)
Temperature (daily mean)	Open Power System Data (2020b)
Water value	ENTSO-E Transparency Platform (2021b), ENTSO-E Transparency Platform (2021d)

Electricity demand is represented by hourly values for the system's electrical load, of which both a day-ahead forecast and the actual values are published by the respective transmission system operators (TSOs) and provided by ENTSO-E Transparency Platform (2021l). The collected load data for the Germany-Luxembourg bidding zone represents 2015 to 2020. In energy system models, electricity demand is usually considered volatile and inflexible in the short term. However, there is typically an option to shed load amid supply scarcity. In our application, we assume the cost of load shedding to be 3,000 €/MWh, as this was the maximum bidding price prior to September 2022[4].

The availability of intermittent renewable energy, namely onshore wind, offshore wind and photovoltaics (PV), depends on meteorological conditions and varies from hour to hour. The feed-in data of these energy sources are provided as hourly day-ahead forecasts by ENTSO-E Transparency Platform (2021h). Despite weather dependency, renewable energy electricity generation can still be intentionally curtailed. Acknowledging the various support schemes for renewable generation in Germany and Europe, which prevent renewable sources from being shut down immediately when negative prices occur, this study assumes curtailment costs of 20 €/MWh_{el}.

For conventional thermal generation, we distinguish between ten technologies and divide further by age if their technical parameters (especially those that impact efficiency) have changed significantly over time. We use 30 capacity clusters to group power plants based on technology and date of commissioning. We derive technology- and age-based efficiencies from Open Power System Data (2020a) data and assign them to the corresponding capacity clusters.

Moreover, we assign the clusters minimum output levels and efficiency losses in part-load operations based on Schröder et al. (2013). Hence, supply that follows fluctuations in demand and renewables is incentivised to shut down due to physical barriers (minimum output levels) and economic incentives (efficiency losses). The capacity, fuel type, generation technology and date of commissioning for units in the German market are derived from BNetzA (2021), UBA (2020) and Open Power System Data (2020a). For the remaining markets considered in our study, we use data from ENTSO-E Transparency Platform (2021j), Open Power System Data (2020a) and EBC (2021).

[4]The maximum bidding price was increased to 4,000 €/MWh on September 20th, 2022.

Power plant efficiency and the costs of fuel and CO_2 emissions form the variable generation costs of conventional thermal technologies. For fuel costs, we apply daily gas prices that are provided by EEX (2021), monthly coal and monthly oil prices from DESTATIS Statistisches Bundesamt (2021). Fuel costs for nuclear and lignite are derived from ENTSO-E (2018) and are assumed not to vary over the time horizon of our study. Prices for CO_2 certificates are taken as weekly data from Sandbag (2020).

Due to the time and additional fuel used by power plants to heat up during a start-up process, fuel and CO_2 prices also impact the cost of starting up a power plant. Further data regarding start-ups (e.g., secondary fuel usage, depreciation) are derived from Schröder et al. (2013).

Electricity generation relies on both the installed capacity and technical availability of power plants. As a result, we consider all scheduled and unscheduled outages that were known prior to the closure of the day-ahead market. Information on hourly outages is obtained from ENTSO-E Transparency Platform (2021n).

In most electricity markets, combined heat and power (CHP) plants are used, where electricity generation and heat supply are interconnected and reliant on each other. To account for this relationship, we apply a must-run condition to all CHP units to ensure operation at a minimum output level, as defined by the heat demand. These output levels are established in two steps. First, we calculate an hourly heat-demand factor consisting of temperature-dependent (spatial heating) and temperature-independent (warm water and process heat) components. The temperature-driven heat demand is calculated using heating degree days derived by mean temperature data obtained from Open Power System Data (2020b), while the temperature-independent heat demand is obtained from hourly and daily consumption patterns provided by Hellwig (2003). Second, we allocate annual electricity generation volumes from CHP plants to each hour of the year based on the hourly heat-demand factor. The data on annual technology-specific electricity generation from CHP units is sourced from European Commission (2021).

Control power is essential for system operators to ensure frequency stability at all times. The day-ahead market is affected by the market for control power provision, meaning that the capacities reserved for control power cannot be placed on the day-ahead market.

The amount of control power to be procured is an average of the tender results taken from Regelleistung.net (2018).

In addition to conventional thermal technologies and intermittent renewables, we consider waste, biomass, energy storage, hydro-reservoirs and run-of-river hydroelectricity. Since the operation of both waste and biomass has largely been historically constant (compare with ENTSO-E Transparency Platform (2021b)), we implement both technologies as base-load.

The energy storage units are divided into high capacity-to-energy ratios and low capacity-to-energy ratios. Storage units with high capacity-to-energy ratios actively charge and discharge. We exclusively consider a subset of pumped storage plants (PSPs) in this group. The overall turbine capacity of these PSPs is detailed by ENTSO-E Transparency Platform (2021j), and the efficiency of a storage cycle is around 75 % (Schröder et al., 2013). For these PSPs, we assume a capacity-to-energy ratio of 1/9 (see DENA, 2010). This means that the plant can generate electricity at full load for nine hours before its storage is emptied. Storage units with low capacity-to-energy ratios comprise long-term PSPs as well as hydro-reservoirs. They are assigned a variable generation cost in the model (i.e., an opportunity cost for water consumption). Using historical electricity prices from ENTSO-E Transparency Platform (2021d) and the observed generation and pumping activities in the respective hour from ENTSO-E Transparency Platform (2021b), we construct a step-wise merit order for long-term PSPs and hydro-reservoirs. Run-of-river and high-capacity-to-energy PSPs are assigned a monthly availability factor derived from the historical generation data from ENTSO-E Transparency Platform (2021b). We assume that 70 % of pump storage capacity belongs to high-capacity-to-energy PSPs, while the remaining 30 % of pump storage capacity belongs to low-capacity-to-energy PSPs.

European electricity markets are highly interconnected through cross-border transmission capacities. Thus, the German electricity market is also integrated into the European electricity system, with a total interconnector capacity of 27 GW, representing more than 30 % of the German peak load[5]. Annual aggregated exports, accounting for approximately 13 % of German consumption in 2019, and imports, making up around 7 % of consumption

[5]Note that the availability of the interconnectors depends on various factors (e.g., congestion within a market zone).

in the same year, are both significant. Our energy system model incorporates net transfer capacities (NTCs) as constraints on transmission between market zones. To achieve this, we use hourly day-ahead NTC forecasts provided by ENTSO-E Transparency Platform (2021f) and JAO Joint Allocation Office (2021).

While parameterised data sets interest numerous stakeholders, replicating these is a tremendous effort (see, e.g., Schröder et al., 2013; Kunz et al., 2017a); thus, our input data can be found in the supplementary materials.

5.4. Methodology

The implementation of the hybrid model is open-source; all data we could make public and the entire source code are available on GitHub under *https://github.com/ProKoMoProject/A-hybrid-model-for-day-ahead-electricity-price-forecasting-combining-fundamental-and-stochastic-mod*.

In this section, we present the components of the hybrid model, starting with the methodologies for the data pre-processing and parameter density forecast steps in Sections 5.4.1 and 5.4.2. Next, we introduce the dispatch market model used to generate the first price estimators in the energy system optimisation step in Section 5.4.3. Finally, we detail the model for the stochastic post-processing step in Section 5.4.4.

5.4.1. Stochastic Data Pre-Processing Step

Modelling the electricity market with a dispatch model requires an understanding of the several various fundamental variables, including demand (represented by load), which is a crucial element. The TSOs provide the actual load and a day-ahead load forecast, which has the potential to be improved, as demonstrated by, for example, Maciejowska et al. (2021) and Möbius et al. (2023). To enhance this forecast for Germany, we use a stochastic model for data pre-processing. Additionally, we model a two-day-ahead load forecast to capture power plant start-ups and shut-downs based on the load of the second following day, using the TSOs' day-ahead load forecast as a starting point.

Day-Ahead Load Forecast

We use the approach initially presented in Möbius et al. (2023) to improve load forecasting. Thus, we occasionally refer to it for detailed specifications and analyses. We propose a purely endogenous time series approach: a model for the TSOs' load forecast error ε_t that depends only on past values of the forecast error itself and, in turn, on the TSOs' load forecast $\hat{l}_t$. The forecast error is the difference between the actual load data l_t and the TSOs' load forecast $\hat{l}_t$. Designing a model for the error and forecasting it enables us to improve the TSOs' load prediction. The resulting load prediction $\hat{l}_t^{\,*}$ at time t is given by

$$\hat{l}_t^{\,*} = \hat{l}_t + \hat{\varepsilon}_t, \tag{5.1}$$

where $\hat{\varepsilon}_t$ is our forecasted TSOs' load prediction error. Thus, $\hat{l}^*$ is an improved load forecast in which we adjust the original forecast for the predictable structure of its error. The sub-index t denotes consecutive hours.

To model and forecast the forecast error ε_t, we use a decomposition model and decompose the error time series into the sum of a seasonal component and a stochastic component (see Lütkepohl (2005); Hyndman and Athanasopoulos (2021); Box et al. (2015) for comprehensive introductions to time series models):

$$\varepsilon_t = SC_t + RC_t, \tag{5.2}$$

where SC_t is a seasonal and RC_t is the remaining, stochastic component at time t.

Capturing a weekly season, the seasonal component SC_t for time t is defined by Formula (5.3) with $HS^{h,wd}$ being the average of TSO forecast errors for hour $h = 1, ..., 24$ and day $wd = 1$ (Monday), ..., 7 (Sunday), and $HoW_t^{h,wd}$ describing dummy variables to address the hour of the day and the day of the week:

$$SC_t = \sum_{h=1}^{24} \sum_{wd=1}^{7} HoW_t^{h,wd} \cdot HS^{h,wd}, \tag{5.3}$$

with

$$HS^{h,wd} := \frac{\sum_{s=t-h-l_w-23}^{t-h-24} \varepsilon_s \cdot HoW_s^{h,wd}}{\sum_{s=t-h-l_w-23}^{t-h-24} HoW_s^{h,wd}}, \tag{5.4}$$

$$HoW_t^{h,wd} = \begin{cases} 1, & \text{if } t \text{ is the h-th hour of the wd-th day of the week,} \\ 0, & \text{otherwise.} \end{cases}$$

For the residual component $RC_t = \varepsilon_t - SC_t$ of the time series, we propose an econometric SARMA $(1,1)\text{x}(1,1)_{24}$ model given by

$$\begin{aligned} RC_t =& \phi_0 + \phi_1 \cdot RC_{t-1} + \phi_{24} \cdot RC_{t-24} - \phi_1\phi_{24} \cdot RC_{t-25} \\ &+ \omega_1 \cdot \psi_{t-1} + \omega_{24} \cdot \psi_{t-24} + \omega_1\omega_{24} \cdot \psi_{t-25} \\ &+ \psi_t, \end{aligned} \tag{5.5}$$

where the innovations are assumed to be homoscedastic and normally distributed. This model contains an additional 24-hour seasonal component, making it stochastic, flexible and dependent on the values of past hours and days. In contrast, SC_t describes a static seasonality.

The model is estimated over a calibration window of one year. Within the hybrid model, the window is constantly rolled over by full days, with the forecast of the next day's 24 hours being made recursively. If no actual data are available due to time points in the future, we use forecast values for the model variables.

Two-Day-Ahead Load Forecast

Power plants make operational start-up and shut-down decisions based on the current day's demand, the demand from the day before and the expected demand on the next day. To account for this in the dispatch model, a forecast of load consumption is needed two days in advance. We use the modelling and forecast of the current load l_t (meaning the TSOs' day-ahead load forecast $\hat{l}_t$) as a starting point from which to forecast the day-ahead forecast for the second following day, resulting in a two-day-ahead forecast $\hat{l}_t^{2DA} = \hat{\hat{l}}_t$.

Therefore, we propose an econometric SARMA $(1,1)\text{x}(1,1)_{24}$ model with an additional exogenous variable, the TSOs' load forecast at lag 168:

$$\begin{aligned}\hat{\hat{l}}_t =& \phi_0 + \phi_1 \cdot \hat{l}_{t-1} + \phi_{168} \cdot \hat{l}_{t-168} + \phi_{24} \cdot \hat{l}_{t-24} - \phi_1\phi_{24} \cdot \hat{l}_{t-25} \\ &+ \omega_1 \cdot \psi_{t-1} + \omega_{24} \cdot \psi_{t-24} + \omega_1\omega_{24} \cdot \psi_{t-25}.\end{aligned} \tag{5.6}$$

The model's innovations ψ_t are assumed to be homoscedastic and normally distributed, meaning $\psi_t \sim N(0, \sigma_\varepsilon^2)$. The model features 24-hour seasonality. Since we also observe weekly seasonality, we include the TSOs' load forecast at the same hour one week earlier, $\hat{l}_{t-168}$, as a regressor.

We calibrate and estimate the model based on window length l_w, which contains one year of historical data. The estimated model is used to recursively (i.e., on an hourly basis) predict the values of each hour of the next day. Since we rely on an autoregressive time series model, day-ahead load forecasts from 168 hours to one hour before the predicted hour are included in the model as explanatory variables for the two-day-ahead prediction. However, this means that some values are unavailable when the forecast is made. They are replaced with recursively forecasted values based on the most recently available observations.

Given the increased uncertainty associated with forecasting two days ahead, our hybrid model incorporates a parameter density forecast that considers various scenarios for the level and development of load, utilising the hourly two-day-ahead load forecast as an input variable.

5.4.2. Parameter Density Forecast Step

To account for uncertainty in two-day-ahead load predictions, scenarios are calculated at the 5 % and 95 % quantiles using QRA. It describes a method for determining quantiles of predictive cumulative distribution functions, which can then be used to construct prediction intervals. A prediction interval is calculated using the $(\alpha/2)$-th and $(1-\alpha/2)$-th quantile of the predictive cumulative distribution function, $\alpha \in (0,1)$, as the lower and upper bound of the interval. QRA is based on quantile regression and aims to model quantiles of real-valued variables that depend on explanatory variables (see, e.g., Koenker and Bassett, 1978). It employs point predictions to explain the q-th quantile of the

conditional distribution of the observation, setting a fixed $q \in (0,1)$. Here, quantile regression uses a vector of regressors $X_t = [1, \hat{l}_t^{2DA}]$, including a value of one for the intercept and the two-day-ahead point prediction for the load at given time t, to calculate the two-day-ahead load prediction in the q-th quantile ($Q_{l_t}(q|\cdot)$) (conditional on additional information):

$$Q_{l_t}(q|X_t) = X_t\beta_q \tag{5.7}$$

Thereby, β_q is a vector of parameters for the q-th quantile. QRA estimates β_q and, thus, the q-th quantile by minimising the pinball loss function of the respective q-th quantile, given by

$$\hat{\beta}_q = \arg\min_{\beta} \Big[\sum_{t:l_t \geq X_t\beta} (q - \mathbf{1}_{l_t < X_t\beta})(l_t - X_t\beta) \Big], \tag{5.8}$$

where $\mathbf{1}$ is the indicator function (see, e.g., Nowotarski and Weron, 2015, 2018).

We use the two-day-ahead load prediction $\hat{l}_t^{2DA}$ and the corresponding load from a one-year historical period to estimate the unknown parameter β_q. After calculating the 5 % and 95 % quantiles, the scenarios cover 90 % of possible load forecast values with $\alpha = 0.9$. With the parameter density forecast and the point forecast of expected value, this approach provides three possible scenarios for the two-day-ahead load: an expected scenario, described with the two-day-ahead load forecast, a low scenario described with the hourly estimated 5 % quantile, and a high scenario described with the hourly estimated 95 % quantile. Motivated by optimal integration rules in Grothe (2013) (and setting $\kappa = 2$, as recommended in that work), we weight the expected value with 2/3 and each quantile with 1/6 to include the scenarios in the *em.power dispatch* model described below.

5.4.3. Energy System Optimisation Step

This section presents the energy system model *em.power dispatch*, which generates wholesale day-ahead price estimators in the hybrid model's energy system optimisation step. The model considers a detailed representation of the key techno-economic aspects

of an integrated European electricity sector, including transmission restrictions between markets, electricity production by CHPs, energy storage and control power provision. For all considered market zones, our model determines the optimal dispatch decisions for various generation and storage technologies, the most effective use of cross-border transmission capacities and the short-run marginal system costs[6], which determine the price estimators for the day-ahead market in hourly resolution.

Since our research focuses on day-ahead price forecasts, the energy system model is developed to reflect the level and quality of information available to market participants on the day before delivery. The model is formulated as a linear optimisation problem minimising total system costs. Ensuring the linear formulation of a highly complex system, we form capacity clusters, parameterising them as described in Section 5.3. Within each capacity cluster, capacity units can be started up, and electricity can be produced in marginal increments (see Müsgens, 2006a). This approach has two key advantages. First, it reduces computational requirements. Second, the problem is differentiable at each point, and the dual variable of the demand constraint can be interpreted as a wholesale market price estimator. Additionally, the accuracy of modelling large energy systems remains reasonably high for our purpose (Müsgens and Neuhoff, 2006).

We implement the resultant imperfect forecasts with two model features. First, we implement a rolling window approach that repeatedly solves three days ($d \in D = \{d, d+1, d+2\}$), as shown in Figure 5.3. In this setting, the 24 hours of the target day are represented by the second day of the horizon ($d+1$). This follows the EPEX spot market organisation, in which 24 hourly day-ahead prices are determined at 12 p.m. on the day before delivery (d). In addition to the target day ($d+1$), we include the day before (d) and the day after ($d+2$). By considering three days in our rolling window, we reduce the problems of starting and ending values, particularly those stemming from power plant start-ups and pump storage plants. Second, we account for the increased uncertainty of the two-day-ahead estimate of key parameters. While parameters for the day d are fully known, and forecasts for $d+1$ are made available by the European Network of Transmission System Operators for Electricity (ENTSO-E), the realisation of key input parameters exhibits higher uncertainty in $d+2$. Therefore,

[6] Technically, the dual variable of demand constraint derives the short-run marginal system cost, also called "shadow price".

we implement probabilistic forecast intervals only in $d+2$, as shown in Figure 5.3. All other days are provided through one scenario. The resulting stochastic rolling window is then repeatedly solved using only data available to market participants when they need to make their decisions. In each model run, we extract the information for the 24 hours of our "target day" – the day ahead.

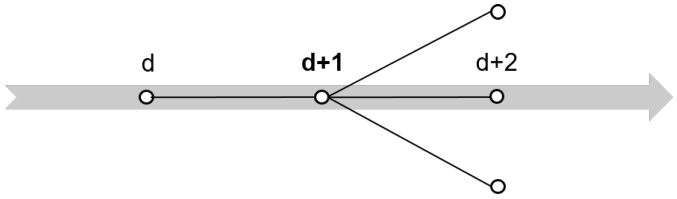

Figure 5.3.: Illustration of the rolling window for the energy system optimisation step.

The optimisation problem is repeatedly solved each day. For the reader's convenience, we provide a nomenclature in Appendix B. Note that all endogenous variables are written in upper case, and all exogenous parameters are written in lower case.

The objective function minimises total system costs (TC) consisting of the expected value of all operational costs (OC) across all three days of a rolling window d^*, given by

$$\min TC = \mathbb{E}_s[OC(s)], \tag{5.9}$$

where our empirical exercise considers three scenarios s to be equally likely to appear.

The operational costs in Formula (5.10) contain all of the short-term costs that generation units face. We include costs at full-load operation ($vc^{FL}_{i,n,d,h}$), additional costs for units that operate at partial load ($vc^{ML}_{i,n,d,h} - vc^{FL}_{i,n,d,h}$) and start-up costs ($sc_{i,n,d,h}$). Note that we apply a linear unit commitment formulation and that all units must produce at least a certain minimum output level (see Formulas (5.12) – (5.16)). Additionally, we account for load-shedding costs ($voll$) and penalty payments for curtailing renewables

($curtc$), as discussed in Section 5.3.

$$\begin{aligned} OC_s = & \sum_{i,n,d,h} G_{i,n,d,h,s} \cdot vc^{FL}_{i,n,d,h} + \sum_{i,n,d,h} SU_{i,n,d,h,s} \cdot sc_{i,n,d,h} \\ & + \sum_{i,n,d,h} (P^{on}_{i,n,d,h,s} - G_{i,n,d,h,s}) \cdot (vc^{ML}_{i,n,d,h} - vc^{FL}_{i,n,d,h}) \cdot g^{min}_i / (1 - g^{min}_i) \\ & + \sum_{stl,n,d,h} G_{stl,n,d,h,s} \cdot wv_{stl,n,d,h} - \sum_{stl,n,d,h} CL_{stl,n,d,h,s} \cdot wv_{stl,n,d,h} \\ & + \sum_{hr,n,d,h} G_{hr,n,d,h,s} \cdot wv_{hr,n,d,h} + \sum_{n,d,h} SHED_{n,d,h,s} \cdot voll \\ & + \sum_{res,n,d,h} CURT_{res,n,d,h,s} \cdot curtc \end{aligned} \tag{5.10}$$

As we apply our model with a rolling window, each model run considers three days d with 24 hours each day, meaning 72 hours per daily model run. Modelling an additional day before and after the target day seems appropriate for storage units operated on a daily cycle. However, storage units (PSPs and seasonal storage units without pumps) have longer than three days of storage cycle. Therefore, PSPs are divided into low-capacity-to-energy storage which operates storage cycles longer than three days, and high-capacity-to-energy storage operating one or more storage cycles within a three-day horizon. The dispatch of the latter is determined endogenously. Low-capacity-to-energy PSPs are assigned a water value $wv_{stl,n,d,h}$ that is implemented as a variable cost factor for electricity generation $G_{stl,n,d,h,s}$ and electricity consumption $CL_{stl,n,d,h,s}$.

Moving beyond pumped storage plants, hydro reservoirs have a natural water feed-in and do not have pumps installed. However, the water budget for electricity generation is limited by seasonal inflow volumes. We also apply a water value $wv_{hr,n,d,h}$ to account for the opportunity costs of electricity generation from hydro reservoirs ($G_{hr,n,d,h,s}$).

Market clearing is ensured by Formula (5.11). For all 72 hours of the given rolling window, demand must equal the sum of generation, load shedding and electricity imports, reduced by the electricity consumption of mid-term energy storage and of long-term energy storage as well as by electricity exports. The dual variable of the demand constraint, expressed in Formula (5.11), is used as an hourly day-ahead wholesale electricity price

estimator.

$$\begin{aligned} l_{n,d,h,s} = & \sum_{i} G_{i,n,d,h,s} - \sum_{stm \subset I} CM_{stm,n,d,h,s} - \sum_{stl \subset I} CL_{stl,n,d,h,s} \\ & + \sum_{nn} (FLOW_{nn,n,d,h,s} - FLOW_{n,nn,d,h,s}) + SHED_{n,d,h,s} \\ & \forall n, nn \in N, d \in D, h \in H, s \in S \end{aligned} \tag{5.11}$$

Note that we apply the improved point forecast for the load created in Section 5.4.1 to Germany in d and $d+1$, as we focus on price predictions for the German market. For all other markets, we implement the original ENTSO-E forecasts. For $d+2$ in Germany, we apply the probabilistic load forecast presented in Section 5.4.2. For the remaining markets, we use the actual realisation of the previous week as a more naive estimator.

Electricity generation by a capacity cluster is limited by upper and lower bounds. The upper bound is formalised in Inequation (5.12). It ensures that electricity generation does not exceed the running capacity ($P^{on}_{i,n,d,h,s}$) in the cluster. The potential to generate electricity by running capacity is further limited by the reserve for positive control power provision ($PCR_{i,n,bp,s}$ and $SCR^{pos}_{i,n,bs,s}$). The lower bound is presented in Inequation (5.13). It states that running capacities must operate at a minimum power level, including the capacity reserved for negative control power provision ($PCR_{i,n,bp}$ and $SCR^{neg}_{i,n,bs,s}$). Note that primary control power provision ($PCR_{i,n,bp,s}$) in Germany is symmetrical (i.e., a unit must provide both positive and negative primary control power). Different positive and negative control power products were introduced for secondary control power. We do not include minute reserve requirements in the model for two reasons. First, fast-reacting units (e.g., hydro, open-cycle gas turbines) can be started up to provide positive minute reserve without being dispatched. Second, both positive and negative reserves can be provided by multiple market players other than the power plants included in the model (e.g., demand flexibility, P2X units, emergency power generators). The hours that belong to bidding blocks are mapped for primary control power by bp and for secondary control power by bs.

$$\begin{aligned} & G_{i,n,d,h,s} \leq P^{on}_{i,n,d,h,s} - PCR_{i,n,bp|h \in bp,s} - SCR^{pos}_{i,n,bs|h \in bs,s} \\ & \forall bp \in BP, bs \in BS, i \in I, n \in N, d \in D, h \in H, s \in S \end{aligned} \tag{5.12}$$

$$P^{on}_{i,n,d,h,s} \cdot g^{min}_{i} + PCR_{i,n,bp|h\in bp,s} + SCR^{neg}_{i,n,bs|t\in bs,s} \leq G_{i,n,d,h,s}$$
$$\forall bp \in BP, bs \in BS, i \in I, n \in N, d \in D, h \in H, s \in S \tag{5.13}$$

The installed capacity limits the running capacity of a power system ($cap_{i,n,d,h}$) in combination with either the availability factor ($af_{i,n,d,h}$) or power plant outages ($out_{i,n,d,h}$), given by

$$P^{on}_{i,n,d,h,s} \leq cap_{i,n,d,h} \cdot af_{i,n} - out_{i,n,d,h} \qquad \forall i \in I, n \in N, h \in H, d \in D, s \in S. \tag{5.14}$$

For thermal generation capacities, we use hourly power plant outages. Renewables are provided with an hourly availability factor, while hydroelectric units are provided with a monthly availability factor.

Formula (5.15) tracks start-up activities ($SU_{i,n,d,h,s}$) that increase running capacity from one hour to another. Due to the non-negativity condition, start-ups are either positive or zero. Formula (5.16) tracks start-up activities from the last hour of a day to the first hour of the following day.

$$P^{on}_{i,n,d,h,s} - P^{on}_{i,n,d,h-1,s} \leq SU_{i,n,d,h,s} \quad \forall i \in I, n \in N, h \in H, d \in D, s \in S \tag{5.15}$$

$$P^{on}_{i,n,d,hfirst,s} - P^{on}_{i,n,d-1,hlast,s} \leq SU_{i,n,d,hfirst,s} \quad \forall i \in I, n \in N, d \in D, s \in S \tag{5.16}$$

The difference between available feed-in from intermittent renewables and their actual generation defines the curtailment of renewables, given by

$$cap_{res,n,d,h} \cdot pf_{res,n,d,h} = G_{res,n,d,h,s} + CURT_{res,n,d,h,s}$$
$$\forall n \in N, res \in I, d \in D, h \in H, s \in S. \tag{5.17}$$

Some power plants are active in both the heat market and the electricity market. Thus, the model implements a must-run condition for such units on the electricity market, which varies over time (e.g., higher in the winter season due to space heating). Depending on hourly heat demand, Formula (5.18) states that the output of a combined heat and power unit is at least equal to the electricity generation linked to the heat production

($chp_{i,n,d,h}$):

$$chp_{i,n,d,h} \leq G_{i,n,d,h,s} \qquad \forall i \in I, n \in N, d \in D, h \in H, s \in S. \tag{5.18}$$

The net transfer capacity ($ntc_{n,nn,d,h}$) constrains the cross-border electricity transfer ($FLOW_{n,nn,d,h,s}$):

$$FLOW_{n,nn,d,h,s} \leq ntc_{n,nn,d,h} \qquad \forall n, nn \in N, d \in D, h \in H, s \in S. \tag{5.19}$$

Formula (5.20) describes the state of the storage level of mid-term storage units. It decreases with electricity generation ($G_{stm,n,d,h}$) and increases with charging ($ST^{in}_{stm,n,d,h,s}$). The efficiency of an entire storage cycle (η_{stm}) is assigned to the charging process.

$$\begin{aligned} &SL_{stm,n,d,h,s} = SL_{stm,n,d,h-1,s} - G_{stm,n,d,h,s} + CM_{stm,n,d,h,s} \cdot \eta_{stm} \\ &\forall stm \in I, n \in N, d \in D, h \in H, s \in S \end{aligned} \tag{5.20}$$

Formula (5.21) ensures the functionality of the storage mechanism between two days:

$$\begin{aligned} SL_{stm,n,d,hfirst,s} =& SL_{stm,n,d-1,hlast,s} - G_{stm,n,d,hfirst,s} \\ &+ CM_{stm,n,d,hfirst,s} \cdot \eta_{stm} \\ &\forall stm \in I, n \in N, d \in D, s \in S. \end{aligned} \tag{5.21}$$

The maximum energy storage capacity ($SL_{stm,n,d,h,s}$) of storage units with high capacity-to-energy ratios is defined by their maximum installed turbine capacity divided by their capacity-to-energy ratio (cer):

$$SL_{stm,n,d,h,s} \leq cap_{stm,n,d,h} \cdot cer \qquad \forall stm \in I, n \in N, d \in D, h \in H, s \in S. \tag{5.22}$$

Formula (5.23) restricts both turbine capacity and pumping capacity, with pumping capacity assumed to be 10 % lower than the turbine capacity:

$$\begin{aligned} &G_{stm,n,d,h,s} + 1.1 \cdot CM_{stm,n,d,h,s} \leq cap_{stm,n,d,h} \\ &\forall stm \in I, n \in N, d \in D, h \in H, s \in S. \end{aligned} \tag{5.23}$$

At the beginning and at the end of each model run, all storage units with high capacity-to-energy ratios must be filled with at least 30 % of their energy level:

$$SL_{stm,n,dfirst,hfirst,s} = 0.3 \cdot cap_{stm,n,d,h} \qquad \forall stm \in I, n \in N, s \in S, \quad (5.24)$$

$$SL_{stm,n,dlast,hlast,s} = 0.3 \cdot cap_{stm,n,dlast,hlast} \qquad \forall stm \in I, n \in N, s \in S. \quad (5.25)$$

Storage plants with low capacity-to-energy ratios are not subject to a storage mechanism. However, these units' electricity generation and consumption are restricted to their installed capacity by

$$G_{stl,n,d,h,s} + CL_{stl,n,d,h,s} \leq cap_{stl,n,d,h} \qquad \forall n \in N, stl \in I, d \in D, h \in H, s \in S. \quad (5.26)$$

Formulas (5.27), (5.28) and (5.29) ensure the control power provision for primary, positive secondary and negative secondary control power.

$$\sum_i PCR_{i,n,bp,s} = pr_n \qquad \forall bp \in BP, n \in N, s \in S \quad (5.27)$$

$$\sum_i SCR^{pos}_{i,n,bs,s} = sr^{pos}_n \qquad \forall bs \in BS, n \in N, s \in S \quad (5.28)$$

$$\sum_i SCR^{neg}_{i,n,bs,s} = sr^{neg}_n \qquad \forall bs \in BS, n \in N, s \in S \quad (5.29)$$

The non-negativity constraint ensures that the individual variables do not show negative values and is given by

$$\begin{aligned} 0 \leq & CL_{stl,n,d,h,s}, CM_{stm,n,d,h,s}, CURT_{res,n,d,h,s}, G_{i,n,d,h,s}, \\ & FLOW_{n,nn,d,h,s}, P_{i,n,d,h,s}, PCR_{i,n,bp,s}, SCR^{neg}_{i,n,bs,s}, SCR^{pos}_{i,n,bs,s}, \\ & SHED_{n,d,h,s}, SL_{stm,n,d,h,s}, SU_{i,n,d,h,s} \\ & \forall n, nn \in N, bp \in BS, bs \in BS, i \in I, n \in N, h \in H, d \in D, s \in S. \end{aligned} \quad (5.30)$$

5.4.4. Stochastic Data Post-Processing Step

In this step, we use a stochastic post-processing technique to refine the estimators produced by the techno-economic energy system model. Specifically, we forecast the errors ε_t of the

day-ahead price estimators $\hat{P}_t$ obtained from the energy system optimisation step, either by a time series based point forecast $\hat{\varepsilon}_t$ or by inferring the forecast errors distribution functions to generate probabilistic day-ahead price predictions. We incorporate exogenous variables such as renewable energy feed-in and weather, as well as lags of the forecast error itself into the time series forecast of ε_t.

We start with the improved point prediction $\hat{P}_t^*$ at time t which is given by

$$\hat{P}_t^* = \hat{P}_t + \hat{\varepsilon}_t, \tag{5.31}$$

where $\hat{P}_t$ is the price prediction from the last step, and $\hat{\varepsilon}_t$ is our model's forecasted price prediction error. Thus, $\hat{P}^*$ constitutes an improved price forecast in which we adjust the forecast from the last step for the stochastic but predictable structure in its error.

We employ two model frameworks – univariate and multivariate – as this approach has been proven to be useful in past research (Ziel and Weron, 2018a). In the univariate framework, we interpret the forecast error time series as one high-frequency time series in an hourly resolution. In the multivariate framework, we split the time series into 24 individual time series, one for each hour, making them in a daily resolution.

For the post-processing setup, subindexes h, d will denote hours one through 24 of day d, with d being consecutive days. So, $P_{1,1}$, for instance, is the actual day-ahead price of the first hour of the first day of the considered period, and $\varepsilon_{5,432}$ is the error of the price estimator of the fifth hour of the 432nd day. This fits best because it enables us to observe a realisation of 24 prices for the hours of the next day simultaneously for electricity prices. Note that if $h-1$ is equal to or less than zero, we would need to shift one day backwards. Likewise, if $h+1$ is greater than 24, we would need to shift one day forward.

We chose a standard econometric time series model for the univariate framework. It consists of endogenous (i.e., autoregressive with moving average structures) and exogenous variables, all of which are integrated into a regression model given by Formula 5.32. To address several seasonal structures included in the time series of the prices' forecast errors $\varepsilon_{h,d}$, we use the first and second observation backwards $(\varepsilon_{h-1,d}, \varepsilon_{h-2,d})$ as well as the first back error $\psi_{h-1,d}$ of the estimated model. Additionally, we use the observation one day before $\varepsilon_{h,d-1}$ (daily structure) and one week before $\varepsilon_{h,d-7}$ (weekly structure) as

endogenous explanatory variables. Considering daily effects, we include the minimum and maximum forecast errors for the day before ($\varepsilon_{min,d-1}, \varepsilon_{max,d-1}$). To account for the strong effects of forecast errors on public holidays, we use a dummy variable $M_{h,d}$ for public holidays as another factor. Additionally, we include an hourly wind forecast $X_{h,d}$.

$$\begin{aligned}\varepsilon_{h,d} =& \phi_0 + \phi_1 \cdot \varepsilon_{h-1,d} + \phi_2 \cdot \varepsilon_{h-2,d} + \phi_3 \cdot \varepsilon_{h,d-1} + \phi_4 \cdot \varepsilon_{h,d-7} + \phi_5 \cdot \psi_{h-1,d} \\ &+ \omega_1 \cdot \varepsilon_{min,d-1} + \omega_2 \cdot \varepsilon_{max,d-1} + \omega_3 \cdot M_{h,d} + \omega_4 \cdot X_{h,d} \\ &+ \psi_{h,d}\end{aligned} \tag{5.32}$$

As in the univariate framework, we use the well-known time series model ARX in the multivariate framework. However, the autoregressive component refers to values of the same hour on previous days. The endogenous variables $\varepsilon_{h,d-1}$ and $\varepsilon_{h,d-7}$ are the forecast errors at the same hour one day prior and seven days prior, respectively. The exogenous variables are the same as in the univariate framework: minimum and maximum forecast errors for the day before, a dummy variable for public holidays and an hourly wind forecast. Thus, the model for the multivariate framework is given by

$$\begin{aligned}\varepsilon_{h,d} =& \phi_0 + \phi_1 \cdot \varepsilon_{h,d-1} + \phi_2 \cdot \varepsilon_{h,d-7} \\ &+ \omega_1 \cdot \varepsilon_{min,d-1} + \omega_2 \cdot \varepsilon_{max,d-1} + \omega_3 \cdot M_{h,d} + \omega_4 \cdot X_{h,d} \\ &+ \psi_{h,d},\end{aligned} \tag{5.33}$$

where ϕ_i, ω_i describe the coefficients that need to be estimated. The innovations ψ are assumed to be homoscedastic and normally distributed in both frameworks, meaning $\psi_{h,d} \sim N(0, \sigma_\epsilon^2)$.

Since we rely on an autoregressive time series model, we need day-ahead spot prices from the last hours before prediction time as explanatory variables. In the multivariate framework, only one step into the future is forecasted at a time due to the separate modelling of each hour. In the univariate framework, 24 values are forecast for the future, with the hours of the next day predicted recursively (i.e., on an hour-by-hour basis). Unavailable variables are replaced with recursively forecasted variables based on the most recent available observations.

In line with approaches previously shown to be effective in the literature (see, e.g., Marcjasz et al., 2018), we vary the presented post-processing models by using different window lengths to estimate the model setup and prevent random choice. We determine the calibration window for 44, 48 and 52 weeks. By using three window lengths and two model frameworks, we end up with six individual sub-models. These sub-models are used to predict the values of the hours h, $h = 1, ..., 24$ of the next day d, and we denote them by $\hat{P}^{uv44}_{h,d}$, $\hat{P}^{uv48}_{h,d}$, $\hat{P}^{uv52}_{h,d}$, $\hat{P}^{mv44}_{h,d}$, $\hat{P}^{mv48}_{h,d}$, $\hat{P}^{mv52}_{h,d}$.

Our final improved point forecast $\hat{P}_t^{\,*}$ is obtained by taking the arithmetic average of the six prices. Despite the potential appeal of using seemingly more sophisticated methods, such as calculating optimal weights via linear regression based on past data, these methods resulted in predictors with higher root mean squared errors (RMSE) and mean absolute errors (MAE), even when we used rolling windows that look into the future. This is mainly due to the additional estimation noise that is introduced when using such methods and may lead to inefficiencies as discussed, e.g., in the context of financial literature in DeMiguel et al. (2009). As a result, we stick with the simpler, yet more robust method of averaging the six individual forecasts.

We now move on to generating probabilistic day-ahead price predictions. To achieve this, we use the six forecasts generated by the individual sub-models to estimate the cumulative distribution function $F_{P_{h,d}}$ of the day-ahead prices. The estimated function $\hat{F}_{P_{h,d}}$ serves as our probabilistic forecast for the price of the next day. We represent the distribution $\hat{F}_{P_{h,d}}$ in terms of its quantiles. Specifically, we employ quantile regression to model the conditional q-th quantile of the cumulative distribution function of the day-ahead prices, where q is a value between 0 and 1. This modelling is accomplished by utilising the six individual point predictions and the following equation:

$$Q_{P_{h,d}}(q|X_{h,d}) = X_{h,d}\beta_q, \tag{5.34}$$

where $X_{h,d} = [1, \hat{P}^{uv44}_{h,d}, \hat{P}^{uv48}_{h,d}, \hat{P}^{uv52}_{h,d}, \hat{P}^{mv44}_{h,d}, \hat{P}^{mv48}_{h,d}, \hat{P}^{mv52}_{h,d}]$ is the vector of regressors containing a value of one for the intercept and the six individual point predictions for the day-ahead price at time h, d. β_q is again estimated by minimising the pinball loss function. To determine the predictive distribution, we forecast multiple quantiles of the distribution.

The coefficients of the regressors are estimated by a calibration window of one year with a distinction made between peak and off-peak hours. Peak hours are defined as those between 8 a.m. and 8 p.m. from Monday to Friday, while off-peak hours are all remaining hours. This distinction is made because peak hours are characterised by high demand for electricity and, therefore, often exhibit higher day-ahead prices. For each quantile q, we estimate two parameter vectors β_q (see Formula (5.8)). Estimating one parameter vector β_q for all day hours proved to be less accurate. Additional information on this matter can be provided upon request.

In summary, our hybrid model includes the following steps. To predict the next day, we first enhance the TSOs' day-ahead load forecast and predict the two-day-ahead load forecast in the stochastic data pre-processing step. We then calculate the two-day-ahead load scenarios in the parameter density forecast step and include them in the *em.power dispatch* in the energy system optimisation step to generate the first price estimators for the day-ahead spot market. Finally, in the stochastic post-processing step, we improve these price estimators with stochastic methods and conduct probabilistic price forecasts. This sequence is repeated continuously, day by day, for all points in time in our observation period. The hybrid model's rolling window approach means that we always use the most up-to-date available data.

5.5. Hybrid Model Results

In this section, we present the day-ahead electricity price forecasts of our hybrid model for Germany from January 2016 to December 2020[7]. Since the day-ahead market is organised in an hourly resolution, our hybrid model calculates point and probabilistic forecasts for each hour of the following day. As the central point of this chapter, we present the overall results of the model (i.e., the point and probabilistic price predictions) and qualitatively detail their place in the literature.

We start by comparing the point forecasts of our hybrid model to those in the literature. With an annual average RMSE of 7.38 €/MWh and MAE of 4.60 €/MWh over the five years from 2016 to 2020, our model aligns well with previous studies. An expert

[7] More precisely, prices cover the German-Austria-Luxembourg bidding zone from January 2016 to September 2018 and the German-Luxembourg bidding zone from October 2018 to December 2020.

model developed by Ziel and Weron (2018a) forecasted electricity prices with an overall MAE of 5.01 €/MWh for 2012 to 2016. Using an autoregressive model with exogenous variables, Maciejowska et al. (2021) achieved a RMSE of 8.43 €/MWh and a MAE of 5.92 €/MWh for 2016 to 2019. For the same period, Qussous et al. (2022) obtained a RMSE of 11.21 €/MWh and a MAE of 7.89 €/MWh, presenting an agent-based power market-simulation model with rule-based bidding strategies. Thus, they developed a non-equilibrium-oriented techno-economic market model aimed to reproduce day-ahead electricity prices. Since they provided extensive information on the error measures, we can use this model for a detailed comparison in the following. However, as the time periods in these presented studies are overlapping with but not identical to our observation period, we also perform a detailed comparison with the LEAR model developed by Lago et al. (2021). The LEAR model's source code is freely available, so we can extend it with data from the years up to 2020. Furthermore, its day-ahead price forecasts are among the most precise in the literature, and its authors are leading scholars in the field of price forecasting. Thus, we can perform a year-by-year comparison with our results. Table 5.2 presents the forecast accuracy of the developed hybrid model, the agent-based market simulation model and the LEAR model, showing the annual RMSE and MAE. It can be seen that the agent-based model has the highest error, which can be attributed to the general difficulties of techno-economic models in making short-term forecasts (the results of the *em.power dispatch* model without further post-processing steps are compiled in Section 5.6.2 and point in the same direction). In contrast, the LEAR model and the proposed hybrid model presented here exhibit similar error measures without larger gaps. Although the LEAR model more often takes the lead, its advantage is limited, as it is a statistical model primarily designed for generating price forecasts. Comparatively, the hybrid model's forecast encompasses the entire market state represented by the energy system model, including information on additional parameters of interest to market participants (e.g., CO_2 emissions, international electricity exchange, and power plant utilisation)[8].

A more detailed evaluation of the prediction errors of the hybrid model is provided in Figures 5.4 and 5.5, which show the RMSE for different criteria, such as base, peak and

[8] Note that while this work focuses exclusively on prices, this model can also be informative about other factors, as discussed in the literature review.

Table 5.2.: RMSE and MAE of day-ahead electricity price forecast through the presented hybrid model, the agent-based model Qussous et al. (2022) and the LEAR model Lago et al. (2021) in [€/MWh].

	RMSE			MAE		
	Hybrid	Agent	LEAR	Hybrid	Agent	LEAR
total	7.38	11.21	7.24	4.60	7.89	4.38
2016	5.82	8.83	5.55	3.48	6.54	3.30
2017	8.79	13.01	7.91	5.25	9.44	4.56
2018	7.28	11.69	6.96	5.07	8.88	4.84
2019	7.05	10.91	7.95	4.43	6.69	4.53
2020	7.63		7.54	4.77		4.65

off-peak hours, and the hours of actual day-ahead price quantiles, respectively. Again, peak hours are those between 8 a.m. and 8 p.m. from Monday to Friday; off-peak hours are the remaining hours. Base hours describe all hours of the day, regardless of the day of the week or hour of the day.

While the errors of 7.47 €/MWh in peak hours and 7.33 €/MWh in off-peak hours seem quite similar over the whole period, Figure 5.5 provides more insight. Therein, we separate the predicted hours into five groups presenting the hours for each confidence interval of realised day-ahead prices in 20 % steps, and calculate and evaluate the RMSE for each group. The figure suggests a relationship between the error in price forecasts and the price level. Throughout the years, the highest RMSE has consistently been identified in the hours with the lowest 20 % and highest 20 % of prices. Based on economic theory, this finding can be explained by start-up costs and their impact on hourly prices. Assuming perfect foresight, Kuntz and Müsgens (2007) have shown that start-up costs are added to fuel costs exclusively during the hour of highest demand in a cycle because additional capacity must be started-up for that hour, which is not needed in any other hour. During the hour of lowest demand, start-up costs are deducted from variable production costs because power plants save costs on re-starts when allowed to continue operations throughout that hour. In contrast, start-up costs do not influence prices during any other hour of a load cycle. The *em.power dispatch* model follows this economic theory when determining wholesale electricity prices based on the shadow prices of the demand constraint. However, in reality, bidders on the day-ahead market face uncertainties with

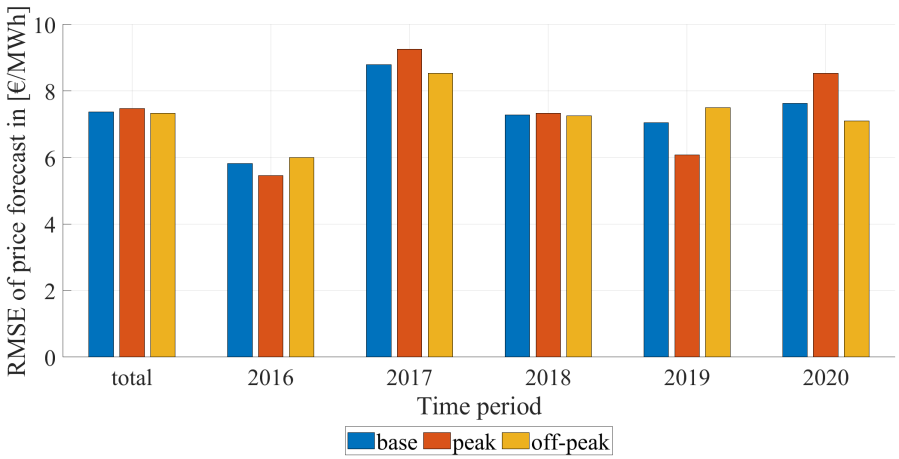

Figure 5.4.: RMSE for base, peak and off-peak hours.

regard to which hour has the highest and lowest residual demand and what magnitude start-up costs have for that day. While uncertainty is always present, its impact is likely higher when start-up costs need to be considered in addition to fuel costs and thus increase price volatility around the highest and lowest price hours. Therefore, negative and positive price peaks are harder to capture and forecast than intermediate price levels. Note that this increased uncertainty in these market conditions affects all point forecasting models. Corresponding figures for the LEAR model show a very similar pattern (Figure 5.6).

We now turn to the analysis of our probabilistic forecasts. We represent the forecast distribution of the day-ahead prices for each forecast hour with quantile estimates in 5 % steps. The quantile estimation for different quantile levels then enables the calculation of forecast intervals, which determine the probability of the day-ahead price being within a certain range.

The first thing to check about probabilistic forecasts is whether they are well calibrated (see, e.g., Gneiting et al., 2007), which means whether forecasted probabilities and observed frequencies coincide. Therefore, Figure 5.7 shows the absolute frequency of all hours in which the day-ahead prices are above or below the forecast quantile limits. A forecast is considered calibrated if the predicted probabilities match the observed frequencies of the target variable over time. Thus, a fully calibrated forecast in a laboratory

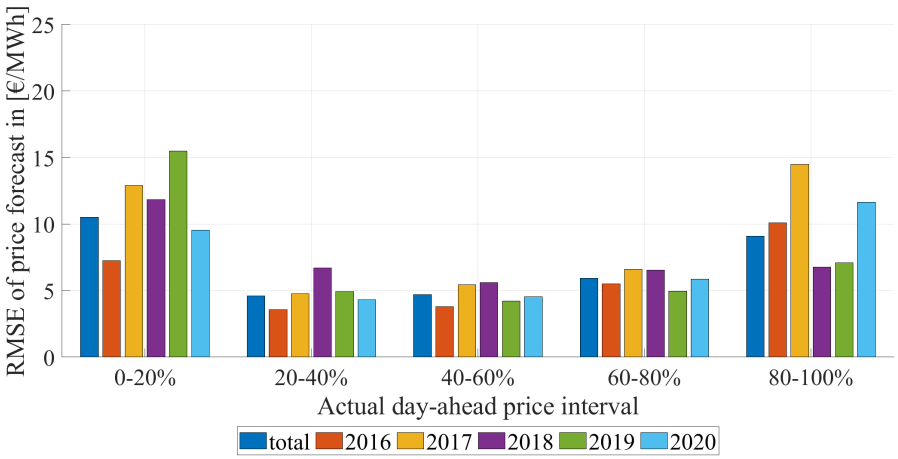

Figure 5.5.: RMSE for hours at different day-ahead price quantiles.

environment would correspond to a uniform distribution. The histogram below shows slightly increasing frequencies towards the outside but forms a good approximation of a uniform distribution generated by randomly drawn numbers. This serves as a quality check for our hybrid model and ensures that the predicted probabilities reflect the true probabilities of the day-ahead prices.

Since peak hours often have higher day-ahead prices than off-peak hours, our hybrid model predicts quantiles with two QRA estimations for each quantile, one for peak hours and one for off-peak hours. Thus, the probabilistic forecasts should be assessed for calibration separately in two disjunctive sub-sets. Figure 5.8 illustrates the calibration of the quantiles for peak hours on the left and off-peak hours on the right. During off-peak hours, there is a higher frequency in the outermost 5 % quantiles on both sides (i.e., at high and low price levels). During peak hours, more actual values exceed the estimated quantile values, especially on the right side of the median. For example, 6.3 % of the hourly values exceed the 95 % quantile value. With a higher frequency in the low 5 % quantile, the lowest prices can be attributed to the price-reducing influence of high electricity generation from renewable energy sources. This is consistent with the proportion of peak hours that show high demand for electricity but also a high feed-in of renewable energies due to high solar radiation or wind speeds and, thus, a high supply.

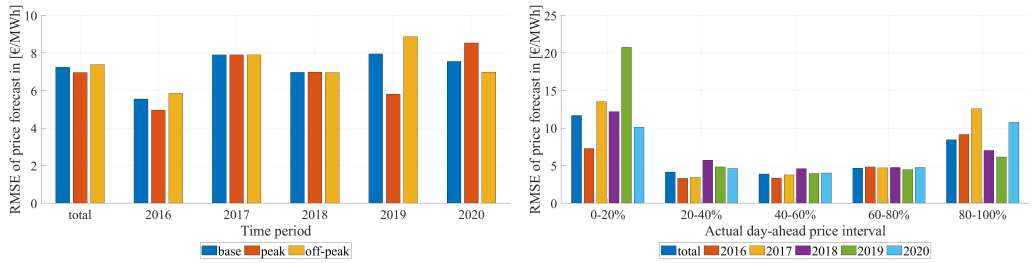

Figure 5.6.: RMSE of the LEAR model's day-ahead price forecast for base, peak and off-peak hours (left) and for hours at different day-ahead price quantiles (right).

The calibration analysis of the predicted quantiles validates the calculated probabilistic forecasts. In the following, we evaluate the hourly distribution of the width of the forecast intervals to obtain more precise and quantified information about market uncertainty and the forecast accuracy that depends on it. Furthermore, we use probabilistic forecasts to calculate the probability of negative prices. Thus, we address the economic interest in including probabilistic forecasts in trading strategies and power plant deployment planning.

During peak hours, the uncertainty and fluctuations of the day-ahead prices are higher than during off-peak hours. This can be explained by a steeper merit order at high-load levels, the occurrence of start-ups during peak hours and the uncertainty of generation from renewable energy sources (especially PV plants, which produce more during peak hours). Our hybrid model captures this uncertainty with its probabilistic forecasts. Figure 5.9 presents box plots that visualise the distribution of the spread between the estimated 95 % quantile and the estimated 5 % quantile for each hour of the day (thus, the width of the 90 % prediction interval). From 8 a.m. to 8 p.m. (daytime), the median spread is wider and outliers are higher than they are at night, reflecting the higher uncertainty and wider range of prices. Although the wider spread of the prediction interval covering 90 % of the potential prices shows that these hours are more difficult to forecast than the night hours, the hybrid model can forecast them as accurately as it can forecast the night hours. The accuracy of point forecasts showed comparable results for peak and off-peak

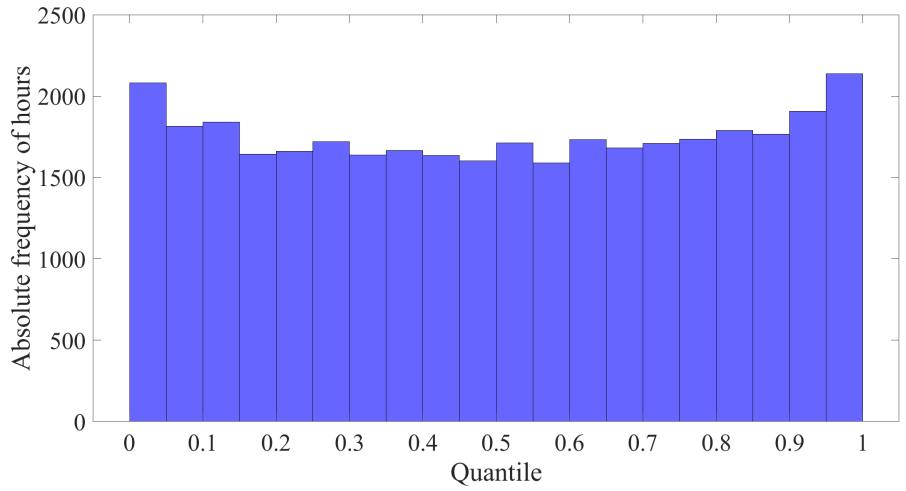

Figure 5.7.: Number of actual prices included in the quantiles estimated in the forecast period from 2017 to 2020.

hours over the entire period (see Figure 5.4). Additionally, the probabilistic forecasts effectively mirror the market's uncertainty.

Figure 5.10 shows the average width of the 90 % prediction interval for each hour of the week, illustrating how easy or difficult it is to forecast the day-ahead electricity price for each individual hour of the week. A wider spread indicates greater uncertainty and less predictability, as the price may take on a wider range of potential values. As previously stated, daytime hours generally exhibit wider intervals than nighttime hours. However, more nuanced patterns are also discernible.

On weekdays (Monday to Friday), the spread of the prediction interval follows a distinct daily course featuring three concave curves with (local) maxima at 3 a.m., 8 a.m. and 4 p.m. The interval is relatively narrow from midnight to 7 a.m. From 7 a.m. to 8 a.m., the interval increases abruptly, posing a major challenge for the forecasting of electricity prices, especially between 4 p.m. and 6 p.m. On weekends (Saturday and Sunday), the interval width is more evenly distributed across all hours but remains high overall and still exhibits a notable decrease between 7 p.m. and 9 p.m. Therefore, predicting day-ahead electricity prices requires careful consideration of the hour of the day and the day of the week on top of all other factors that can affect market dynamics.

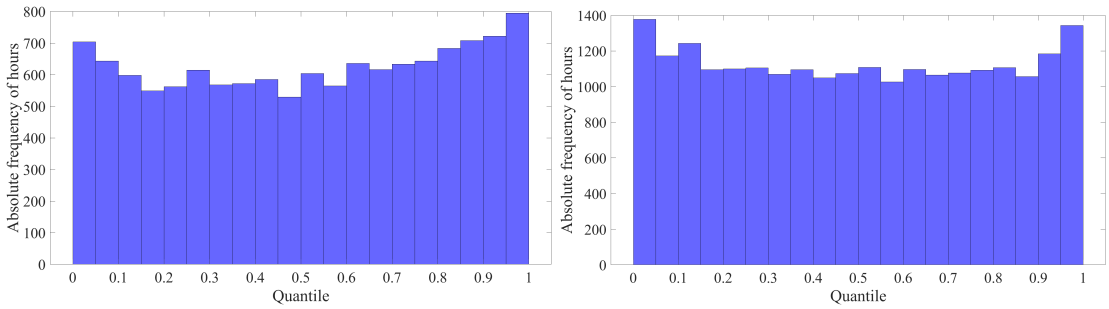

Figure 5.8.: Number of actual prices included in the quantiles estimated in the 2017 to 2020 forecast period, separated for peak (left) and off-peak (right) hours.

Figure 5.11 demonstrates an example of how the probabilistic forecasts account for uncertainty. It shows the course of lower and upper limits in combination with the expected price (the price's point prediction). The presented limits correspond to the estimated 5 % and 95 % quantiles, respectively, and indicate the range of possible outcomes. More precisely, the actual day-ahead electricity price has a 90 % probability of lying within this range. Using the density forecast and predicted bounds, we can make informed risk estimates and probability statements, which can be useful for decision-making amid uncertainty.

Figure 5.12 illustrates the probabilities of negative prices for each hour of the week, as estimated by the density forecast. Notably, negative prices can occur when, for example, increases in generation by renewable energy sources or a large share of must-run capacities (e.g., CHP) force conventional power plant units to shut down, leading to start-up costs when these capacities are needed again. The merit order effect of renewable energies and their regulation, in particular payments for production besides the wholesale electricity market, can exacerbate this situation.

Figure 5.12 reveals that the probability of negative prices is highest on Sundays and public holidays, reaching 10 % to 15 % in some hours. It reflects the increased occurrence of negative prices in these hours in the actual day-ahead prices. This is due to the fact that electricity demand is relatively low during these periods, increasing the likelihood of negative price events. The probability of negative prices is also relatively high (above 5 %) in the early hours of Monday, followed by a slightly higher probability of negative

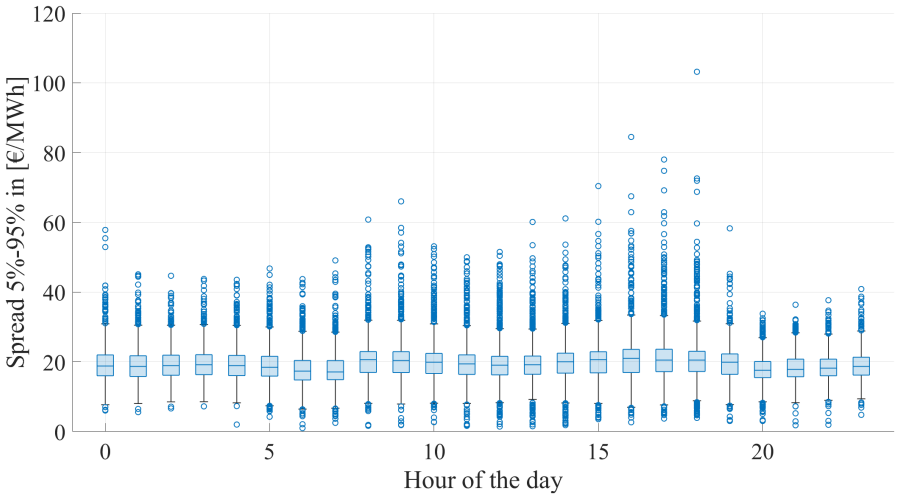

Figure 5.9.: Box plot of the 90 % prediction interval for each hour of the day.

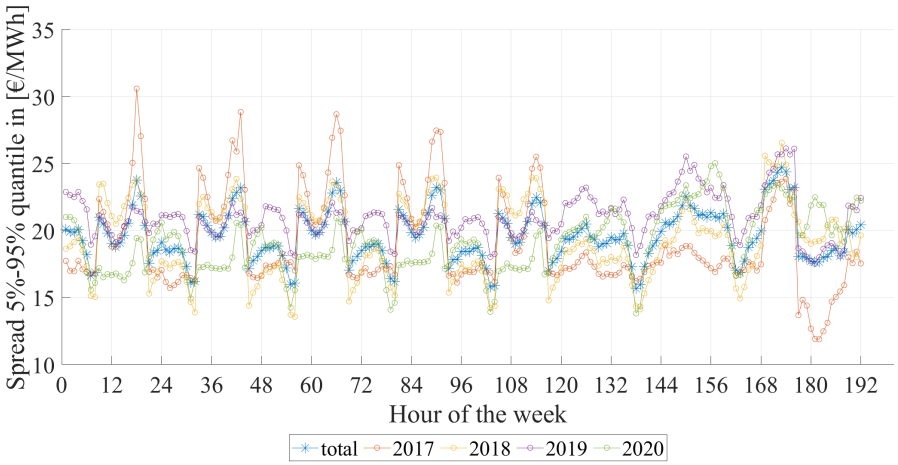

Figure 5.10.: Average spread between the predicted 5 % and 95 % quantiles for the hours of the week.

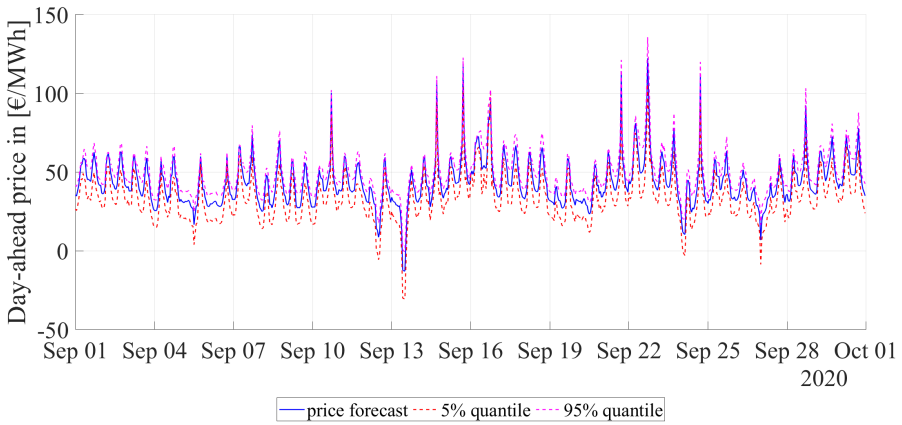

Figure 5.11.: Day-ahead price forecast, lower-bound forecast (5 % quantile) and upper-bound forecast (95 % quantile).

prices in the early hours of the other days of the week. This pattern reflects the low-load behaviour of electricity demand in the early hours combined with the typically high wind feed-in during the night and early morning, which can lead to price drops. On Sundays and holidays, the daytime generation from PV and continuous wind feed-in can increase the likelihood of negative prices due to reduced demand.

The probability values for weekdays (Monday to Friday) are similar in their level and pattern, as these days have comparable fundamental parameters. With the probabilities determined by the density forecasts, bidding strategies, portfolios hedges and power plant usage can be optimised. The risks of negative prices or large price spreads can be incorporated into strategies through the probability statements.

In summary, the results show the high-quality point and probabilistic price forecasts of the hybrid model, which also offers two additional advantages over previous approaches. The integration of a techno-economic energy system model allows for a deeper understanding of (energy) markets. The use of stochastic approaches enables probabilistic price forecasts to quantify uncertainty in these markets and provides valuable information on the probability of negative prices and other market phenomena, helping market participants to make informed decisions and mitigate risks.

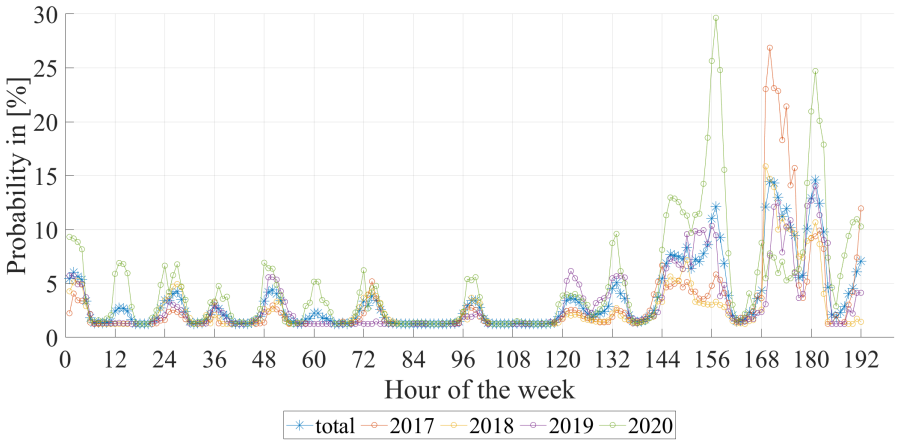

Figure 5.12.: Probability of negative day-ahead prices.

5.6. Analysis of Individual Model Steps

The presented hybrid model is multi-layered. In this section, we offer some insights into the individual components (steps) of the hybrid model. Section 5.6.1 shows the results of the day-ahead load forecasts. Section 5.6.2 provides an evaluation of the price estimators that follow the energy system optimisation step. Finally, section 5.6.3 points out the impact of the six individual price estimators' error forecasts.

5.6.1. Load Forecasts

This section presents the results of the load forecasts, where we compare the RMSE and MAE of TSOs' load forecasts with the improved load forecasts in Table 5.3, showing a significant improvement of 19 % in RMSE and 27 % in MAE. We refer to Möbius et al. (2023) (Chapter 3) for a more detailed analysis.

5.6.2. Price Estimators After the Energy System Optimisation Step

In optimising the energy system model, our hybrid model generates price estimators derived from the dual variable of demand constraint (see Section 5.4.3). Computing the dual variable, the model optimises the energy sector's complex technical and economic interdependencies. In addition to the costs of electricity generation, the model considers

Table 5.3.: RMSE and MAE for the original TSOs' day-ahead load forecast (TSO) and the improved day-ahead load forecast (Impr.), given in [MWh].

	year	total	2016	2017	2018	2019	2020
RMSE	TSO	2,335.49	2,596.48	1,802.61	2,360.51	2,454.70	2,383.23
	Impr.	1,881.64	1,872.44	1,483.45	2,043.87	1,665.76	1,859.29
	% Improvement	19.43	27.89	17.71	13.41	32.14	21.98
MAE	TSO	1,797.05	2,028.44	1,396.45	1,726.67	1,951.00	1,881.84
	Impr.	1,320.83	1,302.17	1,106.12	1,372.55	1,283.17	1,405.71
	% Improvement	26.50	35.80	20.79	20.51	34.23	25.30

unit commitment decisions, such as the start-up and shut-down of generation units, storage operation, limitations on electricity transport to and from neighbouring countries, heat-supply requirements and the provision of control power. All of these techno-economic interdependencies determine the resulting electricity prices and are essential in our model, as they signal both high price peaks and low or even negative electricity prices observable on the market.

Table 5.4 presents the descriptive statistics of the price estimation errors as well as the RMSE and MAE of these price estimators after the energy optimisation step. For all years, the RMSE is 9.50 €/MWh, and the MAE is 6.00 €/MWh. The lowest errors can be observed in 2016, and the highest in 2017. In comparison to state-of-the-art electricity price forecasting models in the literature, the error measurements are larger, and the errors still show structural behaviour. For most years, the error's mean and median are both negative values, meaning that the *em.power dispatch* calculates prices higher than the observed prices on the market. With a value of -15.30 €/MWh for the error's 5 % quantile and a value of 9.60 €/MWh for the error's 95 % quantile, 90 % of the error values lie in this interval.

Figure 5.13 plots the error structure of the entire period divided into the hours of the week. Negative values indicate an average overestimation of the prices in the corresponding hour, while positive values indicate an average underestimation of the prices in the corresponding hour. The figure shows that the errors tend to increase over the weekend, while there is a distinct daily pattern observed (see also Figure 5.14).

Table 5.4.: Descriptive statistics of the error of energy system optimisation step in [€/MWh].

	total	2016	2017	2018	2019	2020
mean	-2.17	-2.23	-3.06	0.02	-0.73	-4.84
median	-1.75	-2.24	-2.75	0.71	-0.23	-3.94
minimum	-143.85	-143.85	-102.45	-81.45	-80.01	-79.05
maximum	105.73	50.62	105.73	55.19	42.87	86.76
5 %-quantile	-15.30	-11.81	-17.77	-13.24	-12.78	-19.50
95 %-quantile	9.60	7.47	10.68	11.40	9.75	6.05
std.	9.25	7.26	11.62	8.61	8.05	9.31

The model tends to underestimate prices during the night while overestimating them in the morning and late afternoon, which is a consistent pattern across all years from 2016 to 2019. While the error structure in 2020 shows some differences, possibly attributed to the COVID-19 pandemic, the model's RMSE per hour of the day does not significantly differ from previous years. We also observe a midday increased error rate and an evening error peak between 4 p.m. to 6 p.m., which is more pronounced in the 2020 data.

Note, however, that we are evaluating here the short-term price prediction of a techno-economic energy system model, which we expect, due to its inability to learn from history, to map the general market situation at these time horizons, but not to form very accurate price estimators. Therefore, the model performs reasonably well with predictable patterns in the errors, which indicate a high potential for the data post-processing step. The effect of this step is presented in the following chapter.

Figure 5.15 illustrates the correlation of the price forecast errors with several exogenous variables. Evidently, wind generation correlates significantly with the price forecast errors from the energy optimisation step and explains 14 % of the overall forecast error's volatility.

5.6.3. Improvement of Price Estimators

The detected systematic deviations and seasonal patterns in the errors of the price estimators following the energy system optimisation step can be captured and predicted by the stochastic model in the post-processing step in a way that improves the price forecast's RMSE for 2016 to 2020 by 22 % through the combination of both model classes.

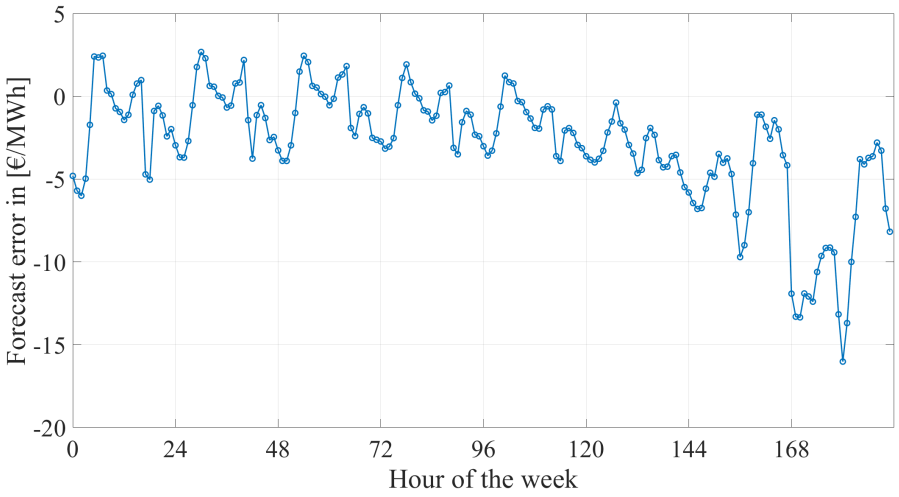

Figure 5.13.: Mean price estimator errors for the hours of the week (including public holidays at hours 168–192) after the energy system optimisation step.

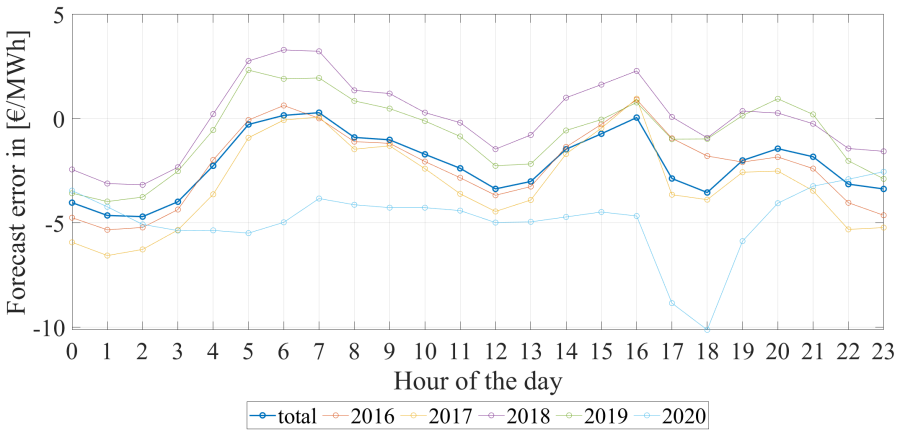

Figure 5.14.: Mean price estimator errors for the hours of the day in each year after the energy system optimisation step.

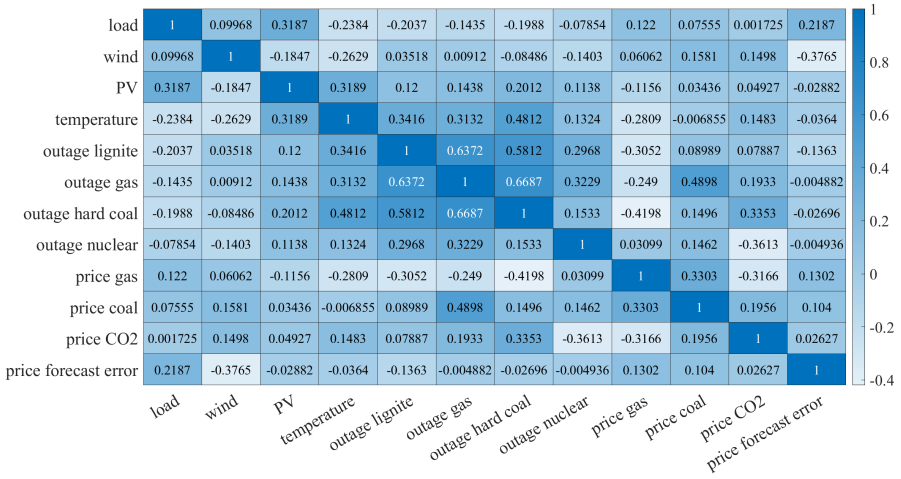

Figure 5.15.: Correlation of possible exogenous variables and the price estimation error.

The statistical data of the hybrid model's forecast error, given in Table 5.5, show that the error is distributed nearly symmetrically with a mean of -0.09 €/MWh and a median of -0.08 €/MWh. Thus, post-processing centres the price forecast error to near zero. At the same time, both the minimum and maximum errors generated decrease each year and over the entire period – as does overall volatility. The post-processing model achieves a reduction of 20 % in the standard deviation of the day-ahead price forecast, compared to the one of the price estimators of the energy system optimisation step.

Table 5.5.: Descriptive statistics of the error of the hybrid model in [€/MWh].

	total	2016	2017	2018	2019	2020
mean	-0.09	0.30	-0.15	1.12	-0.73	-0.99
median	-0.08	0.08	-0.23	1.06	-0.68	-0.50
minimum	-133.44	-133.44	-81.29	-54.41	-79.27	-69.43
maximum	86.10	43.76	74.30	52.72	35.48	86.10
5 %-quantile	-9.58	-6.64	-10.94	-9.09	-9.36	-11.51
95 %-quantile	10.07	8.48	11.21	11.70	9.08	8.24
std.	7.38	5.82	8.79	7.20	7.01	7.56

The stochastic post-processing step consists of six individual sub-models, as described in Section 5.4.4. Each of these sub-models improves the price estimators obtained after the energy system optimisation step (ESM), significantly increasing the forecast

quality, as measured in Table 5.6 by specifying the error measures RMSE and MAE. While the models with multivariate frameworks have lower error measures than those with univariate frameworks over the entire period, the price forecasts of the univariate models are qualitatively better than those of the multivariate models in 2019 and 2020. Figure 5.16 shows the hourly RMSE for each sub-model. Depending on the length of the calibration window, the models of the univariate framework dominate those of the multivariate framework in the first five hours of the day. From that point forward, the multivariate sub-models achieve lower error measures. The result aligns with the expectations of the model specifications. In the univariate framework, the time series is captured as a high-frequency data set, so the forecast includes data up to the last available hour. However, this also requires 24 future values to be forecasted, heightening inaccuracy. With the multivariate framework, a reverse effect is observable due to the split into 24 individual time series, as this split entails even just short steps into the future needing to be forecasted. Still, the most recent available information is only partially considered.

Table 5.6.: Error measurements RMSE and MAE of the sub-models' error time series in [€/MWh].

		Initial	Post-processing							
		ESM	UV42w	UV48w	UV52w	MV42w	MV48w	MV52w	combination	
RMSE	total	9.50	7.57	7.59	7.59	7.51	7.50	7.51	7.38	22 %
	2016	7.60	6.07	6.13	6.09	5.95	5.94	5.92	5.82	23 %
	2017	12.01	9.22	9.20	9.13	8.92	8.86	8.86	8.79	27 %
	2018	8.61	7.49	7.47	7.54	7.40	7.38	7.40	7.28	15 %
	2019	8.09	7.11	7.13	7.14	7.21	7.22	7.21	7.05	13 %
	2020	10.49	7.65	7.69	7.71	7.77	7.79	7.85	7.63	27 %
MAE	total	6.00	4.73	4.75	4.75	4.75	4.74	4.74	4.60	23 %
	2016	4.83	3.69	3.71	3.69	3.64	3.62	3.61	3.48	28 %
	2017	7.09	5.55	5.55	5.51	5.37	5.31	5.28	5.25	26 %
	2018	5.91	5.20	5.18	5.21	5.24	5.23	5.25	5.07	14 %
	2019	5.07	4.46	4.49	4.49	4.61	4.61	4.59	4.43	13 %
	2020	7.13	4.77	4.80	4.83	4.91	4.94	4.99	4.77	33 %

The individual characteristics of the univariate and multivariate frameworks also explain the average errors for each hour of the day (see Figure 5.17) and each hour of the week (see Figure 5.18). While the forecasts of the multivariate sub-models do not indicate a clear daily pattern in the under- or overestimation of values, the univariate

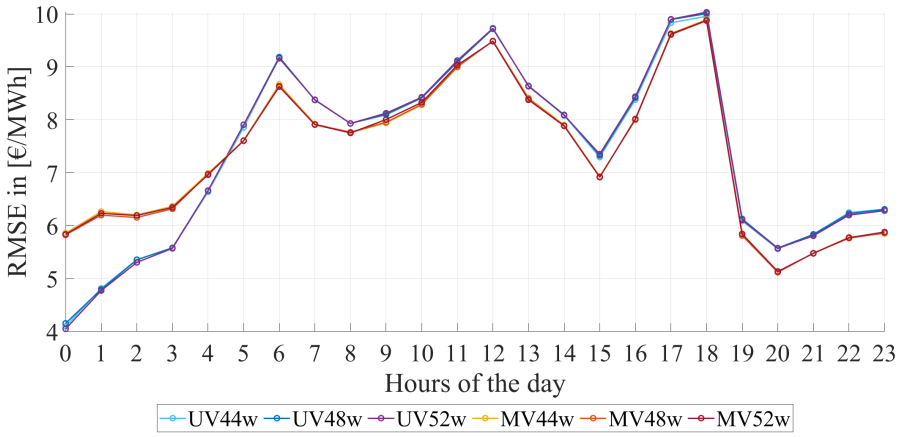

Figure 5.16.: RMSE for univariate and multivariate post-processing sub-models for each hour of the day.

sub-models show a similar daily structure as the price estimators following the energy system optimisation step: underestimation during the hours of 4 to 8 a.m. and 2 to 4 p.m., and overestimation,e.g., during the hours of 17 to 18 p.m. and for the hours from 21 p.m. The average error for weekly hours displays a significantly higher overestimation and underestimation on public holidays. Notably, however, this trend is evident across all forecasts of the univariate and multivariate sub-models.

Table 5.6 presents the error measures for the price forecast that stems from combining the forecasts of individual sub-models. Thus, it depicts the final price forecast of the hybrid model. The RMSE and MAE of this price forecast are lower than the error measures of the individual price forecasts over each individual year as well as the entire period.

Using the multivariate Diebold-Mariano test from the *epftoolbox* by Lago et al. (2021) to compare different model forecasts via hypothesis testing and determine whether one forecast's accuracy is significantly higher than that of the others, we show that the combination of the sub-models is significantly better than all six individual sub-models. The test results are shown in Figure 5.19 as a heatmap illustrating the p-values of the hypothesis that the forecast of the model on the Y-axis is significantly more accurate than the forecast of the model on the X-axis. A p-value close to zero indicates that the

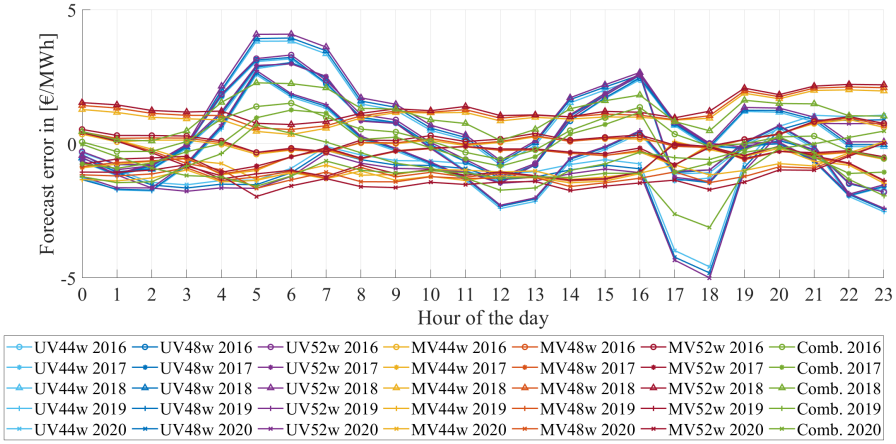

Figure 5.17.: Mean price forecast errors of the individual sub-models and the combined sub-models for the hours of the day in each year.

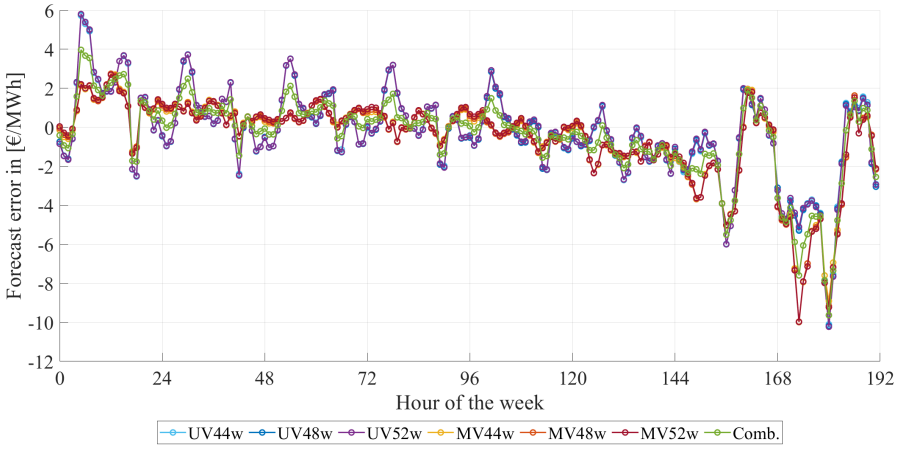

Figure 5.18.: Mean price forecast errors of the individual sub-models and the combined sub-models for the hours of the week (including holidays, hour 168 to 192).

model on the X-axis has a significantly higher forecast accuracy than the model on the Y-axis. The test indicates that, for forecasting day-ahead spot prices, the post-processing model and each stochastic sub-model are significantly better than the energy system model modified by stochastic pre-processing and interweaving, which means the hybrid model after the third step.

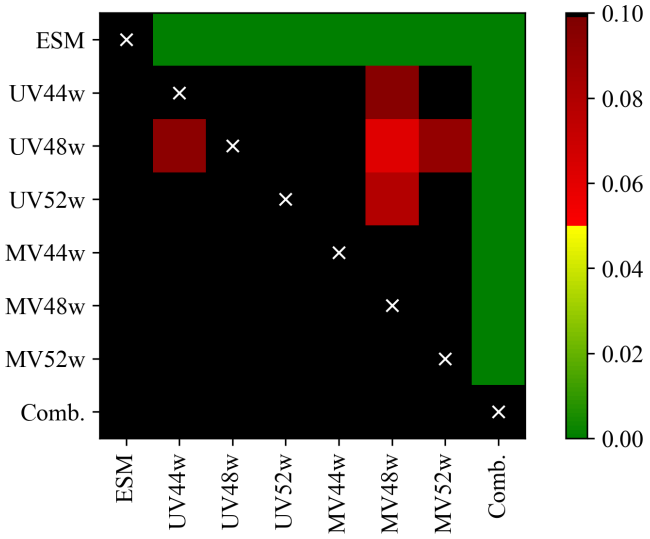

Figure 5.19.: P-value of Diebold-Mariano test for all parts of the stochastic post-processing step (output derived with source code from *epftoolbox* by Lago et al. (2021)).

To better attribute and understand the effect of the stochastic post-processing step, we also determine the improvement in RMSE for each hour of the day and day of the week, as shown in Figure 5.20. Daytime and weekday structures, which can be observed in the price estimators' errors after the energy system optimisation step, are evident in the improvement. This is due in large part to the seasonal components in the stochastic model and the affected autoregressive structures. Notably, the most substantial improvements in terms of percentage are achieved at night. Additionally, weekends and especially holidays see relatively high levels of improvement. In the price estimators, these are the hours and days with the most significant mean error, meaning those with a sizeable mean error and, in turn, the most potential for improvement. Enhancing day-ahead price forecasts by

reducing this error is a key goal of combining techno-economic energy system modelling and stochastic modelling.

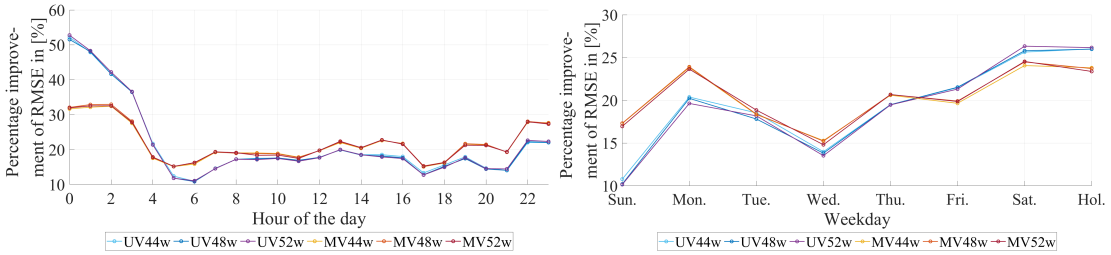

Figure 5.20.: Average RMSE improvement in day-ahead price forecasts for each hour of the day (left) and each day of the week (right).

5.7. Concluding Remarks

This chapter introduced a novel hybrid model for short-term electricity price forecasting, which combines stochastic modelling with (fundamental) techno-economic energy system modelling. The model consists of four steps. First, through stochastic data pre-processing, day-ahead load forecasts are significantly improved, and a load forecast for two days ahead is created. Second, this load forecast is extended by quantile forecasts in three different probable scenarios of hourly load consumption two days in advance using a parameter density forecast step. Third, the modelled quantities and input data are feed into the *em.power dispatch*, a techno-economic market model adapted for predicting day-ahead price estimators. Fourth, the errors of the price estimators from the energy optimisation step are reduced by stochastic models through stochastic data post-processing and complemented by probabilistic forecasts.

The presented hybrid model combines the strengths of stochastic models (strength: trained with price data) and energy system models (strength: insights based on economic theory extending beyond prices). It can be parameterised with data from most energy markets worldwide, providing insights into various energy systems. We demonstrated its performance using German day-ahead electricity market data from January 2016 to December 2020. The price forecasts from the model have an annual average RMSE

of 7.38 €/MWh and an annual average MAE of 4.60 €/MWh. The hybrid model's forecasting accuracy surpasses the majority of benchmarks in the literature and matches the best statistical benchmark identified in the literature. This confirms that techno-economic energy system models can provide valuable input for price forecasting, even for short-term forecasting.

We conducted an in-depth analysis of price forecast quality and identified a notable relationship between the error in price forecasts and the price level. Over the years, the highest RMSE has consistently been found in the hours with the lowest 20 % and the highest 20 % of prices. This result can be explained by start-up costs and their impact on hourly prices, as discussed in Section 5.5, and naturally affects all forecast models.

Additionally, our model provides calibrated density forecasts alongside point forecasts. With these, it can, for example, quantify the probability of negative price events. Our analysis revealed that some hours on Sundays and public holidays have a probability of more than 10 % of becoming negative.

Future research should focus on determining the most suitable model type for cases with varying lead times in price forecasts. As discussed in the first part of this chapter, the relative strength of techno-economic models in handling structural breaks suggests their greater suitability for long-term forecasts (e.g., years ahead), while stochastic models, whether time series-based or artificial intelligence-based, are better suited for short-term forecasts (e.g., intraday). Nevertheless, hybrid models like the one introduced in this work for day-ahead forecasts or similar approaches that combine the advantages of both model classes mentioned above could, if properly adapted, be suitable for performing accurate forecasts with variable lead times. As a result, we think that it is crucial to further explore and develop hybrid models to harness their potential for delivering accurate forecasts across various lead times, making them a valuable addition to the existing forecasting methodologies.

The next chapter summarises this thesis and provides some concluding remarks for further research directions.

6. Conclusion

This thesis contributes to the use of statistical models in the electricity sector to enhance data and forecast accuracy. In particular, we provide a comprehensive data set in a high spatial resolution, which contains generation time series of renewable energy sources and large-scale capacity layouts for onshore wind, offshore wind and solar power plants for nearly 1,500 transmission nodes in mainland Europe. Estimated by an elastic-net regression approach, the layouts mimic the actual generated power by renewable generators very closely and thus are feasible as working layouts. With these layouts, feed-in forecasts for renewable energy sources can be estimated for almost every aggregation level and region for the first time in the literature (see Chapter 2).

Furthermore, we developed a time series model to improve the day-ahead load forecast of TSOs. The model does not require any input variables other than the load forecast error history to significantly improve the transmission system operators' load forecast data in real-time, i.e., the model successively improves each incoming data point. Through the simple prediction model, we enable researchers who use load forecasts as input data to continuously pre-process the data for and improve the results of their models. As an example, we showed an enhancement in a technical-economic power system model and an error reduction of a day-ahead price forecast performed with this model (see Chapter 3).

In addition, we dealt with more complex methods to forecast a forecast error. Specifically, we propose a multidimensional model for generating both point and probabilistic forecasts of prediction errors by building on the idea of improving a point forecast. We used statistical time series and regression models to develop a generally valid forecast model for prediction errors. By proposing a methodology that is not tailored to the errors of a particular prediction but applies to a wide range of target variables, we enable users to improve their predictions and consider the uncertainty and risk of inaccuracy in predictions. This way, the model addresses the strong demand for probabilistic forecasts.

We validated the effectiveness of our method by providing three real data examples. These examples demonstrated the practical benefits of our approach and illustrated how it can be used to improve the accuracy and reliability of forecasts (see Chapter 4).

Finally, we introduced a new approach to enhance a techno-economic energy system model by statistical models. To this end, we used recently introduced approaches to improve data and forecasts and combined them with the energy system model. This was done by developing a multi-stage hybrid model with data pre-processing and data post-processing statistical methods. Through them and their advantages, the innovative hybrid model approach enables the application of fundamental models in the short term. The method yields state-of-the-art day-ahead electricity price forecasts, point and probabilistic, and, thus, can be used to quantify uncertainty in energy markets and develop trading strategies (see Chapter 5).

In summary, this thesis offers new approaches to tackle the increasing uncertainty and complexity caused by liberalisation, the energy transition and the expansion of renewable energies, and the associated challenges. However, some work on the presented topics and approaches remains for further research. For example, it would be interesting to address the limitations of the working layout estimation and the data set for renewable energy sources by extending the methodology through information about storages and curtailments. Furthermore, it would be interesting to consider interdependencies in the uncertainty of forecast error values of the hours of the day and include them in the probabilistic forecast error model. Finally, the hybrid model offers interesting possibilities for further developments and analyses. For example, in order to take greater account of the uncertainty caused by the expansion of renewable energy sources, the introduced methodology for improving a techno-economic energy system model can be expanded to include probabilities and scenarios for renewable energy feed-in.

Appendices

Appendix A.

Data, Code and Sources Availability

The data sets and models developed in each chapter are implemented in the Python™[1] and MATLAB®[2] programming languages and are freely available. Below we provide information on the availability of the individual chapters.

The data and the source code to produce the data set including time series of hourly renewable energy sources power generation and working layouts for the allocation of installed capacity of onshore and offshore wind and PV energy sources, presented in Chapter 2, are openly available. Under *https://github.com/MWaterm/High-Resolution-Working-Layouts-and-Time-Series-for-Renewable-Energy-Generation-in-Europe*, we provide the entire implementation. The data set can be downloaded through the following link: *https://doi.org/10.6084/m9.figshare.22439254.v3*. The data are generated using Copernicus Climate Change Service information [2019-2022], containing modified Copernicus Climate Change Service information [2019-2022].

Data sets related to Chapter 3 and a source code for the entire method are also available in a public GitHub repository. Under *https://github.com/ProKoMoProject/Enhancing-Energy-System-Models-Using-Better-Load-Forecasts*, we provide the code and data for the time series model improving the load forecasts as well as code and data for the techno-economic energy system model. The codes reproduce the benchmarks from the chapter.

The implementation of the forecast error model improving day-ahead forecasts in energy markets, presented in Chapter 4, is provided in another GitHub repository

[1] Used version: 3.9
[2] Used version: R2020b

through the following link: *https://github.com/MWaterm/Forecast-the-forecast-error*. The code presents a ready-to-use application.

The source code to improve a techno-economic energy system model, presented in Chapter 5, is openly available in a repository on GitHub: *https://github.com/ProKoMoProject/A-hybrid-model-for-day-ahead-electricity-price-forecasting-combining-fundamental-and-stochastic-mod*. Therein, we additionally provide all implementations of the resulting hybrid model as well as the generated point and probabilistic day-ahead price forecasts for the German day-ahead electricity market.

Appendix B.

Nomenclature for the Techno-Economic Energy System Model

Sets and indices

BP	Time blocks for primary control power
BS	Time blocks for secondary control power
D	Amount of days of a rolling window that includes $d+0, d+1, d+2$
H	Amount of hours of a day
T	Time steps
$hfirst(H)$	First hour of a day
$hlast(H)$	Last hour of a day
$tfirst(T)$	First hour of a rolling window
$tlast(T)$	Last hour of a rolling window
I	Amount of electricity generation capacity clusters
$N, HR(I)$	Amount of hydro reservoirs [Subset of I]
N, NN	Amount of nodes
$RES(I)$	Amount of intermittent renewables [Subset of I]
$STM(I)$	Amount of mid-term storage [Subset of I]
$STL(I)$	Amount of long-term storage [Subset of I]

Parameters

η_i	Efficiency rate of a generation technology
$af_{i,n,d,h}$	Availability factor for generation capacities
$cap_{i,n,d,h}$	Installed generation capacity in [MW_{el}]
$chp_{i,n,d,h}$	Minimum electricity output of combined heat power units in [MW_{el}/h]
$curtc$	Costs for RES curtailment in [€/MWh_{el}]
$d_{n,d,h}$	Demand forecast on the day-ahead in [MWh_{el}/h]
$d^{d+2}_{n,s,h}$	Scenario-specific demand forecast on the two-day-ahead in [MWh_{el}/h]
cer	Capacity-to-energy ratio for storage that operate actively within a three-day cycle in [MWh_{el}/MW_{el}]
$g^{min}_{i,n,d,h}$	Minimum generation of a running unit in [MW_{el}]
$ntc_{n,nn,d,h}$	Net transfer capacities in [MWh_{el}/h]
$out_{i,n,d,h}$	Power plant outages in [MW_{el}]
$sc_{i,n,d,h}$	Start-up costs in [€/MW_{el}]
$vc^{FL}_{i,n,d,h}$	Variable generation costs at full load in [€/MWh_{el}]
$vc^{ML}_{i,n,d,h}$	Variable generation costs at minimum load in [€/MWh_{el}]
$voll$	Value of lost load in [€/MWh_{el}]
$wv_{i,n,d,h}$	Water value for hydro reservoirs and long-term storage in [€/MWh_{el}]

Variables

$CURT_{i,n,d,h}$	RES curtailment in [MWh_{el}]
$CL_{i,n,d,h}$	Charging activity for long-term storage in [MWh_{el}/h]
$CM_{i,n,d,h}$	Charging activity for mid-term storage in [MWh_{el}/h]
$FLOW_{n,nn,d,h}$	Electricity flow from node n to node nn in [MWh_{el}/h]
$G_{i,n,d,h}$	Electricity generation in [MWh_{el}/h]
$P^{on}_{i,n,d,h}$	Running capacity in [MW_{el}]
$PCR_{i,n,d,h}$	Primary control reserve in [MW_{el}]
$SCR^{pos}_{i,n,d,h}$	Positive secondary control reserve in [MW_{el}]
$SCR^{neg}_{i,n,d,h}$	Negative secondary control reserve in [MW_{el}]
$SHED_{n,d,h}$	Load shedding in [MWh_{el}/h]
$SL_{i,n,d,h}$	Storage level of PSP in [MWh_{el}]
$SU_{i,n,d,h}$	Start-up activity of a generation unit in [MWh_{el}]
TC	Total system costs in [€]

Appendix C.

Supplementary Material for the Load Forecast

Supplementary Material for the Load Forecast (Chapter 3) In this appendix, we provide detailed descriptive statistics of the TSOs' load forecast error and the error measures which result from model estimations with different rolling window lengths of the model presented in Chapter 3.4.1 to enhance the load forecast.

Table C.1.: Weekday wise averaged descriptive statistics of TSOs' load forecast errors for the years 2016 to 2019. All variables are given in [MWh].

Day	Mean	Median	Minimum	Maximum	5%-q.	95%-q.	Std.
Mon.	1,517.71	1,436.63	-6,277.00	12,930.75	-1,895.75	5,111.45	2,159.26
Tue.	1,685.17	1,581.50	-4,867.25	11,469.00	-1,473.05	5,126.95	1,984.32
Wed.	1,601.81	1,516.00	-7,868.50	9,053.75	-1,242.65	4,667.90	1,874.89
Thu.	1,361.43	1,365.25	-17,543.50	9,520.25	-1,372.88	4,330.47	1,896.08
Fri.	944.31	990.75	-10,596.88	9,772.25	-2,060.85	3,911.48	1,892.38
Sat.	-102.26	-43.63	-7,661.75	7,809.00	-2,967.80	2,380.13	1,696.76
Sun.	-378.19	-340.13	-7,752.50	7,522.00	-3,378.53	2,458.15	1,859.72

Table C.2.: Hourly averaged descriptive statistics of TSOs' load forecast errors for the years 2016 to 2019. All variables are given in [MWh].

Hour	Mean	Median	Minimum	Maximum	5%-q.	95%-q.	Std.
1	699.64	742.75	-5,710.00	6,594.75	-2,270.28	3,509.15	1,713.19
2	652.07	696.75	-6,302.25	6,701.50	-2,290.58	3,460.69	1,711.79
3	646.41	657.75	-6,558.25	6,882.75	-2,246.04	3,535.18	1,739.51
4	6,90.28	687.50	-8,539.00	6,888.25	-2,269.38	3,635.30	1,760.22
5	855.45	852.75	-15,353.75	7,617.25	-2,298.63	3,959.94	1,991.04
6	943.53	1,032.50	-17,543.50	9,113.00	-2,658.48	4,335.81	2,295.79
7	946.49	1,075.75	-20,358.00	11,469.00	-2,896.14	4,688.48	2,515.40
8	912.14	1,011.00	-19,681.75	11,152.25	-2,795.23	4,529.93	2,461.27
9	908.80	959.00	-16,540.25	11,658.25	-2,692.56	4,594.01	2,387.68
10	902.67	900.00	-15,234.63	12,930.75	-2,836.34	4,707.63	2,417.03
11	916.34	926.75	-14,149.88	10,484.25	-2,791.68	4,646.26	2,401.02
12	923.30	951.00	-14,261.88	10,471.25	-2,818.44	4,782.05	2,414.55
13	907.81	982.00	-15,839.88	9,777.25	-2,980.00	4,740.98	2,446.60
14	785.04	882.75	-15,116.63	9,306.75	-2,963.74	4,549.70	2,412.79
15	718.73	807.50	-15,220.38	9,510.50	-2,933.24	4,477.88	2,396.13
16	900.33	895.50	-14,434.38	9,520.25	-2,777.48	4,756.91	2,323.86
17	1,080.73	1,051.50	-13,068.00	9,951.25	-2,526.88	4,832.60	2,285.24
18	1,172.53	1,128.00	-12,133.38	10,094.50	-2,110.33	4,819.08	2,140.34
19	1,180.48	1,161.25	-11,652.75	9,409.75	-1,985.76	4,610.81	2,078.72
20	1,061.99	1,071.00	-9,940.75	8,430.50	-1,956.98	4,248.70	1,978.27
21	875.01	909.25	-8,443.13	7,422.00	-2,121.79	3,943.60	1,888.30
22	877.85	872.75	-6,668.50	6,932.25	-2,032.00	3,853.51	1,821.24
23	863.47	806.00	-5,642.38	6,947.25	-1,928.34	3,706.63	1,726.26
24	729.88	763.25	-5,607.88	7,011.50	-2,262.01	3,560.98	1,701.36

Table C.3.: Error measures (MSE, RMSE, MAE) for the the improved day ahead load forecast with a rolling window length of three and six month. MSE is given in [$(\text{MWh})^2$], RMSE and MAE in [MWh].

	total	2017	2018	2019
three month rolling window				
MSE	4,948,990.80	2,272,350.07	4,575,637.58	3,133,176.51
RMSE	2,224.63	1,507.43	2,139.07	1,770.08
MAE	1,691.37	1,132.86	1,462.48	1,377.82
six month rolling window				
MSE	4,016,010.14	4,896,546.88	4,355,814.17	2,795,669.38
RMSE	2,004.00	2,212.81	2,087.06	1,672.03
MAE	1,304.12	1,200.16	1,411.57	1,300.63

Appendix D.

Heat Maps of the Univariate DM Tests

Heat Maps of the Univariate DM Tests (Chapter 4) In this appendix, as a supplement to the analyses in Chapter 4.5.1, we present the evaluations of the univariate DM tests performed for all hours of the day and for the three real data examples load, wind generation and price forecast error. For each example, we provide two figures containing the heat maps of the univariate DM tests for the forecasted values of the hours zero to eleven and twelve to 23. They are arranged in ascending order from left to right and top to bottom.

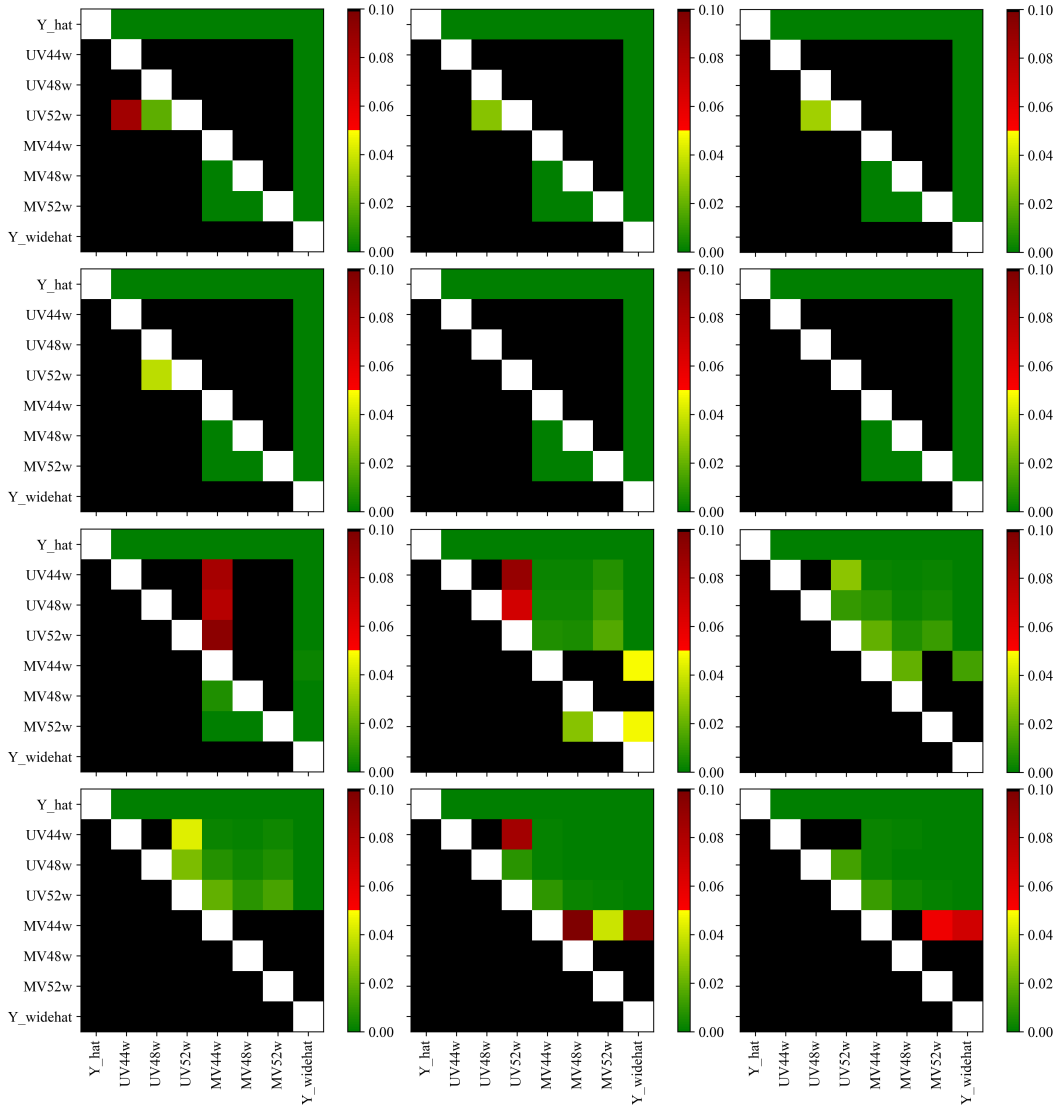

Figure D.1.: Univariate DM tests for the day-ahead electricity load forecast for hours 0 to 11 of the day (output derived with source code from *epftoolbox* by Lago et al. (2021)).

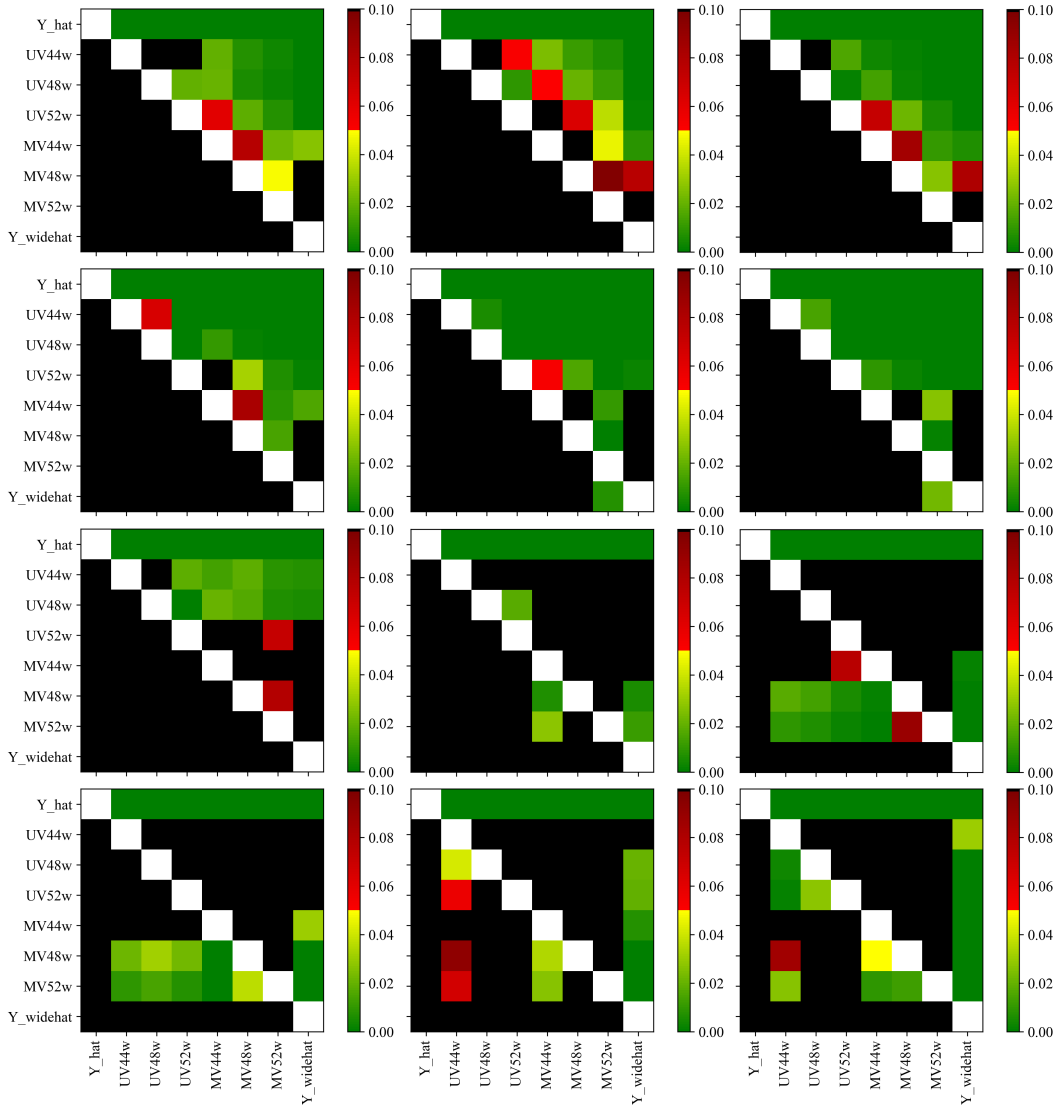

Figure D.2.: Univariate DM tests for the day-ahead electricity load forecast for hours 12 to 23 of the day (output derived with source code from *epftoolbox* by Lago et al. (2021)).

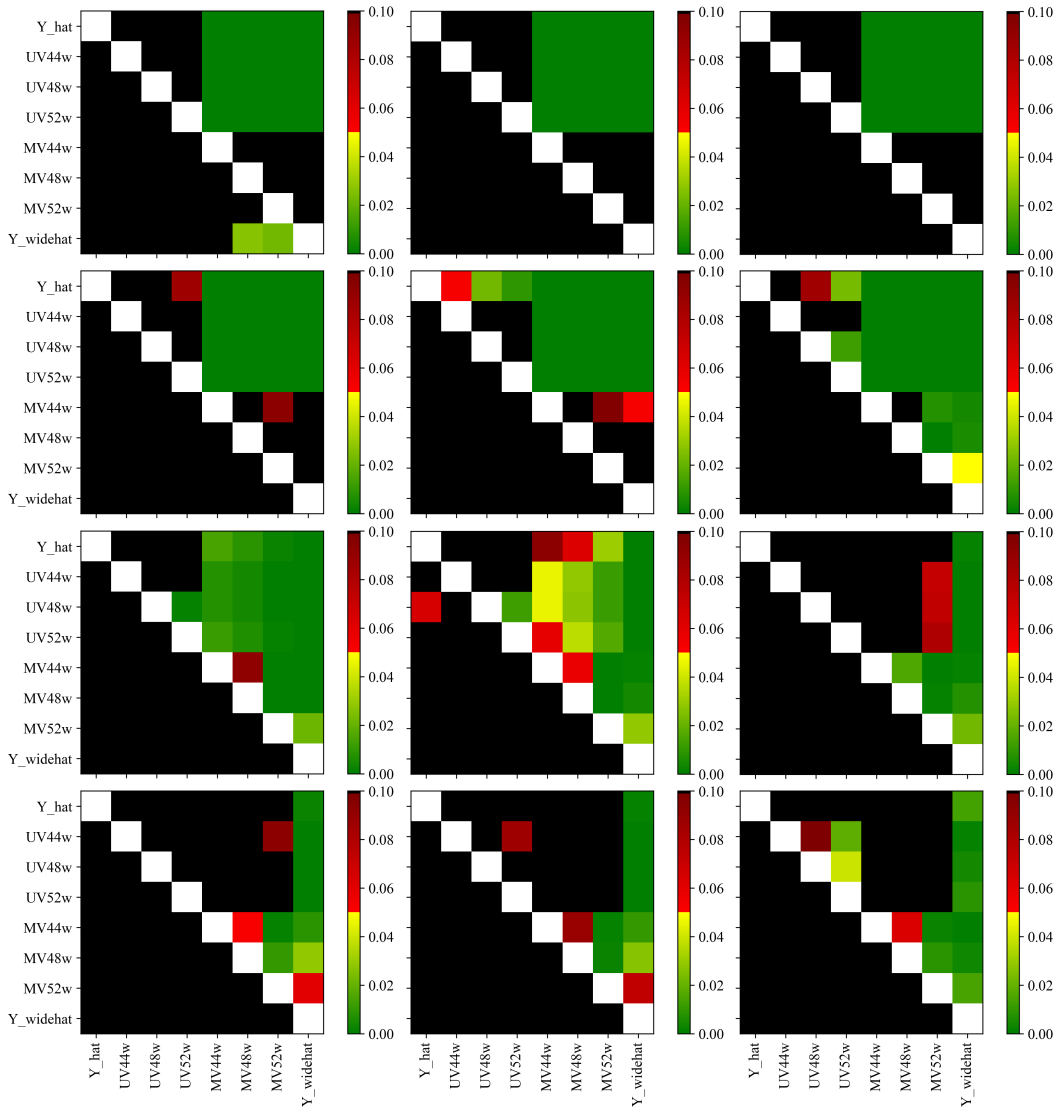

Figure D.3.: Univariate DM tests for the day-ahead wind generation forecast for hours 0 to 11 of the day (output derived with source code from *epftoolbox* by Lago et al. (2021)).

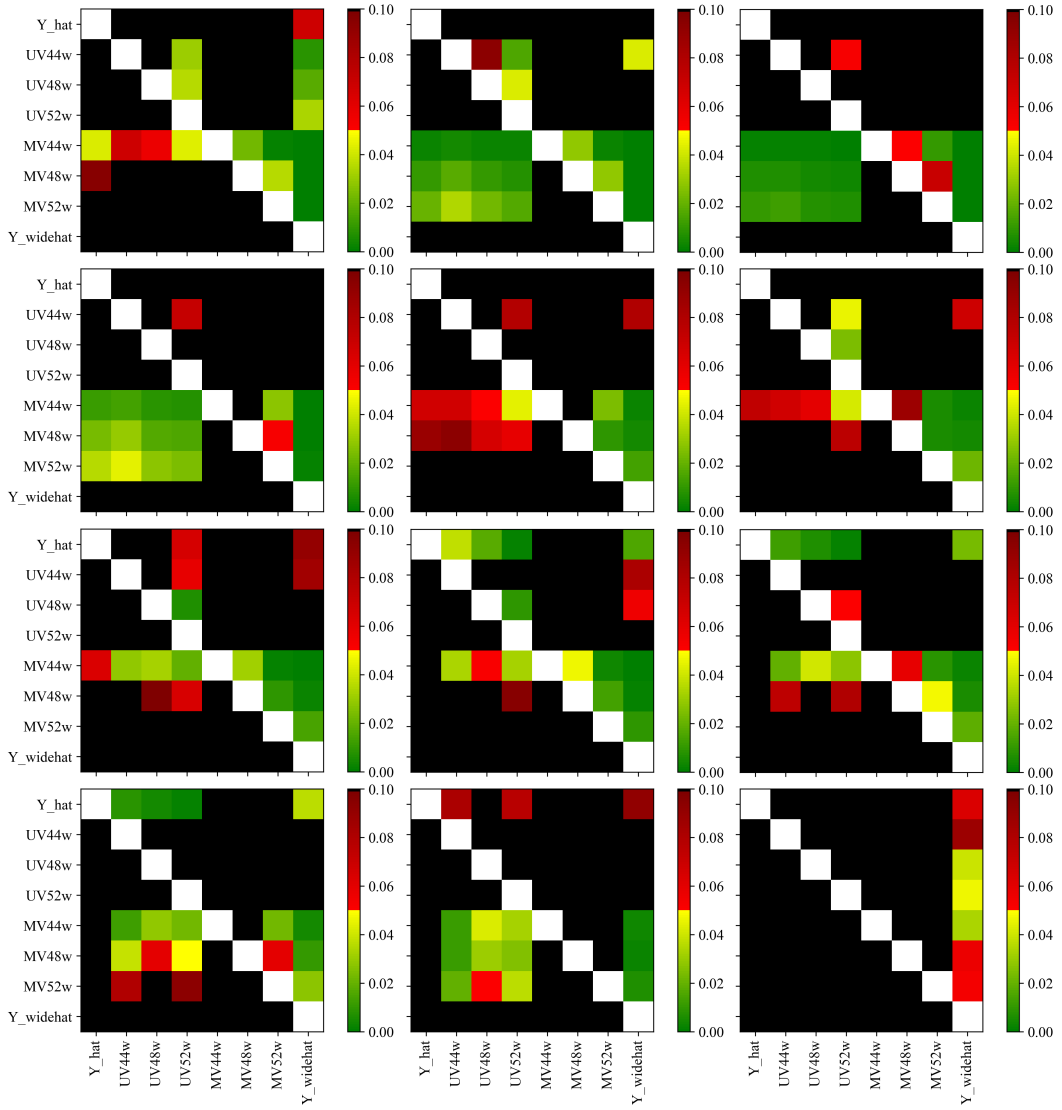

Figure D.4.: Univariate DM tests for the day-ahead wind generation forecast for hours 12 to 23 of the day (output derived with source code from *epftoolbox* by Lago et al. (2021)).

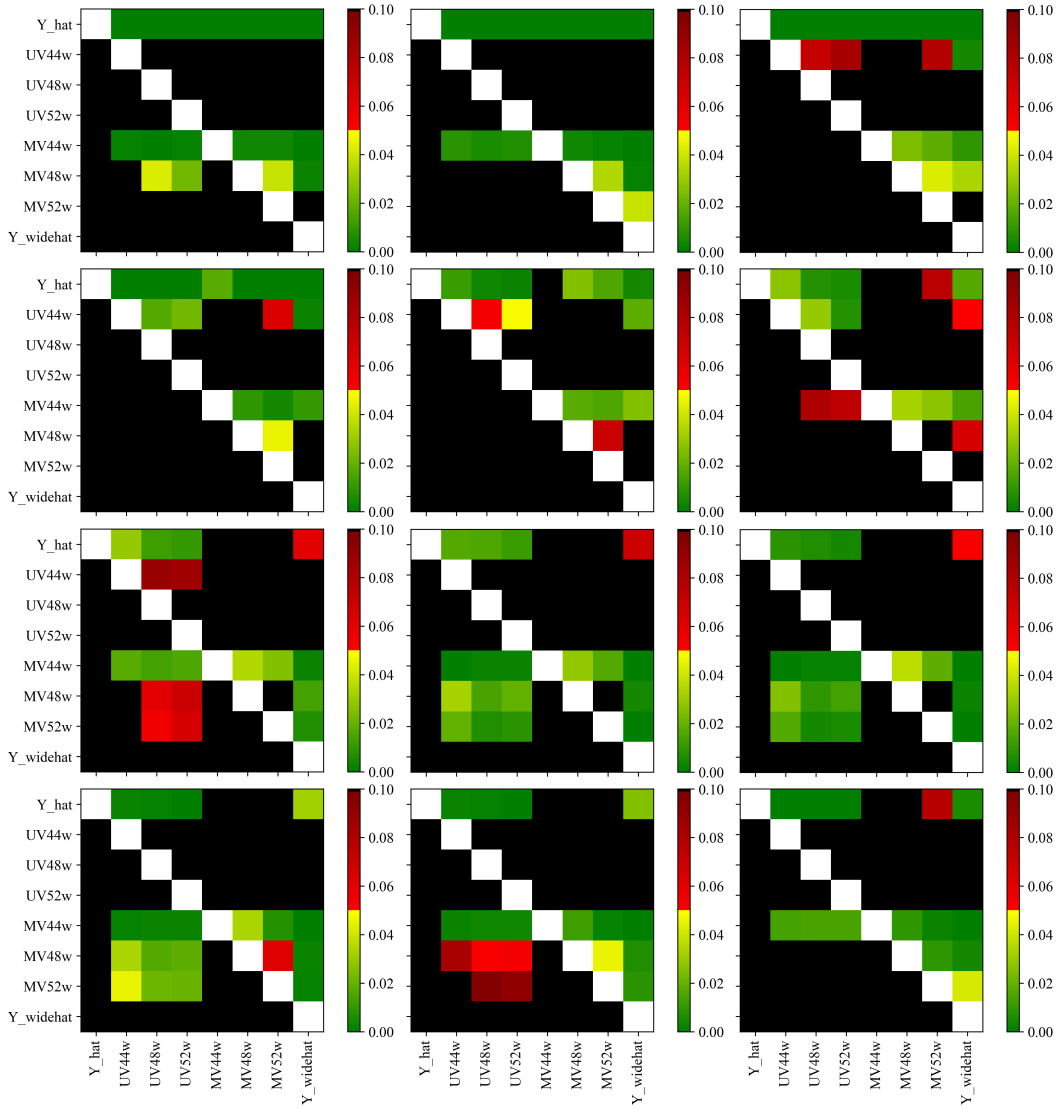

Figure D.5.: Univariate DM tests for the day-ahead electricity price forecast for hours 0 to 11 of the day (output derived with source code from *epftoolbox* by Lago et al. (2021)).

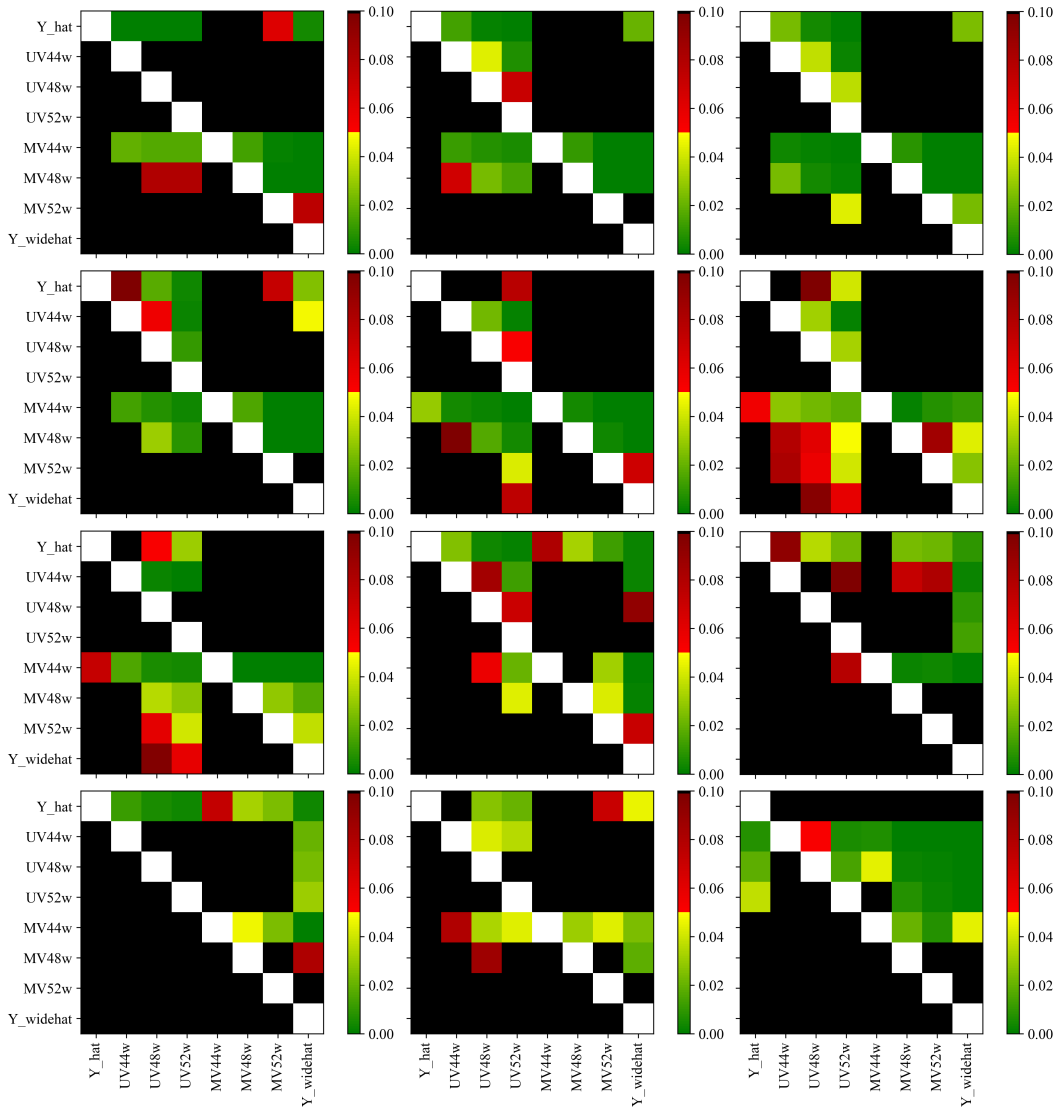

Figure D.6.: Univariate DM tests for the day-ahead electricity price forecast for hours 12 to 23 of the day (output derived with source code from *epftoolbox* by Lago et al. (2021)).

Own Publications

Grothe, O., F. Kächele, and M. Watermeyer (2022): "Analyzing Europe's Biggest Offshore Wind Farms: A Data Set with 40 Years of Hourly Wind Speeds and Electricity Production," *Energies*, 15.

Grothe, O., F. Kächele, and M. Watermeyer (2023): "High-Resolution Working Layouts and Time Series for Renewable Energy Generation in Europe: A Data-Driven Approach for Accurate Fore- and Nowcasting," *Submitted to Renewable Energy*.

Möbius, T., M. Watermeyer, O. Grothe, and F. Müsgens (2023): "Enhancing energy system models using better load forecasts," *Energy Systems*, 1868–3975.

Watermeyer, M., T. Möbius, O. Grothe, and F. Müsgens (2023): "A hybrid model for day ahead electricity price forecasting: Combining fundamental and stochastic modelling," *Submitted to Energy Economics*.

Watermeyer, M., and F. Scheller (2023): "Forecast the forecast error: Improving point forecasts and generating density forecasts in energy markets," *Working paper*.

Bibliography

50Hertz Transmission GmbH, Amprion GmbH, TenneT TSO GmbH, and TransnetBW GmbH (2023): "Szenariorahmen zum Netzentwicklungsplan Strom 2037 mit Ausblick 2045, Version 2023," https://www.netzausbau.de/SharedDocs/Downloads/DE/Bedarfsermittlung/2037/SR/Szenariorahmen_2037_Entwurf.pdf?__blob=publicationFile, accessed on 24-02-2023.

Aggarwal, A. and M. M. Tripathi (2017): "A novel hybrid approach using wavelet transform, time series time delay neural network, and error predicting algorithm for day-ahead electricity price forecasting," in *2017 6th International Conference on Computer Applications In Electrical Engineering-Recent Advances (CERA)*, 199–204.

Aggarwal, S. K., L. M. Saini, and A. Kumar (2009): "Electricity price forecasting in deregulated markets: A review and evaluation," *International Journal of Electrical Power & Energy Systems*, 31, 13–22.

Ahmed, R., V. Sreeram, Y. Mishra, and M. Arif (2020): "A review and evaluation of the state-of-the-art in PV solar power forecasting: Techniques and optimization," *Renewable and Sustainable Energy Reviews*, 124, 109792.

Al-Hamadi, H. and S. Soliman (2004): "Short-term electric load forecasting based on Kalman filtering algorithm with moving window weather and load model," *Electric Power Systems Research*, 68, 47–59.

Ali, Z., G. Putrus, M. Marzband, M. B. Tookanlou, K. Saleem, P. K. Ray, and B. Subudhi (2021): "Online Sensorless Solar Power Forecasting for Microgrid Control and Automation," in *2021 International Symposium of Asian Control Association on Intelligent Robotics and Industrial Automation (IRIA)*, 443–448.

Ambrosius, M., J. Egerer, V. Grimm, and A. H. van der Weijde (2022): "Risk aversion in multilevel electricity market models with different congestion pricing regimes," *Energy Economics*, 105, 105701.

Amjady, N. (2001): "Short-term hourly load forecasting using time-series modeling with peak load estimation capability," *IEEE Transactions on Power Systems*, 16, 798–805.

——— (2006): "Day-ahead price forecasting of electricity markets by a new fuzzy neural network," *IEEE Transactions on Power Systems*, 21, 887–896.

Amjady, N. and M. Hemmati (2006): "Energy price forecasting - problems and proposals for such predictions," *IEEE Power and Energy Magazine*, 4, 20–29.

Andresen, G. B., R. A. Rodriguez, S. Becker, and M. Greiner (2014): "The potential for arbitrage of wind and solar surplus power in Denmark," *Energy*, 76, 49–58.

Andresen, G. B., A. A. Søndergaard, and M. Greiner (2015): "Validation of Danish wind time series from a new global renewable energy atlas for energy system analysis," *Energy*, 93, 1074–1088.

Angamuthu Chinnathambi, R., A. Mukherjee, M. Campion, H. Salehfar, T. M. Hansen, J. Lin, and P. Ranganathan (2019): "A Multi-Stage Price Forecasting Model for Day-Ahead Electricity Markets," *Forecasting*, 1, 26–46.

Antweiler, W. and F. Müsgens (2021): "On the long-term merit order effect of renewable energies," *Energy Economics*, 99, 105275.

Archer, C. L. and M. Z. Jacobson (2007): "Supplying Baseload Power and Reducing Transmission Requirements by Interconnecting Wind Farms," *Journal of Applied Meteorology and Climatology*, 46, 1701–1717.

Baker, R., S. Walker, and J. Wade (1990): "Annual and seasonal variations in mean wind speed and wind turbine energy production," *Solar Energy*, 45, 285–289.

Barthelmie, R., S. Pryor, S. Frandsen, K. Hansen, J. Schepers, K. Rados, W. Schlez, A. Neubert, L. Jensen, and S. Neckelmann (2010): "Quantifying

the impact of wind turbine wakes on power output at offshore wind farms," *Journal of Atmospheric and Oceanic Technology*, 27, 1302 – 1317.

Beran, P., C. Pape, and C. Weber (2019): "Modelling German electricity wholesale spot prices with a parsimonious fundamental model – Validation & application," *Utilities Policy*, 58, 27–39.

Beyer, H. G., G. Heilscher, and S. Bofinger (2004): "A robust model for the MPP performance of different types of PV-modules applied for the performance check of grid connected systems," *EuroSun*.

Bierbrauer, M., S. Trück, and R. Weron (2004): "Modeling electricity prices with regime switching models," *Lecture Notes in Computer Science*, 3039, 859–867.

BNetzA (2021): "Kraftwerksliste der Bundesnetzagentur," `https://www.bundesnetzagentur.de/DE/Sachgebiete/ElektrizitaetundGas/Unternehmen_Institutionen/Versorgungssicherheit/Erzeugungskapazitaeten/Kraftwerksliste/start.html`, accessed on 15-05-2021.

Bordignon, S., D. W. Bunn, F. Lisi, and F. Nan (2013): "Combining day-ahead forecasts for British electricity prices," *Energy Economics*, 35, 88–103.

Borenstein, S., J. B. Bushnell, and F. A. Wolak (2002): "Measuring Market Inefficiencies in California's Restructured Wholesale Electricity Market," *American Economic Review*, 92, 1376–1405.

Box, G. E. P. and G. M. Jenkins (1970): *Time series analysis forecasting and control*, Holden-Day series in time series analysis, San Francisco, Calif. [u.a.]: Holden-Day.

Box, G. E. P., G. M. Jenkins, G. C. Reinsel, and G. M. Ljung (2015): *Time series analysis: forecasting and control*, Wiley series in probability and statistics, Hoboken, New Jersey: John Wiley and Sons Inc., 5th ed.

Brockwell, P. J. and R. A. Davis (2016): *Introduction to Time Series and Forecasting*, Springer International Publishing.

Bundesnetzagentur (2019): "Marktstammdatenregister (MaStR) – core energy market data register," https://www.marktstammdatenregister.de/MaStR, accessed on 15-11-2022.

Bundesnetzagentur für Elektrizität, Gas, Telekommunikation, Post und Eisenbahnen and Bundeskartellamt (2022): "Monitoringbericht 2021," https://www.bundesnetzagentur.de/SharedDocs/Mediathek/Monitoringberichte/Monitoringbericht_Energie2021.pdf?__blob=publicationFile&v=2, accessed on 24-02-2023.

Cancelo, J. R., A. Espasa, and R. Grafe (2008): "Forecasting the electricity load from one day to one week ahead for the Spanish system operator," *International Journal of Forecasting*, 24, 588–602.

Chang, Z., Y. Zhang, and W. Chen (2019): "Electricity price prediction based on hybrid model of adam optimized LSTM neural network and wavelet transform," *Energy*, 187, 115804.

Chen, J.-F., W.-M. Wang, and C.-M. Huang (1995): "Analysis of an adaptive time-series autoregressive moving-average (ARMA) model for short-term load forecasting," *Electric Power Systems Research*, 34, 187–196.

Chen, X., Z. Y. Dong, K. Meng, Y. Xu, K. P. Wong, and H. W. Ngan (2012): "Electricity Price Forecasting With Extreme Learning Machine and Bootstrapping," *IEEE Transactions on Power Systems*, 27, 2055–2062.

Cheng, H., X. Ding, W. Zhou, and R. Ding (2019): "A hybrid electricity price forecasting model with Bayesian optimization for German energy exchange," *International Journal of Electrical Power & Energy Systems*, 110, 653–666.

Christensen, T. M., A. S. Hurn, and K. A. Lindsay (2012): "Forecasting spikes in electricity prices," *International Journal of Forecasting*, 28, 400–411.

Clark, T. E., M. W. McCracken, and E. Mertens (2020): "Modeling Time-Varying Uncertainty of Multiple-Horizon Forecast Errors," *The Review of Economics and Statistics*, 102, 17–33.

Dawid, A. P. (1984): "Present Position and Potential Developments: Some Personal Views: Statistical Theory: The Prequential Approach," *Journal of the Royal Statistical Society. Series A (General)*, 147, 278–292.

de Marcos, R. A., A. Bello, and J. Reneses (2019): "Electricity price forecasting in the short term hybridising fundamental and econometric modelling," *Electric Power Systems Research*, 167, 240–251.

DeMiguel, V., L. Garlappi, and R. Uppal (2009): "Optimal versus naive diversification: How inefficient is the 1/N portfolio strategy," *Review of Financial Studies*, 22, 1915–1953.

DENA (2010): "dena-Netzstudie II. Integration erneuerbarer Energien in die deutsche Stromversorgung im Zeitraum 2015 – 2020 mit Ausblick 2025," `https://www.dena.de/fileadmin/user_upload/Download/Dokumente/Studien__Umfragen/Endbericht_dena-Netzstudie_II.PDF`.

DESTATIS Statistisches Bundesamt (2021): "Erzeugerpreise gewerblicher Produkte (Inlandsabsatz). Preise für leichtes Heizöl, Motorenbenzin und Diesel," `https://www.destatis.de/DE/Themen/Wirtschaft/Preise/Erzeugerpreisindex-gewerbliche-Produkte/_inhalt.html`, accessed on 25-01-2021.

Diebold, F. X. and R. S. Mariano (1995): "Comparing Predictive Accuracy," *Journal of Business & Economic Statistics*, 13, 253–63.

——— (2002): "Comparing Predictive Accuracy," *Journal of Business & Economic Statistics*, 20, 134–144.

Do, L. P. C., K.-H. Lin, and P. Molnár (2016): "Electricity consumption modelling: A case of Germany," *Economic Modelling*, 55, 92–101.

Dudek, G. (2016): "Multilayer perceptron for GEFCom2014 probabilistic electricity price forecasting," *International Journal of Forecasting*, 32, 1057–1060.

Duffie, J. and W. Beckmann (2006): *Solar Engineering of Thermal Processes*, New Jersey: John Wiley and Sons, 3rd ed.

Durisch, W., D. Tille, A. Wörz, and W. Plapp (2000): "Characterisation of photovoltaic generators," *Applied Energy*, 65, 273–284.

EBC (2021): "Europe Beyond Coal: European Coal Plant Database, 25 Jan 2021," `https://beyond-coal.eu/database/`, accessed on 25-01-2021.

EEX (2021): "European Energy Exchange: Historic gas price data," Accessed on 15-05-2021.

Egerer, J., V. Grimm, T. Kleinert, M. Schmidt, and G. Zöttl (2021): "The impact of neighboring markets on renewable locations, transmission expansion, and generation investment," *European Journal of Operational Research*, 292, 696–713.

Eichler, M., O. Grothe, H. Manner, and T. Dennis (2014): "Models for short-term forecasting of spike occurrences in Australian electricity markets: A comparative study," *The Journal of Energy Markets*, 7, 55–81.

Eising, M., H. Hobbie, and D. Möst (2020): "Future wind and solar power market values in Germany — Evidence of spatial and technological dependencies?" *Energy Economics*, 86, 104638.

Engelhorn, T. and T. Möbius (2022): "On the Development of Wind Market Values and the Influence of Technology and Weather: a German Case Study," *Zeitschrift für Energiewirtschaft*, 1–23.

Engelhorn, T. and F. Müsgens (2018): "How to estimate wind-turbine infeed with incomplete stock data: A general framework with an application to turbine-specific market values in Germany," *Energy Economics*, 72, 542–557.

ENTSO-E (2018): "TYNDP 2018 Scenario Report," `https://tyndp.entsoe.eu/tyndp2018/scenario-report`, accessed on 23-02-2022.

ENTSO-E Transparency Platform (2021a): "Actual Generation per Production Type," `https://transparency.entsoe.eu/`, accessed on 15-05-2021.

——— (2021b): "Actual Generation per Production Type," `https://transparency.entsoe.eu/`, accessed on 20-12-2021.

——— (2021c): "Day-ahead Prices," https://transparency.entsoe.eu/, accessed on 15-05-2021.

——— (2021d): "Day-ahead Prices," https://transparency.entsoe.eu/, accessed on 20-12-2021.

——— (2021e): "Forecasted Transfer Capacities - Day Ahead," https://transparency.entsoe.eu/, accessed on 15-05-2021.

——— (2021f): "Forecasted Transfer Capacities - Day Ahead," https://transparency.entsoe.eu/, accessed on 20-12-2021.

——— (2021g): "Generation Forecast - Day ahead," https://transparency.entsoe.eu/, accessed on 15-05-2021.

——— (2021h): "Generation Forecast - Day ahead," https://transparency.entsoe.eu/, accessed on 20-12-2021.

——— (2021i): "Installed Capacities per Production Type," https://transparency.entsoe.eu/, accessed on 15-05-2021.

——— (2021j): "Installed Capacities per Production Type," https://transparency.entsoe.eu/, accessed on 20-12-2021.

——— (2021k): "Total Load - Day Ahead / Actual," https://transparency.entsoe.eu/, accessed on 15-05-2021.

——— (2021l): "Total Load - Day Ahead / Actual," https://transparency.entsoe.eu/, accessed on 20-12-2021.

——— (2021m): "Unavailability of Production and Generation Units," https://transparency.entsoe.eu/, accessed on 15-05-2021.

——— (2021n): "Unavailability of Production and Generation Units," https://transparency.entsoe.eu/, accessed on 20-12-2021.

——— (2022): "Day-ahead Prices," https://transparency.entsoe.eu/, accessed on 10-10-2022.

——— (2023a): "Actual Generation per Production Type," https://transparency.entsoe.eu/, accessed on 13-01-2023.

——— (2023b): "ENTSO-E Transparency Platform," https://transparency.entsoe.eu/, accessed on 13-01-2023.

——— (2023c): "Generation Forecasts for Wind and Solar," https://transparency.entsoe.eu/, accessed on 13-01-2023.

——— (2023d): "Installed Capacity per Production Type," https://transparency.entsoe.eu/, accessed on 24-02-2023.

——— (2023e): "Total Load - Day Ahead / Actual," https://transparency.entsoe.eu/, accessed on 13-01-2023.

European Commission (2019): "COMMUNICATION FROM THE COMMISSION TO THE EUROPEAN PARLIAMENT, THE COUNCIL, THE EUROPEAN ECONOMIC AND SOCIAL COMMITTEE AND THE COMMITTEE OF THE REGIONS The European Green Deal," https://eur-lex.europa.eu/legal-content/EN/TXT/?qid=1576150542719&uri=COM%3A2019%3A640%3AFIN, accessed on 29-12-2021.

——— (2021): "Eurostat Statistics Database," https://ec.europa.eu/eurostat/data/database, accessed on 15-05-2021.

European Commission, Directorate-General for Climate Action, Directorate-General for Energy, Directorate-General for Mobility and Transport, A. De Vita, P. Capros, L. Paroussos, K. Fragkiadakis, P. Karkatsoulis, L. Höglund-Isaksson, W. Winiwarter, P. Purohit, A. Gómez-Sanabria, P. Rafaj, L. Warnecke, A. Deppermann, M. Gusti, S. Frank, P. Lauri, F. Fulvio, A. Florou, M. Kannavou, N. Forsell, T. Fotiou, P. Siskos, P. Havlík, I. Tsiropoulos, S. Evangelopoulou, P. Witzke, M. Kesting, N. Katoufa, I. Mitsios, G. Asimakopoulou, and T. Kalokyris (2021): *EU reference scenario 2020: energy, transport and GHG emissions: trends to 2050*, Publications Office.

Federal Office of Justice and Federal Ministry of Justice (2021): "Gesetz für den Ausbau erneuerbarer Energien (Erneuerbare-Energien-Gesetz - EEG 2021)," .

——— (2022a): "Gesetz über den Bundesbedarfsplan (Bundesbedarfsplangesetz - BBPlG)," http://www.gesetze-im-internet.de/bbplg/BJNR254310013.html, accessed on 24-02-2023.

——— (2022b): "Verordnung zur Sicherung der Energieversorgung über kurzfristig wirksame Maßnahmen (Kurzfristenergieversorgungssicherungsmaßnahmenverordnung - EnSikuMaV)," https://www.gesetze-im-internet.de/ensikumav/BJNR144600022.html, accessed on 05-03-2023.

Frank, C., S. Fiedler, and S. Crewell (2021): "Balancing potential of natural variability and extremes in photovoltaic and wind energy production for European countries," *Renewable Energy*, 163, 674–684.

Garcia, R., J. Contreras, M. van Akkeren, and J. Garcia (2005): "A GARCH forecasting model to predict day-ahead electricity prices," *IEEE Transactions on Power Systems*, 20, 867–874.

Gil, H. A., C. Gomez-Quiles, and J. Riquelme (2012): "Large-scale wind power integration and wholesale electricity trading benefits: Estimation via an ex post approach," *Energy Policy*, 41, 849–859, modeling Transport (Energy) Demand and Policies.

Gneiting, T. (2011): "Making and Evaluating Point Forecasts," *Journal of the American Statistical Association*, 106, 746–762.

Gneiting, T., F. Balabdaoui, and A. E. Raftery (2007): "Probabilistic forecasts, calibration and sharpness," *Journal of the Royal Statistical Society: Series B (Statistical Methodology)*, 69, 243–268.

Gneiting, T. and M. Katzfuss (2014): "Probabilistic Forecasting," *Annual Review of Statistics and Its Application*, 1, 125–151.

Gonzalez, V., J. Contreras, and D. W. Bunn (2012): "Forecasting Power Prices Using a Hybrid Fundamental-Econometric Model," *IEEE Transactions on Power Systems*, 27, 363–372.

González-Aparicio, I., F. Monforti, P. Volker, A. Zucker, F. Careri, T. Huld, and J. Badger (2017): "Simulating European wind power generation applying statistical downscaling to reanalysis data," *Applied Energy*, 199, 155–168.

Green, R. and N. Vasilakos (2010): "Market behaviour with large amounts of intermittent generation," *Energy Policy*, 38, 3211–3220.

Grothe, O. (2013): "A higher order correlation unscented Kalman filter," *Applied mathematics and computation*, 219, 9033–9042.

Grothe, O., F. Kächele, and F. Krüger (2023a): "From point forecasts to multivariate probabilistic forecasts: The Schaake shuffle for day-ahead electricity price forecasting," *Energy Economics*, 106602.

Grothe, O., F. Kächele, and M. Watermeyer (2022): "Analyzing Europe's Biggest Offshore Wind Farms: A Data Set with 40 Years of Hourly Wind Speeds and Electricity Production," *Energies*, 15.

——— (2023b): "High-Resolution Working Layouts and Time Series for Renewable Energy Generation in Europe: A Data-Driven Approach for Accurate Forecasting and Nowcasting," Submitted paper.

Grothe, O. and F. Müsgens (2013): "The influence of spatial effects on wind power revenues under direct marketing rules," *Energy Policy*, 58, 237–247.

Hastie, T., R. Tibshirani, and J. Friedman (2001): *The Elements of Statistical Learning*, Springer Series in Statistics, New York, NY, USA: Springer New York Inc.

Heinisch, V., L. Göransson, R. Erlandsson, H. Hodel, F. Johnsson, and M. Odenberger (2021): "Smart electric vehicle charging strategies for sectoral coupling in a city energy system," *Applied Energy*, 288, 116640.

Hellwig, M. (2003): *Entwicklung und Anwendung parametrisierter Standard-Lastprofile*, Dissertation, Technische Universität München.

Hersbach, H., B. Bell, P. Berrisford, G. Biavati, A. Horányi, J. M. Sabater, J. Nicolas, C. Peubey, R. Radu, I. Rozum, D. Schepers, A. Simmons, C. Soci, D. Dee, and J.-N. Thépaut (2018): "ERA5 hourly data on single levels from 1979 to present. Copernicus Climate Change Service (C3S) Climate Data Store (CDS)." Accessed on 15-11-2022.

Hickey, E., D. G. Loomis, and H. Mohammadi (2012): "Forecasting hourly electricity prices using ARMAX–GARCH models: An application to MISO hubs," *Energy Economics*, 34, 307–315.

Hirth, L. (2013): "The market value of variable renewables: The effect of solar wind power variability on their relative price," *Energy Economics*, 38, 218–236.

Hirth, L., J. Mühlenpfordt, and M. Bulkeley (2018): "The ENTSO-E Transparency Platform – A review of Europe's most ambitious electricity data platform," *Applied Energy*, 225, 1054–1067.

Hoerl, A. E. and R. W. Kennard (2000): "Ridge Regression: Biased Estimation for Nonorthogonal Problems," *Technometrics*, 42, 80–86.

Hong, T., P. Pinson, S. Fan, H. Zareipour, A. Troccoli, and R. J. Hyndman (2016): "Probabilistic energy forecasting: Global Energy Forecasting Competition 2014 and beyond," *International Journal of Forecasting*, 32, 896–913.

Hong, T., P. Pinson, Y. Wang, R. Weron, D. Yang, and H. Zareipour (2020): "Energy Forecasting: A Review and Outlook," *IEEE Open Access Journal of Power and Energy*, 7, 376–388.

Hughes, G. (2012): "The performance of wind farms in the United Kingdom and Denmark," `https://www.ref.org.uk/attachments/article/280/ref.hughes.19.12.12.pdf`, Renewable Energy Foundation, accessed on 03-03-2023.

Huld, T. and A. M. G. Amillo (2015): "Estimating PV Module Performance over Large Geographical Regions: The Role of Irradiance, Air Temperature, Wind Speed and Solar Spectrum," *Energies*, 8, 5159–5181.

Huld, T., G. Friesen, A. Skoczek, R. P. Kenny, T. Sample, M. Field, and E. D. Dunlop (2011): "A power-rating model for crystalline silicon PV modules," *Solar Energy Materials and Solar Cells*, 95, 3359–3369.

Hutcheon, N. and J. W. Bialek (2013): "Updated and validated power flow model of the main continental European transmission network," in *2013 IEEE Grenoble Conference*, 1–5.

Hyndman, R. J. and G. Athanasopoulos (2021): *Forecasting : principles and practice*, Lexington, Ky.: Otexts: Melbourne, Australia, accessed on 04-02-2022.

International Renewable Energy Agency (2023): "IRENASTAT Online Data Query Tool," `https://www.irena.org/Data/Downloads/IRENASTAT`, accessed on 17-02-2023.

Janke, T. and F. Steinke (2020): "Probabilistic multivariate electricity price forecasting using implicit generative ensemble post-processing," in *2020 International Conference on Probabilistic Methods Applied to Power Systems (PMAPS)*, 1–6.

JAO Joint Allocation Office (2021): "ATC for Shadow Auction," `https://www.jao.eu/implict-allocation`, accessed on 15-05-2021.

Jensen, T. V., H. de Sevin, M. Greiner, and P. Pinson (2017): "The RE-Europe data set," The authors are partly supported by the Danish Council for Strategic Research through the project "5s — Future Electricity Markets", no. 12–132636/DSF.

Jensen, T. V. and P. Pinson (2017): "RE-Europe, a large-scale dataset for modeling a highly renewable European electricity system," *Scientific Data*, 4, 170175.

Kaack, L. H., J. Apt, M. G. Morgan, and P. McSharry (2017): "Empirical prediction intervals improve energy forecasting," *Proceedings of the National Academy of Sciences*, 114, 8752–8757.

Kalogirou, S. A. (2014): *Solar energy engineering: processes and systems*, Boston: Academic Press, 2nd ed.

Katzenstein, W., E. Fertig, and J. Apt (2010): "The variability of interconnected wind plants," *Energy Policy*, 38, 4400–4410.

Keles, D., M. Genoese, D. Möst, S. Ortlieb, and W. Fichtner (2013): "A combined modeling approach for wind power feed-in and electricity spot prices," *Energy Policy*, 59, 213–225.

Kenny, D. and S. Fiedler (2022): "Which gridded irradiance data is best for modelling photovoltaic power production in Germany?" *Solar Energy*, 232, 444–458.

Khosravi, A., S. Nahavandi, and D. Creighton (2013): "Quantifying uncertainties of neural network-based electricity price forecasts," *Applied Energy*, 112, 120–129.

Kirchem, D., M. A. Lynch, V. Bertsch, and E. Casey (2020): "Modelling demand response with process models and energy systems models: Potential applications for wastewater treatment within the energy-water nexus," *Applied Energy*, 260, 114321.

Kitzing, L., N. Juul, M. Drud, and T. K. Boomsma (2017): "A real options approach to analyse wind energy investments under different support schemes," *Applied Energy*, 188, 83–96.

Koenker, R. and G. Bassett (1978): "Regression Quantiles," *Econometrica*, 46, 33.

Koirala, B., S. Hers, G. Morales-España, Özge Özdemir, J. Sijm, and M. Weeda (2021): "Integrated electricity, hydrogen and methane system modelling framework: Application to the Dutch Infrastructure Outlook 2050," *Applied Energy*, 289, 116713.

Koivisto, M., G. M. Jónsdóttir, P. Sørensen, K. Plakas, and N. Cutululis (2020): "Combination of meteorological reanalysis data and stochastic simulation for modelling wind generation variability," *Renewable Energy*, 159, 991–999.

Kontogiannis, D., D. Bargiotas, A. Daskalopulu, A. I. Arvanitidis, and L. H. Tsoukalas (2022): "Error Compensation Enhanced Day-Ahead Electricity Price Forecasting," *Energies*, 15.

Kosater, P. and K. Mosler (2006): "Can Markov regime-switching models improve power-price forecasts? Evidence from German daily power prices," *Applied Energy*, 83, 943–958.

Kreith, F. and J. F. Kreider (1978): *Principles of solar engineering*, Series in thermal and fluids engineering, Washington, DC. [u.a.]: Hemisphere Publ. Corp.

Krüger, F. and I. Nolte (2016): "Disagreement versus uncertainty: Evidence from distribution forecasts," *Journal of Banking & Finance*, 72, 172–186.

Kubik, M., D. Brayshaw, P. Coker, and J. Barlow (2013): "Exploring the role of reanalysis data in simulating regional wind generation variability over Northern Ireland," *Renewable Energy*, 57, 558–561.

Kuntz, L. and F. Müsgens (2007): "Modelling start-up costs of multiple technologies in electricity markets," *Mathematical Methods of Operations Research*, 66, 21–32.

Kunz, F., M. Kendziorski, W.-P. Schill, J. Weibezahn, J. Zepter, C. R. von Hirschhausen, P. Hauser, M. Zech, D. Möst, S. Heidari, B. Felten, and C. Weber (2017a): "Electricity, heat, and gas sector data for modeling the German system," DIW Data Documentation 92.

Kunz, F., J. Weibezahn, P. Hauser, S. Heidari, W.-P. Schill, B. Felten, M. Kendziorski, M. Zech, J. Zepter, C. von Hirschhausen, D. Möst, and C. Weber (2017b): "Reference Data Set: Electricity, Heat, and Gas Sector Data for Modeling the German System," `https://doi.org/10.5281/zenodo.1044463`, Zenodo, Version 1.0.0.

Lago, J., G. Marcjasz, B. De Schutter, and R. Weron (2021): "Forecasting day-ahead electricity prices: A review of state-of-the-art algorithms, best practices and an open-access benchmark," *Applied Energy*, 293, 116983.

Lago, J., F. D. Ridder, P. Vrancx, and B. D. Schutter (2018): "Forecasting day-ahead electricity prices in Europe: The importance of considering market integration," *Applied Energy*, 211, 890–903.

Lamont, A. D. (2008): "Assessing the long-term system value of intermittent electric generation technologies," *Energy Economics*, 30, 1208–1231.

Lehna, M., F. Scheller, and H. Herwartz (2022): "Forecasting day-ahead electricity prices: A comparison of time series and neural network models taking external regressors into account," *Energy Economics*, 106, 105742.

Li, G., S. Xie, B. Wang, J. Xin, Y. Li, and S. Du (2020): "Photovoltaic Power Forecasting With a Hybrid Deep Learning Approach," *IEEE Access*, 8, 175871–175880.

Li, Y., R. Wang, Y. Li, M. Zhang, and C. Long (2023): "Wind power forecasting considering data privacy protection: A federated deep reinforcement learning approach," *Applied Energy*, 329, 120291.

Li, Z., Y. Li, Y. Liu, P. Wang, R. Lu, and H. B. Gooi (2021): "Deep Learning Based Densely Connected Network for Load Forecasting," *IEEE Transactions on Power Systems*, 36, 2829–2840.

Lienert, M. and S. Lochner (2012): "The importance of market interdependencies in modeling energy systems – The case of the European electricity generation market," *International Journal of Electrical Power & Energy Systems*, 34, 99–113.

Lin, L., L. Xue, Z. Hu, and N. Huang (2018): "Modular Predictor for Day-Ahead Load Forecasting and Feature Selection for Different Hours," *Energies*, 11.

Ludwig, N., S. Arora, and J. W. Taylor (2022): "Probabilistic load forecasting using post-processed weather ensemble predictions," *Journal of the Operational Research Society*, 0, 1–13.

Lynch, M., M. T. Devine, and V. Bertsch (2019): "The role of power-to-gas in the future energy system: Market and portfolio effects," *Energy*, 185, 1197–1209.

Lütkepohl, H. (2005): *New introduction to multiple time series analysis*, Berlin: Springer.

Maciejowska, K., W. Nitka, and T. Weron (2021): "Enhancing load, wind and solar generation for day-ahead forecasting of electricity prices," *Energy Economics*, 99, 105273.

Maciejowska, K. and J. Nowotarski (2016): "A hybrid model for GEFCom2014 probabilistic electricity price forecasting," *International Journal of Forecasting*, 32, 1051–1056.

Maciejowska, K., J. Nowotarski, and R. Weron (2016): "Probabilistic forecasting of electricity spot prices using Factor Quantile Regression Averaging," *International Journal of Forecasting*, 32, 957–965.

Manner, H., F. Alavi Fard, A. Pourkhanali, and L. Tafakori (2019): "Forecasting the joint distribution of Australian electricity prices using dynamic vine copulae," *Energy Economics*, 78, 143–164.

Manner, H., D. Türk, and M. Eichler (2016): "Modeling and forecasting multivariate electricity price spikes," *Energy Economics*, 60, 255–265.

Marcjasz, G., T. Serafin, and R. Weron (2018): "Selection of Calibration Windows for Day-Ahead Electricity Price Forecasting," *Energies*, 11, 2364.

Marcjasz, G., B. Uniejewski, and R. Weron (2019): "On the importance of the long-term seasonal component in day-ahead electricity price forecasting with NARX neural networks," *International Journal of Forecasting*, 35, 1520–1532.

——— (2020): "Probabilistic electricity price forecasting with NARX networks: Combine point or probabilistic forecasts?" *International Journal of Forecasting*, 36, 466–479.

Mari, C. and E. Mari (2022): "Deep learning based regime-switching models of energy commodity prices," *Energy Systems*.

Misconel, S., C. Zöphel, and D. Möst (2021): "Assessing the value of demand response in a decarbonized energy system – A large-scale model application," *Applied Energy*, 299, 117326.

Misiorek, A., S. Trueck, and R. Weron (2006): "Point and Interval Forecasting of Spot Electricity Prices: Linear vs. Non-Linear Time Series Models," *Studies in Nonlinear Dynamics & Econometrics*, 10.

Morales, J. M., A. J. Conejo, H. Madsen, P. Pinson, and M. Zugno (2014): *Integrating Renewables in Electricity Markets*, International Series in Operations Research & Management Science ; 205SpringerLinkSpringer eBook Collection, Boston, MA: Springer.

Muniain, P. and F. Ziel (2020): "Probabilistic forecasting in day-ahead electricity markets: Simulating peak and off-peak prices," *International Journal of Forecasting*, 36, 1193–1210.

Möbius, T., I. Riepin, F. Müsgens, and A. H. van der Weijde (2021): "Risk aversion in flexible electricity markets," *arXiv*.

Möbius, T., M. Watermeyer, O. Grothe, and F. Müsgens (2023): "Enhancing energy system models using better load forecasts," *Energy Systems*, 1868–3975.

Möst, D. and D. Keles (2010): "A survey of stochastic modelling approaches for liberalised electricity markets," *European Journal of Operational Research*, 207, 543–556.

Müsgens, F. (2006a): "Quantifying Market Power in the German Wholesale Electricity Market Using a Dynamic Multi-Regional Dispatch Model," *The Journal of Industrial Economics*, 54, 471–498.

——— (2006b): "Quantifying Market Power in the German Wholesale Electricity Market Using a Dynamic Multi-Regional Dispatch Model," *The Journal of Industrial Economics*, 54, 471–498.

——— (2020): "Equilibrium prices and investment in electricity systems with CO2-emission trading and high shares of renewable energies," *Energy Economics*, 86, 104107.

Müsgens, F. and K. Neuhoff (2006): "Modelling Dynamic Constraints in Electricity Markets and the Costs of Uncertain Wind Output," .

Nahmmacher, P., E. Schmid, M. Pahle, and B. Knopf (2016): "Strategies against shocks in power systems – An analysis for the case of Europe," *Energy Economics*, 59, 455–465.

Naz, A., M. U. Javed, N. Javaid, T. Saba, M. Alhussein, and K. Aurangzeb (2019): "Short-Term Electric Load and Price Forecasting Using Enhanced Extreme Learning Machine Optimization in Smart Grids," *Energies*, 12.

Nazar, M. S., A. E. Fard, A. Heidari, M. Shafie-khah, and J. P. Catalão (2018): "Hybrid model using three-stage algorithm for simultaneous load and price forecasting," *Electric Power Systems Research*, 165, 214–228.

Nowotarski, J. and R. Weron (2014): "Merging quantile regression with forecast averaging to obtain more accurate interval forecasts of Nord Pool spot prices," in *11th International Conference on the European Energy Market (EEM14)*, 1–5.

——— (2015): "Computing electricity spot price prediction intervals using quantile regression and forecast averaging," *Computational Statistics*, 30, 791–803.

——— (2016): "On the importance of the long-term seasonal component in day-ahead electricity price forecasting," *Energy Economics*, 57, 228–235.

——— (2018): "Recent advances in electricity price forecasting: A review of probabilistic forecasting," *Renewable and Sustainable Energy Reviews*, 81, 1548–1568.

Olamaee, J., M. Mohammadi, A. Noruzi, and S. M. H. Hosseini (2016): "Day-ahead price forecasting based on hybrid prediction model," *Complexity*, 21, 156–164.

Olauson, J. and M. Bergkvist (2015): "Modelling the Swedish wind power production using MERRA reanalysis data," *Renewable Energy*, 76, 717–725.

Open Power System Data (2020a): "Data Package National Generation Capacity. Version 2019-12-02." `https://doi.org/10.25832/national_generation_capacity/2019-12-02`, accessed on 20-12-2020.

——— (2020b): "Data Package Weather Data. Version 2020-09-16." https://doi.org/10.25832/weather_data/2020-09-16, accessed on 20-12-2020.

Panagiotelis, A. and M. Smith (2008): "Bayesian density forecasting of intraday electricity prices using multivariate skew t distributions," *International Journal of Forecasting*, 24, 710–727.

Panapakidis, I. P. and A. S. Dagoumas (2016): "Day-ahead electricity price forecasting via the application of artificial neural network based models," *Applied Energy*, 172, 132–151.

Pape, C., S. Hagemann, and C. Weber (2016): "Are fundamentals enough? Explaining price variations in the German day-ahead and intraday power market," *Energy Economics*, 54, 376–387.

Petropoulos, F., D. Apiletti, V. Assimakopoulos, M. Z. Babai, D. K. Barrow, S. Ben Taieb, C. Bergmeir, R. J. Bessa, J. Bijak, J. E. Boylan, J. Browell, C. Carnevale, J. L. Castle, P. Cirillo, M. P. Clements, C. Cordeiro, F. L. Cyrino Oliveira, S. De Baets, A. Dokumentov, J. Ellison, P. Fiszeder, P. H. Franses, D. T. Frazier, M. Gilliland, M. S. Gönül, P. Goodwin, L. Grossi, Y. Grushka-Cockayne, M. Guidolin, M. Guidolin, U. Gunter, X. Guo, R. Guseo, N. Harvey, D. F. Hendry, R. Hollyman, T. Januschowski, J. Jeon, V. R. R. Jose, Y. Kang, A. B. Koehler, S. Kolassa, N. Kourentzes, S. Leva, F. Li, K. Litsiou, S. Makridakis, G. M. Martin, A. B. Martinez, S. Meeran, T. Modis, K. Nikolopoulos, D. Önkal, A. Paccagnini, A. Panagiotelis, I. Panapakidis, J. M. Pavía, M. Pedio, D. J. Pedregal, P. Pinson, P. Ramos, D. E. Rapach, J. J. Reade, B. Rostami-Tabar, M. Rubaszek, G. Sermpinis, H. L. Shang, E. Spiliotis, A. A. Syntetos, P. D. Talagala, T. S. Talagala, L. Tashman, D. Thomakos, T. Thorarinsdottir, E. Todini, J. R. Trapero Arenas, X. Wang, R. L. Winkler, A. Yusupova, and F. Ziel (2022): "Forecasting: theory and practice," *International Journal of Forecasting*, 38, 705–871.

Pfenninger, S. and I. Staffell (2016): "Long-term patterns of European PV output using 30 years of validated hourly reanalysis and satellite data," *Energy*, 114, 1251–1265.

Phipps, K., S. Lerch, M. Andersson, R. Mikut, V. Hagenmeyer, and N. Ludwig (2022): "Evaluating ensemble post-processing for wind power forecasts," *Wind Energy*, 25, 1379–1405.

Piasecki, A., J. Jurasz, and A. Kies (2019): "Measurements and reanalysis data on wind speed and solar irradiation from energy generation perspectives at several locations in Poland," *SN Applied Sciences*, 1.

Plaga, L. S. and V. Bertsch (2023): "Methods for assessing climate uncertainty in energy system models — A systematic literature review," *Applied Energy*, 331, 120384.

Qussous, R., N. Harder, and A. Weidlich (2022): "Understanding Power Market Dynamics by Reflecting Market Interrelations and Flexibility-Oriented Bidding Strategies," *Energies*, 15.

Rafiei, M., T. Niknam, and M. Khooban (2017): "Probabilistic electricity price forecasting by improved clonal selection algorithm and wavelet preprocessing," *Neural Computing and Applications*, 28.

Rajagukguk, R. A., R. A. A. Ramadhan, and H.-J. Lee (2020): "A Review on Deep Learning Models for Forecasting Time Series Data of Solar Irradiance and Photovoltaic Power," *Energies*, 13.

Regelleistung.net (2018): "List of tenders capacity," `https://www.regelleistung.net/ext/`, accessed on 12-12-2021.

Reindl, D., W. Beckman, and J. Duffie (1990a): "Diffuse fraction correlations," *Solar Energy*, 45, 1–7.

——— (1990b): "Evaluation of hourly tilted surface radiation models," *Solar Energy*, 45, 9–17.

Riepin, I., T. Möbius, and F. Müsgens (2021): "Modelling uncertainty in coupled electricity and gas systems—Is it worth the effort?" *Applied Energy*, 285, 116363.

Rodrigues, F. and A. Trindade (2018): "Load forecasting through functional clustering and ensemble learning," *Knowledge and Information Systems*, 57, 229–244.

Rose, S. and J. Apt (2015): "What can reanalysis data tell us about wind power?" *Renewable Energy*, 83, 963–969.

Sandbag (2020): "CO2 emission allowance," `https://sandbag.be/index.php/carbon-price-viewer/`, accessed on 20-02-2020.

Sauma, E. E., S. S. Oren, E. E. Sauma, and S. S. Oren (2006): "Proactive planning and valuation of transmission investments in restructured electricity markets," *Journal of Regulatory Economics*, 30, 261–290.

Scheller, F. and T. Bruckner (2019): "Energy system optimization at the municipal level: An analysis of modeling approaches and challenges," *Renewable and Sustainable Energy Reviews*, 105, 444–461.

Schill, W. P., M. Pahle, and C. Gambardella (2017): "Start-up costs of thermal power plants in markets with increasing shares of variable renewable generation," *Nature Energy*, 2, 1–6.

Schill, W.-P. and A. Zerrahn (2018): "Long-run power storage requirements for high shares of renewables: Results and sensitivities," *Renewable and Sustainable Energy Reviews*, 83, 156–171.

Schröder, A., F. Kunz, J. Meiss, R. Mendelevitch, and C. von Hirschhausen (2013): "Current and Prospective Costs of Electricity Generation until 2050," *DIW Data Documentation*, 68.

Schön, C., J. Dittrich, and R. Müller (2019): "The Error is the Feature: How to Forecast Lightning using a Model Prediction Error," in *Proceedings of the 25th ACM SIGKDD International Conference on Knowledge Discovery and Data Mining*, ACM, 2979–2988.

Seinfeld, J. H. and S. N. Pandis (2016): *Atmospheric Chemistry and Physics: From Air Pollution to Climate Change*, Wiley, 3rd ed.

Sensfuss, F., M. Ragwitz, and M. Genoese (2008): "The merit-order effect: A detailed analysis of the price effect of renewable electricity generation on spot market prices in Germany," *Energy Policy*, 36, 3086–3094.

Sgarciu, S., D. Scholz, and F. Müsgens (2023): "How CO2 prices accelerate decarbonisation – The case of coal-fired generation in Germany," *Energy Policy*, 173, 113375.

Shahid, F., A. Zameer, M. Afzal, and M. Hassan (2020): "Short term solar energy prediction by machine learning algorithms," *arXiv*.

Singh, A. K., Ibraheem, S. Khatoon, M. Muazzam, and D. K. Chaturvedi (2012): "Load forecasting techniques and methodologies: A review," in *2012 2nd International Conference on Power, Control and Embedded Systems*, 1–10.

Spencer, J. W. (1971): "Fourier series representation of the position of the sun," *Search*, 2, 172+.

Staffell, I. and R. Green (2014): "How does wind farm performance decline with age?" *Renewable Energy*, 66, 775–786.

Staffell, I. and S. Pfenninger (2016): "Using bias-corrected reanalysis to simulate current and future wind power output," *Energy*, 114, 1224–1239.

Steinert, R. and F. Ziel (2019): "Short- to mid-term day-ahead electricity price forecasting using futures," *Energy Journal*, 40, 105–127.

Suganthi, L. and A. A. Samuel (2012): "Energy models for demand forecasting a review," *Renew Sustain Energy Rev*, 16, 1223–1240.

Sunderland, K. M., M. Narayana, G. Putrus, M. F. Conlon, and S. McDonald (2016): "The cost of energy associated with micro wind generation: International case studies of rural and urban installations," *Energy*, 109, 818–829.

Tan, Z., J. Zhang, J. Wang, and J. Xu (2010): "Day-ahead electricity price forecasting using wavelet transform combined with ARIMA and GARCH models," *Applied Energy*, 87, 3606–3610.

Tawn, R. and J. Browell (2022): "A review of very short-term wind and solar power forecasting," *Renewable and Sustainable Energy Reviews*, 153, 111758.

TenneT TSO GmbH (2023): "Project SuedLink," `https://www.tennet.eu/de/de/projekte/suedlink`, accessed on 24-02-2023.

TransnetBW GmbH (2023): "Project SuedLink," `https://www.transnetbw.de/de/netzentwicklung/projekte/suedlink`, accessed on 24-02-2023.

UBA (2020): "Umweltbundesamt: Datenbank "Kraftwerke in Deutschland"," `https://www.umweltbundesamt.de/dokument/datenbank-kraftwerke-in-deutschland`, accessed on 20-02-2020.

Uniejewski, B., G. Marcjasz, and R. Weron (2019): "On the importance of the long-term seasonal component in day-ahead electricity price forecasting: Part II — Probabilistic forecasting," *Energy Economics*, 79, 171–182, energy Markets Dynamics in a Changing Environment.

Uniejewski, B., J. Nowotarski, and R. Weron (2016): "Automated Variable Selection and Shrinkage for Day-Ahead Electricity Price Forecasting," *Energies*, 9.

Uniejewski, B. and R. Weron (2021): "Regularized quantile regression averaging for probabilistic electricity price forecasting," *Energy Economics*, 95, 105121.

Vaillancourt, K., O. Bahn, E. Frenette, and O. Sigvaldason (2017): "Exploring deep decarbonization pathways to 2050 for Canada using an optimization energy model framework," *Applied Energy*, 195, 774–785.

van der Weijde, A. H. and B. F. Hobbs (2012): "The economics of planning electricity transmission to accommodate renewables: Using two-stage optimisation to evaluate flexibility and the cost of disregarding uncertainty," *Energy Economics*, 34, 2089–2101.

Ventosa, M., Álvaro Baíllo, A. Ramos, and M. Rivier (2005): "Electricity market modeling trends," *Energy Policy*, 33, 897–913.

Wan, C., Z. Xu, Y. Wang, Z. Y. Dong, and K. P. Wong (2014): "A Hybrid Approach for Probabilistic Forecasting of Electricity Price," *IEEE Transactions on Smart Grid*, 5, 463–470.

Wang, D., J. Gan, J. Mao, F. Chen, and L. Yu (2023): "Forecasting power demand in China with a CNN-LSTM model including multimodal information," *Energy*, 263, 126012.

Wang, H., Z. Lei, X. Zhang, B. Zhou, and J. Peng (2019): "A review of deep learning for renewable energy forecasting," *Energy Conversion and Management*, 198, 111799.

Wang, X., P. Guo, and X. Huang (2011): "A Review of Wind Power Forecasting Models," *Energy Procedia*, 12, 770–778, the Proceedings of International Conference on Smart Grid and Clean Energy Technologies (ICSGCE 2011).

Watermeyer, M., T. Möbius, O. Grothe, and F. Müsgens (2023): "A hybrid model for day-ahead electricity price forecasting: Combining fundamental and stochastic modelling," Submitted paper.

Watermeyer, M. and F. Scheller (2023): "Forecast the forecast error: Improving point forecasts and generating density forecasts in energy markets," Working paper.

Weigt, H. and C. von Hirschhausen (2008): "Price formation and market power in the German wholesale electricity market in 2006," *Energy Policy*, 36, 4227–4234, transition towards Sustainable Energy Systems.

Weron, R. (2006): *Modeling and forecasting electricity loads and prices : a statistical approach*, Wiley finance series, Chichester [u.a.]: Wiley & Sons.

——— (2014): "Electricity price forecasting: A review of the state-of-the-art with a look into the future," *International Journal of Forecasting*, 30, 1030–1081.

Weron, R. and A. Misiorek (2005): "Modeling and forecasting electricity loads: A comparison," *Proceedings of the European Electricity Market EEM-04*.

——— (2008): "Forecasting spot electricity prices: A comparison of parametric and semiparametric time series models," *International Journal of Forecasting*, 24, 744–763.

Weron, R. and F. Ziel (2019): "Electricity price forecasting," in *Routledge Handbook of Energy Economics*, Routledge, 506–521.

Wu, Z., X. Zhao, Y. Ma, and X. Zhao (2019): "A hybrid model based on modified multi-objective cuckoo search algorithm for short-term load forecasting," *Applied Energy*, 237, 896–909.

Yang, Y., J. Wu, Y. Chen, and C. Li (2013): "A New Strategy for Short-Term Load Forecasting," *Abstract and Applied Analysis*, 2013.

Yang, Z., L. Ce, and L. Lian (2017): "Electricity price forecasting by a hybrid model, combining wavelet transform, ARMA and kernel-based extreme learning machine methods," *Applied Energy*, 190, 291–305.

Zhang, J., Z. Tan, and Y. Wei (2020): "An adaptive hybrid model for short term electricity price forecasting," *Applied Energy*, 258, 114087.

Zhao, J. H., Z. Y. Dong, Z. Xu, and K. P. Wong (2008): "A Statistical Approach for Interval Forecasting of the Electricity Price," *IEEE Transactions on Power Systems*, 23, 267–276.

Zhou, M., Z. Yan, Y. Ni, G. Li, and Y. Nie (2006): "Electricity price forecasting with confidence-interval estimation through an extended ARIMA approach," *Generation, Transmission and Distribution, IEE Proceedings*, 187–195.

Ziel, F. (2018): "Modeling public holidays in load forecasting: a German case study," *Journal of Modern Power Systems and Clean Energy*, 6, 191–207.

Ziel, F. and R. Weron (2018a): "Day-ahead electricity price forecasting with high-dimensional structures: Univariate vs. multivariate modeling frameworks," *Energy Economics*, 70, 396–420.

——— (2018b): "Day-ahead electricity price forecasting with high-dimensional structures: Univariate vs. multivariate modeling frameworks," *Energy Economics*, 70, 396–420.

Zou, H. and T. Hastie (2005): "Regularization and variable selection via the elastic net," *Journal of the Royal Statistical Society: Series B (Statistical Methodology)*, 67, 301–320.

Eidesstattliche Versicherung

gemäß § 13 Abs. 2 Ziff. 3 der Promotionsordnung des Karlsruher Instituts für Technologie für die KIT-Fakultät für Wirtschaftswissenschaften

1. Bei der eingereichten Dissertation zu dem Thema *Advancing Energy Transition: Statistical Approaches to Pan-European Feed-in Data Sets, Enhanced Data Quality and Improved Forecasting* handelt es sich um meine eigenständig erbrachte Leistung.

2. Ich habe nur die angegebenen Quellen und Hilfsmittel benutzt und mich keiner unzulässigen Hilfe Dritter bedient. Insbesondere habe ich wörtlich oder sinngemäß aus anderen Werken übernommene Inhalte als solche kenntlich gemacht.

3. Die Arbeit oder Teile davon habe ich bislang nicht an einer Hochschule des In- oder Auslands als Bestandteil einer Prüfungs- oder Qualifikationsleistung vorgelegt.

4. Die Richtigkeit der vorstehenden Erklärungen bestätige ich.

5. Die Bedeutung der eidesstattlichen Versicherung und die strafrechtlichen Folgen einer unrichtigen oder unvollständigen eidesstattlichen Versicherung sind mir bekannt. Ich versichere an Eides statt, dass ich nach bestem Wissen die reine Wahrheit erklärt und nichts verschwiegen habe.

Karlsruhe, 12. April 2023

(Mira Watermeyer)